

5. Fields in Plane-Stratified Regions

5.1 INTRODUCTION

Representations of Green's functions for regions with planar stratification along z , derived in Sec. 2.3, require knowledge of eigenfunctions in the domain transverse to z , and of their z -dependent modal amplitudes. Eigenfunction solutions for various cross-sectional domains have been given in Chapter 3, while Sec. 2.4 contains information on modal voltage and current amplitudes. For transversely unbounded regions, the eigenfunctions form a continuous spectrum (see Sec. 3.2). The resulting Green's function representations then involve single or double integrals that must be evaluated for extraction of explicit information on field behavior. Of special interest in radiation and diffraction theory are far fields, for which the integrals may be reduced by the asymptotic methods discussed in Chapter 4. Contributions from saddle points and singularities in the integrands result in wave constituents that can be interpreted as geometric-optical and diffracted ray fields. This chapter explores these aspects in detail for time-harmonic and impulsive excitation of a number of plane-stratified configurations.

The discussion begins in Sec. 5.2 with a summary of steady-state and time-dependent electromagnetic field representations and their scalarization. These formal results for arbitrary longitudinal stratification are specialized to unbounded cross sections viewed either as rectangular or cylindrical waveguides excited by time-harmonic and pulsed point or line sources, and also by moving sources. Analytic properties of typical representation integrals and asymptotic forms for the far-zone (or high-frequency) solution are summarized in Sec. 5.3, with emphasis on a physical interpretation of wave species resulting from saddle points, poles, and branch points.

Attention is given to specific geometrical configurations, the simplest being the unbounded homogeneous dielectric medium in Sec. 5.4. While the Green's

functions for various source configurations in such a medium can be derived directly in closed form, we treat modal representations and their asymptotic reduction to illustrate relevant concepts and techniques for simple examples. The discussion proceeds to sources in the presence of a semiinfinite dielectric medium (Sec. 5.5) for which the far-zone field contains not only the direct, reflected, and refracted contributions of geometrical optics but also diffracted constituents in the form of surface waves and (or) lateral waves (the latter are associated with phenomena of total reflection). Consideration is given to transition regions wherein the field cannot be described in terms of these distinct wave types; analytically, transition effects arise from a confluence of saddle points and pole or branch-point singularities in the integral representation. The nature of geometric-optical and diffraction fields becomes evident from the study of transient propagation (Sec. 5.5d), which permits tracking of various wavefronts and thus clarifies corresponding time-harmonic phenomena.

Section 5.6 is concerned with fields excited by sources in the presence of a dielectric slab. This configuration exhibits effects of multiple reflection between the slab boundaries and, when the dielectric constant in the slab exceeds that in the exterior medium, of wave trapping. The energy in the trapped or surface waves is confined to the slab region and transported in the direction parallel to the boundaries, whence a field representation in terms of modes guided along a transverse coordinate ρ is appropriate for emphasizing such wave phenomena. The ρ -transmission representation can be constructed directly on use of the slab eigenfunctions developed in Sec. 3.3c, or by contour deformation from the z -transmission representation; the latter procedure involves the characteristic Green's functions of Sec. 3.3a and illustrates the general theory of alternative representations presented in Sec. 3.3c. Analogous considerations apply to the constant-impedance boundary treated in Sec. 5.7, which may, under suitable conditions, also guide a surface wave. Section 5.7d contains an example of excitation by an aperture, thereby demonstrating how Green's function solutions are used for synthesizing distributed source configurations.

The preceding examples comprise plane-stratified regions with piecewise constant properties along z for which the modal Green's function solutions can be obtained in terms of trigonometric or exponential functions as in Sec. 2.4. For continuous stratification, treated in Secs. 5.8 and 5.9, the non-uniform transmission-line theory of Sec. 3.3b is applicable and yields formal results for arbitrary inhomogeneity profiles, as summarized in Sec. 5.8b. Explicit solutions can be obtained either for "slowly varying" inhomogeneities or for special profiles. For the former, the geometrical-optics method introduced in Sec. 1.7 is applicable and is illustrated in detail in Sec. 5.8c. Alternatively, one may proceed as in Sec. 5.8d from modal representation integrals, simplified on use of the WKB approximations (Sec. 3.5c) for modal Green's functions. When applicable, asymptotic evaluation of the integrals yields the geometric-optical field but unlike the direct geometric-optical method in Sec. 5.8c, also provides

field solutions in transition regions near caustics; to accommodate these regions, the asymptotic evaluation must account for the confluence of two saddle points in the integrand (see Sec. 4.5a).

Special inhomogeneous stratifications are exemplified in Sec. 5.9 by the inverse-square and continuous-transition (Epstein) profiles. Particular attention is given to the inverse-square medium, which possesses a number of interesting properties. Its transmission-line solutions involve the well-explored Bessel functions, so various analytical and asymptotic aspects of the general procedure in Sec. 5.8 can be verified in detail. The simplicity of the solution carries over to the study of ducted propagation in Sec. 5.9b. Two-dimensional radiation and diffraction problems in the inverse-square medium are closely related to a class of rotationally symmetric scattering problems in three dimensions; utilization of this analogy in Sec. 5.9c provides insight into a number of two-dimensional and three-dimensional radiation and scattering processes.

5.2 FIELD REPRESENTATIONS IN REGIONS WITH PIECEWISE CONSTANT PROPERTIES

5.2a Derivation of the Time-Harmonic Field From Scalar Potentials

The electromagnetic fields excited by time-harmonic electric point currents $\mathbf{J}(\mathbf{r}, t) = \mathbf{J}^o \delta(\mathbf{r} - \mathbf{r}') e^{j\omega t}$ and magnetic point currents $\hat{\mathbf{M}}(\mathbf{r}, t) = \mathbf{M}^o \delta(\mathbf{r} - \mathbf{r}') e^{j\omega t}$ may be represented at $\mathbf{r} \neq \mathbf{r}'$ as [see Eq (2.3.6)]†

$$\mathbf{E}(\mathbf{r}, \mathbf{r}') = \nabla \times \nabla \times \mathbf{z}_0 \Pi'(\mathbf{r}, \mathbf{r}') - j\omega \mu \nabla \times \mathbf{z}_0 \Pi''(\mathbf{r}, \mathbf{r}'), \quad (1a)$$

$$\mathbf{H}(\mathbf{r}, \mathbf{r}') = j\omega \epsilon \nabla \times \mathbf{z}_0 \Pi'(\mathbf{r}, \mathbf{r}') + \nabla \times \nabla \times \mathbf{z}_0 \Pi''(\mathbf{r}, \mathbf{r}'), \quad (1b)$$

where the E - and H -mode Hertz potentials Π' and Π'' , respectively, are related via Eqs. (2.3.24) and (2.3.25) to the scalar functions \mathcal{S}' and \mathcal{S}'' ,

$$\Pi'(\mathbf{r}, \mathbf{r}') = \frac{1}{j\omega \epsilon} \mathbf{J}^o \cdot \nabla' \times \nabla' \times \mathbf{z}_0 \mathcal{S}'(\mathbf{r}, \mathbf{r}') - \mathbf{M}^o \cdot \nabla' \times \mathbf{z}_0 \mathcal{S}'(\mathbf{r}, \mathbf{r}'), \quad (1c)$$

$$\Pi''(\mathbf{r}, \mathbf{r}') = \mathbf{J}^o \cdot \nabla' \times \mathbf{z}_0 \mathcal{S}''(\mathbf{r}, \mathbf{r}') + \frac{1}{j\omega \mu} \mathbf{M}^o \cdot \nabla' \times \nabla' \times \mathbf{z}_0 \mathcal{S}''(\mathbf{r}, \mathbf{r}'). \quad (1d)$$

It may be recalled that the operations in Eqs. (1c) and (1d) imply that

$$\mathbf{A} \cdot \nabla' \times \mathbf{z}_0 = -\mathbf{A}_t \times \mathbf{z}_0 \cdot \nabla'_t, \quad (1e)$$

$$\mathbf{A} \cdot \nabla' \times \nabla' \times \mathbf{z}_0 = \mathbf{A}_t \cdot \nabla'_t \frac{\partial}{\partial z'} - A_z \nabla'^2_t, \quad (1f)$$

where \mathbf{A} is any vector and ∇'_t operates on the source-point (primed) coordinates. Equations (1e) and (1f) illuminate the role played by the transverse and longitudinal vector components of the source configuration. In particular, a longitudinal electric current element $\mathbf{J}^o = \mathbf{z}_0 J_z^o$, $\mathbf{M}^o = 0$, contributes only to

†Time-dependent quantities in this chapter will be distinguished by a superscript circumflex.

$\Pi'(\mathbf{r}, \mathbf{r}')$, thereby exciting E modes only, and a longitudinal magnetic current element $\mathbf{M}^o = z_0 M_z^o, \mathbf{J}^o = 0$, generates only H modes, whereas both mode types are excited by a transversely directed source of either electric or magnetic current.

It has been shown [Eqs. (2.3.32) and (2.3.33)] that if $\mathbf{E}(\mathbf{r}, \mathbf{r}')$ and $\mathbf{H}(\mathbf{r}, \mathbf{r}')$ satisfy the Maxwell field equations for point current excitation, then $\mathcal{S}'(\mathbf{r}, \mathbf{r}')$ and $\mathcal{S}''(\mathbf{r}, \mathbf{r}')$ satisfy the differential equation

$$(\nabla^2 + k^2) \nabla'_i \mathcal{S}'(\mathbf{r}, \mathbf{r}') = \delta(\mathbf{r} - \mathbf{r}'), \quad k^2 = \omega^2 \mu \epsilon, \quad (2)$$

subject to appropriate boundary conditions. By defining[†]

$$-\nabla_i^2 \mathcal{S}'(\mathbf{r}, \mathbf{r}') = G'(\mathbf{r}, \mathbf{r}'), \quad -\nabla_i^2 \mathcal{S}''(\mathbf{r}, \mathbf{r}') = G''(\mathbf{r}, \mathbf{r}'), \quad (3a)$$

one may relate \mathcal{S}' and \mathcal{S}'' to the corresponding Green's functions G' and G'' of the scalar wave equation since

$$(\nabla^2 + k^2) \frac{G'(\mathbf{r}, \mathbf{r}')}{G''(\mathbf{r}, \mathbf{r}') } = -\delta(\mathbf{r} - \mathbf{r}'). \quad (3b)$$

It may be noted from Eqs. (1c)–(1f) that the derivation of the Hertz potentials and thence of the fields for arbitrary source orientation does not require a knowledge of \mathcal{S}' and \mathcal{S}'' but rather of $\nabla'_i \mathcal{S}'$ and $\nabla'_i \mathcal{S}''$. This aspect is of importance since the latter quantities are sometimes determined more easily than \mathcal{S}' and \mathcal{S}'' and they also do not exhibit convergence difficulties associated with certain spectral representations of \mathcal{S}' and \mathcal{S}'' . Furthermore, for purely longitudinal sources, the significant quantities are $\nabla_i^2 \mathcal{S}'$ and (or) $\nabla_i^2 \mathcal{S}''$, whence in this instance the fields may be derived from the scalar Green's functions in Eqs. (3). Since an arbitrarily oriented source may be decomposed into a transverse and longitudinal part, it is useful to list the corresponding reduction of Eqs. (1c) and (1d) for these separate cases. When the source is transverse ($J_z^o = M_z^o = 0$),

$$\Pi'(\mathbf{r}, \mathbf{r}') = \left(\frac{1}{j\omega\epsilon} \mathbf{J}_i^o \cdot \frac{\partial}{\partial z'} + \mathbf{M}_i^o \times \mathbf{z}_0 \right) \cdot \nabla'_i \mathcal{S}'(\mathbf{r}, \mathbf{r}'), \quad (4a)$$

$$\Pi''(\mathbf{r}, \mathbf{r}') = \left(\mathbf{z}_0 \times \mathbf{J}_i^o + \frac{1}{j\omega\mu} \mathbf{M}_i^o \cdot \frac{\partial}{\partial z'} \right) \cdot \nabla'_i \mathcal{S}''(\mathbf{r}, \mathbf{r}'), \quad (4b)$$

whereas for a longitudinal source ($J_z^o = M_z^o = 0$),

$$\Pi'(\mathbf{r}, \mathbf{r}') = \frac{J_z^o}{j\omega\epsilon} G'(\mathbf{r}, \mathbf{r}'), \quad \Pi''(\mathbf{r}, \mathbf{r}') = \frac{M_z^o}{j\omega\mu} G''(\mathbf{r}, \mathbf{r}'). \quad (4c)$$

For certain simple problems, Eqs. (2) and (3) may be solved directly, but generally it is necessary to resort to appropriate representations. From a transmission-line analysis along the z axis, with eigenfunctions evaluated in the cross section transverse to z , one has the following solutions in terms of a modal expansion [Eqs. (2.3.24a) and (2.3.25a)]:

[†]The operator ∇_i^2 could have been replaced by $\nabla_i'^2$ [see Eqs. (2.3.32b) and (2.3.33b)].

$$\mathcal{S}'(\mathbf{r}, \mathbf{r}') = \frac{1}{j\omega\epsilon(z')} \sum_i \frac{\Phi_i(\rho)\Phi_i^*(\rho')}{k_{ii}^2} Y'_i(z, z'), \quad k_{ii}' \neq 0, \quad (5a)$$

$$\mathcal{S}''(\mathbf{r}, \mathbf{r}') = \frac{1}{j\omega\mu(z')} \sum_i \frac{\psi_i(\rho)\psi_i^*(\rho')}{k_{ii}^2} Z''_i(z, z'), \quad k_{ii}'' \neq 0, \quad (5b)$$

and also, from Eqs. (2.3.32b) and (2.3.33b),

$$G'(\mathbf{r}, \mathbf{r}') = \frac{1}{j\omega\epsilon(z')} \sum_i \Phi_i(\rho)\Phi_i^*(\rho') Y'_i(z, z'), \quad (5c)$$

$$G''(\mathbf{r}, \mathbf{r}') = \frac{1}{j\omega\mu(z')} \sum_i \psi_i(\rho)\psi_i^*(\rho') Z''_i(z, z'). \quad (5d)$$

The notation $\epsilon(z')$ and $\mu(z')$ for a multilayered region implies that these quantities are to be evaluated in the medium containing the source point z' . When no argument is indicated, ϵ and μ refer to the medium properties at the observation point. It is recalled that $\Phi_i(\rho)$ and $\psi_i(\rho)$ are the scalar eigenfunctions that have been listed in Chapter 3 for a variety of cross sections. $Y'_i(z, z')$ and $Z''_i(z, z')$ are, respectively, the E -mode current excited by a unit voltage generator and the H -mode voltage excited by a unit current generator (see Figs. 2.6 and 2.7), and they are related as follows to the one-dimensional E - and H -mode Green's functions:

$$Y'_i(z, z') = j\omega\epsilon(z')g'_{zi}(z, z'), \quad Z''_i(z, z') = j\omega\mu(z')g''_{zi}(z, z'), \quad (6a)$$

where $g'_{zi}(z, z')$ and $g''_{zi}(z, z')$ satisfy the equation

$$\left(\frac{d^2}{dz^2} + \kappa_i^2 \right) g_{zi}(z, z') = -\delta(z - z'), \quad \kappa_i^2 = k^2 - k_{ii}^2, \quad (6b)$$

subject to appropriate boundary conditions at the endpoints of the z domain. It is to be anticipated from Eqs. (5a) and (5b) that difficulties in the representation arise when the eigenvalue $k_{ii} = 0$ is admitted, as may be the case for continuous spectral distributions [see the footnote to Eq. (2.3.24a)].

The preceding considerations make evident that the basic problem involves the determination of the scalar functions \mathcal{S}' , \mathcal{S}'' or G' , G'' specified by the differential equations (2) and (3b), respectively; some simple boundary conditions permit the direct integration of these equations in closed form, whereas more general cases require the series or integral solutions resulting from an eigenfunction expansion.

5.2b Modal Representations for Unbounded Cross Sections

Since the configurations to be analyzed possess transversely unbounded cross sections, the transverse eigenvalue problem is highly degenerate and many alternative choices of coordinate systems are possible. The most useful for point-source and transverse-line-source excitation are the circular cylindrical and rectangular, respectively, since they account in the most direct manner for the symmetry properties of the associated fields. In view of the absence of transverse boundaries, the eigenvalue problems for the E and H modes are identical

so that $\Phi_i = \psi_i$, and the distinction between the E - and H -mode Green's functions resides solely in their longitudinal dependence. For the rectangular waveguide description, one obtains via Eqs. (5c), (5d), (6a), (6b), and (3.2.40) the double Fourier integral representation,

$$G(\mathbf{r}, \mathbf{r}') = \frac{1}{4\pi^2} \int_{-\infty}^{\infty} \int_{-\infty}^{\infty} e^{-j\xi(x-x') - j\eta(y-y')} g_{zi}(z, z') d\xi d\eta. \quad (7)$$

While the circular waveguide description can be obtained in a similar manner on use of Eqs. (3.2.78) instead of Eqs. (3.2.40), it is instructive to develop the resulting representation directly from Eq. (7).¹ We consider an integral of the form

$$I = \int_{-\infty}^{\infty} \int_{-\infty}^{\infty} f(k_t) e^{-jk_t(\rho-\rho')} dk_t, \quad \mathbf{k}_t = \mathbf{x}_0 \xi + \mathbf{y}_0 \eta, \quad (7a)$$

with $k_t = |\mathbf{k}_t|$ and $dk_t = d\xi d\eta$. On introducing polar coordinates (ρ, ϕ) and (k_t, α) in the ρ and \mathbf{k}_t spaces via $\rho = \rho(\mathbf{x}_0 \cos \phi + \mathbf{y}_0 \sin \phi)$, $\mathbf{k}_t = k_t(\mathbf{x}_0 \cos \alpha + \mathbf{y}_0 \sin \alpha)$, and noting that $d\mathbf{k}_t = k_t dk_t d\alpha$, one rewrites Eq. (7a) as

$$I = \int_0^{\infty} dk_t k_t f(k_t) \int_0^{2\pi} d\alpha e^{-jk_t \rho \cos(\alpha - \phi)} e^{jk_t \rho' \cos(\alpha - \phi')}. \quad (7b)$$

Replacement of each of the exponentials in Eq. (7b) by the series expansion

$$e^{j\beta \cos \xi} = \sum_{m=-\infty}^{\infty} j^m J_m(\beta) e^{jm\xi}, \quad (7c)$$

interchange of the orders of summation and integration, and reduction of the α integral, yields the Fourier–Bessel representation for I in Eq. (7a):

$$I = 2\pi \sum_{m=-\infty}^{\infty} e^{-jm(\phi-\phi')} \int_0^{\infty} dk_t k_t f(k_t) J_m(k_t \rho) J_m(k_t \rho'). \quad (7d)$$

Thus, the circular waveguide description of $G(\mathbf{r}, \mathbf{r}')$ is in the notation of Eq. (3.2.78) (with ξ denoting k_t),

$$G(\mathbf{r}, \mathbf{r}') = \frac{1}{2\pi} \sum_{m=-\infty}^{\infty} e^{-jm(\phi-\phi')} \int_0^{\infty} \xi J_m(\xi \rho) J_m(\xi \rho') g_{zi}(z, z') d\xi. \quad (8a)$$

For subsequent application, it will be useful to employ instead of Eq. (8a) a representation involving a range of integration in ξ from $-\infty$ to $+\infty$. Provided that $g_{zi}(z, z')$ is an even function of ξ , a requirement satisfied by the longitudinal Green's functions to be encountered subsequently, the desired representation may be derived as in Eqs. (3.2.64)–(3.2.73) and yields

$$G(\mathbf{r}, \mathbf{r}') = \frac{1}{4\pi} \sum_{m=-\infty}^{\infty} e^{-jm(\phi-\phi')} \int_{-\infty, \xi > \pi}^{\infty} \xi J_m(\xi \rho_{<}) H_m^{(2)}(\xi \rho_{>}) g_{zi}(z, z') d\xi. \quad (8b)$$

The lower integration limit indicates that the branch point at $\xi = 0$ introduced by the transformation is avoided as in Fig. 3.2.10(b). The choice of transformation involving $H_m^{(2)}$ instead of $H_m^{(1)}$ is motivated by the fact that, for a time dependence $\exp(j\omega t)$, the former satisfies the radiation condition at $\rho \rightarrow \infty$ in a natural manner and facilitates subsequent asymptotic evaluation of the integral (see Sec. 5.3d).

Since $k_{ii}^2 = \xi^2 + \eta^2$ and $k_{ii}^2 = \xi^2$ for the rectangular and circular waveguide representations, respectively, it follows from Eqs. (5a), (5b), and (6a) that in rectangular coordinates,

$$\mathcal{S}(\mathbf{r}, \mathbf{r}') = \frac{1}{4\pi^2} \int_{-\infty}^{\infty} \int_{-\infty}^{\infty} \frac{e^{-j\xi(x-x') - j\eta(y-y')}}{\xi^2 + \eta^2} g_{zi}(z, z') d\xi d\eta, \quad (9)$$

whereas in circular cylindrical coordinates,

$$\mathcal{S}(\mathbf{r}, \mathbf{r}') = \frac{1}{2\pi} \sum_{m=-\infty}^{\infty} e^{-jm(\phi-\phi')} \int_0^{\infty} \frac{1}{\xi} J_m(\xi\rho) J_m(\xi\rho') g_{zi}(z, z') d\xi, \quad (10a)$$

$$\mathcal{S}(\mathbf{r}, \mathbf{r}') = \frac{1}{4\pi} \sum_{m=-\infty}^{\infty} e^{-jm(\phi-\phi')} \int_{-\infty}^{\infty} \frac{1}{\xi} J_m(\xi\rho_-) H_m^{(2)}(\xi\rho_+) g_{zi}(z, z') d\xi, \quad (10b)$$

where $g_{zi}(z, z')$ depends on k_{ii} via the longitudinal propagation constant $\kappa_i = (k^2 - k_{ii}^2)^{1/2}$. The occurrence of $k_{ii} = 0$ in the continuous spectrum of eigenvalues leads to the previously mentioned convergence difficulties in Eqs. (9) and (10a), so these results must be regarded as purely formal. However, the functions $\nabla'_i \mathcal{S}$, from which the Hertz potentials are calculated via Eqs. (4a) and (4b), have valid representations, as will be demonstrated for Eq. (10a). In cylindrical coordinates, $\nabla'_i = \rho'_0(\partial/\partial\rho') + \phi'_0(\partial/\rho' \partial\phi')$. The convergence problem arises from the $m = 0$ term only, since for $m \neq 0$, the behavior $J_m(\xi\rho) \sim (\xi\rho)^m$ as $\xi \rightarrow 0$ assures regularity of the integrand at $\xi = 0$. The differentiation of the $m = 0$ terms with respect to ρ' results in the occurrence of $\xi J'_0(\xi\rho') \sim \xi^2$ in the numerator of the integrand, so the integral representation for $(\partial/\partial\rho') \mathcal{S}$ is regular at $\xi = 0$. The derivative of the $m = 0$ term with respect to ϕ' vanishes identically since this term is independent of ϕ' . Thus, the modal representation for $\nabla'_i \mathcal{S}$ is regular at $\xi = 0$, with the implication that the differentiations are performed on the summands (or integrands) of Eqs. (5a) and (5b).†

Point-source excitation

The suitability of the circular waveguide representation for point-source-excitation problems may be made manifest if the coordinate system is chosen so that $\rho' = 0$ (i. e., the source is located on the z axis). For a longitudinal dipole, the electromagnetic fields may be derived directly from $G(\mathbf{r}, \mathbf{r}')$ [see Eq. (4c)], which reduces in view of $J_0(0) = 1$, $J_m(0) = 0$, $m \neq 0$, to

$$G(\mathbf{r}, \mathbf{r}') = \frac{1}{4\pi} \int_{-\infty}^{\infty} \xi H_0^{(2)}(\xi\rho) g_{zi}(z, z') d\xi, \quad \rho' = 0. \quad (11)$$

For transverse source vector distributions, the requisite scalar functions are the potentials Π' and Π'' in Eqs. (4a) and (4b). When $\rho' \rightarrow 0$ in the previously discussed representation for $\nabla'_i \mathcal{S}$ derived from Eqs. (10a) and (10b), one may

†In the derivation of Eqs. (2.3.24) and (2.3.25), it was assumed that derivative operations can be commuted with the summation in Eqs. (2.3.24a) and (2.3.25a). This is not the case for integral representations as in Eq. (10a), whence one must consider $\nabla'_i \mathcal{S}'$ and $\nabla'_i \mathcal{S}''$, as noted above.

verify that only the $m = 1$ terms contribute, whence

$$\nabla'_t \mathcal{S}(\mathbf{r}, \mathbf{r}') = \begin{cases} \mathbf{p}_0 \frac{1}{2\pi} \int_0^\infty J_1(\xi\rho) g_{zi}(z, z') d\xi, & \rho' = 0, \\ \mathbf{p}_0 \frac{1}{4\pi} \int_{-\infty}^\infty H_1^{(2)}(\xi\rho) g_{zi}(z, z') d\xi, & \end{cases} \quad (12a)$$

$$(12b)$$

where \mathbf{p}_0 is the radial unit vector in the plane transverse to z : $\mathbf{p}_0 = \mathbf{x}_0 \cos \phi + \mathbf{y}_0 \sin \phi$.

Line-source excitation

When the excitation is in the form of a line distribution of sources confined to the plane $z = z'$, it is convenient to choose the rectangular waveguide representation and to orient one of the transverse coordinate axes, say x , along the source direction. The resulting simplification of Eqs. (7) and (9), a consequence of integration over x' to synthesize the line distribution, is not impaired when the source elements are phased progressively according to $\exp(-j\alpha x')$, where α is a real constant. Moreover, the orientation of the elements with respect to the line axis is arbitrary (Fig. 5.2.1). It follows that the relevant forms of

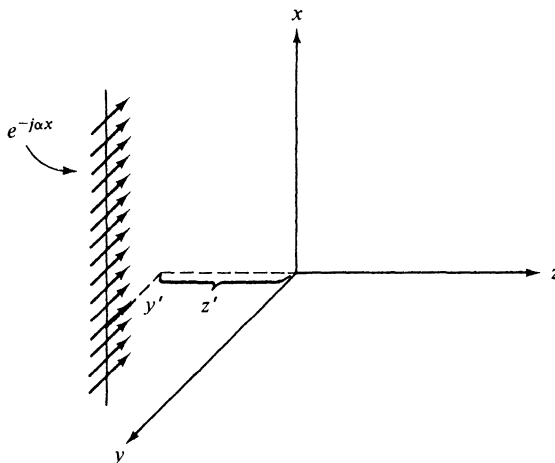


FIG. 5.2.1 Line source of arbitrarily oriented, progressively phased current elements.

$G(\mathbf{r}, \mathbf{r}')$ and $\mathcal{S}(\mathbf{r}, \mathbf{r}')$ are obtained by multiplying Eqs. (7) and (9) by $\exp(-j\alpha x')$ and integrating between $x' = -\infty$ and $x' = +\infty$; a subsequent interchange of the orders of integration and the recognition that $\int_{-\infty}^{\infty} \exp[-j(\alpha - \xi)x'] dx' = 2\pi\delta(\alpha - \xi)$ leads to the two-dimensional forms

$$\bar{G}(\mathbf{r}, \hat{\mathbf{p}}') = \int_{-\infty}^{\infty} e^{-j\alpha x'} G(\mathbf{r}, \mathbf{r}') dx' = e^{-j\alpha x} \bar{G}(\hat{\mathbf{p}}, \hat{\mathbf{p}}'), \quad \hat{\mathbf{p}} = (y, z), \quad (13)$$

where $\bar{G}(\hat{\mathbf{p}}, \hat{\mathbf{p}}')$ is the two-dimensional Green's function

$$\tilde{G}(\hat{\mathbf{p}}, \hat{\mathbf{p}}') = \frac{1}{2\pi} \int_{-\infty}^{\infty} e^{-j\eta(y-y')} g_{zi}(z, z') d\eta. \quad (13a)$$

Similarly, from Eq. (9),

$$\tilde{\mathcal{S}}(\mathbf{r}, \hat{\mathbf{p}}') = e^{-j\alpha x} \tilde{G}(\hat{\mathbf{p}}, \hat{\mathbf{p}}'), \quad (14)$$

where

$$\tilde{\mathcal{S}}(\hat{\mathbf{p}}, \hat{\mathbf{p}}') = \frac{1}{2\pi} \int_{-\infty}^{\infty} \frac{e^{-j\eta(y-y')}}{\eta^2 + \alpha^2} g_{zi}(z, z') d\eta. \quad (14a)$$

In Eqs. (13a) and (14a), the longitudinal propagation constant occurring in $g_{zi}(z, z')$ is to be written as $\kappa_i = (k^2 - \alpha^2 - \eta^2)^{1/2}$.

Unless $\alpha = 0$, no difficulty at $\eta = 0$ is encountered in the integral representation in Eq. (14a), and one may derive the potential functions $\bar{\Pi}'(\mathbf{r}, \hat{\mathbf{p}}')$ and $\bar{\Pi}''(\mathbf{r}, \hat{\mathbf{p}}')$ from Eqs. (4a) and (4b) by substituting Eq. (14) and replacing ∇'_t by $-j\alpha \mathbf{x}_0 + \mathbf{y}_0 (\partial/\partial y')$. When $\alpha = 0$, the integral representation for $\nabla'_t \tilde{\mathcal{S}}$ possesses a simple pole at $\eta = 0$. This pole is of no consequence since it does not contribute to fields obtained from $\tilde{\mathcal{S}}$ by differentiation operations involving single or double derivatives with respect to y [see Eqs. (1) and Eqs. (5.4.31)].

5.2c Fields Excited by Impulsive Sources

When the sources are stationary in space but have an impulsive time dependence

$$\hat{\mathbf{J}}(\mathbf{r}, t) = \mathbf{J}(\mathbf{r})\delta(t - t'), \quad \hat{\mathbf{M}}(\mathbf{r}, t) = \mathbf{M}(\mathbf{r})\delta(t - t'), \quad (15)$$

then since $\delta(t - t') = (2\pi)^{-1} \int_{-\infty}^{\infty} \exp(j\omega t - j\omega t') d\omega$, the resulting transient electromagnetic fields may be inferred from the time-harmonic solutions in Sec. 5.2a upon multiplication by $(2\pi)^{-1} \exp(j\omega t - j\omega t')$ and integration between $-\infty$ and $+\infty$ over the frequency variable $\omega = k\bar{c} = k/\sqrt{\mu\epsilon}$, where \bar{c} is the speed of light in a medium with *non-dispersive* dielectric constant ϵ and permeability μ .† This implies via Eqs. (1) that the vector fields $\hat{\mathbf{E}}(\mathbf{r}, \mathbf{r}'; t, t')$ and $\hat{\mathbf{H}}(\mathbf{r}, \mathbf{r}'; t, t')$ for an impulsive point source are derivable from the time-dependent scalar Hertz potentials $\hat{\Pi}(\mathbf{r}, \mathbf{r}'; t, t')$ or from their time derivatives (a multiplicative factor $j\omega$ is replaced by $\partial/\partial t$), and the Hertz potentials may in turn be obtained from $\hat{\mathcal{S}}(\mathbf{r}, \mathbf{r}'; t, t')$ or $\hat{G}(\mathbf{r}, \mathbf{r}'; t, t')$. It is sometimes more convenient to deal not with the source current densities $\hat{\mathbf{J}}$ and $\hat{\mathbf{M}}$ but rather with the dipole moments $\hat{\mathbf{p}}$ and $\hat{\mathbf{m}}$ defined as

$$\hat{\mathbf{J}}(\mathbf{r}, t) = \frac{\partial}{\partial t} \hat{\mathbf{p}}(\mathbf{r}, t), \quad \hat{\mathbf{M}}(\mathbf{r}, t) = \frac{\partial}{\partial t} \hat{\mathbf{m}}(\mathbf{r}, t), \quad (16)$$

since one avoids thereby the necessity of time integration of the space- and

†While all physical media exhibit dispersion, the results derived on the basis of dispersionless materials are meaningful when the transient source distribution has a *confined* frequency spectrum over which ϵ and μ are essentially frequency independent. The impulse excitations discussed here may be used to synthesize physically realizable source functions with these spectral characteristics.

time-dependent functions $\hat{\mathcal{S}}$ or \hat{G} [factor of $(j\omega)^{-1}$ in Eqs. (1c), (1d), and (4c)]. Thus, the fields generated by a longitudinally directed electric or magnetic dipole having a moment density

$$\hat{\mathbf{p}}(\mathbf{r}, t) = \mathbf{z}_0 \hat{p} \delta(\mathbf{r} - \mathbf{r}') \delta(t - t'), \quad \hat{\mathbf{m}}(\mathbf{r}, t) = \mathbf{z}_0 \hat{m} \delta(\mathbf{r} - \mathbf{r}') \delta(t - t') \quad (17)$$

are obtained from Eqs. (1a), (1b), and (4c) as [see also Eqs. (1.1.53)]

$$\hat{\mathbf{E}}(\mathbf{r}, \mathbf{r}'; t, t') = \frac{\hat{p}}{\epsilon} \nabla \times \nabla \times \mathbf{z}_0 \hat{G}'(\mathbf{r}, \mathbf{r}'; t, t') - \hat{m} \nabla \times \mathbf{z}_0 \frac{\partial}{\partial t} \hat{G}''(\mathbf{r}, \mathbf{r}'; t, t'), \quad (18a)$$

$$\hat{\mathbf{H}}(\mathbf{r}, \mathbf{r}'; t, t') = \hat{p} \nabla \times \mathbf{z}_0 \frac{\partial}{\partial t} \hat{G}'(\mathbf{r}, \mathbf{r}'; t, t') + \frac{\hat{m}}{\mu} \nabla \times \nabla \times \mathbf{z}_0 \hat{G}''(\mathbf{r}, \mathbf{r}'; t, t'), \quad (18b)$$

where the dielectric constant ϵ and the permeability μ are assumed to be frequency independent (non-dispersive medium). \hat{G} is the space- and time-dependent Green's function

$$\hat{G}(\mathbf{r}, \mathbf{r}'; t, t') = \frac{1}{2\pi} \int_{-\infty}^{\infty} G_{\omega}(\mathbf{r}, \mathbf{r}') e^{j\omega(t-t')} d\omega, \quad (18c)$$

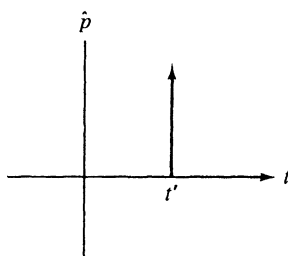
which satisfies the differential equation

$$\left(\nabla^2 - \frac{1}{c^2} \frac{\partial^2}{\partial t^2} \right) \hat{G}(\mathbf{r}, \mathbf{r}'; t, t') = -\delta(\mathbf{r} - \mathbf{r}') \delta(t - t'), \quad (18d)$$

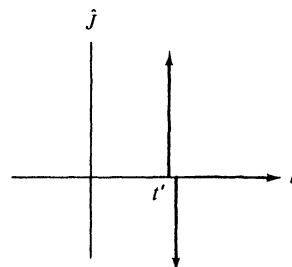
$$\bar{c} = \frac{1}{\sqrt{\mu\epsilon}} = c \sqrt{\frac{\mu_0\epsilon_0}{\mu\epsilon}},$$

subject to the same spatial boundary conditions as $G_{\omega}(\mathbf{r}, \mathbf{r}')$, and to the temporal (causality) condition that all fields vanish prior to $t = t'$. μ_0 and ϵ_0 are the constitutive parameters in vacuum. The subscript ω has been added to the time-harmonic solution $G(\mathbf{r}, \mathbf{r}')$ to emphasize its dependence on frequency. Analogous expressions may be obtained for transversely directed dipole sources. The temporal profiles corresponding to the excitation functions in Eq. (17) are shown in Fig. 5.2.2.

It has been shown in Sec. 1.6b that the recovery of the transient solution from the time-harmonic result is accomplished directly if the integral represen-



(a) Dipole moment



(b) Current

FIG. 5.2.2 Corresponding dipole moment and current profiles.

tation for the latter can be cast into a special form. In particular, if it is possible to write G_ω as a Laplace integral,

$$G_\omega(\mathbf{r}, \mathbf{r}') = \int_0^\infty e^{-st} A(\mathbf{r}, \mathbf{r}'; \tau) d\tau, \quad s = j\omega, \quad (19a)$$

where A is independent of s , then from the definition of the Laplace transform,

$$\hat{A}(\mathbf{r}, \mathbf{r}'; t, t') = A(\mathbf{r}, \mathbf{r}'; t - t'). \quad (19b)$$

Included in the category of integrals expressible as in Eq. (19a) is the generic radiation integral in Eq. (5.3.14),

$$I_\omega(L, \bar{\alpha}) = \int_{\bar{P}} e^{-jkL \cos(w - \bar{\alpha})} f(w) dw, \quad (20)$$

where \bar{P} is the contour shown in Fig. 5.3.5b. The parameters L and $\bar{\alpha}$ are assumed to be positive, $\bar{\alpha}$ being restricted to the range $0 < \bar{\alpha} < \pi/2$, and the function $f(w)$ is independent of $k = \omega/\bar{c}$, where $\bar{c} = (\mu\epsilon)^{-1/2}$ is the speed of light in the medium. As observed in this chapter and in Chapter 6, a number of time-harmonic radiation and diffraction problems can be expressed in this form. Since the analysis in Eqs. (1.6.34)–(1.6.41) is based on an assumed time dependence $\exp(-i\omega t)$, we repeat the principal steps for the presently used $\exp(j\omega t)$. Introducing $\omega \rightarrow -js$ in Eq. (20), one may write

$$I_\omega(L, \bar{\alpha}) = \int_{-j\infty}^{j\infty} e^{-s(L/\bar{c}) \cos w} f(w + \bar{\alpha}) dw, \quad (21)$$

where it has been assumed that the function $f(w)$ has no singularities in the strip $0 < |\operatorname{Re} w| < \pi/2$. The contour deformation employed in achieving Eq. (21) is justified as in Eq. (1.6.38).

On successive changes of variable $\beta = -jw$ and $\tau = (L/\bar{c}) \cosh \beta$, one obtains†

$$I_\omega(L, \bar{\alpha}) = j \int_{L/\bar{c}}^\infty e^{-s\tau} \frac{b(\tau)}{\sqrt{\tau^2 - (L/\bar{c})^2}} d\tau, \quad (22a)$$

$$b(\tau) = f\left[\bar{\alpha} + j \cosh^{-1}\left(\frac{\bar{c}\tau}{L}\right)\right] + f\left[\bar{\alpha} - j \cosh^{-1}\left(\frac{\bar{c}\tau}{L}\right)\right], \quad (22b)$$

whence on comparison with Eq. (19a),

$$A(\tau) = \begin{cases} 0, & \tau < \frac{L}{\bar{c}}, \\ \frac{jb(\tau)}{\sqrt{\tau^2 - L^2/\bar{c}^2}}, & \tau > \frac{L}{\bar{c}}. \end{cases} \quad (23)$$

If $v(w) = jf(w)$ is real for real values of w , then $v(w^*) = v^*(w)$ and

$$jb(\tau) = 2\operatorname{Re}\left\{jf\left[\bar{\alpha} + j \cosh^{-1}\left(\frac{\bar{c}\tau}{L}\right)\right]\right\}. \quad (23a)$$

Several applications of this result are given in the following sections.

†If the exponential in Eq. (21) has some other form $\exp[-s(L/\bar{c})h(w)]$, the variable τ is defined as $\tau = (L/\bar{c})h(w)$.

5.2d Fields Excited by Charges in Uniform Rectilinear Motion

Transient fields may also be excited when the location of the source changes with time, even though the source strength itself is non-varying. The simplest class of such problems involves uniform motion of an electric charge along a straight-line path. The results are of interest for studies of the interaction of high-speed charged particles with material media of various types (dielectrics, plasmas, etc.), and bear on such physical applications as the absorption of protons in "swimming-pool" atomic reactors, or the excitation of low-frequency noise in the earth's exosphere by streams of charges emanating from the sun.

A point charge of strength q is assumed to move with constant speed v parallel to the x axis of a rectangular coordinate system. The current density $\hat{J}(\mathbf{r}, t)$ associated with this moving charge is

$$\hat{J}(\mathbf{r}, t) = x_0 q v \delta(x - vt) \delta(y - y') \delta(z - z'); \quad (24)$$

its Fourier spectrum function $J(\mathbf{r}, \omega)$ is obtained as

$$\begin{aligned} J(\mathbf{r}, \omega) &= \int_{-\infty}^{\infty} \hat{J}(\mathbf{r}, t) e^{-j\omega t} dt = x_0 q e^{-j(k_0/\beta)x} \delta(\hat{p} - \hat{p}'), \\ \hat{p} &= (y, z), \quad \beta = \frac{v}{c} < 1, \quad k_0 = \frac{\omega}{c} = \omega \sqrt{\mu_0 \epsilon_0}, \end{aligned} \quad (25)$$

where c is the speed of light in vacuum. Thus, the associated time-harmonic source distribution $J(\mathbf{r}, \omega)$ is a line current with a linearly varying phase [see Eqs. (13) and (14)], and the radiation from the point charge moving in various environments can be obtained from the time-harmonic line-source solutions via the inverse Fourier transform. Applications to special geometries, and discussion of concomitant Cerenkov-type effects, may be found in Secs. 5.4e and 5.5j.

While application of the inverse Fourier transform is essential for the determination of the real, time-dependent electromagnetic fields $\hat{\mathbf{E}}(\mathbf{r}, t)$ and $\hat{\mathbf{H}}(\mathbf{r}, t)$ excited by moving charges, it can be avoided for the evaluation of the total radiated energy, which is often of more interest than the fields themselves. The Poynting vector

$$\hat{\mathbf{P}}(\mathbf{r}, t) = \hat{\mathbf{E}}(\mathbf{r}, t) \times \hat{\mathbf{H}}(\mathbf{r}, t) \quad (26)$$

represents the flow of electromagnetic field energy per unit area per unit time. To calculate the radiated energy, one defines a total energy flow vector $\mathbf{W}(\mathbf{r})$ per unit area as

$$\mathbf{W}(\mathbf{r}) = \int_{-\infty}^{\infty} \hat{\mathbf{P}}(\mathbf{r}, t) dt. \quad (27)$$

We now substitute for $\hat{\mathbf{E}}$ and $\hat{\mathbf{H}}$ their Fourier integral representations; these may be written conveniently in terms of $f(\mathbf{r}, \omega)$ and a complex-conjugate function $f^*(\mathbf{r}, \omega)$. Since $\hat{f}(\mathbf{r}, t)$ is real, one notes from

$$f(\mathbf{r}, \omega) = \int_{-\infty}^{\infty} \hat{f}(\mathbf{r}, t) \exp(-j\omega t) dt$$

that $f(\mathbf{r}, -\omega) = f^*(\mathbf{r}, \omega)$:

$$\hat{f}(\mathbf{r}, t) = \frac{1}{2\pi} \int_0^\infty f(\mathbf{r}, \omega) e^{j\omega t} d\omega + \frac{1}{2\pi} \int_0^\infty f^*(\mathbf{r}, \omega) e^{-j\omega t} d\omega. \quad (28)$$

Thus, upon assuming the interchangeability of the t and ω integrations,

$$\begin{aligned} 4\pi^2 \mathbf{W}(\mathbf{r}) &= \int_0^\infty d\omega \int_0^\infty d\omega' \left[\mathbf{E}(\mathbf{r}, \omega) \times \mathbf{H}(\mathbf{r}, \omega') \int_{-\infty}^\infty e^{j(\omega+\omega')t} dt \right. \\ &\quad + \mathbf{E}^*(\mathbf{r}, \omega) \times \mathbf{H}(\mathbf{r}, \omega') \int_{-\infty}^\infty e^{-j(\omega-\omega')t} dt \\ &\quad + \mathbf{E}(\mathbf{r}, \omega) \times \mathbf{H}^*(\mathbf{r}, \omega') \int_{-\infty}^\infty e^{j(\omega-\omega')t} dt \\ &\quad \left. + \mathbf{E}^*(\mathbf{r}, \omega) \times \mathbf{H}^*(\mathbf{r}, \omega') \int_{-\infty}^\infty e^{-j(\omega-\omega')t} dt \right], \end{aligned} \quad (29)$$

and, since $\int_{-\infty}^\infty e^{-j\alpha t} dt = 2\pi\delta(\alpha)$,

$$\mathbf{W}(\mathbf{r}) = \frac{1}{\pi} \operatorname{Re} \int_0^\infty \mathbf{P}(\mathbf{r}, \omega) d\omega, \quad \mathbf{P}(\mathbf{r}, \omega) = \mathbf{E}(\mathbf{r}, \omega) \times \mathbf{H}^*(\mathbf{r}, \omega). \dagger \quad (30)$$

Hence,

$$\mathbf{W}_\omega(\mathbf{r}) = \frac{1}{\pi} \operatorname{Re} \mathbf{P}(\mathbf{r}, \omega), \quad (31)$$

represents the total energy flow per unit area in the frequency interval between ω and $\omega + d\omega$.

The total energy flowing through a plane $z = \text{constant}$, per unit angular frequency at ω , is given by

$$W_\omega(z) = \int_S \mathbf{W}_\omega(\mathbf{r}) \cdot \mathbf{z}_0 dS, \quad (32)$$

where S is the cross-sectional area transverse to z . Upon substituting the modal representations [see Eqs. (2.2.8)]

$$\mathbf{E}_i(\mathbf{r}, \omega) = \sum_i V'_i(z, \omega) \mathbf{e}'_i(\mathbf{p}) + \sum_i V''_i(z, \omega) \mathbf{e}''_i(\mathbf{p}), \quad (33a)$$

$$\mathbf{H}_i(\mathbf{r}, \omega) \times \mathbf{z}_0 = \sum_i I'_i(z, \omega) \mathbf{e}'_i(\mathbf{p}) + \sum_i I''_i(z, \omega) \mathbf{e}''_i(\mathbf{p}), \quad (33b)$$

into Eq. (32), inverting the orders of summation and integration, and recalling the orthonormality properties (2.2.11b) of the vector-mode functions, one finds

$$W_\omega(z) = \frac{1}{\pi} \operatorname{Re} \left[\sum_i V'_i(z, \omega) I'^*(z, \omega) + \sum_i V''_i(z, \omega) I''*(z, \omega) \right]. \quad (34)$$

Thus, W_ω is given as a superposition of individual mode powers and involves only the modal amplitudes V_i and I_i . Finally, the total energy W flowing through a plane $z = \text{constant}$ is given by

$$W(z) = \int_S \mathbf{W}(\mathbf{r}) \cdot \mathbf{z}_0 dS = \int W_\omega(z) d\omega. \quad (35)$$

[†]The equality of Eqs. (27) and (30) is known as Parseval's formula ² [see also Eq. (1.2.27)].

Although the analysis in Eqs. (26)–(35) has been performed in the context of radiation from moving charges, it should be noted that the above energy calculation, and in particular the modal result in Eq. (34), is more generally applicable.

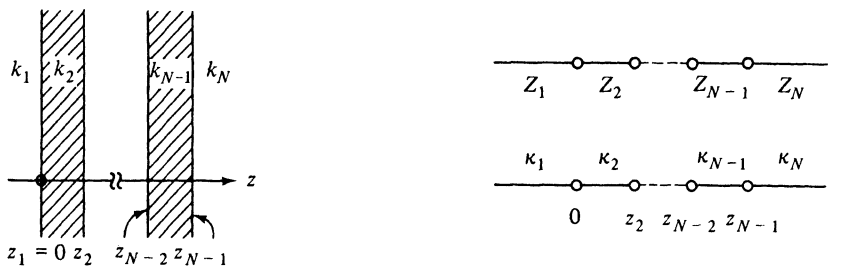
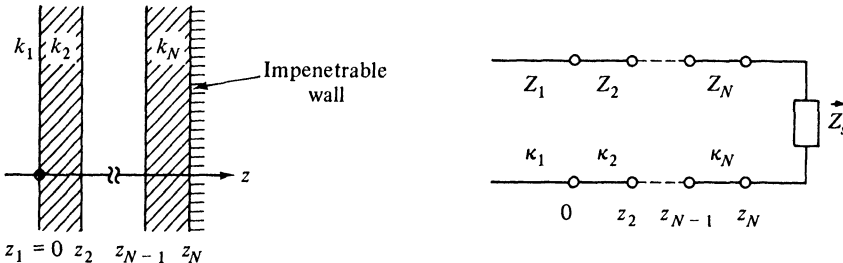
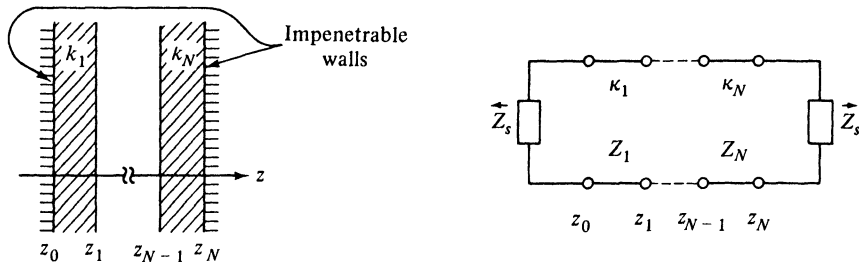
5.3 INTEGRATION TECHNIQUES

5.3a Analytical Properties of the Representation Integrals

Calculation of the multidimensional Green's functions from the integral representations in Eqs. (5.2.7)–(5.2.14) requires knowledge of the one-dimensional modal Green's functions $g_{zi}(z, z')$; determination of the latter from Eq. (5.2.6b) implies specification of the detailed properties of the region along the z coordinate. While g_{zi} thus depends on the nature of the z stratification, general asymptotic properties of the field can be inferred from the analytic behavior of the integrands without restriction to specific geometries. The discussion in this section is concerned with the contribution to the asymptotic field solution from stationary (saddle) points, poles, and branch points in the integral representations, and with the physical interpretation of the corresponding wave types. These general results are applied to specific geometrical configurations in the remaining sections of this chapter.

The longitudinal Green's functions $g_{zi}(z, z')$, left unspecified so far, depend on the integration variables ξ or η via the longitudinal propagation constant $\kappa_i = (k^2 - k_{ii}^2)^{1/2}$. In a multilayered region with piecewise constant $\epsilon_\beta, \mu_\beta, \beta = 1, 2, \dots, N$, g_{zi} is a function of the various propagation constants $\kappa_{i\beta} = (k_\beta^2 - k_{ii}^2)^{1/2}$, where $k_\beta = \omega(\mu_\beta \epsilon_\beta)^{1/2}$. The functional dependence of g_{zi} will be shown to be even with respect to $\kappa_{i\beta}$ in a β th layer of finite width along z , whereas this is not the case in a semiinfinite region. Since an even function of $\kappa_{i\beta}$ possesses a series expansion in powers of $(\kappa_{i\beta})^{2n}$, $n = 0, 1, 2, \dots$, g_{zi} is regular at the point $\kappa_{i\beta} = 0$ in the complex k_{ii} plane. On the other hand, for a semiinfinite section characterized by ϵ_1, μ_1 (extending to $z = -\infty$) or ϵ_N, μ_N (extending to $z = +\infty$), the lack of evenness implies the existence of first-order branch points at $k_{ii} = \pm k_1$ or $k_{ii} = \pm k_N$, respectively. Thus, the longitudinal Green's function g_{zi} for a region containing an arbitrary number of layers exhibits branch points at $k_{ii} = \pm k_1, \pm k_N$ when both $z = -\infty$ and $z = +\infty$ are accessible, branch points at either $\pm k_1$ or $\pm k_N$ when an impenetrable boundary prevents accessibility to $z = +\infty$ or $z = -\infty$, respectively (see Sec. 5.7), and no branch points when two impenetrable boundaries confine the region to a finite z interval (see Fig. 5.3.1). The presence of boundaries also gives rise, in general, to simple pole singularities in g_{zi} (see Secs. 5.5 and 5.6).

The precise form of $g_{zi}(z, z')$ depends on the details of the stratification along the z direction, and methods for its construction are discussed in Secs. 2.4 and 3.3b. In view of the differential equation (5.2.6b), the solution is synthesized in terms of trigonometric or exponential functions. While for a mul-

(a) Branch points at $k_t = \pm k_1, \pm k_N$ (b) Branch points at $k_t = \pm k_1$ 

(c) No branch points

FIG. 5.3.1 Various physical regions, modal network representations, and the corresponding branch-point singularities of the modal Green's function in the complex k_t plane. The modal subscript i has been omitted and $\kappa_\beta = \sqrt{k_\beta^2 - k_t^2}$.

tilayered configuration $g_{\alpha}(z, z')$ may be quite complicated [see Eqs. (2.4.28)], it has a simple generic form when both the source point and the observation point are located in a seminfinite region [e. g., in the region $z < 0$ in Figs.

5.3.1(a) or 5.3.1(b)]. In this instance, the Green's function is composed of an "incident" wave appropriate to an infinite region with wavenumber k_1 and a "reflected" wave whose amplitude is determined by the details of the configuration in the half-space $z > 0$. In particular [see Eqs. (2.4.29c) and (2.4.29d) with $\vec{\Gamma}_i(z_0) = 0$],

$$g_{zi}(z, z') = \frac{1}{2j\kappa_{i_1}} [e^{-j\kappa_{i_1}|z-z'|} \mp \vec{\Gamma}_i(0)e^{j\kappa_{i_1}(z+z')}], \quad z, z' < 0, \quad (1)$$

where $\vec{\Gamma}_i(0)$, the modal (voltage) reflection coefficient looking into the region $z > 0$ from $z = 0$ in region 1, is expressed in terms of the modal input impedance $\vec{Z}_i(0)$, as follows :

$$\vec{\Gamma}_i(0) = \frac{\vec{Z}_i(0) - Z_{i_1}}{\vec{Z}_i(0) + Z_{i_1}}. \quad (1a)$$

The $-$ and $+$ signs in Eq. (1) are associated with the *E*-mode and *H*-mode problems, respectively [see Eqs. (5.2.6a), (2.4.29c) and (2.4.29d)]. $\vec{Z}_i(0)$ may be determined by a repeated application of Eq. (2.4.10), which relates the input impedance $\vec{Z}_i(z_{\beta-1})$ at $z_{\beta-1}$ to the input impedance $\vec{Z}_i(z_\beta)$ at z_β :

$$\frac{\vec{Z}_i(z_{\beta-1})}{Z_{i\beta}} = \frac{1 + j[\vec{Z}_i(z_\beta)/Z_{i\beta}] \cot [\kappa_{i\beta}(z_{\beta-1} - z_\beta)]}{[\vec{Z}_i(z_\beta)/Z_{i\beta}] + j \cot [\kappa_{i\beta}(z_{\beta-1} - z_\beta)]}, \quad (1b)$$

with $Z_{i\beta}$ denoting the characteristic impedance in the region between $z_{\beta-1}$ and z_β [Eq. (2.2.15)];

$$Z_{i\beta} = \frac{\kappa_{i\beta}}{\omega\epsilon_\beta} \text{ for } E \text{ modes}; \quad Z_{i\beta} = \frac{\omega\mu_\beta}{\kappa_{i\beta}} \text{ for } H \text{ modes}. \quad (1c)$$

The primes and double primes that distinguish *E*- and *H*-mode quantities, respectively, have been omitted for convenience.

For a determination of the singularities of $g_{zi}(z, z')$ in the complex k_{ii} plane, it suffices to examine the singularities of the reflection coefficient $\vec{\Gamma}_i(0)$ or equivalently, the branch points and zeros of the total impedance function $\vec{Z}_i(0) = [\vec{Z}_i(0) + Z_{i1}]$.† The zeros of $\vec{Z}_i(0)$ locate pole singularities which are descriptive of the waves guided in the direction transverse to z [see Secs. 5.5 and 5.6; these waves may be either of the surface-wave (modal) or leaky-wave (usually non-modal) type]. Concerning branch-point singularities, one observes from Eq. (1b) that $\vec{Z}_i(z_{\beta-1})$ is an even function of $\kappa_{i\beta}$ and therefore regular at $k_{ii} = \pm k_\beta$ since $Z_{i\beta}$ is an odd function of $\kappa_{i\beta}$ and $\vec{Z}_i(z_\beta)$ is a function only of κ_{in} , $n \geq \beta + 1$. Since the expression for $\vec{Z}_i(0)$ is deduced by repeated application of Eq. (1b), it follows that $\vec{Z}_i(0)$ is an even function of all $\kappa_{i\beta}$ associated

†For configurations containing stratification or boundaries in the region $z < 0$ as well, the total impedance function is replaced by $\vec{Z}_i(0) = \vec{Z}_i(0) + \vec{Z}_i(0)$ [see Eqs. (2.4.28)].

with layers of finite width. If the last (N th) layer extends to infinity, its input impedance is given by Z_{IN} , which is an odd function of κ_{IN} and hence possesses branch-point singularities at $k_t = \pm k_N$. On the other hand, for an impenetrable wall at z_N , $\vec{Z}_i(z_N) = \vec{Z}_s$, and no branch points are introduced since the surface impedance \vec{Z}_s is a constant independent of k_t . Analogous considerations apply to $\vec{Z}_i(0)$. The results stated in Fig. 5.3.1 are therefore verified.

Since the branch points lie on the integration paths when k_ρ is real (lossless medium), the disposition of the contours in Eqs. (5.2.7)–(5.2.14) near the singularities must be clarified. For example, in Eq. (5.2.8b), where $k_t = \xi$, branch points due to κ_{tt} occur at $\xi = \pm k_1$. While the determination of the proper integration paths can be carried out for real k_1 (see Sec. 5.3b), it is simpler for the present to assume slight dissipation, so that for an $\exp(j\omega t)$ time dependence $k = \omega[\mu(\epsilon_r - j\epsilon_i)]^{1/2}$ has a small negative imaginary part, where ϵ_r and ϵ_i are the real and imaginary parts, respectively, of the dielectric constant ϵ . Thus the branch points are displaced from the real ξ and η axes into the fourth and second quadrants of the complex ξ and η planes. If one now lets $\epsilon_i \rightarrow 0$, it follows that the path of integration should be indented around the singularities into the first or third quadrants, respectively, for branch-point locations on the positive or negative axes (Fig. 5.3.2). Concerning the convergence of the integral (for a lossless medium) with real k^2 , we recall the restriction that for non-propagating modes (imaginary κ_i), $\kappa_i = -j|\kappa_i|$, so finiteness of the integral is assured [see Eqs. (2.2.15)]. Phrased more generally, for complex values of

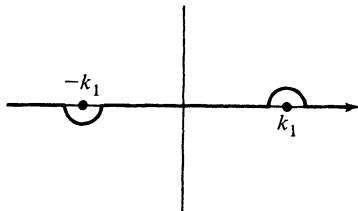


FIG. 5.3.2 Avoidance of branch-point singularities in the complex ξ plane [$\exp(j\omega t)$ dependence].

ξ relevant to subsequent contour deformation, we impose on the square root the condition $\text{Im}\sqrt{k^2 - \xi^2} < 0$ along the path, which then guarantees convergence of the exponential terms in Eq. (1). The regions in the complex ξ plane for which $\text{Im}\sqrt{k^2 - \xi^2}$ is negative are examined in Sec. 5.3b for various choices of branch cuts that make the integrand single valued on a multisheeted Riemann surface. Analogous considerations may be applied to the double integral in Eq. (5.2.7), for example, where $k_t^2 = \xi^2 + \eta^2$. Branch points in the ξ and η integrals now occur at $\pm\sqrt{k_1^2 - \eta^2}$ and $\pm\sqrt{k_1^2 - \xi^2}$, respectively.

Pole singularities of $g_{zi}(z, z')$ may also lie on the integration path, and their avoidance may be clarified by considerations analogous to the above, either by displacement from the real axis through the assumption of small loss, or by

imposition of the radiation condition on possible residue contributions to the field at infinity.

5.3b Definition of $\kappa(\xi) = \sqrt{k^2 - \xi^2}$ in the Complex ξ Plane

As observed previously, the Green's function integrands in Sec. 5.2b may contain branch-point singularities arising, for example, from the mode wave-number $\kappa_i = \sqrt{k^2 - \xi^2}$. To assure a unique specification of integrands in the complex ξ plane it is necessary to discuss in detail the analytic properties of the square-root function $\kappa_i \equiv \kappa(\xi)$. When ξ is real and $|\xi| < k$, k being assumed real for the moment, the guided wave along z is propagating and hence the propagation constant κ is real and positive, consistent with a positive modal characteristic impedance [see Eq. (2.2.15)]. Thus, we require a definition of $\kappa(\xi)$ such that

$$\sqrt{k^2 - \xi^2} > 0, \quad -k < \xi < k. \quad (2)$$

To ensure that integrands remain bounded as $|\kappa(\xi)| |z - z'| \rightarrow \infty$, it is necessary to impose restrictions on the imaginary part of κ . For the time dependence $\exp(j\omega t)$, the required restriction for real ξ is $\kappa = -j|\kappa|$ (i.e., $\text{Im } \kappa < 0$ when $|\xi| > k$).† If ξ is allowed to be complex, the condition $\text{Im } \kappa < 0$ will be imposed for all permitted complex values of κ . The analytic continuation of ξ from real to complex values is required for subsequent deformation of the integration contours.

To make the definition of the double-valued function $\kappa(\xi)$ unique, a two-sheeted complex ξ plane is necessary, with branch cuts providing the means of passing from one Riemann sheet to the other.³ The selection of branch cuts is arbitrary but determines the disposition of those regions of the complex ξ plane in which $\text{Im } \kappa < 0$, or $\text{Im } \kappa > 0$. Three particularly useful choices are shown in Fig. 5.3.3. Let us define

$$(k - \xi) = |k - \xi| e^{i\alpha}, \quad (k + \xi) = |k + \xi| e^{i\beta}, \quad \alpha, \beta \text{ real}, \quad (3a)$$

with the angles α and β so selected as to make $\alpha = 0$ and $\beta = 0$ when ξ is real and $|\xi| < k$ on the top sheet. Hence,

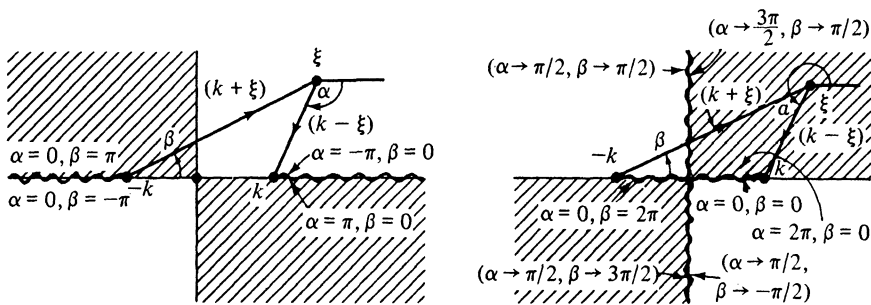
$$\sqrt{k^2 - \xi^2} = |\sqrt{k^2 - \xi^2}| e^{i(\alpha+\beta)/2}, \quad (3b)$$

where we have chosen the positive sign of the square root. i is the imaginary unit and does not refer in this context to a harmonic time dependence of the field. To satisfy condition (2) it is required that

$$\alpha + \beta = 0, \quad \text{when } -k < \xi < k. \quad (4a)$$

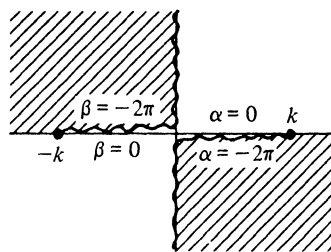
Consider now the choice of branch cuts in the first part of Fig. 5.3.3 (a). With the angles α and β defined as shown, it is evident that condition (4a) is

†This requirement, and also (2), follows from the radiation condition, which demands that the energy radiated by the source to distant observation points is bounded and outgoing (see Sec. 1.5.b).



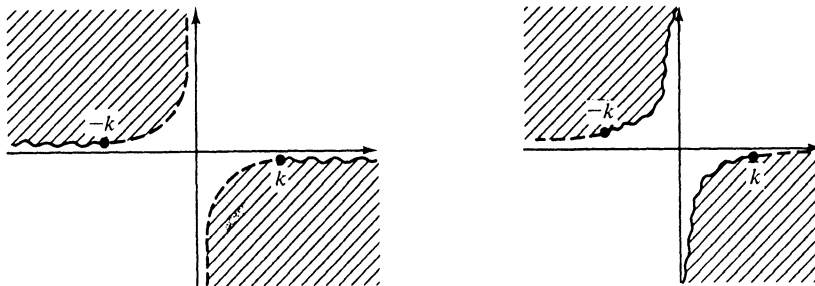
- (1) $\text{Im } \kappa > 0$ in shaded region
 $\text{Im } \kappa < 0$ in unshaded region
 $\text{Re } \kappa > 0$ on entire top sheet

- (2) $\text{Im } \kappa > 0$ on entire top sheet
 $\text{Re } \kappa > 0$ in unshaded region
 $\text{Re } \kappa < 0$ in shaded region



- (3) $\text{Im } \kappa < 0$ on entire top sheet
 $\text{Re } \kappa > 0$ in unshaded region
 $\text{Re } \kappa < 0$ in shaded region

(a) k real



- (1) $\text{Im } \kappa > 0$ in shaded region
 $\text{Im } \kappa < 0$ in unshaded region
 $\text{Re } \kappa > 0$ on entire top sheet

- (2) $\text{Im } \kappa < 0$ on entire top sheet
 $\text{Re } \kappa > 0$ in unshaded region
 $\text{Re } \kappa < 0$ in shaded region

(b) $\text{Im } k < 0$

FIG. 5.3.3 Analytic properties of $\sqrt{k^2 - \xi^2}$ in various complex ξ planes.

met since $\alpha = \beta = 0$ when $-k < \xi < k$. This position of the branch cuts restricts the ranges of α and β on the top sheet to†

$$-\pi < \alpha < \pi, \quad -\pi < \beta < \pi. \quad (4b)$$

In accord with the usual convention, an angle is counted positive or negative if measured in a counterclockwise or clockwise sense, respectively, from the horizontal axis. The arguments α and β of $(k - \xi)$ and $(k + \xi)$ on the upper and lower sides of the branch cuts have been shown explicitly. Since $0 > (\alpha + \beta) > -\pi$ in the first and third quadrants of the complex ξ plane, one notes from Eq. (3b) that $\sin[(\alpha + \beta)/2] < 0$ (i.e., $\text{Im } \kappa < 0$ in these regions). Conversely, $0 < \alpha + \beta < \pi$ in the second and fourth quadrants, implying that $\text{Im } \kappa > 0$. It also follows that $\text{Re } \kappa > 0$ on the entire top sheet. All these conditions are reversed in the corresponding quadrants of the second Riemann sheet. The branch cuts in the first part of Fig. 5.3.3(a) evidently follow the contours $\text{Re } \kappa = 0$.

In an alternative choice of branch cuts in the second part of Fig. 5.3.3(a), drawn along contours on which $\text{Im } \kappa = 0$, one notes again that α and β are so defined as to satisfy Eq. (4a). In this instance, $0 < \alpha + \beta < 2\pi$ in all quadrants, so $\text{Im } \kappa > 0$ on the entire top sheet. [This choice is pertinent for field problems involving an assumed $\exp(-i\omega t)$ time dependence.] The behavior of $\text{Re } \kappa$ in the different quadrants is also shown. If the branch cuts are drawn along the contours $\text{Im } \kappa = 0$ in the manner shown in the third part of Fig. 5.3.3(a) then $\text{Im } \kappa < 0$ on the entire top sheet and the algebraic sign of $\text{Re } \kappa$ is as indicated. Again, the algebraic signs of $\text{Re } \kappa$ and $\text{Im } \kappa$ in the various quadrants on the second sheet are the reverse of those on the first sheet.

In the above discussion, k was assumed to be real. Since all physical media have some loss, it is also pertinent to treat the case of a lossy dielectric wherein, for an assumed time dependence $\exp(j\omega t)$, $\epsilon = \epsilon_r - j\sigma/\omega$, σ = conductivity of medium. Correspondingly, $k = \omega\sqrt{\mu\epsilon}$ has a negative imaginary part. As for real k , it is convenient to choose the branch cuts along the contours on which $\text{Re } \kappa$ or $\text{Im } \kappa$ vanishes. These contours are determined by enforcing $\alpha + \beta = 0, \pm 2\pi, \dots$ for $\text{Im } \kappa = 0$ and $\alpha + \beta = \pm\pi, \pm 3\pi, \dots$ for $\text{Re } \kappa = 0$. Since

$$\tan \alpha = \frac{k_i - \xi_i}{k_r - \xi_r}, \quad \tan \beta = \frac{k_i + \xi_i}{k_r + \xi_r}, \quad (5a)$$

one finds that both $\text{Re } \kappa = 0$ and $\text{Im } \kappa = 0$ along the hyperbolas

$$\xi_r \xi_i = k_r k_i.$$

ξ_r , k_r , and ξ_i , k_i denote the real and imaginary parts, respectively, of ξ and k . One verifies readily that $\text{Re } \kappa = 0$ on those portions of the curves for which $|\xi_r| > k_r$, while $\text{Im } \kappa = 0$ for $|\xi_r| < k_r$. The corresponding behavior of κ in the complex ξ plane is shown in Figs. 5.3.3(b) for $k_i < 0$. One notes that as

†Conditions (4a) and (4b) constitute the definition of $\sqrt{k^2 - \xi^2}$ on the first branch of the two-sheeted Riemann surface. A definition on the second branch would involve $\pi < \alpha < 3\pi$ or $\pi < \beta < 3\pi$, for example.

$k_i \rightarrow 0$ in Fig. 5.3.3(b), one obtains the configurations in the first and third parts of Fig. 5.3.3(a). If $k_i > 0$ [for fields having an assumed time dependence $\exp(-i\omega t)$], one has a subdivision of the ξ plane which is obtainable from that in Fig. 5.3.3(b) by a reflection of all curves about either the real or the imaginary ξ axis [see Fig. 5.5.4(b)]. The various regions must then be so assigned as to reduce to those in Figs. 5.3.3(a) in the limit $k_i \rightarrow 0$.

A simple rule may be stated for the assignment of the algebraic signs of $\operatorname{Re} \kappa$ and $\operatorname{Im} \kappa$ in various portions of the complex ξ plane. It follows from the recognition that sign changes in $\operatorname{Re} \kappa$ or $\operatorname{Im} \kappa$ can occur only when ξ crosses the contours $\operatorname{Re} \kappa = 0$ or $\operatorname{Im} \kappa = 0$, respectively. Thus, if branch cuts are chosen along the contours $\operatorname{Im} \kappa = 0$, for example, the sign of $\operatorname{Im} \kappa$ is constant on either the top sheet or the bottom sheet, since the crossing of the $\operatorname{Im} \kappa = 0$ curve leads from one sheet to the other. It then suffices to specify $\operatorname{Re} \kappa$ and $\operatorname{Im} \kappa$ consistently at a single point on the top sheet, for example at $\xi = 0$, since one may then deduce the sign alternations in $\operatorname{Re} \kappa$ from the crossings of the $\operatorname{Re} \kappa = 0$ contours. In this manner, one may arrive directly at the designation in the second part of Fig. 5.3.3(b) if the top sheet is chosen so that $\kappa_t = +k$ at $\xi = 0$.

5.3c The Transformation $\xi = k \sin w$

To facilitate subsequent function-theoretic manipulations involving integrals of the type occurring in Eqs. (5.2.11)–(5.2.14), it is desirable to introduce a new complex variable w via the transformation

$$\xi = k \sin w, \quad (6)$$

which identifies w as a complex angle variable and makes $\kappa_i = (k^2 - \xi^2)^{1/2} = 0$ a regular point in the w plane. The transcendental function $\sin w$ is single-valued. From its periodicity property $\sin(w + 2n\pi) = \sin w$, $n = \pm 1, \pm 2, \dots$, it is evident that a multiplicity of w values corresponds to the same value of ξ . Thus, the entire ξ plane can be mapped into various adjacent sections of "width" 2π in the w plane. The inverse function $\sin^{-1}(\xi/k)$ in the ξ plane is multiple valued, implying the existence of branch points in that plane. The branch points occur at those points in the ξ plane for which the mapping derivative $d\xi/dw$ vanishes in the w plane and are of the order of the zero of $d\xi/dw$. Since $d\xi/dw = k \cos w$, the branch points are situated at $\xi = \pm k$ and are of the first order.

To investigate in detail the properties of the mapping from the ξ to the w plane, we separate Eq. (6) into its real and imaginary parts (k is assumed to be real) :

$$\xi_r = k \sin w_r \cosh w_i, \quad \xi_i = k \cos w_r \sinh w_i, \quad (7)$$

where

$$\xi = \xi_r + i\xi_i, \quad w = w_r + iw_i, \quad (7a)$$

with ξ_r , ξ_i , w_r , and w_i real. As shown in Fig. 5.3.4(a), the four quadrants in the ξ plane map in the w plane into corresponding regions, identified via Eq. (7),

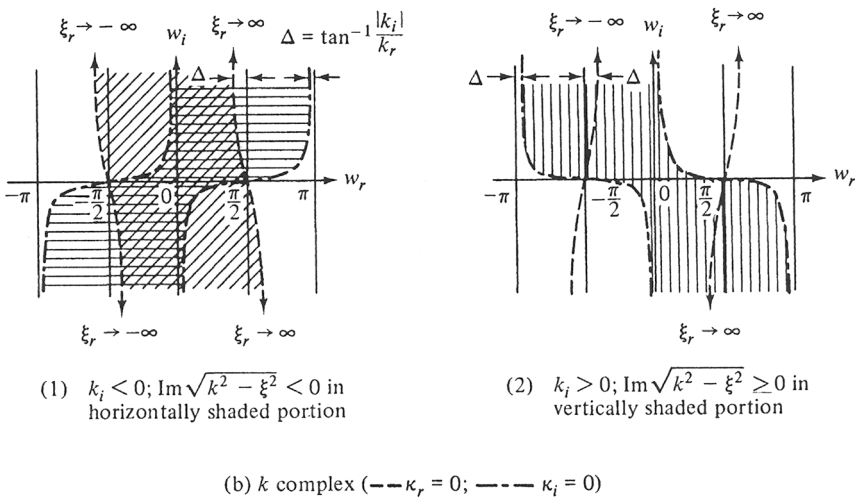
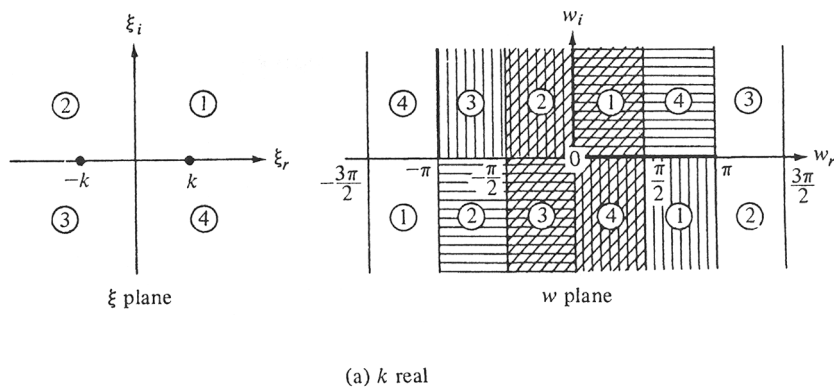


FIG. 5.3.4 Mapping from the complex ξ plane to the complex w plane.

which bear the same numbers as those in the ξ plane. One notes the repetitive character of the regions in the w plane as w_r changes by multiples of 2π . Thus, the two-sheeted ξ plane can be mapped, for example, into the strip $-\pi < w_r < \pi$ in the w plane. The top sheet of the Riemann surface in the ξ plane as shown in Fig. 5.3.4(a) maps, for example, into the strip $-\pi/2 < w_r < \pi/2$ in the w plane; each neighboring strip of width π in the w plane can then represent the other sheet of the Riemann surface in the complex ξ plane. Thus, in the mapping from the ξ plane to the w plane, the Riemann sheets in the former appear as adjacent regions in the latter.

The detailed correspondence between regions in the complex w plane and those in the two-sheeted ξ plane depends on the choice of branch cuts in the ξ

plane. To assess this correspondence in a simple manner we utilize the behavior of

$$\kappa = \sqrt{k^2 - \xi^2} = +k \cos w = k(\cos w_r \cosh w_i - i \sin w_r \sinh w_i). \quad (8)$$

With $\kappa(0) = k$, the plus sign in Eq. (8) is chosen to make the point $\xi = 0$ correspond to $w = 0$. For a choice of branch cuts as in the first part of Fig. 5.3.3(a), $\text{Im } \kappa$ is positive in quadrants 2 and 4 and negative in quadrants 1 and 3. From Eq. (8), $\text{Im } \kappa = -k \sin w_r \sinh w_i$, so one can identify the regions in the w plane of Fig. 5.3.4(a), shaded with slanted lines, as corresponding to those on the entire top sheet of the Riemann surface in the first part of Fig. 5.3.3(a). Similarly, the vertically shaded regions in the w plane correspond to the choice of branch cuts in the second part of Fig. 5.3.3(a) with $\text{Im } \kappa > 0$ on the entire top sheet; the horizontally shaded regions correspond to the third part of Fig. 5.3.3(a) with $\text{Im } \kappa < 0$ on the entire top sheet.

When k is complex,

$$\begin{aligned} \kappa_r &= k_r \cos w_r \cosh w_i + k_i \sin w_r \sinh w_i, \\ \kappa_i &= k_i \cos w_r \cosh w_i - k_r \sin w_r \sinh w_i, \end{aligned} \quad (8a)$$

so the boundary curves $\kappa_r = 0$, $\kappa_i = 0$ in the complex w plane appear as in Fig. 5.3.4(b). As $|w_i| \rightarrow \infty$, these curves are asymptotic to the lines $w_r = \pi/2 \pm \Delta$, etc., as shown. The various shaded regions in the w plane of Fig. 5.3.4(a) are therefore distorted. The slanted and horizontally shaded regions in the first part of Fig. 5.3.4(b) correspond to the entire top sheets of the Riemann surfaces in the ξ planes in the first and second parts of Fig. 5.3.3(b), respectively. In the horizontally shaded domain of Fig. 5.3.4(b), $\text{Im } \kappa < 0$. Analogous considerations apply to the second part of Fig. 5.3.4(b), wherein $\text{Im } \kappa > 0$ in the vertically shaded domain.

5.3d Asymptotic Evaluation of a Typical Radiation Integral for the Incident and Reflected Fields

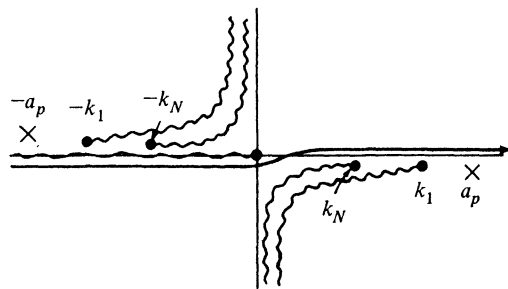
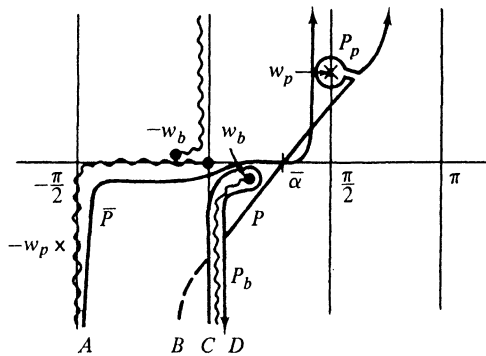
The preliminaries of Secs. 5.3a–5.3c facilitate the asymptotic evaluation of integrals of the form given in Eqs. (5.2.11)–(5.2.14), with g_{zi} specified as in Eq. (1). For an assumed $\exp(j\omega t)$ time dependence, generic forms of these integrals are, for the point-source problem,

$$I_1 = \int_{-\infty e^{-j\pi}}^{\infty} H_n^{(2)}(\xi\rho) e^{-j\kappa_{11}\xi} f_1(\xi) d\xi, \quad n = 0, 1, \quad (9a)$$

and, for the line-source problem,

$$I_2 = \int_{-\infty}^{\infty} e^{-j\eta(y-y')} e^{-j\kappa_{11}\bar{z}} f_2(\eta) d\eta, \quad (9b)$$

where the positive distance parameter \bar{z} may represent either $|z - z'|$ or $|z + z'|$, and the functions $f_{1,2}$ are independent of the space coordinates but possess branch-point and (or) pole singularities in the complex ξ or η plane. A typical integration path is shown in Fig. 5.3.5(a), wherein the branch-point singularities

(a) Complex ξ or η planes (in η plane, omit branch point at $\eta = 0$)(b) w plane (w_b corresponds to k_N , w_p corresponds to a_p , branch point at $w = 0$ corresponds to branch point at $\xi = 0$)FIG. 5.3.5 Integration paths ($e^{j\omega t}$ dependence).

at $\pm k_1$, and $\pm k_N$ and the pole singularities at $\pm a_p$ have been slightly displaced from the real axis to signify the presence of small loss: In the lossless limit, the required indentations of the integration path around the singularities are thereby evident. The branch point at the origin arises from the Hankel function in Eq. (9a) and is not present in the corresponding η -plane description of Eq. (9b). Branch cuts have been drawn so that $\text{Im } \kappa_1$ and $\text{Im } \kappa_N$ are negative on the entire top sheet of the multisheeted Riemann surface (see Fig. 5.3.3).

Since one of the aims of the presentation in this book is to provide familiarity with field solutions corresponding to either an $\exp(j\omega t)$ or an $\exp(-i\omega t)$ time dependence, it is appropriate to give as well the $\exp(-i\omega t)$ forms of Eqs. (9a) and (9b). To pass from one formulation to the other, one replaces j by $-i$, thereby performing essentially a complex conjugation. The resulting modification affects not only the appearance of the integrands but also the paths of in-

tegration on which the radiation condition is satisfied. Thus, it is now necessary to have $\text{Im } \kappa > 0$ to provide for the decay of non-propagating wave solutions $\exp(i\kappa_i z)$. The generic radiation integrals for the $\exp(-i\omega t)$ variation are given by

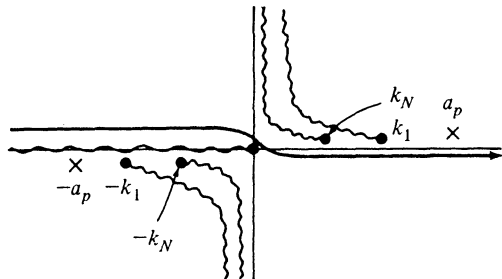
$$I_1 = \int_{-\infty e^{i\pi}}^{\infty} H_n^{(1)}(\xi\rho) e^{i\kappa_{11}z} f_1(\xi) d\xi, \quad (10a)$$

and

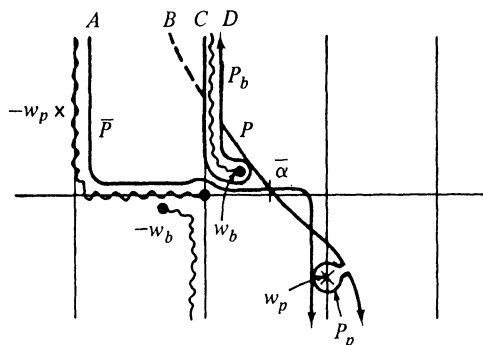
$$I_2 = \int_{-\infty}^{\infty} e^{i\eta(y-y')} e^{i\kappa_{11}z} f_2(\eta) d\eta, \quad (10b)$$

and the corresponding integration paths and singularities are shown in Fig. 5.3.6(a) [see Fig. 3.2.10(a) in connection with Eq. (10a)].

It is convenient to transform from the complex wavenumber variables ξ or η to the complex angle variable w via $\xi = k_1 \sin w$ or $\eta = k_1 \sin w$, since the branch-point pair at $\pm k_1$ in Figs. 5.3.5(a) or 5.3.6(a) may thereby be removed



(a) Complex ξ or η planes
(in η plane, omit branch point at $\eta = 0$)



(b) w plane (w_b corresponds to k_N , w_p corresponds to a_p , branch point at $w = 0$ corresponds to branch point at $\xi = 0$)

FIG. 5.3.6 Integration paths ($e^{-i\omega t}$ dependence).

and the subsequent calculation facilitated. In view of the mapping properties described in Sec. 5.3c, the configuration in the complex w plane is as shown in Figs. 5.3.5(b) and 5.3.6(b), with \bar{P} representing the transformed integration contour. Upon introducing polar coordinates L and $\bar{\alpha}$ via

$$\left. \begin{aligned} \rho \\ y - y' \end{aligned} \right\} = L \sin \bar{\alpha}, \quad \bar{z} = L \cos \bar{\alpha}, \quad (11)$$

one obtains the following expressions for the point-source problem with an $\exp(j\omega t)$ dependence,

$$I_1 = k_1 \int_{\bar{P}} H_n^{(2)}(k_1 L \sin \bar{\alpha} \sin w) e^{-jk_1 L \cos \bar{\alpha} \cos w} f_1(k_1 \sin w) \cos w dw, \quad (12a)$$

and, for the line-source problem,

$$I_2 = k_1 \int_{\bar{P}} e^{-jk_1 L \cos(w - \bar{\alpha})} f_2(k_1 \sin w) \cos w dw. \quad (12b)$$

Analogous results are found for the $\exp(-i\omega t)$ dependence. In Eq. (12a), L is the spherical polar distance from $\rho = 0$, $\bar{z} = 0$, and $\bar{\alpha} \leq \pi/2$ is the angle between L and the \bar{z} axis, whereas in Eq. (12b), L is the cylindrical polar distance from $y = y'$, $\bar{z} = 0$, and the polar angle $\bar{\alpha}$ may range from $-\pi/2$ to $+\pi/2$.

Equation (12b) is already in the form suitable for an asymptotic evaluation by the method of steepest descent (Sec. 4.1), since for observation points in the far zone, the large parameter $k_1 L$ appears in the exponential term, and the function $f_2 \cos w$ is slowly varying by comparison. To achieve a similar formulation for Eq. (12a) and its counterpart for the $\exp(-i\omega t)$ case, one may employ the large-argument approximation for the Hankel functions [see also Eqs. (5.4.37)]:

$$H_n^{(2)}(u) \sim \sqrt{\frac{2}{\pi u}} e^{-j(u-n\pi/2-\pi/4)} \left[1 + O\left(\frac{1}{u}\right) \right],$$

$$|u| \gg n, \quad -2\pi < \arg u < \pi, \quad (13a)$$

$$H_n^{(1)}(u) \sim \sqrt{\frac{2}{\pi u}} e^{j(u-n\pi/2-\pi/4)} \left[1 + O\left(\frac{1}{u}\right) \right],$$

$$|u| \gg n, \quad -\pi < \arg u < 2\pi, \quad (13b)$$

provided that $k_1 L \sin \bar{\alpha} \gg 1$ and that the integration paths are deformed away from the origin sufficiently to assure $|k_1 L \sin \bar{\alpha} \sin w| \gg 1$ along \bar{P} . The restrictions on $\arg(\sin w)$ are met on \bar{P} and various deformed contours employed subsequently. Equations (12a) and (12b) are then both represented by an integral of the form

$$I = \int_{\bar{P}} f(w) \exp \left[\begin{aligned} -j \\ +i \end{aligned} \right] k_1 L \cos(w - \bar{\alpha}) dw \quad \left(\begin{aligned} e^{j\omega t} \\ e^{-i\omega t} \end{aligned} \text{ dependence} \right), \quad (14)$$

where f takes on values appropriate to the point-source or line-source excitation.

The asymptotic evaluation of I for large values of $k_1 L$ is performed directly by the methods described in Chapter 4. The integration path \bar{P} is first deformed into the steepest-descent path P through the saddle point at $w = \bar{\alpha}$ [see Fig.

4.2.2, where $P \equiv \tilde{P}_z$ is shown for the $\exp(-i\omega t)$ case]; this path distortion is permissible since both \tilde{P} and P terminate at $|w| \rightarrow \infty$ in regions wherein the exponential in Eq. (14) decays, thereby eliminating contributions from contour segments connecting the endpoints. For certain saddle-point locations, it may happen that singularities in the finite portion of the w plane must be crossed during the path deformation. These pole or branch-point singularities must then be surrounded by appropriate contours P_p and P_b , respectively, as shown in Figs. 5.3.5(b) and 5.3.6(b). When the branch point at w_b is intercepted, the steepest-descent path passes through the branch cut onto the second Riemann sheet; connection between the endpoints A and B of \tilde{P} and P is brought about by the path segments AC , CD (along P_b) and DB , with no contribution arising from AC and DB .[†] Thus, for the $\exp(-i\omega t)$ dependence, Eq. (14) may be re-written in terms of a “steepest-descent representation” as

$$\begin{aligned} I = & \int_P \cdots dw + U(\bar{\alpha} - \bar{\alpha}_b) \int_{P_b} \cdots dw \\ & + U(\bar{\alpha} - \bar{\alpha}_p) 2\pi i [(w - w_p) f(w)]_w \exp [ik_1 L \cos(w_p - \bar{\alpha})], \end{aligned} \quad (15)$$

where $U(x)$ is the Heaviside unit function, which equals unity when x is positive and vanishes when x is negative, while $\bar{\alpha}_b$ and $\bar{\alpha}_p$ are those values of $\bar{\alpha}$ for which the steepest-descent path crosses the branch-point and pole singularities, respectively. From Eq. (4.2.29) it is concluded that

$$\bar{\alpha}_{p,b} = \operatorname{Re} w_{p,b} - \cos^{-1} \operatorname{sech} (\operatorname{Im} w_{p,b}). \quad (15a)$$

The residue contribution arising from a (simple) pole at w_p has been exhibited explicitly in the last term of Eq. (15).

The integrals over the paths P and P_b cannot generally be reduced further, but they may be simplified by asymptotic techniques when $(k_1 L)$ is large. From Eqs. (4.2.1a), one has, for the saddle-point contribution,

$$\int_P f(w) e^{ik_1 L \cos(w - \bar{\alpha})} dw \sim \sqrt{\frac{2\pi}{k_1 L}} f(\bar{\alpha}) e^{i(k_1 L - \pi/4)} \left[1 + O\left(\frac{1}{k_1 L}\right) \right]. \quad (16a)$$

Similarly, when P_b encircles the branch point in the positive sense, Eq. (4.8.3) yields for the branch-cut integral contribution,

$$\begin{aligned} & \int_{P_b} f(w) \exp [ik_1 L \cos(w - \bar{\alpha})] dw \\ & \sim \frac{2\sqrt{\pi}}{|k_1 L \sin(\bar{\alpha} - w_b)|^{3/2}} \left[\sqrt{w - w_b} \frac{df(w)}{dw} \right]_{w_b} \\ & \exp [ik_1 L \cos(w_b - \bar{\alpha})] \exp \left(-i \frac{3}{2} \left\{ \frac{\pi}{2} + \arg [k_1 \sin(w_b - \bar{\alpha})] \right\} \right), \end{aligned} \quad (16b)$$

where it has been assumed that $\sqrt{w - w_b} df/dw$ is finite at w_b , a behavior ex-

[†]The Riemann surface is associated with the branch points of $f(w)$ at $\pm w_b$ that arise from the corresponding singularities at $\pm k_N$ in the ξ or η planes. Since these singularities do not occur in the exponential term in Eq. (14), this function has identical decay characteristics on either Riemann sheet.

hibited by functions encountered in an actual calculation. For the $\exp(+j\omega t)$ dependence, i in Eqs. (15) and (16) is replaced by $-j$. One observes that for real values of w_p and w_b , the residue contribution in Eq. (15) is dominant at large distances since it behaves like $O(1)$ in $k_1 L$, whereas the saddle-point and branch-point contributions decay like $(k_1 L)^{-1/2}$ and $(k_1 L)^{-3/2}$, respectively. On the other hand, when w_p is complex, the residue contribution has an exponential decay factor which may render the saddle-point result dominant. It may also be remarked that the field due to the saddle point is observed everywhere, while the pole or branch-point fields are generally confined to special regions delimited by the Heaviside unit functions in Eq. (15). For the class of problems to be considered in this chapter, the poles account for surface waves and leaky waves, the branch points yield lateral waves, and the saddle points furnish the direct, reflected, and refracted fields of geometrical optics; the result in Eq. (16a) may be interpreted as a local plane-wave field propagating along L with varying amplitude.

An interesting schematization of the relation between propagating wave solutions in the wavenumber ξ or η and angle w planes, and their relevance to the saddle-point condition, may be realized with the aid of the wavenumber surface. This surface, traced out by the endpoints of the wave vector \mathbf{k}_1 for plane waves propagating in all possible directions, is a sphere since the medium is isotropic. The outward normal to the surface, evidently parallel to \mathbf{k}_1 and defining the direction of the power-flow vector $\bar{\mathbf{S}}$, is also called the *ray direction* (see the discussion in Sec. 1.6b). Propagating plane-wave solutions are characterized by real values of the wavenumbers ξ (or η) and κ , and their relation to the propagation angle w is as shown in Fig. 5.3.7(a). The saddle point in the radiation integral is situated at $w = \bar{\alpha}$ (or $\xi, \eta = k_1 \sin \bar{\alpha}$), where $\bar{\alpha}$ is the angle between the \bar{z} axis and the radius vector from the origin at $L = 0$ to the observation point [Fig. 5.3.7(b)]. Thus, one may find the saddle point graphically from the wavenumber plot by constructing a normal to the surface in the direction parallel to L and by reading off the corresponding values of w , ξ , or η .

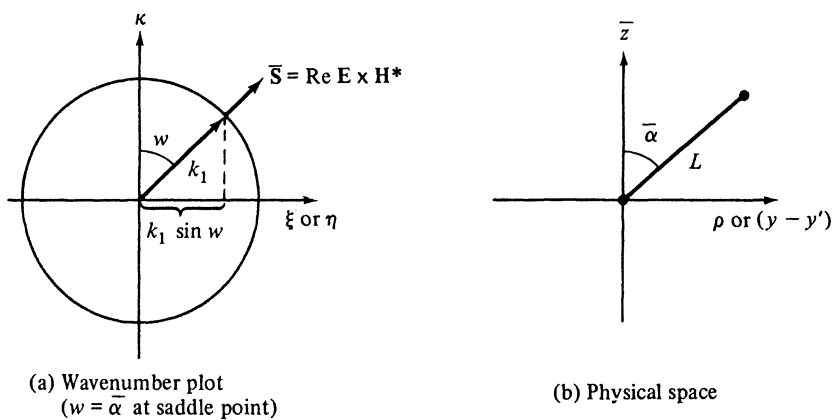


FIG. 5.3.7 Wavenumber surface and saddle-point condition.

Although this graphical visualization is not too important in the present case of an isotropic medium since the propagation characteristics are so simple, it aids greatly in an anisotropic environment (see Secs. 1.6b and 8.3). The saddle point locates the region of major contribution to the steepest-descent integral, and the saddle-point value, $w = \bar{\alpha}$ or ξ , $\eta = k_1 \sin \bar{\alpha}$ selects that particular plane wave which establishes the local field and carries energy along the radial direction L to the corresponding observation point; more precisely, the field is established by a wavepacket having a small spread of angles or wavenumbers about the saddle-point value. This physical interpretation gives insight into the mechanism of energy transfer to the radiation field and is obtained directly from the wave-number diagram.

The simple formulas in Eqs. (16a) and (16b) fail when $\bar{\alpha} \rightarrow w_p$ and w_b , respectively; in this instance, the saddle point is situated near a singularity, and the asymptotic evaluation must be performed in a more refined manner. As noted in Secs. 4.4a and 4.4c, the modified formula, valid for arbitrary proximity of a pole and a saddle point, involves Fresnel integrals, whereas the modified result for neighboring saddle point and branch point is given in terms of a Weber (parabolic cylinder) function.

5.3e General Properties of Pole and Branch-Point Wave Contributions

The asymptotic results in Eqs. (15) and (16) contain wave contributions that arise from poles or branch points of the reflection coefficient $\vec{\Gamma}_r(0)$ in Eq. (1); these singularities in the complex w plane are located at $w_\mu = w_{\mu_r} + iw_{\mu_i} = w_p$, or w_b , where w_{μ_r} and w_{μ_i} denote the real and imaginary parts of w_μ , respectively. Apart from a possible algebraic dependence on the space coordinates, a typical wave constituent is characterized by the exponential behavior

$$\exp[ik_1 L \cos(w_\mu - \bar{\alpha})] = \\ \exp[ik_1 L \cosh w_{\mu_r} \cos(w_{\mu_r} - \bar{\alpha})] \exp[-k_1 L \sinh w_{\mu_r} \sin(\bar{\alpha} - w_{\mu_r})], \quad (17)$$

representing for real k_1 a non-uniform plane wave whose phase fronts advance along the direction $\bar{\alpha} = w_{\mu_r}$ (direction of constant amplitude) and whose amplitudes change most rapidly in the perpendicular direction $\bar{\alpha} = w_{\mu_r} \pm \pi/2$ (direction of constant phase). The phase velocity $v = \omega/(k_1 \cosh w_{\mu_r})$ is seen to be smaller than the ω/k_1 value for a uniform plane wave. In particular, when $w_{\mu_r} = \pi/2$, $w_{\mu_i} < 0$, the phase fronts propagate transverse to \bar{z} and the amplitude decays along \bar{z} only [see the definitions of L and $\bar{\alpha}$ in Eq. (11)], thereby characterizing the field as a *surface wave* carrying energy in the direction parallel to an interface at $\bar{z} = 0$ (Secs. 5.6 and 5.7). On the other hand, when $0 < w_{\mu_r} < \pi/2$, $w_{\mu_i} > 0$, energy is transferred out of the interface, and yields a *leaky wave* (Sec. 5.6). Important in a physical interpretation of these plane-wave solutions is their domain of existence in the asymptotic field, described essentially by that range of observation angles $\bar{\alpha}$ for which the singularity w_μ is encountered during the deformation of the original integration contour \tilde{P} into the steepest-descent path P in Fig. 5.3.6(b); the explicit separation of the contributions from a

singularity and from the saddle point applies only when these points are “widely separated” (see Sec. 4.1). If $\bar{\alpha}_\mu$ denotes the value of $\bar{\alpha}$ for which P just passes through w_μ [see Eq. (15a)], then when w_μ is situated above and (or) to the right of the original path \bar{P} in Fig. 5.3.8(a), the singularity contributes in the range $\bar{\alpha}_\mu < \bar{\alpha} < \pi/2$, with $(\bar{\alpha}_\mu - w_{\mu r}) \geq 0$ when $w_{\mu i} \geq 0$. For the remaining locations

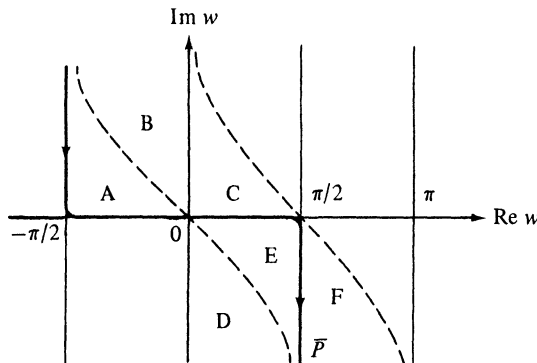
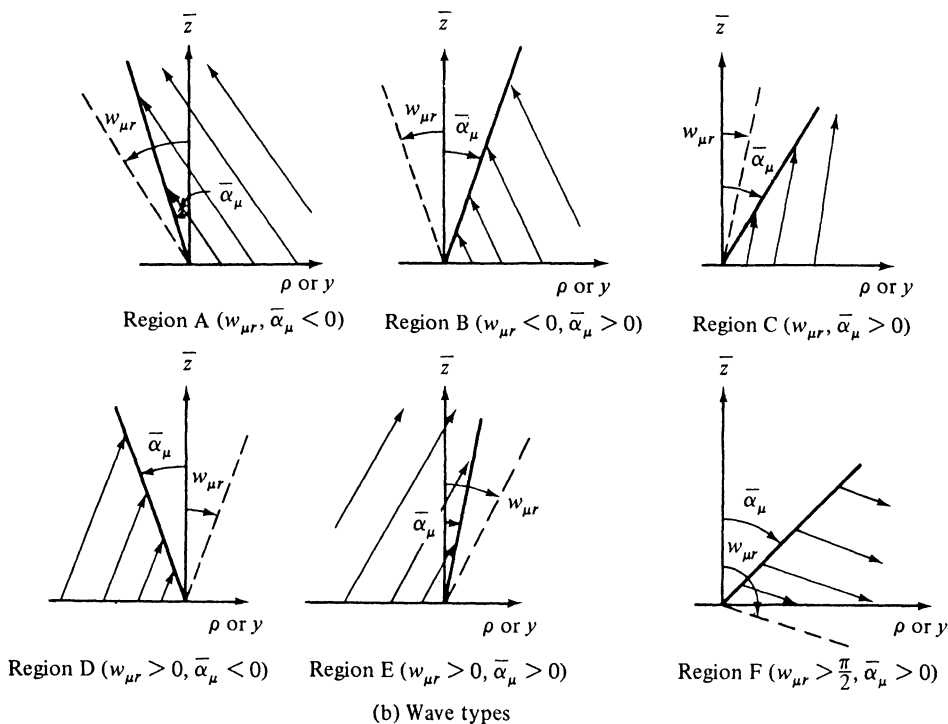
(a) Location of singularities [$\exp(-i\omega t)$ dependence].

FIG. 5.3.8 Physical characteristics of waves arising from singularities of the modal reflection coefficient $\vec{\Gamma}_i(0)$ [Eq. (1)] in the complex w plane.

of w_μ in the semistrip $0 < w_r < \pi/2$, $w_i < 0$, the contribution appears in the complementary region $0 < \bar{\alpha} < \bar{\alpha}_\mu$ and $(\bar{\alpha}_\mu - w_{\mu r}) < 0$ with $w_{\mu i} < 0$. One observes from Eq. (17) that the corresponding field decays exponentially in its domain of existence along any radial direction leading from $L = 0$ to a distant observation point; inclusion and far-zone interpretation of the wave in Eq. (17) is therefore significant, although, taken by itself without reference to the mechanism of excitation, this field may be an improper solution of the Maxwell equations. In this connection one should note that improper, or non-modal (non-spectral), singularities lie in the region $\text{Im } \kappa_\mu = \text{Im } \sqrt{k^2 - k_{\mu r}^2} < 0$ corresponding, for the assumed $\exp(-i\omega t)$ dependence, to the improper sheet of the complex transverse wavenumber k_t plane [see, for example, region C in Fig. 5.3.8(a)].

These remarks are illustrated in Fig. 5.3.8, which exhibits the wave types arising from singularity contributions in various parts of the complex w plane.⁵ The dashed lines in the first figure represent the steepest-descent paths through saddle points at $w = 0$ and $w = \pi/2$, respectively, and provide the partitioning of the w plane. The parallel lines (rays) in the remaining plots represent the direction of phase propagation (and energy flow) in the inhomogeneous plane wave whose domain of existence is bounded by the observation angle $\bar{\alpha}_r$; the rays are parallel to the line $\bar{\alpha} = w_{\mu r}$ and perpendicular to the equiphasic planes (not shown); the wave amplitude is constant along a ray but changes elsewhere. Increased spacing between the rays indicates that the amplitude decreases in this direction. While the physical domain for radiation from a point source is confined to $\rho > 0$ or $0 \leq \bar{\alpha} \leq \pi/2$, some of the plots extend also into the region $\bar{\alpha} < 0$ relevant for line-source excitation [see Eq. (11)]. One observes that with the exception of waves arising from region C , all wave types have decreasing intensities as the observation point moves either along the \bar{z} or ρ directions away from the source region $\rho = \bar{z} = 0$. It is also noted that the waves corresponding to regions A through E carry energy away from the interface (i.e., they “leak” into the exterior region $\bar{z} > 0$), while the wave from region F supplies energy to overcome losses in the medium occupying the half-space $\bar{z} < 0$ (see Secs. 5.5–5.7). Furthermore, the waves arising from regions A , B , D , and E are backward, since their energy-flow characteristics are toward the source plane $\rho = 0$; these features are of importance in connection with the imposition of a radiation condition. While these aspects are valid for lossy or lossless stratification in $\bar{z} < 0$, it is worth mentioning explicitly the non-dissipative case. In this instance, w_μ in region F moves onto the line $w_r = \pi/2$ (i.e., $w_{\mu r} = \pi/2$) and one obtains a forward surface wave, as mentioned earlier. If the structure exhibits a singularity that moves onto the line $w_r = \pi/2$ from region E , the corresponding surface wave is backward.

Wave types arising from regions A through E in the complex w plane of Fig. 5.3.8 carry power in the direction $w_{\mu r}$ toward the vicinity of the surface $\bar{\alpha} = \bar{\alpha}_\mu$, which bounds their domain of existence. It is natural to ask what happens to this energy. We recall at this point that the singularity contribution

constitutes only a portion of the asymptotic field solution and that there is present in all observation regions a “space wave”, arising from the saddle-point evaluation in Eq. (16a), which transports the radiated energy into the far zone $k_1 L \rightarrow \infty$. Because of their exponential decay with L , the waves arising from w_μ are not observable at very great distances from the source and it appears, therefore, that the energy carried by them is converted into the radially propagating space wave in the vicinity of the angle $\tilde{\alpha} = \tilde{\alpha}_\mu$. The radial decay along $\tilde{\alpha}_\mu$ is smallest when $\tilde{\alpha}_\mu \approx w_{\mu r}$ (i.e., when the complex singularity w_μ lies near the real w axis); one may then expect its presence to be strongly noticeable in the radiation field since appreciable coupling occurs between the two wave types when they propagate essentially along the direction $\tilde{\alpha}_\mu$. For a pole singularity, it is simple to verify the validity of this statement by observing that, as a function of the observation angle $\tilde{\alpha}$, the space-wave amplitude in Eq. (16a) may become quite large near $\tilde{\alpha}_\mu$ when $f(w)$ has a pole at $w_\mu = w_{\mu r} + iw_{\mu i}$, with $|w_{\mu i}| \ll 1$. Under these conditions, the strongly excited complex pole dominates the field near the source and gives rise to a peak in the radiation pattern near $\tilde{\alpha} = \tilde{\alpha}_\mu$.⁴ For a branch-point contribution, the additional algebraic decay factor $[k_1 L \sin(\tilde{\alpha} - w_b)]^{-3/2}$ in Eq. (16b) implies that strong interaction near $\tilde{\alpha}_\mu \approx w_{\mu r}$ takes place with the $O(1/k_1 L)^{-3/2}$ term in the saddle-point result of Eq. (16a).

5.3f Asymptotic Evaluation of a Typical Radiation Integral for the Transmitted Fields

The calculation of fields transmitted across an interface is more involved than that of direct or reflected fields since the modal Green's function $g_{zi}(z, z')$ has a more complicated form. This is true even for the case of a single plane interface at $z = 0$ separating two semiinfinite dielectrics (Fig. 5.5.1), for which $\vec{\Gamma}_i(0)$ in Eq. (1) is given in Eqs. (5.5.12). The form of $g_{zi}(z, z')$ for $z > 0$ may be inferred from that for $z < 0$ by invoking the required continuity at $z = 0$ and recognizing that to satisfy the radiation condition at $z = +\infty$ for a time dependence $\exp(+j\omega t)$, the solution must have the dependence $\exp(-jk_{i2}z)$. Thus, for $z' < 0, z > 0$,

$$g_{zi}(z, z') = g_{zi}(0, z')e^{-jk_{i2}z} = \frac{1}{2jk_{i1}} [1 \mp \vec{\Gamma}_i(0)] e^{-jk_{i1}|z'| - jk_{i2}z}, \quad (18)$$

where κ_{i1} and κ_{i2} are the modal propagation constants in regions 1 and 2, respectively, and the + and - signs refer, respectively, to the E and H modes. Since the generic forms of the resulting radiation integrals in Eqs. (9) contain integrands wherein both $\kappa_{i1} = \sqrt{k_1^2 - k_i^2}$ and $\kappa_{i2} = \sqrt{k_2^2 - k_i^2}$ appear in the exponent, k_i being either ξ or η , it follows that the transformations $k_i = k_1 \sin w$ or $k_i = k_2 \sin w$ do not bring about simplifications analogous to those in Eq. (14). The difficulty can be circumvented by assuming that $k_2 z \gg k_1 |z'|$ (observation point located very far from the interface), in which instance the $\exp(-jk_{i1}|z'|)$ term may be considered part of the slowly varying amplitude function f_1 or f_2 in Eqs. (9). The change of variable $k_i = k_2 \sin w$ then leads to

a formulation directly analogous to the one in Eq. (14), thereby making the subsequent discussion applicable. In a similar manner, one may treat the case $k_2 z \ll k_1 |z'|$, with $\exp(-jk_{i2}z)$ now playing the role of a slowly varying factor.

An asymptotic evaluation based on the preceding assumptions, although adequate for far-field calculations, does not yield information about the important case where $k_{i1,2}$ are large but z and z' are unrestricted. In this regime of geometrical optics, neither of the exponential terms in Eq. (18) may be regarded as slowly varying, and both must be retained in the saddle-point calculation. There is no simple transformation from the ξ or η plane to the w plane furnishing an exponential as in Eq. (14), so an alternative approach is required. The procedure to be described is carried out directly in the plane of the transverse wavenumbers. As before, we consider the typical integral which, for the $\exp(j\omega t)$ dependence, is

$$I = \int_{-\infty}^{\infty} e^{-jq(\eta)} \bar{f}(\eta) d\eta, \quad q(\eta) = \eta y + \kappa_{i1}|z'| + \kappa_{i2}z, \quad (19a)$$

or, alternatively, for the $\exp(-i\omega t)$ dependence,

$$I = \int_{-\infty}^{\infty} e^{iq(\eta)} \bar{f}(\eta) d\eta. \quad (19b)$$

The integration paths are specified in Figs. 5.3.5(a) and 5.3.6(a). The saddle points η_s in the integrand, located at $dq/d\eta = 0$, are determined by the implicit relation

$$y + \frac{d\kappa_{i1}}{d\eta} |z'| + \frac{d\kappa_{i2}}{d\eta} z = 0 \quad \text{at} \quad \eta = \eta_s. \quad (19c)$$

Explicit specification of the *complete* steepest-descent path SDP through a saddle point at η_s , defined by the requirement $\operatorname{Re} q(\eta) = \operatorname{Re} q(\eta_s)$ (see Sec. 4.1b), is rather difficult. However, its progress *near* η_s is determined simply: Along a $\pm 45^\circ$ line with respect to the real η axis if the saddle point is of the first order and real [see Fig. 4.2.1; the present discussion treats only non-evanescent waves arising from real saddle points with $\kappa_{i1,2}(\eta_s)$ real, i.e., $|\eta_s| < k_{i1,2}$]. One may now consider the alternative path in Fig. 5.3.9, which proceeds along SDP near η_s ; its remaining portions C , drawn parallel to the real η axis for simplicity, lie in

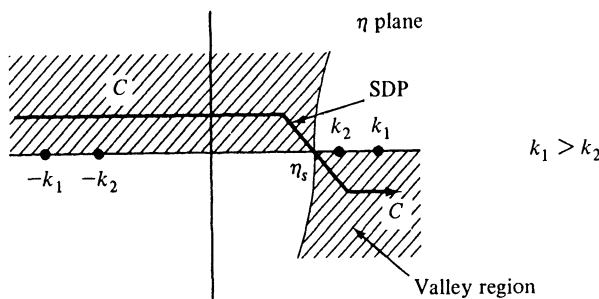


FIG. 5.3.9 Modified integration path when $d^2q/d\eta^2|_{\eta_s} < 0$ ($e^{-i\omega t}$ dependence).

“valley” regions of the complex η plane, wherein $\exp [iq(\eta)]$ decays (drawing of the branch cuts has been omitted). Since $|\eta_s| < k_{1,2}$, no branch points are intercepted during the path deformation. Possible residue contributions due to intercepted pole singularities are treated as before.

Since $\text{Im } q(\eta) > 0$ in the shaded region of Fig. 5.3.9, the principal contribution to the integral arises from the path segment SDP in the vicinity of η_s . Although the SDP does not go to infinity, the error due to truncation at some finite point in a valley region is exponentially small and may be neglected [see Eq. (4.1.17)]. Equation (4.2.1) or (4.2.20a) then yields the saddle-point approximation of Eq. (19b),

$$I_{SDP} \sim \sqrt{\frac{2\pi}{|d^2q/d\eta^2|_{\eta_s}}} \bar{f}(\eta_s) \exp [iq(\eta_s) + i(\pi/4) \operatorname{sgn}(d^2q/d\eta^2)_{\eta_s}]. \quad (20)$$

When the $\kappa_{i2}z$ term in Eq. (19c) is omitted and the substitution $\eta_s = k_1 \sin \bar{\alpha}$ is made, this result reduces to the one in Eq. (16a). Since the procedure leading to Eq. (20) does not involve the *complete* steepest-descent path, the exponentially small error bound on Eq. (20) is weaker than that for Eq. (16a) [see remarks following Eq. (4.2.18)]. However, when exponentially small contributions are neglected, Eq. (20) is sufficiently accurate.

A significant graphical interpretation of the saddle-point condition may be given. Upon writing

$$\tan \bar{\alpha}_1 = -\frac{\partial \kappa_{i1}}{\partial \eta} \Big|_{\eta_s}, \quad \tan \bar{\alpha}_2 = -\frac{\partial \kappa_{i2}}{\partial \eta} \Big|_{\eta_s}, \quad \kappa_{i1,2} = \sqrt{k_{1,2}^2 - \eta^2} \quad (21)$$

one obtains, from Eq. (19c),

$$y - z \tan \bar{\alpha}_2 - |z'| \tan \bar{\alpha}_1 = 0 \quad \text{at } \eta_s. \quad (22)$$

This equation for a straight line may be interpreted graphically: fields reach an observation point (y, z) in the region $z > 0$ via the ray trajectories 1 and 2 in Fig. 5.3.10(b) in such a manner that the real angles $\bar{\alpha}_1$ and $\bar{\alpha}_2$ satisfy the required plane-wave refraction law (Snell’s law) at the interface. This follows from Eq. (21), whence $\bar{\alpha}_1$ and $\bar{\alpha}_2$ define, respectively, the inclination of the normals to the κ_{i1} versus η and κ_{i2} versus η wavenumber plots in Fig. 5.3.10(a); since $\eta_s = k_1 \sin \bar{\alpha}_1 = k_2 \sin \bar{\alpha}_2$, Snell’s law is satisfied by these angles. The saddle-point condition, in conjunction with the wavenumber surface, therefore permits a ray-optical interpretation consistent with the constructs of geometrical optics. The saddle-point condition for the reflected field may be interpreted in a similar manner from the integral in Eq. (10b) and the resulting ray trajectory is shown dashed in Fig. 5.3.10.

It may easily be verified, in accord with expectations from ray optics, that the term $\exp [iq(\eta_s)]$ in Eq. (20) expresses precisely the phase change for a wave propagating along the trajectories 1 and 2 in Fig. 5.3.10. As noted above, $\eta_s = k_1 \sin \bar{\alpha}_1 = k_2 \sin \bar{\alpha}_2$, and similarly, $\kappa_{i1}(\eta_s) = k_1 \cos \bar{\alpha}_1$, $\kappa_{i2}(\eta_s) = k_2 \cos \bar{\alpha}_2$. When these relations as well as Eqs. (19c) and (21) are employed, one may

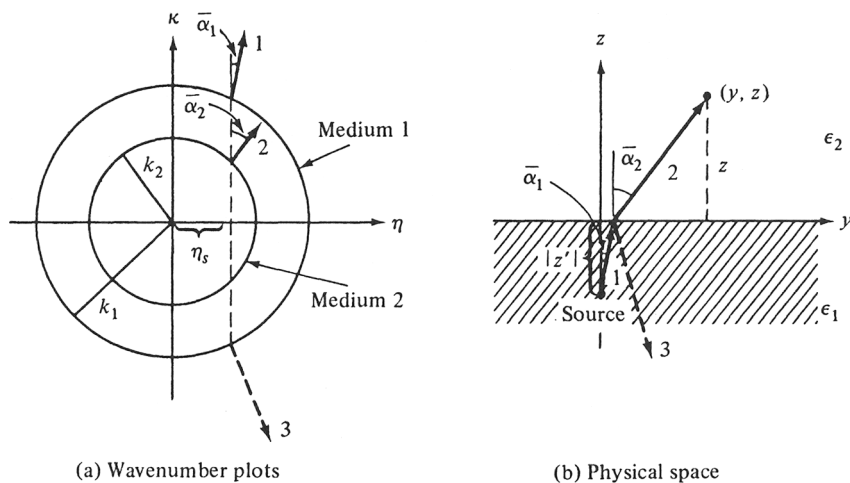


FIG. 5.3.10 Interpretation of the saddle-point condition for $k_1 > k_2$.

write

$$q(\eta_s) = k_1 L_1 + k_2 L_2, \quad (23)$$

where L_1 and L_2 are the lengths along rays 1 and 2, respectively. The amplitude term in Eq. (20) also conforms with ray optics as shown in Eqs. (5.5.9).

5.4 SOURCES IN AN UNBOUNDED DIELECTRIC

The results of the general discussion in Secs. 5.2 and 5.3 are now applied to problems involving various source configurations in an unbounded homogeneous medium. As noted in Sec. 5.2, the electromagnetic fields can be derived from the scalar functions G' , G'' or \mathcal{S}' , \mathcal{S}'' so primary emphasis is placed on the determination of these functions. Although some of the solutions in this simple environment may be obtained by direct integration of the differential equations, the method of modal representations is employed to illustrate implications of this more general procedure in elementary terms. In the format to be adopted, the statement of the problem and its solution are listed in the beginning, followed by a discussion of the physical interpretation of the result, and finally by a section summarizing relevant analytical steps. In this manner, the essential properties of the field may be surveyed succinctly, without the danger of hiding them in analytical details. To conform with general practice in the theory of radiation and diffraction, the final results are presented for the $\exp(-i\omega t)$ dependence, although some of the preliminary work involving modal analysis and network concepts is performed for the $\exp(j\omega t)$ dependence conventional in the latter context.

5.4a Dipoles Oriented Along z

Time-harmonic electric source current density

$$\hat{\mathbf{J}}(\mathbf{r}, t) = Il\delta(\mathbf{r})e^{-i\omega t}\mathbf{z}_0. \quad (1)$$

The fields of a source oriented as shown in Fig. 5.4.1 can be derived from

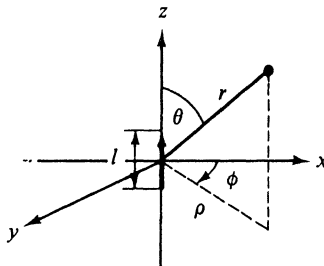


FIG. 5.4.1 Coordinate system.

the three-dimensional E -mode Green's function $G' = G_f$ defined by [see Eq. (5.2.3b)]

$$(\nabla^2 + k^2)G_f(\mathbf{r}, \mathbf{r}') = -\delta(\mathbf{r} - \mathbf{r}'), \quad (2a)$$

subject to a radiation condition at infinity. The solution for $\mathbf{r}' = 0$, obtained by direct integration of Eq. (2a), is given by [see Eq. (1.1.31), on multiplication by $\exp(-i\omega t')$ and integration over t']

$$G_f(\mathbf{r}, \mathbf{r}') = \frac{e^{ikr}}{4\pi r}, \quad (2b)$$

where $k = \omega\sqrt{\mu\epsilon}$ while ϵ and μ are the dielectric constant and permeability of the medium, respectively. The root-mean-square field components, obtained via Eqs. (5.2.1a), (5.2.1b), and (5.2.4c) (with $G' = G_f$) are, in spherical coordinates,

$$E_r = \sqrt{\frac{\mu}{\epsilon}} \frac{Ik l \cos \theta e^{ikr}}{2\pi kr^2} \left(1 + \frac{i}{kr}\right), \quad (3a)$$

$$E_\theta = -\sqrt{\frac{\mu}{\epsilon}} \frac{iIk l \sin \theta e^{ikr}}{4\pi r} \left(1 + \frac{i}{kr} - \frac{1}{(kr)^2}\right), \quad (3b)$$

$$H_\phi = -\frac{iIk l \sin \theta e^{ikr}}{4\pi r} \left(1 + \frac{i}{kr}\right), \quad (3c)$$

$$H_r = H_\theta = E_\phi = 0, \quad (3d)$$

where I is the current in the element and l is its length. For arbitrary source location at $\mathbf{r}' \neq 0$, one replaces r by $|\mathbf{r} - \mathbf{r}'|$ in Eq. (2b) and rederives the equivalent of Eqs. (3). The results remain valid in the dissipative case $\text{Im } k > 0$. The average radiated power density \bar{S} is given by

$$\tilde{S}_r = \operatorname{Re}(E_\theta H_\phi^*) = \sqrt{\frac{\mu}{\epsilon}} \frac{|Ik|_l^2 \sin^2 \theta}{(4\pi)^2 r^2}, \quad (4a)$$

$$\tilde{S}_\theta = \tilde{S}_\phi = 0, \quad (4b)$$

and the total radiated power P is [see Eq. (1.2.29)]

$$P = \int_0^\pi \tilde{S}_r \cdot 2\pi r^2 \sin \theta \, d\theta = \sqrt{\frac{\mu}{\epsilon}} \frac{|Ik|_l^2}{6\pi}. \quad (5)$$

The asymptotic field solution in the far zone $kr \gg 1$ contains to $O(1/kr)$ the components E_θ and H_ϕ only; their values are inferred from Eqs. (3b) and (3c) upon retaining only the first term inside the parentheses.

Discussion

Only E modes (with respect to z) are excited. The far field is transverse to the radius vector from the source to the observation point, and the transverse components account for the radiation of energy [see Eqs. (4)]. The mechanism of energy transport into the far zone may be schematized in ray-optical terms as in Fig. 5.4.2, where it is recalled (see Sec. 1.6) that the direction of a ray at

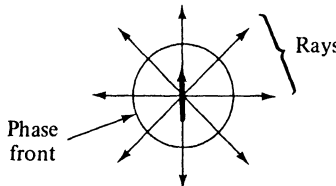


FIG. 5.4.2 Ray diagram.

a given point coincides with that of the power density vector $\tilde{\mathbf{S}}$ (see also Fig. 5.3.7). The equiphasic surfaces (phase fronts) perpendicular to the rays are spherical, and the field strength along a ray decays according to $1/r$.

Normalization for plane wave incidence

If the source point \mathbf{r}' moves to infinity the field observed at finite \mathbf{r} behaves like a plane wave since the curvature of the resulting spherical wavefront is negligible over any finite region. To make these remarks quantitative, we examine Eq. (2), with $r \rightarrow |\mathbf{r} - \mathbf{r}'|$, in the limit $\mathbf{r}' \rightarrow \infty$ and also introduce the source strength $J^o = Il$. Since

$$|\mathbf{r} - \mathbf{r}'| = [r^2 + r'^2 - 2rr' \cos \gamma]^{1/2}, \quad (6)$$

with γ representing the angle between the vectors \mathbf{r} and \mathbf{r}' , and

$$\cos \gamma = \frac{\mathbf{r} \cdot \mathbf{r}'}{rr'} = \cos \theta \cos \theta' + \sin \theta \sin \theta' \cos(\phi - \phi'), \quad (6a)$$

one obtains, upon expansion by the binomial theorem,[†]

[†]From Eq. (6a), one obtains $|\mathbf{r} - \mathbf{r}'| \sim r' - r \cos \gamma + O(1/r')$ as $r' \rightarrow \infty$. For the determination of the amplitude, it is sufficient to approximate $|\mathbf{r} - \mathbf{r}'|$ by r' as r' becomes very large. However, for the determination of the phase we can neglect only those terms which tend to zero as $r' \rightarrow \infty$ [i.e., terms of $O(1/r')$].

$$J^o G_f(\mathbf{r}, \mathbf{r}') \sim A \exp \{-ikr[\cos \theta \cos \theta' + \sin \theta \sin \theta' \cos(\phi - \phi')]\}, \\ r' \rightarrow \infty, \quad (6b)$$

where

$$A = \frac{J^o e^{ikr'}}{4\pi r'}. \quad (6c)$$

The right-hand side of Eq. (6b) represents a plane wave with amplitude A incident along a vector defined by the angular spherical coordinates (θ', ϕ') . To keep A finite as $r' \rightarrow \infty$, it is necessary to increase the source strength J^o proportionally with r' . If the incident plane wave is to have unit amplitude, one sets $A = 1$. From the above one can formulate a simple rule for passing from a Green's function corresponding to a *unit* strength point-source excitation at \mathbf{r}' to excitation by a *unit* amplitude plane wave: One first lets $r' \rightarrow \infty$ along the desired direction (θ', ϕ') and then sets $(1/4\pi r') \exp(ikr') = 1$.

Modal procedure

Although Eq. (2a) may be integrated directly to yield the closed-form expression for the free-space Green's function in Eq. (2b), such a procedure is generally not successful for other geometrical configurations containing interfaces perpendicular to z . It is therefore instructive to study the solution of Eq. (2a) by the modal analysis and synthesis procedure employed in these more general cases. The relevant representation is the one in Eq. (5.2.11). Since the z domain is bilaterally unbounded, the modal Green's function $g_{zi}(z, z')$ is given by the first term in Eq. (5.3.1) [note $\exp(+j\omega t)$ dependence],

$$g_{zi}(z, z') = \frac{e^{-j\sqrt{k^2 - \xi^2}|z|}}{2j\sqrt{k^2 - \xi^2}}, \quad z' = 0. \quad (7)$$

Thus,

$$G_f = -\frac{j}{8\pi} \int_{-\infty \exp(-j\pi)}^{\infty} \xi H_0^{(2)}(\xi\rho) \frac{\exp(-j\sqrt{k^2 - \xi^2}|z|)}{\sqrt{k^2 - \xi^2}} d\xi, \quad (7a)$$

with the integration path given in Fig. 5.3.5a (the singularities shown in the figure at $\pm k_N, \pm a_p$ are omitted). In the w plane, with $\xi = k \sin w$,

$$G_f = -\frac{jk}{8\pi} \int_{\bar{P}} \sin w H_0^{(2)}(kr \sin \theta \sin w) e^{-jkr \cos \theta \cos w} dw, \quad (7b)$$

where the contour \bar{P} is shown in Fig. 5.3.5b and (r, θ) are the spherical polar coordinates. Comparison of Eqs. (7b), (5.3.13a), and (5.3.14) leads to the identification

$$f(w) = -\frac{jk}{8\pi} \sqrt{\frac{2 \sin w}{\pi kr \sin \theta}} e^{j\pi/4}, \quad (8)$$

so that, from Eq. (5.3.16a), for the $\exp(+j\omega t)$ dependence,

$$G_f \sim \frac{e^{-jkr}}{4\pi r} \left[1 + O\left(\frac{1}{kr}\right) \right], \quad kr \sin \theta \gg 1. \quad (9)$$

The corresponding result for the $\exp(-i\omega t)$ dependence follows on letting $j \rightarrow -i$. It is of interest to note that the expression in Eq. (9) is independent of

$\sin \theta$, although in the derivation it had to be assumed that $\sin \theta \neq 0$. This lack of dependence on $\sin \theta$ indicates that the approximate result in Eq. (9) should remain valid even as $\sin \theta \rightarrow 0$. [By orienting the polar axis along a new direction $\hat{\theta} = 0$, one derives Eq. (9) subject to $kr \sin \hat{\theta} \gg 1$, whence the original direction $\theta = 0$ is now included in the permitted range.]

Upon comparing Eq. (9) (with $j \rightarrow -i$) and Eq. (2b), one notes that the approximate and exact solutions agree perfectly. It is implied thereby that in the asymptotic representation of the integral in Eq. (7b), all higher-order terms involving powers of $1/(kr)^n$, $n = 2, 3, \dots$, vanish. This may be verified upon evaluation of the first few higher-order terms via the procedure described in Sec. 4.2b. It should be emphasized that in this more accurate evaluation, the asymptotic representation of the Hankel function must include higher-order terms.

Alternative representations

Since the integral in Eq. (5.2.8b), and the one in Eq. (7a) derived therefrom for the special case of a source at the coordinate origin in an unbounded medium, has the generic form given in Eq. (3.3.37), it is expected to be useful for the derivation of an alternative result by contour deformation. To illustrate these manipulations for the $\exp(-i\omega t)$ dependence, we rewrite Eq. (7a) as

$$G_f = \frac{i}{8\pi} \int_{-\infty \exp(i\pi)}^{\infty} \xi H_0^{(1)}(\xi\rho) \frac{e^{i\sqrt{k^2 - \xi^2}|z|}}{\sqrt{k^2 - \xi^2}} d\xi, \quad (10)$$

with the path defined in Fig. 5.4.3 [see also Fig. 5.3.6(a)]. Since the branch cuts have been chosen so that $\text{Im } \sqrt{k^2 - \xi^2} > 0$ on the entire top sheet of the Riemann surface [see Fig. 5.3.3(a)], the exponential term in Eq. (10) decays

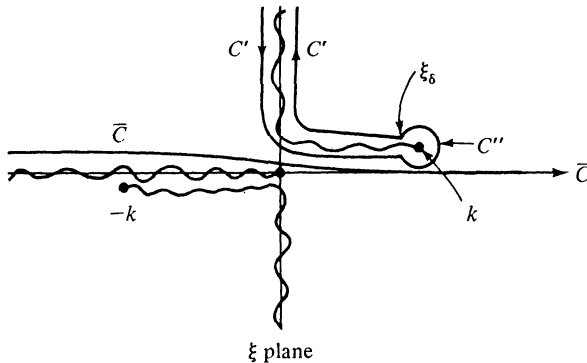


FIG. 5.4.3 Contours employed for alternative representations.

everywhere at $|\xi| \rightarrow \infty$. Since $H_0^{(1)}(\xi\rho)$ decays exponentially when $|\xi| \rightarrow \infty$, $\text{Im } \xi > 0$ [see Eq. (5.3.13b)], the contour \bar{C} can be deformed for any ρ and $|z|$ away from the origin into the contour $C' + C''$ enclosing the upper branch cut. C'' is a circular contour centered at $\xi = k$ with a small, but finite, radius $\delta = |\xi_\delta - k|$. Although the integrand in Eq. (10) grows like $1/\sqrt{\delta}$ on C'' , the

integral itself is $O(\sqrt{\delta})$, as can be verified upon expanding the regular portion of the integrand in a power series about $\xi = k$ and carrying out the integration over C' . Hence, the contribution from the integration over C'' vanishes as $\delta \rightarrow 0$.

Upon introducing the change of variable

$$\zeta = \sqrt{k^2 - \xi^2}, \quad \text{i.e., } \xi d\xi = -\zeta d\zeta,$$

in the remaining integral over C' (with $\delta = 0$), one notes that ζ is real and varies from $+\infty$ to $-\infty$ as ξ moves along C' in the direction shown in Fig. 5.4.3 [see Fig. 5.3.3(a) for determination of the sign of $\operatorname{Re} \zeta$]. Thus, Eq. (10) transforms into

$$G_f = \frac{i}{8\pi} \int_{-\infty}^{+\infty} H_0^{(1)}[\sqrt{k^2 - \zeta^2}\rho] e^{i\zeta|z|} d\zeta, \quad (11)$$

where the restriction $\operatorname{Im} \sqrt{k^2 - \zeta^2} > 0$ must be imposed to assure the decay of the Hankel function as $|\zeta| \rightarrow \infty$, and $\sqrt{k^2 - \zeta^2}$ is chosen positive for $-k < \zeta < k$. The path of integration relative to the branch points at $\zeta = \pm k$ proceeds in the same manner as shown in Fig. 5.4.3 for the ζ plane. Upon changing ζ into $(-\zeta)$ in Eq. (11), one obtains the same integral except that $\exp(i\zeta|z|)$ is replaced by $\exp(-i\zeta|z|)$. Thus, the algebraic sign of the exponent is of no consequence and we may replace $|z|$ by z .

The various representations for G_f in the parameter range $0 < \rho < \infty$, $-\infty < z < \infty$, obtained in Eqs. (2b), (10), (11), and (5.2.7) are summarized below for the case where the source point is situated at $\rho' = z' = 0$ and for an $\exp(-i\omega t)$ time dependence:

$$G_f(r, 0) = \frac{e^{ik\sqrt{\rho^2 + z^2}}}{4\pi\sqrt{\rho^2 + z^2}}, \quad (12a)$$

$$G_f(r, 0) = \frac{i}{8\pi^2} \int_{-\infty}^{\infty} \int_{-\infty}^{\infty} \frac{e^{i(\xi x + ny) + i\sqrt{k^2 - \xi^2 - \eta^2}|z|}}{\sqrt{k^2 - \xi^2 - \eta^2}} d\xi d\eta, \quad (12b)$$

$$G_f(r, 0) = \frac{i}{8\pi} \int_{\infty \exp(i\pi)}^{\infty} \xi H_0^{(1)}(\xi\rho) \frac{e^{i\sqrt{k^2 - \xi^2}|z|}}{\sqrt{k^2 - \xi^2}} d\xi, \quad (12c)$$

$$G_f(r, 0) = \frac{i}{8\pi} \int_{-\infty}^{\infty} H_0^{(1)}[\sqrt{k^2 - \zeta^2}\rho] e^{i\zeta z} d\zeta. \quad (12d)$$

Equation (12a) is the closed-form result, Eqs. (12b) and (12c) are z -transmission modal representations involving plane-wave and cylindrical-wave mode functions, respectively, in the cross-sectional domain, while Eq. (12d) is a radial transmission formulation involving a plane-wave modal representation in the z domain. Equation (12b) is the most cumbersome since it involves a double integral. The more convenient integral representations in Eqs. (12c) and (12d) have different convergence properties. In the z -transmission representation in Eq. (12c), the integrand decays rapidly for $|\xi| > k$ when $|z|$ is large, while in the radial transmission formulation in Eq. (12d), the integrand decays rapidly for $|\zeta| > k$ when ρ is large. Although these properties are inconsequential in

the present instance where an exact solution is known in closed form, analogous considerations are important for more general problems that cannot be solved explicitly. Moreover, the radial transmission formulation is frequently more useful for the derivation of results appropriate to a source distributed along z . In this case, one first replaces z by $z - z'$ in Eqs. (12) to obtain the expression for a point source at z' . If the source distribution ranges between the limiting values z_1 and z_2 along the z direction, then $|z - z'|$ must be represented discontinuously for observation points z lying in the interval $z_1 < z < z_2$; that is $|z - z'| = \pm(z - z')$ for $z \gtrless z'$. The integration over z' required for the response to the distributed source is then performed more conveniently in Eq. (12d) than in Eq. (12c), since the former has a dependence on $z - z'$ which does not require a breakup of the integration interval into regions $z' < z$ and $z' > z$.

Pulsed electric source current density

$$\hat{\mathbf{j}}(\mathbf{r}, t) = \hat{p}\delta(\mathbf{r}) \frac{d}{dt} \delta(t) \mathbf{z}_0. \quad (13)$$

The fields excited by this source distribution with impulsive *dipole moment* $\hat{\mathbf{p}}(\mathbf{r}, t) = \hat{p}\delta(\mathbf{r})\delta(t)\mathbf{z}_0$ can be derived via Eqs. (5.2.18) (with $\hat{G}' = \hat{G}_f$) from the space- and time-dependent Green's function defined by

$$\left(\nabla^2 - \frac{1}{c^2} \frac{\partial^2}{\partial t^2} \right) \hat{G}_f(\mathbf{r}, \mathbf{r}'; t, t') = -\delta(\mathbf{r} - \mathbf{r}')\delta(t - t'), \quad \bar{c} = \frac{1}{\sqrt{\mu\epsilon}}, \quad (14a)$$

subject to quiescence when $t < t'$. The solution for $\mathbf{r}' = 0, t' = 0$, is given by

$$G_f(\mathbf{r}, \mathbf{r}'; t, t') = \frac{\delta(t - r/\bar{c})}{4\pi r}, \quad (14b)$$

and follows at once from Eqs. (2) and (5.2.19) [with $A = (1/4\pi r)\delta(\tau - r/\bar{c})$] [see also Eqs. (1.1.15)]. The (scalar) disturbance is spherically symmetric about the source (see Fig. 5.4.2), propagates outward with velocity \bar{c} , and at r has a functional dependence on time identical with that at the source (Fig. 5.4.4).

If the source is moved to infinity along the x axis so that the incident field is in the form of a plane wave propagating along the x direction, the steady-state behavior for the $\exp(j\omega t)$ variation is expressed in terms of the potential

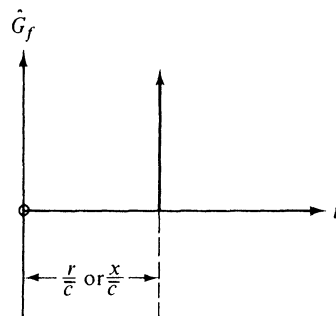


FIG. 5.4.4 Impulsive scalar point source or plane-wave response observed at a distance r and x , respectively.

function $G = \exp(-jk|x|)$. Since the k dependence in this expression is the same as in Eq. (2b), it is concluded that the field of an impulsive plane wave is characterized by the potential function (see Fig. 5.4. 4.),†

$$\hat{G}_f(x, t) = \delta\left(t - \frac{|x|}{c}\right). \quad (15)$$

Magnetic dipole source

The fields for the time-harmonic magnetic current density

$$\hat{\mathbf{M}}(\mathbf{r}, t) = Vl\delta(\mathbf{r})e^{-i\omega t}\mathbf{z}_0, \quad (16)$$

where V is the voltage across the element and l is its length, are derived from the H -mode Green's function $G'' = G_f$, in Eqs. (2) since in an unbounded medium, the E - and H -mode Green's functions satisfy the same boundary conditions (radiation condition at infinity) and are therefore identical. The results are dual to those obtained for the electric dipole ($E \rightarrow H$, $H \rightarrow -E$, $I \rightarrow V$, $\mu \leftrightarrow \epsilon$). A similar statement applies to the pulsed excitation.

5.4b Dipoles Oriented Transverse to z

Time-harmonic electric source current density

$$\hat{\mathbf{J}}(\mathbf{r}, t) = Il\delta(\mathbf{r})e^{-i\omega t}\mathbf{y}_0. \quad (17)$$

Evaluation of the fields is carried out in terms of the steady-state scalar functions $\mathcal{S}' = \mathcal{S}'' = \mathcal{S}_f$ defined by [see Eq. (5.2.2)]

$$(\nabla^2 + k^2)\nabla_t^2 \mathcal{S}_f(\mathbf{r}, \mathbf{r}') = \delta(\mathbf{r} - \mathbf{r}'), \quad k^2 = \omega^2\mu\epsilon, \quad (18)$$

subject to a radiation condition at infinity. The following solutions obtain for $\mathbf{r}' = 0$ [see Eq. (2b)]:

$$\nabla_t^2 \mathcal{S}_f(\mathbf{r}, \mathbf{r}') = -\frac{e^{ik\sqrt{\rho^2+z^2}}}{4\pi\sqrt{\rho^2+z^2}}, \quad r = \sqrt{\rho^2+z^2}, \quad \rho = \sqrt{x^2+y^2}, \quad (19a)$$

and, by direct integration [see Eq. (2l)],

$$\frac{\partial \mathcal{S}_f}{\partial \rho} = \frac{i}{4\pi k\rho} \left[e^{ik\sqrt{\rho^2+z^2}} - e^{ik|z|} \right]. \quad (19b)$$

The electromagnetic fields may be calculated from $\nabla_t' \mathcal{S}_f(\mathbf{r}, \mathbf{r}') = -\nabla_t \mathcal{S}_f(\mathbf{r}, \mathbf{r}') = -\mathbf{p}_0(\partial/\partial\rho)\mathcal{S}_f(\mathbf{r}, \mathbf{r}')$ via Eqs. (5.2.4a), (5.2.4b) and (5.2.1a), (5.2.1b). (Note: $\partial/\partial z' \rightarrow -\partial/\partial z$, and $\mathbf{x}_0 \cdot \mathbf{p}_0 = x/\rho$, $\mathbf{y}_0 \cdot \mathbf{p}_0 = y/\rho$). One finds for the x component of the magnetic field at the point $\mathbf{r} = (x, y, z)$,

$$H_x = H'_x + H''_x, \quad (20)$$

where H'_x is the E -mode contribution,

$$H'_x = Il \left[\frac{x^2 - y^2}{4\pi\rho^4} \left(e^{ikz} - \frac{z}{r} e^{ikr} \right) + \frac{y^2 z e^{ikr}}{4\pi\rho^2 r^2} \left(\frac{1}{r} - ik \right) \right], \quad (20a)$$

†Note from Eqs. (7) and (5.2.6b) that $G = \exp(-jk|x|)$ satisfies the equation $[d^2/dx^2 + k^2]G = -2jk\delta(x)$, whence in view of $k = \omega/c$, $j\omega \rightarrow (\partial/\partial t)$, the source giving rise to \hat{G}_f in Eq. (15) is $(2/c)\delta(x) d\delta(t)/dt$.

and H''_x is the H -mode contribution,

$$H''_x = Il \left[\frac{y^2 - x^2}{4\pi\rho^4} \left(e^{ikz} - \frac{z}{r} e^{ikr} \right) + \frac{x^2 z e^{ikr}}{4\pi\rho^2 r^2} \left(\frac{1}{r} - ik \right) \right], \quad (20b)$$

or, upon combining,

$$H_x = \frac{ze^{ikr} Ikl}{4\pi r^2} \left(\frac{1}{kr} - i \right). \quad (20c)$$

Analogous expressions are obtained for the other field components. The radiated power density is the same as for the z -directed current element in Eqs. (4) and (5) except that θ is now measured from the positive x axis. The physical interpretation of the result is the same as in Fig. 5.4.2.

Discussion

While the total fields in the present case are identical with those in Eqs. (3), provided that the y axis is chosen as the polar axis of the spherical coordinate system, the calculation shows that both E modes and H modes with respect to a preferred direction are excited by a transverse current element.⁶ The results become significant when the medium is stratified along the z direction since the E - and H -mode constituents of the fields are then affected unequally (i.e., $\mathcal{S}' \neq \mathcal{S}''$). Moreover, fields radiated by a current element transverse to the optic axis in a uniaxially anisotropic region may be inferred by applying to Eqs. (20a) and (20b) different coordinate scaling transformations, thereby necessitating the availability of these explicit formulas (see Sec. 7.2c).

Equation (19b) is obtained from Eq. (19a) by recognizing that, in view of the rotational symmetry of \mathcal{S}_f with respect to the z axis, $\nabla_t^2 = (1/\rho)(\partial/\partial\rho) \cdot (\rho\partial/\partial\rho)$. Thus, by integration, noting that $\partial\mathcal{S}_f/\partial\rho$ is bounded at $\rho = 0$,

$$\rho \frac{\partial\mathcal{S}_f}{\partial\rho} = - \int_0^\rho \rho \frac{e^{ik\sqrt{\rho^2+z^2}}}{4\pi\sqrt{\rho^2+z^2}} d\rho = \frac{i}{4\pi k} \int_0^\rho \frac{d}{d\rho} [e^{ik\sqrt{\rho^2+z^2}}] d\rho, \quad (21)$$

thereby confirming the result in Eq. (19b). It may also be noted that with g_{st} given by Eq. (7), the resulting integrals in Eqs. (5.2.12) may be evaluated in closed form via Eq. (19b). (Note: $j \rightarrow -i$.)

Time-harmonic magnetic source current density

$$\hat{\mathbf{M}}(\mathbf{r}, t) = Vl\delta(\mathbf{r})e^{-i\omega t}\mathbf{y}_0. \quad (22)$$

The results in this case are obtainable from those for the electric current element by the duality replacements $E \rightarrow H$, $H \rightarrow -E$, $I \rightarrow V$, and $\mu \leftrightarrow \epsilon$.

Pulsed electric or magnetic source currents

These problems are treated in detail in Sec. 1.1b [see Eqs. (1.1.43)–(1.1.46)].

5.4c Line Currents Oriented Transverse to z

Time-harmonic electric source current density

$$\hat{\mathbf{J}}(\mathbf{r}, t) = I\delta(\hat{\mathbf{p}} - \hat{\mathbf{p}}')e^{-i\omega t}\mathbf{x}_0. \quad (23)$$

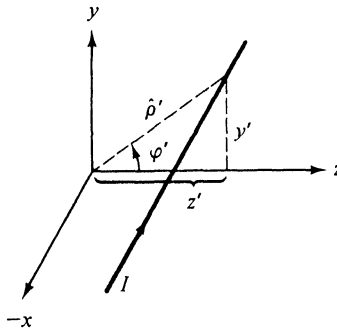


FIG. 5.4.5 Line source.

The electromagnetic fields of a source oriented as in Fig. 5.4.5 are derived from the two-dimensional Green's function \bar{G}_f , which satisfies the differential equation [two-dimensional analogue of Eq. (5.2.3b)]

$$(\nabla^2 + k^2)\bar{G}_f(\hat{\mathbf{p}}, \hat{\mathbf{p}}') = -\delta(\hat{\mathbf{p}} - \hat{\mathbf{p}}'),$$

$$\hat{\mathbf{p}} = (y, z) = (\hat{\rho}, \varphi), \quad \frac{\partial}{\partial x} \equiv 0, \quad (24)$$

subject to a radiation condition at infinity. The solution is given by

$$\bar{G}_f(\hat{\mathbf{p}}, \hat{\mathbf{p}}') = \frac{i}{4} H_0^{(1)}(k|\hat{\mathbf{p}} - \hat{\mathbf{p}}'|), \quad (25)$$

where $k = \omega\sqrt{\mu\epsilon}$. For $\hat{\mathbf{p}}' = 0$, the fields are

$$E_x = i\omega\mu I \bar{G}_f = -\frac{\omega\mu}{4} I H_0^{(1)}(k\hat{\rho}), \quad E_\rho = E_\varphi = 0, \quad (26a)$$

$$H_\varphi = -\frac{i}{\omega\mu} \frac{\partial E_x}{\partial \hat{\rho}} = -\frac{ik}{4} I H_1^{(1)}(k\hat{\rho}), \quad H_\rho = H_z = 0, \quad (26b)$$

where I is the source current and $\hat{\rho}$ and φ represent polar coordinates in the yz plane. (Note the cyclic order: $\mathbf{x}_0 \times \varphi_0 = \hat{\mathbf{p}}_0$.) The radiated power density \tilde{S} per unit length along x is

$$\tilde{S}_\rho = \operatorname{Re}(E_x H_\varphi^*) = \sqrt{\frac{\mu}{\epsilon}} \frac{k}{8\pi\hat{\rho}} |I|^2, \quad (27a)$$

$$\tilde{S}_\varphi = \tilde{S}_x \equiv 0, \quad (27b)$$

and the total radiated power P per unit length along x ,

$$P = \sqrt{\frac{\mu}{\epsilon}} \frac{k}{4} |I|^2. \quad (28)$$

The asymptotic field solution at large distance from the source is obtained upon replacing the Hankel functions by their large-argument approximation in Eq. (5.3.13b):

$$E_x \sim -\frac{\omega\mu I}{2\sqrt{2\pi k}\hat{\rho}} e^{i(k\hat{\rho}-\pi/4)} \left[1 + O\left(\frac{1}{k\hat{\rho}}\right) \right], \quad (29a)$$

$$H_\varphi \sim -\frac{1}{2} \sqrt{\frac{k}{2\pi\hat{\rho}}} I e^{i(k\hat{\rho}-\pi/4)} \left[1 + O\left(\frac{1}{k\hat{\rho}}\right) \right]. \quad (29b)$$

The inclusion of a phase progression in the transverse current distribution in Eq. (23) leads to a more complicated description [see Eqs. (5.2.1) and (5.2.14)] which is avoided by the alternative coordinate orientation in Eq. (45) (see also Sec. 5.4e).

Normalization for plane-wave incidence

As in Eqs. (6), we can readily formulate the rule for passing from the line-source excitation in Eq. (23) to a plane-wave excitation by letting the source point $\hat{\rho}' \rightarrow \infty$. Since

$$|\hat{\rho} - \hat{\rho}'| = [\hat{\rho}^2 + \hat{\rho}'^2 - 2\hat{\rho}\hat{\rho}' \cos(\varphi - \varphi')]^{1/2}, \quad (30a)$$

one obtains, upon use of Eq. (5.3.13b) in Eq. (25), by considerations analogous to those leading from Eq. (6a) to Eq. (6b),

$$\begin{aligned} \bar{G}_f(\hat{\rho}, \hat{\rho}') &\sim A \exp[-ik\hat{\rho} \cos(\varphi - \varphi')], \\ A &= \frac{1}{4} \sqrt{\frac{2}{\pi k \hat{\rho}'}} \exp\left[i\left(k\hat{\rho}' + \frac{\pi}{4}\right)\right], \quad \hat{\rho}' \rightarrow \infty. \end{aligned} \quad (30b)$$

The term $\exp[-ik\hat{\rho} \cos(\varphi - \varphi')]$ in Eq. (30b) represents a plane wave of unit amplitude incident along the direction φ' . Thus, to pass from a result derived for a *unit* strength line source located at $\hat{\rho}'$ to the result for a *unit* amplitude plane wave incident along the direction φ' , one first lets $\hat{\rho}' \rightarrow \infty$ and then sets $A = 1$.

Discussion

The configuration in Fig. 5.4.5 follows from that in Fig. 5.2.1 when the current elements are oriented along the line axis. The electric field generated by the line source has a single axial component, whereas the magnetic field is circular about the source axis. Energy flows out radially from the source and the energy transport mechanism may be schematized as in Fig. 5.4.2, with the dipole replaced by the line current. The far fields decay according to $\hat{\rho}^{-1/2}$, characteristic for the two-dimensional case.

While transverse currents generally excite both *E* and *H* modes with respect to *z*, the lack of a phase progression along the source implies that $\partial/\partial x = \partial/\partial x' = 0$ in Eqs. (5.2.1) or (5.2.4a), (5.2.4b), with \mathcal{S}' and \mathcal{S}'' replaced by their two-dimensional analogues $\bar{\mathcal{S}}' = \bar{\mathcal{S}}'' = \bar{\mathcal{S}}_f$ in Eqs. (5.2.14) (with $\alpha = 0$). It then follows that the *E*-mode Hertz potential $\bar{\Pi}'(\mathbf{r}, \hat{\rho}) = 0$, and the *H*-mode potential

$$\bar{\Pi}''(\mathbf{r}, \hat{\rho}') = I \frac{\partial}{\partial y'} \bar{\mathcal{S}}_f(\mathbf{r}, \hat{\rho}'). \quad (31)$$

Thus, from Eqs. (5.2.1),

$$\mathbf{E} = -\mathbf{x}_0 j \omega \mu I \frac{\partial^2}{\partial y \partial y'} \bar{\mathcal{S}}_f = \mathbf{x}_0 j \omega \mu I \frac{\partial^2 \bar{\mathcal{S}}_f}{\partial y^2} = -\mathbf{x}_0 j \omega \mu I \bar{G}_f, \quad (31a)$$

thereby confirming Eq. (26a) (with $j \rightarrow -i$). Similarly, Eq. (26b) follows from

$$\mathbf{H} = -I \left(\mathbf{y}_0 \frac{\partial}{\partial z} - \mathbf{z}_0 \frac{\partial}{\partial y} \right) \frac{\partial^2 \bar{G}_f}{\partial y^2} = -I \mathbf{x}_0 \times \hat{\nabla}_t \bar{G}_f. \quad (31b)$$

The solution in Eq. (25) may be obtained by direct integration of Eq. (24). With $\hat{\rho}' = 0$, \bar{G}_f is recognized to be symmetrical about $\hat{\rho} = 0$, so $\nabla^2 \rightarrow (\partial/\hat{\rho}\partial\hat{\rho})(\hat{\rho}\partial/\partial\hat{\rho})$. For $\hat{\rho} \neq 0$, Eq. (24) is solved by

$$\bar{G}_f(\hat{\rho}) = AH_0^{(1)}(k\hat{\rho}) + BH_0^{(2)}(k\hat{\rho}), \quad (32a)$$

where A and B are constants. To satisfy the radiation condition at infinity for an assumed time dependence $\exp(-i\omega t)$, we must retain only the function $H_0^{(1)}(k\hat{\rho})$ [see Eqs. (5.3.13)], so $B = 0$. For evaluation of A , Eq. (24) is integrated over a circular region S with radius $\hat{\rho}$, where $\hat{\rho} \rightarrow 0$. Since

$$H_0^{(1)}(k\hat{\rho}) \rightarrow i \frac{2}{\pi} \ln \hat{\rho}, \quad \hat{\rho} \rightarrow 0, \quad (32b)$$

one notes that, as $\hat{\rho} \rightarrow 0$,

$$-1 = \int_S (\nabla^2 + k^2) \bar{G}_f dS = \oint_s \frac{\partial \bar{G}_f}{\partial \hat{\rho}} ds = i4A, \quad (32c)$$

where s is the circumference of the circular region S . Thus, $A = i/4$, and $\bar{G}_f(\hat{\rho}) = (i/4)H_0^{(1)}(k\hat{\rho})$. Equation (25) follows upon shifting the source point to an arbitrary location $\hat{\rho}'$. Correspondingly, for the $\exp(+j\omega t)$ dependence, $\bar{G}_f(\hat{\rho}) = -(j/4)H_0^{(2)}(k\hat{\rho})$.

Modal procedure

Since the source distribution is comprised of transverse electric currents, the modal network problem may be schematized as in Fig. 5.4.6. The resulting modal Green's function is the same as in Eq. (7), so from Eq. (5.2.13a),

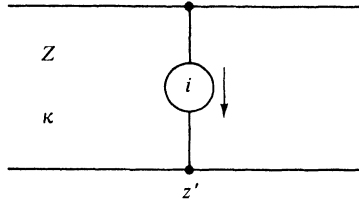


FIG. 5.4.6 Modal network problem.

$$\bar{G}_f(\hat{\rho}, \hat{\rho}') = \frac{-j}{4\pi} \int_{-\infty}^{\infty} \frac{\exp[-j\eta(y - y') - j\sqrt{k^2 - \eta^2}|z - z'|]}{\sqrt{k^2 - \eta^2}} d\eta. \quad (33)$$

The path of integration proceeds relative to the branch points at $\eta = \pm k$ as in Fig. 5.3.5 (a); the branch point at $\eta = 0$ in the figure is absent in this case. Upon transforming variables $\eta = k \sin \varphi$, and employing the polar coordinates

$$y - y' = R \sin \varphi, \quad |z - z'| = R \cos \varphi, \quad 0 < \varphi < \frac{\pi}{2}, \quad (34)$$

one obtains the contour-integral representation

$$\left(-\frac{j}{4} H_0^{(2)}(k|\hat{\mathbf{p}} - \hat{\mathbf{p}}'|) \right) \equiv -\frac{j}{4} H_0^{(2)}(kR), \quad (35a)$$

$$\bar{G}_f(\hat{\mathbf{p}}, \hat{\mathbf{p}}') = \begin{cases} -\frac{j}{4\pi} \int_{\bar{P}} e^{-jkR \cos(w-\varphi)} dw, \\ -\frac{j}{4\pi} \int_{\bar{P}} e^{-jkR \cos w} dw. \end{cases} \quad (35b)$$

The path \bar{P} in the complex w plane is shown in Fig. 5.3.5(b). If one introduces $w - \varphi$ as a new variable in Eq. (35b), one obtains the representation in Eq. (35c). Since $0 < \varphi < \pi/2$ and the integrand contains no singularities [i.e., the branch cut in Fig. 5.3.5(b) is absent], the path \bar{P} is equivalent to any contour which begins in the w plane in the section $0 > \operatorname{Re} w > -\pi$, $\operatorname{Im} w < 0$, and ends in the section $0 < \operatorname{Re} w < \pi$, $\operatorname{Im} w > 0$. The right-hand side of Eq. (35c) is independent of φ , as it must be in view of the closed-form result in Eq. (35a). The integral representation (35c) and that in Eq. (36c) below for the Hankel function was first derived by Sommerfeld (for a detailed discussion see reference 7).

Upon starting from the $\exp(-i\omega t)$ formulation, one deduces, in a similar manner,

$$\left(-\frac{i}{4} H_0^{(1)}(kR), \right) \quad (36a)$$

$$\bar{G}_f(\hat{\mathbf{p}}, \hat{\mathbf{p}}') = \frac{i}{4\pi} \int_{-\infty}^{\infty} \frac{\exp[i\eta(y-y') + i\sqrt{k^2 - \eta^2}|z-z'|]}{\sqrt{k^2 - \eta^2}} d\eta, \quad (36b)$$

$$\left(\frac{i}{4\pi} \int_{\bar{P}} e^{ikR \cos w} dw, \right) \quad (36c)$$

where the contours of integration in Eqs. (36b) and (36c) are the same as those in Figs. 5.3.6(a) and 5.3.6(b), respectively. Via the integral expressions in Eqs. (35) and (36), the outgoing cylindrical waves as given by the Hankel functions are represented as a superposition of plane waves with complex angles of incidence.

From an asymptotic evaluation of the Sommerfeld integral representations in Eqs. (35c) and (36c), one readily derives by considerations analogous to those following Eq. (5.3.14) the first-order asymptotic formulas in Eqs. (5.3.13). For a complete asymptotic expansion of $H_0^{(1)}(kR)$ for large values of kR , one employs Eqs. (4.2.18) instead of the first-order asymptotic approximation in Eq. (4.2.1a). Upon introducing into Eq. (36c) the change of variable $\cos w = 1 + is^2$, $-\infty < s < \infty$, one obtains, via Eq. (4.2.18a),

$$\begin{aligned} H_0^{(1)}(kR) &= \frac{1}{\pi} \int_{\bar{P}} e^{ikR \cos w} dw = \frac{1}{\pi} e^{ikR} \int_{-\infty}^{\infty} G(s) e^{-kRs^2} ds \\ &\sim \frac{e^{ikR}}{\pi} G_e \left[\sqrt{-\frac{d}{d(kR)}} \right] \sqrt{\frac{\pi}{kR}}. \end{aligned} \quad (37a)$$

From Eqs. (4.2.27a) and (4.2.30c), $G(s) = dw/ds = \sqrt{2} e^{-is/4} [1 - (is^2/2)]^{-1/2}$, whence, from Eq. (4.2.18c),

$$G_e \left[\sqrt{-\frac{d}{d(kR)}} \right] = \sqrt{2} e^{-is/4} \left[1 + \frac{i}{4} \frac{d}{d(kR)} - \frac{3}{32} \frac{d^2}{d(kR)^2} + \dots \right]. \quad (37b)$$

Time-harmonic electric source current density

$$\hat{\mathbf{J}}(\mathbf{r}, t) = I \delta(\hat{\mathbf{p}} - \hat{\mathbf{p}}') e^{-i\omega t} \mathbf{z}_0. \quad (38)$$

The electromagnetic fields for a \mathbf{z}_0 -directed line-source configuration at $\hat{\mathbf{p}}'$ are derived from the Green's function $\tilde{G}_f(\hat{\mathbf{p}}, \hat{\mathbf{p}}')$ in Eq. (25). For $\hat{\mathbf{p}}' = 0$, the fields are as follows:

$$H_x = I \frac{\partial}{\partial y} \tilde{G}_f(\hat{\mathbf{p}}, \hat{\mathbf{p}}') = -\frac{ik}{4} \sin \varphi H_1^{(1)}(k\hat{\rho}), \quad H_y = H_z = 0, \quad (39a)$$

$$E_\beta = -\frac{i}{\omega \epsilon \hat{\rho}} \frac{\partial H_x}{\partial \varphi}, \quad E_\varphi = \frac{i}{\omega \epsilon} \frac{\partial H_x}{\partial \hat{\rho}}, \quad E_x = 0. \quad (39b)$$

$\hat{\rho} = \sqrt{y^2 + z^2}$ is the distance from the source to the observation point, and φ is the angle between $\hat{\rho}$ and the positive z axis. Asymptotic solutions for the field are obtained by substitution of the formula in Eq. (5.3.13b).

Discussion

The configuration in Fig. 5.4.7 follows from that in Fig. 5.2.1 when the current elements are oriented along z . The fields are not symmetrical about the line-source axis but exhibit a pattern similar to that for the point dipole in Eqs. (3). Energy into the far field is transported along straight-line trajectories emanating radially from the source (see Fig. 5.4.2). Since the electric currents in Eq. (38) are longitudinal, only E modes with respect to z are excited and the Hertz potential function $\tilde{\Pi}'(\mathbf{r}, \hat{\mathbf{p}}')$ is proportional to $\tilde{G}_f(\hat{\mathbf{p}}, \hat{\mathbf{p}}')$ [see Eq. (5.2.4c)]. Equations (39) then follow directly from Eqs. (5.2.1a) and (5.2.1b).

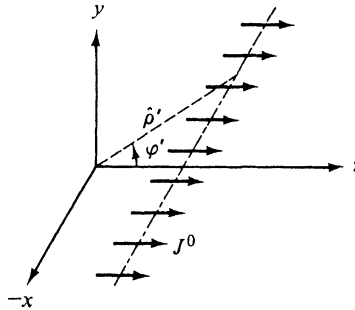


FIG. 5.4.7 Dipole line source.

In this instance a modal-analysis procedure involves the network problem schematized in Fig. 5.4.8 and leads to an integral representation as in Eq. (33).

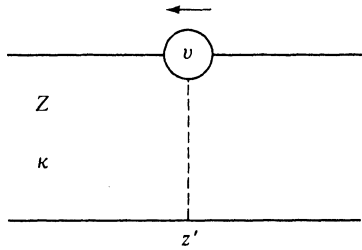


FIG. 5.4.8 Modal network problem.

Time-harmonic magnetic current density

Problems involving the magnetic current densities

$$\hat{\mathbf{M}}(\mathbf{r}, t) = V\delta(\hat{\mathbf{p}} - \hat{\mathbf{p}}')e^{-i\omega t}\mathbf{z}_0, \quad (40a)$$

or

$$\hat{\mathbf{M}}(\mathbf{r}, t) = V\delta(\hat{\mathbf{p}} - \hat{\mathbf{p}}')e^{-i\omega t}\mathbf{z}_0, \quad (40b)$$

are dual to the corresponding cases in Eqs. (23) and (38), respectively. Results are obtained via the duality replacements $E \rightarrow H$, $H \rightarrow -E$, and $I \rightarrow V$. Also, the modal network problems in Figs. 5.4.6 and 5.4.8 are interchanged.

Pulsed source currents

Since the time-harmonic fields excited by the current distributions in Eqs. (23), (38), (40a) and (40b) are derivable from the Green's function $\tilde{G}_f(\hat{\mathbf{p}}, \hat{\mathbf{p}}')$ in Eq. (25), the transient fields may be obtained from a knowledge of the corresponding time-dependent Green's function $\hat{G}_f(\hat{\mathbf{p}}, \hat{\mathbf{p}}'; t, t')$, which satisfies the differential equation

$$\left(\frac{\partial^2}{\partial y^2} + \frac{\partial^2}{\partial z^2} - \frac{1}{\bar{c}^2} \frac{\partial^2}{\partial t^2} \right) \hat{G}_f(\hat{\mathbf{p}}, \hat{\mathbf{p}}'; t, t') = -\delta(\hat{\mathbf{p}} - \hat{\mathbf{p}}')\delta(t - t'),$$

$$\bar{c} = \frac{1}{\sqrt{\mu\epsilon}} \quad (41)$$

subject to quiescence when $t < t'$. The solution for $t' = 0$, $\hat{\mathbf{p}}' = 0$, is

$$\hat{G}_f = \begin{cases} \frac{1}{2\pi} \frac{1}{\sqrt{t^2 - (\hat{\mathbf{p}}/\bar{c})^2}}, & t > \frac{\hat{\mathbf{p}}}{\bar{c}}, \\ 0, & t < \frac{\hat{\mathbf{p}}}{\bar{c}}, \end{cases} \quad (42a)$$

$$(42b)$$

where $\hat{\mathbf{p}} = \sqrt{y^2 + z^2}$. The solution for arbitrary $\hat{\mathbf{p}}'$, t' is obtained by the replacements $\hat{\mathbf{p}} \rightarrow |\hat{\mathbf{p}} - \hat{\mathbf{p}}'|$, $t \rightarrow t - t'$. For example, when the source configuration in Fig. 5.4.7 has the temporal dependence

$$\hat{\mathbf{J}}(\mathbf{r}, t) = \delta(\hat{\mathbf{p}})I(t)\mathbf{z}_0, \quad I(t) = \frac{d\hat{\mathbf{p}}(t)}{dt} = \hat{\mathbf{p}} \frac{d}{dt} \delta(t), \quad (43)$$

where $\hat{\mathbf{p}}$ is the dipole moment strength, it follows from Eqs. (39) (see also Sec. 5.2c) that the transient fields are given by

$$\hat{H}_x = \hat{p} \frac{\partial^2}{\partial t \partial y} \hat{G}_f, \quad \hat{E}_\rho = -\hat{p} \frac{1}{\epsilon \hat{\rho}} \frac{\partial^2}{\partial \phi \partial y} \hat{G}_f, \quad \hat{E}_\phi = \hat{p} \frac{1}{\epsilon} \frac{\partial^2}{\partial \hat{\rho} \partial y} \hat{G}_f. \quad (44)$$

[Note that $(\partial^2/\partial \phi \partial y) \neq (\partial^2/\partial y \partial \phi)$ since $y = y(\hat{\rho}, \phi)$.] The fields due to the other source arrangements may be obtained in a similar manner.

\hat{G}_f in Eqs. (42) represents a cylindrically symmetrical disturbance spreading outward from the source with speed \bar{c} and reaching an observation point $\hat{\rho}$ at a time $t = \hat{\rho}/\bar{c}$. Although the action of the source is confined to the instant $t = 0$, a response of decreasing intensity persists at $\hat{\rho}$ after the passing of the initial wave front (Fig. 5.4.9).

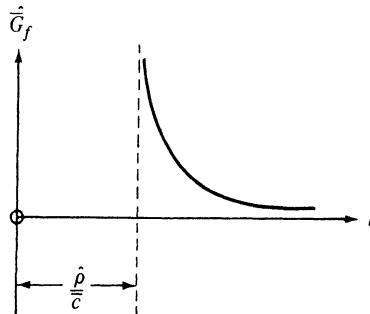


FIG. 5.4.9 Pulsed scalar line-source response observed at a distance $\hat{\rho}$.

The solution in Eq. (42) may be deduced directly by the method described in Sec. 5.2c. From the integral representation for the time-harmonic Green's function in Eq. (35c) with $\hat{\rho}' = 0$, one identifies $\bar{\alpha} = 0$, $L = \hat{\rho}$, $f(w) = -j/4\pi$ in Eq. (5.2.20). The transient result then follows from Eqs. (5.2.19) and (5.2.23) (see also Sec. 1.6b).

5.4d Line Currents Oriented Along z

Time-harmonic electric current density

$$\hat{\mathbf{J}}(\mathbf{r}, t) = I \delta(\mathbf{p} - \mathbf{p}') e^{i\alpha z} e^{-i\omega t} \mathbf{z}_0. \quad (45)$$

Since the current distribution is oriented along z , the fields may be derived from the scalar Green's function

$$\tilde{G}'(\mathbf{r}, \mathbf{p}') = e^{i\alpha z} \tilde{G}_f(\mathbf{p}, \mathbf{p}'), \quad \mathbf{p} = (x, y) = (\rho, \phi), \quad (46a)$$

where \tilde{G}_f satisfies the differential equation

$$\begin{aligned} (\nabla_t^2 + \hat{\kappa}^2) \tilde{G}_f(\mathbf{p}, \mathbf{p}') &= -\delta(\mathbf{p} - \mathbf{p}'), \quad \hat{\kappa}^2 = k^2 - \alpha^2, \\ \nabla_t^2 &= \frac{1}{\rho} \frac{\partial}{\partial \rho} \rho \frac{\partial}{\partial \rho} + \frac{1}{\rho^2} \frac{\partial^2}{\partial \phi^2}, \end{aligned} \quad (46b)$$

subject to a radiation condition at infinity. The solution for $\mathbf{p}' = 0$ is given via Eq. (25) as

$$\bar{G}_f(\rho, \rho') = \frac{i}{4} H_0^{(1)}(\hat{\kappa}\rho), \quad \text{Im } \hat{\kappa} \geq 0, \quad (47)$$

and the fields are then obtained from Eqs. (5.2.1a), (5.2.1b) and (5.2.4c):

$$E_\rho = \frac{I}{-i\omega\epsilon} \frac{\partial^2 \bar{G}_f}{\partial \rho \partial z} = \frac{I\alpha\hat{\kappa}}{-i4\omega\epsilon} e^{i\alpha z} H_1^{(1)}(\hat{\kappa}\rho), \quad (48a)$$

$$E_z = \frac{I}{i\omega\epsilon} \left[\nabla_i^2 \bar{G}_f + e^{i\alpha z} \delta(\rho - \rho') \right] = \frac{-\hat{\kappa}^2 I}{4\omega\epsilon} e^{i\alpha z} H_0^{(1)}(\hat{\kappa}\rho), \quad (48b)$$

$$H_\phi = \frac{i\hat{\kappa}}{4} I e^{i\alpha z} H_1^{(1)}(\hat{\kappa}\rho), \quad (48c)$$

$$E_\phi = H_\rho = H_z = 0. \quad (48d)$$

When $\alpha = 0$ (i.e., $\hat{\kappa} = k$) one has $E_\rho = 0$, and the expressions for E_z and H_ϕ agree with those for E_x and H_ϕ , respectively, in Eqs. (26), allowance being made for different coordinate designations.

For large values of $|\hat{\kappa}\rho|$, one can employ the asymptotic approximation (5.3.13) for the Hankel functions and obtain for the fields observed at large distances from the source:

$$E_\rho \sim \frac{I\alpha\hat{\kappa}e^{i\pi/4}}{2\omega\epsilon\sqrt{2\pi\hat{\kappa}\rho}} e^{i(\hat{\kappa}\rho + \alpha z)} \sim -\frac{\alpha}{\hat{\kappa}} E_z \sim \frac{\alpha}{\omega\epsilon} H_\phi. \quad (49)$$

Upon defining for $\alpha < k$ an angle ψ and unit vector \mathbf{R}_0 (see Fig. 5.4.10) as

$$\alpha = k \cos \psi, \quad \hat{\kappa} = k \sin \psi, \quad \mathbf{R}_0 = \rho_0 \sin \psi + z_0 \cos \psi, \quad (50)$$

one notes that

$$\mathbf{E} \sim (\mathbf{R}_0 \times \boldsymbol{\phi}_0) \frac{k}{\hat{\kappa}} E_z; \quad \mathbf{H} \sim -\boldsymbol{\phi}_0 \frac{\omega\epsilon}{\hat{\kappa}} E_z \sim \sqrt{\frac{\epsilon}{\mu}} \mathbf{R}_0 \times \mathbf{E}. \quad (51)$$

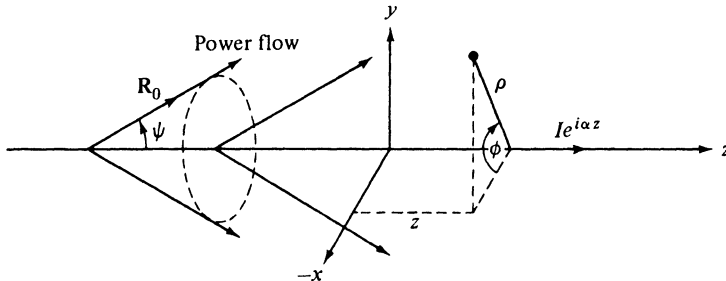


FIG. 5.4.10 Progressively phased line current.

Discussion

The line-source Green's function in Eq. (46a) is related to the point-source Green's function $G_f(\mathbf{r}, \mathbf{r}')$ in Eq. (2) by a continuous superposition of source elements along the z axis:

$$\bar{G}'(\mathbf{r}, \rho') = \int_{-\infty}^{\infty} e^{i\alpha z'} G_f(\mathbf{r}, \mathbf{r}') dz' = \int_{-\infty}^{\infty} e^{i\alpha z'} \frac{e^{ik\sqrt{\rho^2 + (z-z')^2}}}{4\pi\sqrt{\rho^2 + (z-z')^2}} dz', \quad (52)$$

and this integral is expressible in closed form via Eq. (47) [see Eqs. (12a) and (12d), which are Fourier transforms of this result]. The transition from Eq. (5.2.3b) to Eqs. (46) is evident.

The far fields behave locally like plane waves propagating in the \mathbf{R}_0 direction at an angle ψ with the line-source axis. This observation can be highlighted by writing Eq. (49) as

$$E_z \sim A \frac{e^{i\mathbf{k}\cdot\mathbf{R}}}{\sqrt{kR}}, \quad A = -\frac{i\omega\mu \sin \psi e^{-i\pi/4}}{2\sqrt{2\pi}}, \quad (53a)$$

where the propagation vector \mathbf{k} and the distance vector \mathbf{R} are defined as

$$\mathbf{k} = k\mathbf{R}_0, \quad \mathbf{R} = \rho_0\rho + z_0z. \quad (53b)$$

The factor A is a constant for a given line-source distribution, and the factor $1/\sqrt{kR}$ accounts for the cylindrical spreading of the wave as it progresses outward from the source. The wave observed at (ρ, z) appears to originate from a point on the line source that is connected to the observation point by a vector of length R making an angle ψ with the source axis (see Fig. 5.4.10). The angle ψ decreases to zero as $\alpha \rightarrow k$ (i.e., as the phase velocity along the line source approaches that of a wave in free space).

When $\alpha > k$, $\hat{\kappa}$ in Eq. (46b) is imaginary and one must choose $\hat{\kappa} = i\sqrt{\alpha^2 - k^2}$. In this instance, the fields at large distances from the source decay exponentially with ρ . It is to be noted that when $\alpha < k$ the phase velocity along the z direction is given by $v_p = \omega/\alpha > c$, where $c = \omega/k$ is the velocity of light in the medium, while $\alpha > k$ yields $v_p < c$. These ranges of α characterize "fast" and "slow" waves, respectively, as compared with the velocity of light. From the above results it is recognized that fast waves radiate energy into the space surrounding the current distribution, while the energy in the slow waves is confined to the immediate vicinity of the source currents and travels along the direction of current flow [see Eqs. (48), with $\hat{\kappa}$ imaginary, whence E_ϕ and H_ϕ are in time phase, while E_z and H_ϕ are 90° out of phase]. These considerations apply not only to the present problem, wherein the source distribution is specified, but also to diffraction problems, wherein one encounters induced currents with fast or slow phase variations.

The above-described radiation characteristics of the phased line source may also be inferred directly from the wavenumber diagram in Fig. 5.3.7. In the present instance, the longitudinal wavenumber κ has the prescribed value α , so only the intersection of the plane $\kappa = \alpha$ with the surface is relevant. When $\alpha < k$, the $\kappa = \alpha$ plane intersects the wavenumber surface [Fig. 5.4.11(a)], and the plane-wave solutions corresponding to this intersection (i.e., the normals to the sphere) give rise to the conical ray diagram in Fig. 5.4.10. When $\alpha > k$, no intersection occurs [Fig. 5.4.11(b)], thereby eliminating propagating wave solutions with real values of the transverse wavenumber $\hat{\kappa}$.

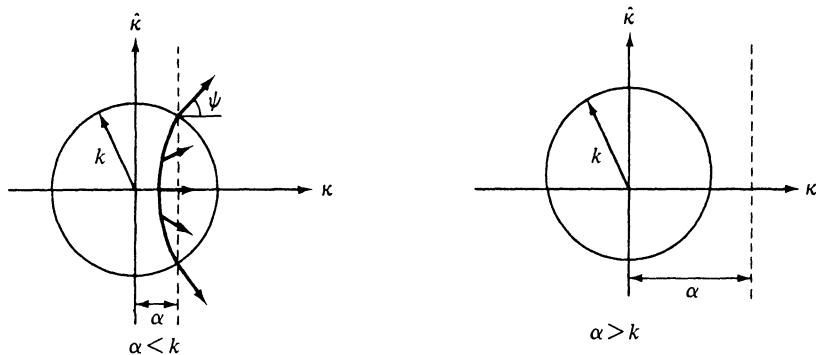
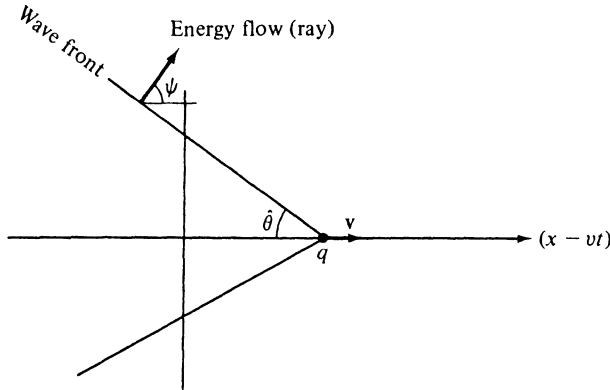


FIG. 5.4.11 Use of wavenumber plot.

5.4e Point Charge in Uniform Straight Motion

$$\hat{\mathbf{J}}(\mathbf{r}, t) = qv\delta(x - vt)\delta(\hat{\mathbf{p}} - \hat{\mathbf{p}}')\mathbf{x}_0. \quad (54)$$

The fields produced by a point charge q moving, as shown Fig. 5.4.12, with constant speed v along a straight-line path parallel to the x axis in a medium

FIG. 5.4.12 Point charge moving in an infinite medium with $\epsilon > c^2/v^2$.

with frequency independent dielectric constant $\epsilon = \bar{\epsilon}\epsilon_0$ and vacuum permeability $\mu = \mu_0$ are derivable from a function $\hat{G}(\mathbf{r}, t)$ which satisfies the differential equation

$$\left(\nabla^2 - \frac{\bar{\epsilon}}{c^2} \frac{\partial^2}{\partial t^2}\right) \hat{G}(\mathbf{r}, t) = -\delta(\hat{\mathbf{p}} - \hat{\mathbf{p}}')\delta\left(t - \frac{x}{v}\right), \quad (55)$$

$$\hat{\mathbf{p}} = (y, z) = (\hat{p}, \varphi)$$

subject to initial conditions discussed subsequently. The solution for $\hat{\mathbf{p}}' = 0$ is given by

$$\hat{G}(\mathbf{r}, t) = \begin{cases} 0, & t - \frac{x}{v} < \frac{\hat{\rho}\gamma}{c}, \\ \frac{1}{2\pi\sqrt{(t - x/v)^2 - (\hat{\rho}\gamma/c)^2}}, & t - \frac{x}{v} > \frac{\hat{\rho}\gamma}{c}, \end{cases} \quad (55a)$$

$$(55b)$$

when $\gamma = \sqrt{\bar{\epsilon}} - (1/\beta)^2$ is positive. $\bar{\epsilon} = \epsilon/\epsilon_0$ is the dielectric constant normalized to its value ϵ_0 in vacuum and $\beta = v/c$ the ratio of the particle speed to the speed of light in vacuum (i.e., $\beta < 1$). It is thereby implied that Eqs. (55) are valid only when the particle speed is high enough to assure $\bar{\epsilon} > (c/v)^2$. At low speeds, where $\bar{\epsilon} < (c/v)^2$, one has, instead,

$$\hat{G}(\mathbf{r}, t) = \frac{1}{4\pi\sqrt{(t - x/v)^2 + (\hat{\rho}|\gamma|/c)^2}}, \quad |\gamma| = \sqrt{\frac{1}{\beta^2} - \bar{\epsilon}}. \quad (56)$$

For $\hat{\rho} \neq 0$, one replaces $\hat{\rho}$ by $|\hat{\rho} - \hat{\rho}'|$.

To determine the electromagnetic fields, one performs the differentiations

$$\hat{E}_\rho = \frac{-q}{v\epsilon_0\bar{\epsilon}} \frac{\partial}{\partial \hat{\rho}} \hat{G}, \quad (57a)$$

$$\hat{E}_x = \frac{-q\gamma^2}{c^2\epsilon_0\bar{\epsilon}} \frac{\partial}{\partial t} \hat{G}, \quad (57b)$$

$$\hat{H}_\varphi = -q \frac{\partial}{\partial \hat{\rho}} \hat{G}, \quad (57c)$$

where $\hat{\rho}$ and φ are cylindrical coordinates in the $y - z$ plane. In particular, for the low-speed case $\bar{\epsilon} < 1/\beta^2$,

$$\hat{E}_\rho = \frac{q}{4\pi\epsilon_0\bar{\epsilon}} \frac{\hat{\rho}}{\sqrt{1 - \beta^2\bar{\epsilon}\{[(x - vt)^2/(1 - \beta^2\bar{\epsilon})] + \hat{\rho}^2\}^{3/2}}}, \quad (58a)$$

$$\hat{E}_x = \frac{q}{4\pi\epsilon_0\bar{\epsilon}} \frac{x - vt}{\sqrt{1 - \beta^2\bar{\epsilon}\{[(x - vt)^2/(1 - \beta^2\bar{\epsilon})] + \hat{\rho}^2\}^{3/2}}}, \quad (58b)$$

$$\hat{H}_\varphi = \frac{qv}{4\pi} \frac{\hat{\rho}}{\sqrt{1 - \beta^2\bar{\epsilon}\{[(x - vt)^2/(1 - \beta^2\bar{\epsilon})] + \hat{\rho}^2\}^{3/2}}}. \quad (58c)$$

The radial energy flow through a unit area in a cylindrical surface with radius $\hat{\rho}$ surrounding the particle trajectory is, in the frequency interval from ω to $\omega + d\omega$,

$$W_\omega(\mathbf{r}) = \begin{cases} 0, & \bar{\epsilon} < \left(\frac{c}{v}\right)^2, \\ \frac{q^2\omega(1 - 1/\bar{\epsilon}\beta^2)}{8\pi^2 c^2 \epsilon_0 \hat{\rho}}, & \bar{\epsilon} > \left(\frac{c}{v}\right)^2. \end{cases} \quad (59a)$$

$$(59b)$$

The *total* energy radiated per unit length of particle trajectory is

$$W = 2\pi\hat{\rho} \int_0^\omega W_\omega(\mathbf{r}) d\omega = \frac{q^2}{4\pi\epsilon_0 c^2} \int_0^\omega \omega \left(1 - \frac{1}{\bar{\epsilon}\beta^2}\right) d\omega, \quad (60)$$

where $\hat{\omega}$ is the limiting frequency for which $\bar{\epsilon}(\hat{\omega})\beta^2 = 1$ (i.e., $\bar{\epsilon}\beta^2 < 1$ for $\omega > \hat{\omega}$). If $\bar{\epsilon}$ is assumed frequency independent, W becomes infinite; the dielectric constant of all *physical* media is frequency dependent and approaches that of vacuum as the frequency increases without limit; it therefore exhibits a cutoff frequency $\hat{\omega}$.

Discussion

As shown in Fig. 5.4.12, Eqs. (55) reveal that the electromagnetic fields trail behind the moving charge inside a cone making an angle $\hat{\theta}$ with the x axis; since the speed of the particle in this regime is greater than the speed $c/\sqrt{\bar{\epsilon}}$ of a wave propagating in the medium, the electromagnetic disturbance cannot run ahead of the particle. The cone is defined by the equation $vt - x = \hat{\rho}\gamma\beta$, so

$$\cot \hat{\theta} = \gamma\beta = \sqrt{\bar{\epsilon}\beta^2 - 1}, \quad \beta = \frac{v}{c}. \quad (61)$$

In a coordinate system fixed to the moving charge, the electromagnetic fields are zero when $\theta > \hat{\theta}$ and are derivable from Eq. (55b) when $\theta < \hat{\theta}$. The normal direction to the conical wave front is given by the previously defined angle $\psi = (\pi/2) - \hat{\theta} = \cos^{-1}(1/\beta\sqrt{\bar{\epsilon}})$. The presence of the wave front indicates that radiation takes place, the associated phenomena being generally referred to as Cerenkov radiation. These results were first derived by Frank and Tamm⁸ to explain radiation observed from fast charged particles in media with large refractive index.

No radiation occurs in the slow-speed case $\bar{\epsilon} < 1/\beta^2$; this parameter range includes the vacuum $\bar{\epsilon} = 1$. The fields are similar to those in the electrostatic problem $v = 0$ and may, in fact, be derived therefrom by an application of the Lorentz transformation.⁹ While for $v = 0$, $\hat{E}_x/\hat{E}_\beta = x/\hat{\rho}$, the effect of the motion is to shrink this ratio to $(x - vt)/\hat{\rho}$, so the field intensity seen by a stationary observer is no longer symmetrical about the charge.

To construct the solutions in Eqs. (55) and (56), it is useful to observe that the fields produced by the source distribution in Eq. (54) are related intimately to the fields of a progressively phased line current extending over the entire trajectory. This follows from the recognition that the Fourier spectrum of the current distribution $\hat{\mathbf{J}}$ in Eq. (54) is given for $\hat{\rho}' = 0$ by [see Eq. (5.2.25)]

$$\mathbf{J}(\mathbf{r}, \omega) = \int_{-\infty}^{\infty} \hat{\mathbf{J}}(\mathbf{r}, t) e^{-j\omega t} dt = q\delta(\hat{\rho})e^{-j(\omega/v)x_0}, \quad (62)$$

representative of a line distribution with a phase progression given by $\alpha = \omega/v$ [see Eq. (45)]. The results in Sec. 5.4d are therefore directly applicable, allowance being made for the different time dependence ($i \rightarrow -j$) and also for the differently oriented coordinate system; the charge travels along the x axis in order to facilitate subsequent analysis when the medium exhibits stratification along z . From Eqs. (46) and (47), one has for the relevant time-harmonic Green's function,

$$G(\mathbf{r}, \omega) = \frac{-j}{4} e^{-j(k_0/\beta)x} H_0^{(2)}(k_0 \hat{\rho} \gamma), \quad k_0 = \frac{\omega}{c}, \quad \beta = \frac{v}{c}, \quad (63)$$

with the ω dependence exhibited explicitly. The corresponding time-harmonic fields are then calculated as in Eqs. (48) and lead (with $\partial/\partial t \leftrightarrow j\omega$) to Eqs. (57).

$G(\mathbf{r}, \omega)$ satisfies the differential equation [see Eq. (46b)]

$$\left(\hat{\nabla}_t^2 + \frac{\omega^2}{c^2} \bar{\epsilon} - \frac{\omega^2}{v^2} \right) G(\mathbf{r}, \omega) = -\delta(\hat{\rho} - \hat{\rho}') e^{-j(\omega/v)x}, \quad \hat{\nabla}_t^2 = \nabla^2 - \frac{\partial^2}{\partial x^2}, \quad (63a)$$

which can be written in the following alternative forms upon inclusion of the time factor $\exp(j\omega t)$:

$$\left. \begin{aligned} & \left(\nabla^2 - \frac{\bar{\epsilon}}{c^2} \frac{\partial^2}{\partial t^2} \right) \\ & \left(\hat{\nabla}_t^2 - \frac{\gamma^2}{c^2} \frac{\partial^2}{\partial t^2} \right) \\ & \left(\hat{\nabla}_t^2 + \beta^2 |\gamma|^2 \frac{\partial^2}{\partial x^2} \right) \end{aligned} \right\} G(\mathbf{r}, \omega) e^{j\omega t} = -\delta(\hat{\rho} - \hat{\rho}') e^{j\omega(t-x/v)}, \quad (63b)$$

where $\gamma^2 = \bar{\epsilon} - (1/\beta)^2$. The time-dependent Green's function

$$\hat{G}(\mathbf{r}, t) = \frac{1}{2\pi} \int_{-\infty}^{\infty} G(\mathbf{r}, \omega) e^{j\omega t} d\omega \quad (64)$$

is recovered from Eqs. (63b) upon multiplication by $1/2\pi$ and integration over ω , and the first of Eqs. (63b) is then transformed into Eq. (55).

The second of Eqs. (63b),

$$\left(\hat{\nabla}_t^2 - \frac{\gamma^2}{c^2} \frac{\partial^2}{\partial t^2} \right) \hat{G}(\mathbf{r}, t) = -\delta(\hat{\rho} - \hat{\rho}') \delta\left(t - \frac{x}{v}\right), \quad (64a)$$

is of the same form as Eq. (41) provided that the positive constant c^2 is replaced by the positive constant c^2/γ^2 , and $t' = x/v$. x can be regarded as a parameter since it does not occur in the differential operator on the left-hand side of Eq. (64a). The solution in Eqs. (42) then furnishes directly the result in Eqs. (55a) and (55b).

When γ^2 is negative, the third of Eqs. (63b),

$$\left(\hat{\nabla}_t^2 + \beta^2 |\gamma|^2 \frac{\partial^2}{\partial x^2} \right) \hat{G}(\mathbf{r}, t) = -\delta(\hat{\rho} - \hat{\rho}') \delta\left(t - \frac{x}{v}\right), \quad (64b)$$

is useful. Upon introducing a new variable $\bar{x} = x/\beta|\gamma|$, the differential operator on the left-hand side becomes the Laplacian in the \bar{x}, y, z coordinate space. Furthermore, $\delta(t - x/v) \rightarrow \delta(t - \bar{x}|\gamma|/c) = (c/|\gamma|)\delta(\bar{x} - \bar{x}')$, where $\bar{x}' = ct/|\gamma|$ plays the role of a parameter. The transformed problem therefore requires the evaluation of the static Green's function G_s in the \bar{x}, y, z space, which, upon inclusion of the multiplicative factor $c/|\gamma|$, yields, for $\hat{\rho}' = 0$,

$$G_s = \frac{c/|\gamma|}{4\pi\sqrt{\hat{\rho}^2 + [\bar{x} - (ct/|\gamma|)]^2}} \quad (65)$$

This expression, when transformed back into the x, y, z space, leads to Eq. (56).

As in Sec. 5.4d, the parameter $\alpha = k_0/\beta = \omega/v$ in the time-harmonic problem determines whether radiation does, or does not, take place. When $\alpha < k_0\sqrt{\bar{\epsilon}}$, radiation occurs, whereas no energy escapes from the vicinity of the source when $\alpha > k_0\sqrt{\bar{\epsilon}}$. These conditions are equivalent to the previously stated $\beta^2\bar{\epsilon} > 1$ and $\beta^2\bar{\epsilon} < 1$, respectively. The direction of propagation of the waves in the radiating case is given via Fig. 5.4.11 by the angle ψ . This figure demonstrates furthermore that the radiation characteristics of the moving particle may be inferred *directly* from the wavenumber surface for the medium: One first constructs the plane $\kappa = k_0/\beta$, where in this instance, κ is taken as the wavenumber along x . When this plane intersects the sphere $k = k_0\sqrt{\bar{\epsilon}}$, radiation leaves the particle axis along the conical trajectories shown. When no intersection occurs, there is no radiation. If $\bar{\epsilon}$ is assumed to be frequency independent, all plane waves in the radiating case leave at the same angle ψ , thereby establishing the wave-front in Fig. 5.4.12. From a physical viewpoint, the particle excites those plane waves whose phase speeds $v_p > c/\sqrt{\bar{\epsilon}}$ along its trajectory are equal to v ; evidently, this condition, the "Cerenkov coherence condition," cannot be met when $v < c/\sqrt{\bar{\epsilon}}$.

The energy flow in the frequency interval from ω to $\omega + d\omega$ is evaluated from the time-harmonic fields via Eqs. (48) (modified as noted above) and (5.2.31) and leads directly to Eqs. (59) upon use of the Wronskian relation: $J_0(w)(d/dw)N_0(w) - N_0(w)(d/dw)J_0(w) = 2/\pi w$. Formula (59a) confirms that no radiation takes place when $\bar{\epsilon}\beta^2 < 1$.

Modal representation

While the most direct method of determining the radiation from a moving charge utilizes a cylindrical coordinate system centered on the charge trajectory along x , it is possible by an alternative approach to view the configuration as a waveguide along z in which the moving charge sets up a transverse electric current. This procedure is unnecessarily complicated in an unbounded homogeneous medium but becomes essential when the region is stratified along z . Since a problem in the latter category is to be examined subsequently, it is useful to consider the required formulation even for the simple case of infinite space. Again, the Fourier transform is taken with respect to time, thereby rendering the phased line source in Eq. (62) as the relevant excitation. Since in many applications the radiated energy rather than the fields is the quantity of primary interest, we shall formulate the problem in terms of the modal voltages and currents in the relevant formula [Eq. (5.2.34)].

The steady-state modal network problem is sketched in Fig. 5.4.6, whence for $z > z'$,

$$V_i(z, \omega) = -\frac{Z_i(\omega)i_i(\omega)}{2} e^{-j\kappa_i(\omega)(z-z')} = Z_i(\omega)I_i(z, \omega), \quad (66)$$

where i_i , Z_i , and κ_i are the current generator strength, modal characteristic impedance, and propagation constant, respectively, and the dependence on ω

has been indicated explicitly. The vector-mode functions are [Eqs. (2.3.1)]

$$\mathbf{e}'_i(\mathbf{p}) = -\frac{\nabla_t \Phi_i(\mathbf{p})}{k'_{ii}}, \quad \mathbf{e}''_i(\mathbf{p}) = \mathbf{z}_0 \times \frac{\nabla_t \psi_i(\mathbf{p})}{k''_{ii}}. \quad (67)$$

Since all field quantities excited by the current distribution in Eq. (62) have an x dependence given by $\exp(-jk_0x/\beta)$, one may define the scalar mode functions Φ_i and ψ_i as

$$\Phi_i(\mathbf{p}) = \psi_i(\mathbf{p}) = \frac{1}{\sqrt{2\pi}} e^{-jny} e^{-j(k_0/\beta)x}, \quad -\infty < \eta < \infty, \quad (67a)$$

whence

$$k'_{ii} = k''_{ii} = \sqrt{\left(\frac{k_0}{\beta}\right)^2 + \eta^2}, \quad \sum_i \rightarrow \int_{-\infty}^{\infty} d\eta. \quad (67b)$$

Upon substituting Eqs. (62) and (67) into Eq. (2.2.14b), one finds, with $y' = 0$,

$$i'_i = \frac{-jq(k_0/\beta)}{\sqrt{2\pi} k'_{ii}}, \quad i''_i = \frac{-jq\eta}{\sqrt{2\pi} k''_{ii}}, \quad (68a)$$

while, from Eqs. (2.2.15),

$$Z'_i = \frac{\kappa'_i}{\omega \epsilon_0 \bar{\epsilon}}, \quad Z''_i = \frac{\omega \mu_0}{\kappa''_i}, \quad \kappa'_i = \sqrt{k_0^2 \bar{\epsilon} - k'^2_{ii}} = \kappa''_i. \quad (68b)$$

To calculate $W_\omega(z)$ from Eq. (5.2.34), we note first that

$$V'_i I'^*_i + V''_i I''^*_i = \frac{Z'_i |i'_i|^2}{4} + \frac{Z''_i |i''_i|^2}{4} = \frac{q^2 k_0^2 \gamma^2}{8\pi \omega \epsilon_0 \bar{\epsilon} \kappa'_i}, \quad (69)$$

where γ is defined in connection with Eq. (55b). This expression is real only when κ'_i is real, so the integration over η in Eq. (5.2.34) extends only over the interval $|\eta| \leq k_0\gamma$:

$$W_\omega(z) = \frac{q^2 k_0^2 \gamma^2}{8\pi^2 \omega \epsilon_0 \bar{\epsilon}} \int_{-k_0\gamma}^{k_0\gamma} \frac{d\eta}{\sqrt{k_0^2 \gamma^2 - \eta^2}} = \frac{q^2 k_0^2 \gamma^2}{8\pi \omega \epsilon_0 \bar{\epsilon}}. \quad (70)$$

This result represents the energy radiated through a plane $z > z'$. By symmetry, an equal amount is radiated through a plane $z < z'$, so the total radiated energy per unit length in x , in the frequency interval between ω and $\omega + d\omega$, is given by $2W_\omega(z)$, which is identical with the result $2\pi\hat{\rho}W_\omega(\mathbf{r})$, with $W_\omega(\mathbf{r})$ given in Eq. (59b).

5.4f Ring Currents

Circular ring currents represent another important simple form of field excitation arising in various physical applications. We consider two types of ring currents (Fig. 5.4.13) distinguished by currents flowing parallel to the ring axis or along the ring periphery, respectively. The former is termed a “dipole ring source”; the latter is merely called a “ring source.” Unlike the field due to a scalar point or line source of constant strength, which depends only on the

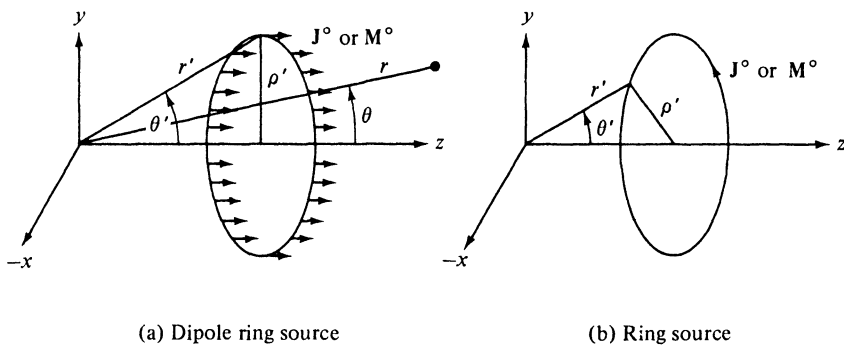


FIG. 5.4.13 Ring currents.

distance measured from the source, the ring-source field is also a function of the angle of observation measured from the ring axis.

Time-harmonic longitudinal electric source current density

$$\hat{\mathbf{J}}(\mathbf{r}, t) = J^0 \delta(\rho - \rho') \delta(z - z') e^{in\phi} e^{-i\omega t} \mathbf{z}_0. \quad (71)$$

Since the currents are longitudinal, the fields may be derived via Eqs. (5.2.1) and (5.2.4c) from a scalar Green's function $\hat{G}_f(\mathbf{r}; \mathbf{r}', \theta')$, obtained by integration of the free-space Green's function $G_f(\mathbf{r}, \mathbf{r}')$ in Eq. (2b) (with $r \rightarrow |\mathbf{r} - \mathbf{r}'|$) around the contour of the ring:

$$\hat{G}_f(\mathbf{r}, \mathbf{r}', \theta') = \rho' \int_{-\pi}^{\pi} e^{in\phi'} G_f(\mathbf{r}, \mathbf{r}') d\phi', \quad (72a)$$

$$= \frac{\rho'}{4\pi} \int_{-\pi}^{\pi} e^{in\phi'} \frac{e^{ik|\mathbf{r}-\mathbf{r}'|}}{|\mathbf{r} - \mathbf{r}'|} d\phi', \quad (72b)$$

where $|\mathbf{r} - \mathbf{r}'|$ in a spherical coordinate representation is defined in Eq. (6). It is observed from Eq. (71) that the source distribution may possess a progressive phase shift given by $\exp(in\phi)$, where n is an integer or zero. It does not appear to be possible to evaluate the integral in Eq. (72b) in closed form. However, for a far-field evaluation (see also Sec. 5.9c) we may employ the asymptotic approximation $|\mathbf{r} - \mathbf{r}'| \sim r - r' \cos \gamma$, whence [see Eqs. (6)]

$$\frac{e^{ik|\mathbf{r}-\mathbf{r}'|}}{|\mathbf{r} - \mathbf{r}'|} \sim \frac{e^{ik(r - r' \cos \gamma)}}{r}, \quad r \gg r'. \quad (73a)$$

Since

$$\int_{-\pi}^{\pi} e^{-ix \cos \psi - in\psi} d\psi = 2\pi e^{-inx/2} J_n(x), \quad (73b)$$

and the upper and lower limits of integration in Eq. (72b) can be replaced by $\pi + \phi$ and $-\pi + \phi$, respectively, one obtains, via Eqs. (72b) and (73a), the far-field form of \hat{G}_f ,

$$\hat{G}_f(\mathbf{r}, \mathbf{r}', \theta') \sim \frac{e^{ik(r - r' \cos \theta \cos \theta')}}{2r} \rho' e^{in(\phi - \pi/2)} J_n(kr' \sin \theta \sin \theta'), \quad r \gg r'. \quad (74)$$

The radial variation $(1/r) \exp(ikr)$ indicates that the far field progresses as a spherical wave.

Discussion

The physical interpretation of Eq. (74) differs for various values of source radius $\rho' = r' \sin \theta'$. If $x \ll 1$, then $J_n(x) \sim x^n$, so $\hat{G}_f \propto L(k\rho')^n$ for very small values of $k\rho'$, where $L = 2\pi\rho'$ is the length of the ring source. Thus, the far fields radiated by a ring source with small $k\rho'$ are very small except when $n = 0$, as for a constant current distribution; in this case $J_0(x) \sim 1$, $x \rightarrow 0$, and $\hat{G}_f \rightarrow LG_f$. If $k\rho'$ is large but much smaller than kr , one distinguishes the separate ranges $k\rho' \sin \theta > n$ and $k\rho' \sin \theta < n$. Let us assume that n is likewise large; then, for $x \ll n$, $J_n(x) \sim (x/n)^n$, while for $x \gg n$, one employs $2J_n(x) = H_n^{(1)}(x) + H_n^{(2)}(x)$, with the asymptotic formulas for the Hankel functions given in Eqs. (37) or (5.3.13). Thus, for observation angles θ small enough so that $k\rho' \sin \theta \ll n$, the fields radiated by a ring source become very small.

On the other hand, when $k\rho' \sin \theta \gg n$, use of Eqs. (5.3.13) yields

$$\hat{G}_f \sim \frac{e^{i(n\phi + \pi/4)}}{2r\sqrt{2\pi k} \sin \theta} \sqrt{\frac{\rho'}{\theta}} \{ e^{ik[r-r' \cos(\theta-\theta')]} + e^{-i(n+1/2)\pi} e^{ik[r-r' \cos(\theta+\theta')]} \} \quad (75)$$

which may be written as

$$\hat{G}_f \sim e^{in\phi} \sqrt{\frac{r' \sin \theta'}{r \sin \theta}} \{ \bar{G}_f[r - r' \cos(\theta - \theta')] + \Gamma \bar{G}_f[r - r' \cos(\theta + \theta')] \}, \quad (76)$$

where

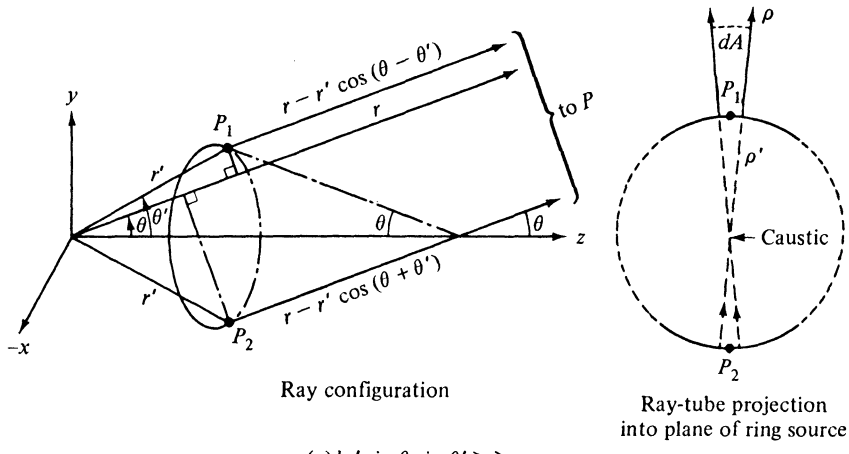
$$\Gamma = (-i)(-1)^n \quad (76a)$$

and $\bar{G}_f(r)$ is the line-source Green's function in Eq. (25),

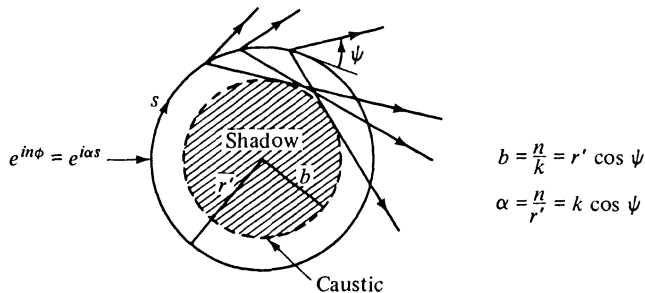
$$\bar{G}_f(r) = \frac{i}{4} H_0^{(1)}(kr) \sim \frac{e^{i(kr + \pi/4)}}{2\sqrt{2\pi kr}}, \quad kr \gg 1. \quad (76b)$$

Equation (76) admits a direct ray-optical interpretation. Since $k\rho'$ is large, the ring source may be regarded as a superposition of linear elements. Introducing $s = \rho'\phi$ as the distance variable along the ring, one may write $\exp(in\phi) = \exp(i\alpha s)$, $\alpha = n/\rho'$ where α is the wavenumber descriptive of the phased excitation in Eq. (71). The radiation characteristics of linearly phased line currents are discussed in Sec. 5.4d, and one notes from Fig. 5.4.10 that each element emits geometric optical rays at an angle $\psi = \cos^{-1}(\alpha/k)$ with respect to the element axis. For the case considered, $k\rho' \gg n$, whence $\psi \approx \pi/2$ and the rays leave each element almost perpendicularly. Thus, a distant observation point P is reached by two rays originating, respectively, at the nearest and farthest points P_1 and P_2 on the ring [Fig. 5.4.14(a)]; the corresponding distances measured along these rays are $[r - r' \cos(\theta - \theta')]$ and $[r - r' \cos(\theta + \theta')]$. The two \bar{G}_f functions in Eq. (76) therefore represent the scalar fields radiated by unit strength linear current elements located at P_1 and P_2 . The factor Γ multiplying the contribution from P_2 is separated into two parts as in Eq. (76a). The $(-1)^n$ term accounts for the phase difference $\exp(in\pi)$ between the source

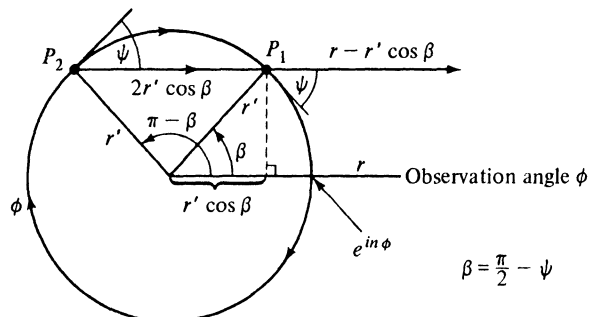
elements at P_1 and P_2 . The $-i$ term represents the phase change experienced by a ray on crossing a caustic; such a caustic (ray envelope) exists on the ring axis since all rays emanating from the source converge thereon. When



$$(a) kr' \sin \theta \sin \theta' \gg n$$



$$(b) kr' > n, \quad \theta = \theta' = \pi/2 - \text{general ray picture}$$



$$(c) kr' > n, \quad \theta = \theta' = \pi/2 - \text{rays reaching distant observation point}$$

FIG. 5.4.14 Geometrical interpretation of radiation from a large ring source.

the observation point is located in a plane described by the azimuthal coordinate ϕ , the source element at A in Fig. 5.4.14(a) has the phase $\exp(in\phi)$, thereby explaining the occurrence of this factor in Eq. (76). Finally, the $\sqrt{\rho'/\rho}$ term in Eq. (76) accounts for the fact that source elements in the vicinity of P_1 and P_2 are not collinear but lie on the ring; when projected into the plane of the ring, ray-tube cross sections dA exhibit a divergence ρ/ρ' in addition to that descriptive of a straight-line current. Since the field amplitude along a ray varies inversely with the square root of the ray-tube cross section, the result in Eq. (76) follows [see Eq. (1.7.37) wherein ψ denotes a phase function]. Evidently, the divergence factor transforms the cylindrical wave near a ring element into a spherical wave far from the element.

Equations (75) or (76) become invalid as $\sin \theta \rightarrow 0$, as evidenced by the resulting divergence of the formulas. In this transition range, where observation points lie near or on the caustic, one must employ Eq. (74).

In Eq. (75) it was assumed that $kr' \sin \theta' \sin \theta \gg n$, so the simple asymptotic approximation in Eq. (37) for the Hankel functions could be used. If one seeks an approximate representation of Eq. (74) which is valid for both n and $k\rho' \sin \theta$ large, one must employ the more accurate asymptotic representations below [see Eqs. (4.5.33) and (4.5.34)]. For $1 - n/x \gg x^{-2/3}$,

$$H_n^{(1,2)}(x) \sim \sqrt{\frac{2}{\pi x \cos \beta}} e^{\pm i x [\cos \beta + (\beta - \pi/2) \sin \beta] \mp i \pi/4}, \quad \sin \beta = \frac{n}{x}. \quad (77a)$$

For $(n/x) - 1 \gg x^{-2/3}$,

$$H_n^{(1,2)}(x) \sim \mp i \sqrt{\frac{2}{\pi x \sinh \psi}} e^{x(\psi \cosh \psi - \sinh \psi)}, \quad \cosh \psi = \frac{n}{x}, \quad (77b)$$

$$J_n(x) \sim \frac{1}{\sqrt{2\pi x \sinh \psi}} e^{-x(\psi \cosh \psi - \sinh \psi)}.$$

For $|1 - n/x| = O(x^{-2/3})$,

$$H_n^{(1,2)}(x) \sim \frac{2^{1/3}}{n^{1/3}} [\text{Ai}(-2^{1/3}\tau) \mp i \text{Bi}(-2^{1/3}\tau)], \quad \tau = n^{-1/3}(x - n), \quad (77c)$$

where $\text{Ai}(\alpha)$ and $\text{Bi}(\alpha)$ are the Airy functions defined in Sec. 4.2e. The above representations, though written for real positive n and x , hold also for selected complex ranges. Formulas for $J_n(x)$ are obtained from Eqs. (77a) or (77c) via $2J_n = H_n^{(1)} + H_n^{(2)}$. For the range $n/x > 1$, a special formula is required since $H_n^{(1)} + H_n^{(2)} \sim 0$ from Eq. (77b). Equations (77) highlight the fact that $J_n(x)$ is a propagating wave function when $n < x$, an attenuating wave function when $n > x$, and goes through a transition range when $n \approx x$.

If one examines Eq. (74) in the range where n is large and $k\rho' > n$, but where it is not required that $k\rho' \gg n$ then use of Eq. (77a) reveals a more complicated asymptotic behavior than that exhibited in Eq. (75). Owing to the presence of additional phase terms, the two ray contributions at P do not appear to originate from the nearest and farthest points on the ring but from shifted positions. The radiation mechanism in this case is illustrated in Fig. 5.4.14(b), where we restrict ourselves for simplicity to observation points lying in the plane of the

ring source ($\theta = \theta' = \pi/2$). As before, rays leave each ring-source element with an inclination measured by the angle $\psi = \cos^{-1}(\alpha/k)$. For wavenumbers α characterizing “slow” waves ($\alpha = n/r' > k$), the angle ψ is complex, no real rays exist, and the fields are confined to the vicinity of the ring source and propagate along the direction of current flow. In the “fast” wave case $\alpha < k$, radiation occurs in accord with the ray picture shown in Fig. 5.4.14(b). $\alpha \approx k$ corresponds to the transition range $n \approx kr'$ noted in connection with Eqs. (77). When $kr' \gg n$, [i.e., the spatial period $(2\pi r')/n$ comprises many wavelengths], one obtains the situation depicted in Fig. 5.4.14(a), wherein the angle $\psi \approx \pi/2$. The validity of this interpretation is verified upon examining in Eq. (74) the exponential terms $\exp(i\chi_{1,2})$ resulting after substitution of Eq. (77a) for $J_n(kr')$. One finds that

$$\chi_1 = k(r - r' \cos \beta) + n(\phi - \beta) + \frac{\pi}{4},$$

$$\chi_2 = k(r + r' \cos \beta) + n(\phi - \pi + \beta) - \frac{\pi}{4}.$$

The physical significance of these phase functions is appreciated from Fig. 5.4.14(c), wherein the field radiated to a distant point (r, ϕ) is examined, r being the distance from the center of the ring. According to the ray picture in Fig. 5.4.14(b), the field comprises contributions from two rays originating at P_1 and P_2 in Fig. 5.4.14(c). The ray emanating from P_1 travels a distance $(r - r' \cos \beta)$ with an associated phase $k(r - r' \cos \beta)$. The phase of the source distribution at P_1 is $n(\phi - \beta)$, yielding a total phase at (r, ϕ) identical with that in χ_1 , save for the $\pi/4$ term, which arises in conjunction with the radiation from a line source as noted in Eq. 76(b). The same interpretation applies to χ_2 relative to the ray from P_2 , except for an additional phase shift of $-\pi/2$ which is contributed when this ray crosses the caustic at the shadow boundary [see Fig. 5.4.14(b)].

Figure 5.4.14(b) schematizes the radiation mechanism not only for the case $kr \gg kr' > n$, but also for $kr' \gg kr > n$, wherein the field is observed in the interior of the ring. Unless $\psi \approx \pi/2$, there exists a “shadow” region which is not penetrated by real rays. The envelope of the ray family (caustic), a circle with radius $b = r' \cos \psi$, bounds the shadow region in the plane of the ring source. The analytical formulation for the field in the interior of the ring is obtained from Eq. (74) by interchanging r and r' and letting $\theta = \theta' = \pi/2$. The field behavior is then governed primarily by the factor $J_n(kr)$, which gives rise to propagating waves (real rays) when $n < kr$, attenuating waves when $n > kr$ (shadow region), with the transition occurring at $r \approx b = n/k$. An alternative, and more extensive, ray-optical treatment proceeding directly from Eqs. (72) is given in Sec. 5.9c.

Modal representation (circular waveguide)

A circular-waveguide representation for the scalar ring-source Green's function \mathring{G}_f defined in Eq. (72a) is obtained from Eqs. (5.2.8a) or (5.2.8b), with Eq. (7), upon carrying out the integration over ϕ' [$\exp(j\omega t)$ dependence]:

$$\hat{G}_f(\mathbf{r}; \rho', z') = \frac{-j\rho'}{2} e^{-jn\phi} \int_0^\infty \xi J_n(\xi\rho) J_n(\xi\rho') \frac{e^{-j\sqrt{k^2 - \xi^2}|z-z'|}}{\sqrt{k^2 - \xi^2}} d\xi, \quad (78a)$$

$$= \frac{-j\rho'}{4} e^{-jn\phi} \int_{\infty e^{-j\pi}}^\infty \xi H_n^{(2)}(\xi\rho_>) J_n(\xi\rho_<) \frac{e^{-j\sqrt{k^2 - \xi^2}|z-z'|}}{\sqrt{k^2 - \xi^2}} d\xi. \quad (78b)$$

The singularities and path of integration appropriate to the integral representation in Eq. (78b) are shown in Fig. 5.3.5(a). Upon letting $z' = 0$ for convenience, introducing the change of variable $\xi = k \sin w$ and the polar coordinates (r, θ) , one obtains for $\rho > \rho'$ the following representation in the w plane;

$$\hat{G}_f = \frac{-jk\rho'}{4} e^{-jn\phi} \int_{\bar{P}} \sin w H_n^{(2)}(kr \sin \theta \sin w) J_n(k\rho' \sin w) e^{-jkr \cos \theta \cos w} dw, \quad (79)$$

with the path \bar{P} shown in Fig. 5.3.5(b). For $\rho < \rho'$, ρ and ρ' in Eq. (79) are interchanged.

To effect an approximate evaluation of the integral in Eq. (79) for the case where the observation point is situated very far from the ring source (i.e., $kr \rightarrow \infty$) one may represent the Hankel function by its asymptotic form in Eq. (5.3.13) subject to the condition that $\sin \theta \sin w \neq 0$ along the path of integration. Moreover, since the source radius ρ' is finite, we may treat $J_n(k\rho' \sin w)$ as a slowly varying function, compared with $H_n^{(2)}(kr \sin \theta \sin w)$, as $kr \rightarrow \infty$, or, less stringently, when $r \sin \theta \gg \rho'$, $kr \gg 1$. Thus, the pertinent formulation becomes

$$\hat{G}_f \sim \frac{-j\rho' e^{-jn(\phi-\pi/2)+jn/4}}{4} \sqrt{\frac{2k}{\pi r \sin \theta}} \int_{\bar{P}} \sqrt{\sin w} J_n(k\rho' \sin w) e^{-jkr \cos(w-\theta)} dw. \quad (80)$$

The asymptotic evaluation of the integral in Eq. (80) proceeds in direct analogy with that in Eq. (5.3.14), with $f(w) = \sqrt{\sin w} J_n(k\rho' \sin w)$, etc. Use of $j \rightarrow -i$ and Eq. (5.3.16a) [for $\exp(-i\omega t)$ dependence] then yields the first-order asymptotic approximation in Eq. (74). It is to be noted that the asymptotic evaluation is carried out under the restriction $r \sin \theta \gg \rho'$, while the direct derivation leading to Eq. (74) shows that this result is valid for all θ in the range $0 \leq \theta \leq \pi$.

Time-harmonic azimuthal electric source current density

$$\hat{\mathbf{J}}(\mathbf{r}, t) = I\delta(\rho - \rho')\delta(z - z')e^{jn\phi}e^{-i\omega t}\phi_0. \quad (81)$$

For a calculation of the radiation from the ring source in Fig. 5.4.13(b), wherein source currents with a progressive phase variation $\exp(in\phi)$ flow in the azimuthal direction, one may utilize the previously derived results for a transverse (to z) current element in Sec. 5.4b. For an azimuthal electric current element, for example, we let $\mathbf{J}^o = \phi_0 \mathbf{J}^o$, $\mathbf{M}^o \equiv 0$, and obtain for the potential functions in Eqs. (5.2.1) [$\exp(j\omega t)$ dependence],

$$j\omega\epsilon\Pi'(\mathbf{r}, \mathbf{r}') = \mathbf{J}^o \frac{1}{\rho'} \frac{\partial^2}{\partial \phi' \partial z'} \mathcal{S}_f, \quad \Pi''(\mathbf{r}, \mathbf{r}') = -\mathbf{J}^o \frac{\partial \mathcal{S}_f}{\partial \rho'}, \quad (82)$$

with \mathcal{S}_f given in Eq. (5.2.10b), with Eq. (7); it is recalled that the representation for \mathcal{S}_f in Eq. (5.2.10b) is to be considered as purely formal, but that

the functions $\partial \mathcal{S}_f / \partial \phi'$ and $\partial \mathcal{S}_f / \partial \rho'$ are meaningful after the partial differentiations have been carried out on the integrand of \mathcal{S}_f .

The potential functions for the ring source are now deduced from an integration as in Eq. (72a), with $i \rightarrow -j$. One notes that, for $n \neq 0$, both E and H modes are excited (i.e., the radiation from the ring source gives rise to longitudinal electric and magnetic fields). For the special case of a constant ring-source distribution $n = 0$, the potential $\hat{\Pi}'$ vanishes. The associated electric and magnetic fields are then obtained via Eqs. (5.2.1) and (82). The electric field has only a ϕ component, which is given by

$$\hat{\mathbf{E}}(\mathbf{r}) = \phi_0 \frac{j\omega\mu \partial \hat{\Pi}''}{\partial \rho} = -\phi_0 j\omega\mu J^0 \frac{\partial^2 \hat{\mathcal{S}}_f}{\partial \rho \partial \rho''}, \quad (83a)$$

where from an integration of Eq. (5.2.10b), with Eq. (7),

$$\frac{\partial^2 \hat{\mathcal{S}}_f}{\partial \rho \partial \rho'} = \frac{-jp'}{2} \int_0^\infty \frac{\xi J_1(\xi\rho) J_1(\xi\rho') \exp(-j\sqrt{k^2 - \xi^2} |z - z'|)}{\sqrt{k^2 - \xi^2}} d\xi. \quad (83b)$$

Upon comparing Eqs. (78a) and (83b) one notes that

$$\left. \frac{\partial^2 \hat{\mathcal{S}}_f}{\partial \rho \partial \rho'} \right|_{n=0} = (e^{jn\phi} \hat{G}_f)_{n=1}. \quad (83c)$$

Thus, the previously obtained asymptotic results for \hat{G}_f can be employed directly for the determination of the far fields in the present problem. Results for the $\exp(-i\omega t)$ dependence are obtained on letting $j \rightarrow -i$.

Time-harmonic magnetic current distributions

The results in this instance are obtained from those above by the duality replacements $E \rightarrow H$, $H \rightarrow -E$, $J^0 \rightarrow M^0$, $I \rightarrow V$, and $\mu \leftrightarrow \epsilon$.

5.5 SOURCES IN THE PRESENCE OF A SEMIINFINITE DIELECTRIC MEDIUM

5.5a Time-harmonic Longitudinal Electric Current Element

$$\hat{\mathbf{J}}(\mathbf{r}, t) = Il\delta(\rho)\delta(z - z')e^{-i\omega t}\mathbf{z}_0. \quad (1)$$

We consider the physical configuration in Fig. 5.5.1, wherein a longitudinal electric current element of strength $J^0 = Il$, with I the current in the element and l its infinitesimal length, is situated at the point $z' < 0$ on the z axis in the presence of a dielectric interface at $z = 0$. The medium in the half-space $z < 0$ is characterized by a dielectric constant ϵ_1 and a permeability μ , while the analogous constants for the half-space $z > 0$ are ϵ_2 and μ . Unlike the problem of the dipole in free space, this problem cannot be solved in terms of a single simple function of the spatial coordinates so that one must resort to a modal technique. With z as the transmission coordinate, the electromagnetic fields are derived from a scalar E -mode Green's function $G(\mathbf{r}, \mathbf{r}')$ [see Eqs. (5.2.1) and (5.2.4c)], which satisfies the separate differential equations

$$(\nabla^2 + k_1^2)G'_1(\mathbf{r}, \mathbf{r}') = -\delta(\mathbf{r} - \mathbf{r}'), \quad z < 0, \quad (2a)$$

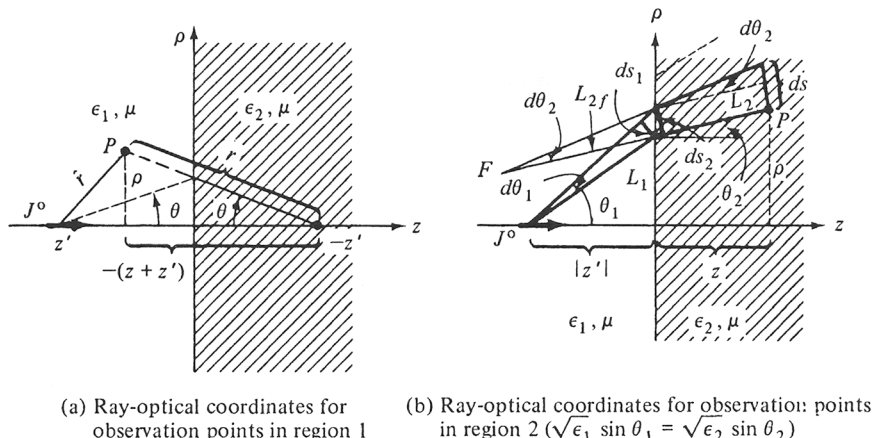


FIG. 5.5.1 Semiinfinite dielectric medium with a longitudinal current element.

$$(\nabla^2 + k_z^2)G'_2(\mathbf{r}, \mathbf{r}') = 0, \quad z > 0, \quad (2b)$$

subject to a radiation condition at infinity in both regions, and to the following continuity requirements at $z = 0$ [see Eqs. (2.3.36) et seq.]:

$$G'_1 = G'_2, \quad \frac{1}{\epsilon_1} \frac{\partial G'_1}{\partial z} = \frac{1}{\epsilon_2} \frac{\partial G'_2}{\partial z} \quad \text{at } z = 0, \quad (2c)$$

where $k_{1,2}^2 = \omega^2 \mu \epsilon_{1,2}$. In cylindrical coordinates with $\mathbf{r} = (\rho, z)$ and $\mathbf{r}' = (0, z')$, one obtains, for $z < 0$,

$$G'_1(\mathbf{r}, \mathbf{r}') = G_{f1}(\mathbf{r}, \mathbf{r}') + G'_s(\mathbf{r}, \mathbf{r}'), \quad (3)$$

where $G_{f1} = (1/4\pi\hat{r}) \exp(i k_1 \hat{r})$, with $\hat{r} = |\mathbf{r} - \mathbf{r}'|$, is the free-space Green's function in Eq. (5.4.2) (Fig. 5.5.1). G'_s , expressive of the interface effect, is represented by an integral extending either over the transverse wavenumber ξ or over the complex angle variable w :

$$G'_s = \frac{-i}{8\pi} \int_{-\infty e^{i\pi}}^{\infty} \xi H_0^{(1)}(\xi\rho) \frac{\exp[-i\sqrt{k_1^2 - \xi^2}(z + z')]}{\sqrt{k_1^2 - \xi^2}} \Gamma(\xi) d\xi, \quad (3a)$$

$$= \frac{-ik_1}{8\pi} \int_{-\bar{P}} \sin w H_0^{(1)}(k_1 r \sin \theta \sin w) e^{ik_1 r \cos \theta \cos w} \Gamma(k_1 \sin w) dw, \quad (3b)$$

with the integration paths given in Fig. 5.3.6. The two representations are related via the transformation $\xi = k_1 \sin w$; spherical coordinates with respect to the image point have been introduced through the definitions

$$\rho = r \sin \theta, \quad -(z + z') = r \cos \theta > 0, \quad 0 \leq \theta \leq \frac{\pi}{2}, \quad (3c)$$

and Γ is the *E*-mode reflection coefficient

$$\Gamma(\xi) = \frac{\sqrt{k_1^2 \epsilon - \xi^2} - \epsilon \sqrt{k_1^2 - \xi^2}}{\sqrt{k_1^2 \epsilon - \xi^2} + \epsilon \sqrt{k_1^2 - \xi^2}}, \quad \epsilon = \frac{\epsilon_2}{\epsilon_1}, \quad (3d)$$

whence

$$\Gamma(k_1 \sin w) = \frac{\sqrt{\epsilon - \sin^2 w} - \epsilon \cos w}{\sqrt{\epsilon - \sin^2 w} + \epsilon \cos w}. \quad (3e)$$

The Green's function $G'_1(\mathbf{r}, \mathbf{r}')$ in the region $z > 0$ can be represented as in Eq. (3a) provided that

$-\exp[-i\sqrt{k_1^2 - \xi^2}(z + z')] \Gamma(\xi)$ is replaced by

$$[1 - \Gamma(\xi)] \exp(i\sqrt{k_1^2 - \xi^2} z - i\sqrt{k_1^2 - \xi^2} z'). \quad (4)$$

For large values of $k_1 r$ but for arbitrary values of $k_1 \hat{r}$, where r and \hat{r} are the distances from the image and source points, respectively [Fig. 5.5.1(a)], the integrals for G'_1 in Eqs. (3a) and (3b) may be evaluated asymptotically. Saddle-point integration yields the following result, which in the region $z < 0$ generally dominates other contributions mentioned subsequently:

$$G'_1 \sim \frac{e^{ik_1 t}}{4\pi\hat{r}} - \Gamma(k_1 \sin \theta) \frac{e^{ik_1 r}}{4\pi r} \left[1 + O\left(\frac{1}{k_1 r}\right) \right], \quad \theta \approx 0, \quad (5)$$

where

$$\Gamma(k_1 \sin \theta) = \frac{\sqrt{\epsilon - \sin^2 \theta} - \epsilon \cos \theta}{\sqrt{\epsilon - \sin^2 \theta} + \epsilon \cos \theta}. \quad (5a)$$

Equation (5) is valid provided that the observation point is not too near the interface ($\theta \approx \pi/2$) or the dipole axis ($\theta \approx 0$). This result, with the exclusion of the generically indicated higher-order terms, can be deduced *directly* by arguments of *geometrical optics* (see Discussion).

In addition to the geometric-optical field, which arises from the saddle point at $w = \theta$ in the integrand, there are other possible contributions to G'_1 from branch-point and pole singularities representative of distinct *diffracted* field types. The branch point singularity at $w_b = \sin^{-1} \sqrt{\epsilon}$ furnishes the following *additional* term G'_{sb} to the asymptotic expression for G'_1 :

$$G'_{sb} \sim -\frac{e^{i\pi/4}}{8\pi} \sqrt{\frac{2k_1}{\pi r \sin \theta}} \frac{2 \exp[ik_1(\sqrt{1-\epsilon}|z+z'| + \sqrt{\epsilon}\rho) - i\pi/4]}{[k_1(\sqrt{\epsilon}|z+z'| - \sqrt{1-\epsilon}\rho)]^{3/2}(1-\epsilon)^{1/4}} \sqrt{\frac{2\pi}{\epsilon}} U(\theta - \hat{\theta}). \quad (6)$$

The Heaviside unit function U vanishes when $\theta < \hat{\theta}$ and equals unity when $\theta > \hat{\theta}$, while $\hat{\theta}$ is that value of the observation angle for which the steepest-descent path through the saddle point $w = \theta$ crosses the branch point at w_b [see Eq. (5.3.15a)]:

$$\hat{\theta} = \operatorname{Re} w_b - \cos^{-1} \operatorname{sech}(\operatorname{Im} w_b), \quad w_b = \sin^{-1} \sqrt{\epsilon}, \quad \epsilon = \frac{\epsilon_2}{\epsilon_1}. \quad (6a)$$

This "lateral wave" field (see Fig. 5.5.2) decays according to $(k_1 \cdot \text{distance})^{-2}$ [see Eq. (6)], more rapidly than the geometric-optical field in Eq. (5). Moreover, when the medium in $z > 0$ is denser than in $z < 0$ ($\epsilon > 1$), or when

losses are present ($\text{Im } \epsilon > 0$), there are also exponential decays, so G'_{sb} is usually negligible under these conditions. An important exception occurs when medium 1 is lossy and medium 2 is lossless, so $\text{Im } k_1 > 0$, $\text{Im } k_2 = 0$. The geometric-optical field in Eq. (5) is then strongly damped, whereas the damping in Eq. (6) arises only from the factor multiplying $|z + z'|$, but not from the factor $k_1\sqrt{\epsilon} = k_2$ multiplying ρ . Thus, G'_{sb} dominates when the lateral distance ρ is large and medium 1 has dissipation (see the discussion relating to Fig. 5.5.2). It may also be noted that $\Gamma(k_1 \sin \theta) \rightarrow 1$ and $r \rightarrow \hat{r}$ when $\theta \rightarrow \pi/2$, so the geometric-optical field vanishes near the interface; the $O(1/k_1^2 r^2)$ term, next in the asymptotic expansion in Eq. (5), then becomes relevant together with G'_{sb} when the region is lossless.

For highly dissipative dielectrics filling the half-space $z > 0$ (i.e., $|\epsilon| \gg 1$, $\arg \epsilon \approx \pi/2$), G'_{sb} is negligible but a further modification must be considered for observation points near the interface. The pole singularity[†] in Eq. (3e) is then found to be located near the saddle point and the composite contribution to the field becomes

$$G'_1 \sim \frac{e^{ik_1 \hat{r}}}{4\pi \hat{r}} + \frac{e^{ik_1 r}}{4\pi r} - \frac{\theta - w_p}{8\pi} \hat{\Gamma}(k_1 \sin \theta) \sqrt{\frac{2k_1}{r}} e^{i(k_1 r + \pi/4)} \{ \}, \quad (7)$$

$$\{ \} = i2e^{-k_1 r b^2} Q(-ib\sqrt{k_1 r}) + T(0) \frac{1}{\sqrt{k_1 r}}, \quad (7a)$$

where $\hat{\Gamma} = 1 + \Gamma$, and

$$\begin{aligned} b &= \sqrt{2} e^{i\pi/4} \sin \frac{w_p - \theta}{2}, \quad w_p \approx \frac{\pi}{2} + \frac{e^{-i\pi/4}}{\sqrt{|\epsilon|}}, \\ T(0) &= \frac{\sqrt{2} e^{-i\pi/4}}{\theta - w_p} + \frac{e^{-i\pi/4}}{\sqrt{2} \sin [(w_p - \theta)/2]}, \\ Q(y) &= \int_y^\infty e^{-x^2} dx. \end{aligned} \quad (7b)$$

This expression is uniformly valid for all observation angles $0 < \theta \leq \pi/2$ in the half-space $z < 0$ and for arbitrary ϵ_2 ; it may be shown to reduce to Eq. (5) when $\theta \not\approx \pi/2$. For the special case of large dissipation in medium 2 ($\arg \epsilon \approx \pi/2$) and no loss in medium 1, and for $\theta = \pi/2$ (source and observation point on the interface), the contribution from the second term in Eq. (7a) is small compared with the first term and can therefore be neglected. Via Eq. (7b), Eq. (7) can then be written in the following form to yield for G'_1 along the interface,

$$G'_1 \sim \frac{e^{ik_1 r}}{2\pi r} [1 + i2\sqrt{\zeta} e^{-\zeta} Q(-i\sqrt{\zeta})], \quad k_1 r \gg 1, \quad |\epsilon| \gg 1, \quad \arg \epsilon \approx \frac{\pi}{2}, \quad (8)$$

where the parameter ζ is Sommerfeld's "numerical distance"¹⁰

$$\zeta = \frac{k_1 r}{2|\epsilon|}. \quad (8a)$$

[†]When medium 2 is a plasma for which it is possible to have $\epsilon_2 < -\epsilon_1$, with $\epsilon_1 > 0$, then the pole may contribute in a manner different from that described here; see Sec. 5.5k.

Alternatively, upon recognizing that $Q(-i\sqrt{\zeta}) = Q(0) - \int_0^{-i\sqrt{\zeta}} e^{-x^2} dx$, with $Q(0) = \sqrt{\pi}/2$, one can rewrite Eq. (8) as

$$G'_1 \sim \frac{e^{ik_1 r}}{2\pi r} \left[1 + i\sqrt{\pi\zeta} e^{-\zeta} - i2\sqrt{\zeta} e^{-\zeta} \int_0^{-i\sqrt{\zeta}} e^{-x^2} dx \right]. \quad (8b)$$

The first term on the right-hand side of Eq. (8b) represents the solution for waves propagating along a perfectly conducting surface ($|\epsilon| = \infty$); the second term stems from the fact that $|\epsilon|$ is large but finite. While for small ζ the first term is predominant, the second and third terms grow in importance with increasing ζ and actually approach -1 when $\zeta \gg 1$ [see Eq. (4.4.20)]. Thus, the wave character depends quite strongly on the numerical distance. The second term in Eq. (8b) represents a "surface wave," as is evident upon identifying its contribution to G'_1 as proportional $(1/\sqrt{\xi_p r}) \exp(i\xi_p r)$, where $\xi_p r = k_1 r \sin \omega_p \approx k_1 r + i\zeta$ (see the discussion to follow). However, at very large distances (ζ large) the effect of the surface-wave contribution is nullified by the third term in Eq. (8b), whence the discussion of its predominant existence in the dipole field has only limited validity.

In the region $z > 0$ a saddle-point evaluation of the integral in Eq. (3a) for large real values of $k_{1,2}$ yields by Eq. (4) the first-order result

$$G'_2(\mathbf{r}, \mathbf{r}') \sim \frac{e^{i(k_1 L_1 + k_2 L_2)}}{4\pi\sqrt{k_1 \rho}} \frac{\sqrt{\sin \theta_1}}{\cos \theta_1} \frac{1}{\sqrt{\frac{L_1}{k_1 \cos^2 \theta_1} + \frac{L_2}{k_2 \cos^2 \theta_2}}} [1 - \Gamma(k_1 \sin \theta_1)], \quad (9)$$

where the distances $L_{1,2}$ and the angles $\theta_{1,2}$ are defined in Fig. 5.5.1(b). Higher-order contributions arising from the saddle-point calculation have not been included in Eq. (9). This expression for G'_2 may be deduced completely by considerations of *geometrical optics* (see Discussion). When $\theta_1 \approx \pi/2$ and L_2 is small the geometric-optical formula must be corrected in a manner similar to that described for the region $z < 0$.¹¹

Discussion

The approximate evaluation of the integral representations for G'_s in Eqs. (3) has received a great deal of attention in the literature because of its relevance to the study of the propagation of electromagnetic waves along the earth's surface (to a first approximation, the earth's sphericity and the effect of the ionosphere are neglected). Difficulties in an asymptotic evaluation of the appropriate ξ plane integrals arise because in addition to branch points at $\xi = 0$ and $\xi = \pm k_1$, the integrand in Eq. (3a) possesses first-order branch points at $\xi_b = \pm k_1 \sqrt{\epsilon}$ and simple pole singularities at the zeros ξ_p of the denominator on the right-hand side of Eq. (3d). Sommerfeld¹⁰ obtained the first formal solution in terms of the circular waveguide (cylindrical coordinate) representation in Eq. (3a) and carried out an asymptotic evaluation for large values of $k_1 r$. In this evaluation he chose to deform the contour of integration and there-

by to cross a pole of the integrand. The resulting residue contribution, as noted from Eq. (3a) for $z' = 0$ (source point located on the interface), has a coordinate dependence given by

$$H_0^{(1)}(\xi_p \rho) \exp[+i\sqrt{k_1^2 - \xi_p^2}|z|] \sim (1/\sqrt{\xi_p \rho}) \exp[i\sqrt{k_1^2 - \xi_p^2}|z| + i\xi_p \rho],$$

where, if ϵ_2 is complex, $\text{Im}\sqrt{k_{1,2}^2 - \xi_p^2} > 0$ for the $\exp(-i\omega t)$ time convention. The associated fields decay exponentially away from the interface for both $z < 0$ and $z > 0$, as noted from Eq. (4); the residue contribution thus has the character of a “surface wave,” first discussed by Zenneck, “guided” by the interface. Because of its inverse $\sqrt{\rho}$ radial decay at large distances, slower than the $1/r$ variation of the primary field G_{f1} , a great deal of discussion has ensued about the independent existence of this wave and its utilization for the transmission of radio waves over long distances. In view of the voluminous literature on this subject, we abstain from discussing the historical development of this problem; for an appreciation thereof, the reader is referred to Reference 12. As seen from the asymptotic evaluation for source and observation points located near the interface [Eq. (8b)], the far field radiated by a dipole antenna can be represented so as to exhibit a surface-wave term. However, the simultaneous presence of other terms nullifies the effect of the surface wave except over a restricted range of values of Sommerfeld’s numerical distance parameter $\zeta = k_1 r / 2|\epsilon|$. Hence despite the fact that the surface wave represents a field type that can be independently sustained on a lossy interface, its isolation from the other contributions to the field radiated by a dipole source has only limited validity.

The aforementioned complications are absent when the source point and (or) the observation point are located far from the interface, in which instance the asymptotic formulas in Eqs. (5) and (9) describe the field behavior. These partial results may be derived completely via considerations of geometrical optics. With reference to an observation point P in Fig. 5.5.1(a), the first and second terms of the field response, as expressed in Eq. (5), evidently comprise a direct-wave and a reflected-wave contribution, respectively. The contribution from the direct wave is identical with that observed in an infinite medium with wavenumber k_1 . The reflected-wave contribution can be interpreted as a geometric-optical term arising from a ray which reaches the observation point after being reflected from the interface at the angle of incidence (dashed lines in Fig. 5.5.1). The distance from the source to P along this trajectory is r [see also Fig. 1.7.9(a) and Eq. (1.7.64b) for the analogous line-source problem]. Alternatively, the reflected-wave contribution can be viewed as arising from a weighted image source situated as in Fig. 5.5.1 in an infinite medium with wavenumber k_1 . The amplitude function of the reflected ray appearing to originate at the image point contains the factor $-\Gamma(k_1 \sin \theta)$, the reflection coefficient for a plane wave, polarized with magnetic vector parallel to the interface (this is the relevant polarization for the dipole in Fig. 5.5.1) and incident on the interface at an angle θ with respect to the normal direction.¹³ The geo-

metric-optical field is modified by terms of $O(1/k_1^2 r^2)$, which represent higher-order terms in the asymptotic evaluation (these terms are not evaluated explicitly here).

The ray-optical interpretation of Eq. (9) is somewhat more involved since the ray paths now proceed in both regions. With reference to Fig. 5.5.1(b), the evaluation of the field according to geometrical optics requires the following steps, motivated by the fact that the field along a ray propagates locally like that of a plane wave having the appropriate polarization (see Sec. 1.7b):

1. Determination of a ray path connecting the source point and observation point in a manner such that the ray reflection and refraction laws (same as for plane waves) are satisfied at the interface.

2. Evaluation of the initial field G'_{20} on the refracted ray by calculating the incident field on the interface and multiplying by the plane-wave transmission coefficient.

3. Evaluation of the phase at P by adding to the phase of G'_{20} the appropriate phase increment along L_2 .

4. Evaluation of the amplitude at P by multiplying $|G'_{20}|$ by the square root of the refracted ray-tube cross-section ratio at the interface and at P .

Item 1 leads to the ray path in Fig. 5.5.1(b), with the angles θ_1 and θ_2 related by the plane-wave refraction law (Snell's law); both rays are contained in a plane normal to the interface, a feature not necessarily satisfied when anisotropic media are involved (see Fig. 1.7.4). To construct the field G'_{20} in item 2, we recognize that the incident field on the interface is given by $(4\pi L_1)^{-1} \exp(i k_1 L_1)$ and the plane-wave transmission coefficient by $[1 - \Gamma(k_1 \sin \theta_1)]$ [see also Eq. (5), with $\hat{r} = r = L_1$, and the continuity requirement $G'_1 = G'_2$ at $z = 0$]. The phase increment along the refracted ray path (item 3) is given by $k_2 L_2$. For determination of the amplitude in item 4, reference is made to the incident and refracted tubes formed by closely neighboring rays [Fig. 5.5.1(b)]. The intensity at P is related to the intensity at the interface by the area ratio

$$\frac{dA_2}{dA} = \frac{2\pi|z'| \tan \theta_1}{2\pi\rho} \frac{ds_2}{ds}, \quad (9a)$$

where ds_2 and ds are the cross-sectional length elements in a ρz section through the conically spreading ray tube; the rotational symmetry of the ray structure with respect to the z axis has been used in deriving Eq. (9a). Thus, the geometrical optics solution at an observation point (ρ, z) in region 2 is [see Eq. (1.7.37)].¹¹

$$G'_{20}|_{\text{opt}} = \left\{ \frac{e^{ik_1 L_1}}{4\pi L_1} [1 - \Gamma(k_1 \sin \theta_1)] \right\} e^{ik_2 L_2} \sqrt{\frac{dA_2}{dA}}. \quad (9b)$$

The quantity in the braces represents the field G'_{20} at the interface, and the remaining factors account for the phase and amplitude change along the refracted ray away from the interface.

To establish the equivalence of Eqs. (9) and (9b), one may employ the following geometrical relations deducible from Fig. 5.5.1(b):

$$ds = ds_2 + L_2 d\theta_2 = (L_2 + L_{2f})d\theta_2, \quad (9c)$$

$$ds_2 = ds_1 \frac{\cos \theta_2}{\cos \theta_1} = L_1 \frac{\cos \theta_2}{\cos \theta_1} d\theta_1 = L_{2f} d\theta_2,$$

so that in view of $d\theta_1/d\theta_2 = (k_2/k_1)(\cos \theta_2/\cos \theta_1)$, derived from Snell's law $k_1 \sin \theta_1 = k_2 \sin \theta_2$,

$$\frac{ds_2}{ds} = \frac{L_{2f}}{L_2 + L_{2f}}, \quad L_{2f} = L_1 \frac{k_2}{k_1} \frac{\cos^2 \theta_2}{\cos^2 \theta_1}. \quad (9d)$$

L_{2f} represents the length of the refracted ray tube from the virtual focus F in Fig. 5.5.1(b) to the interface. When Eqs. (9d) and (9a) are substituted into Eq. (9b), one obtains Eq. (9). It has therefore been shown that the first-order saddle-point contributions to the reflected or refracted fields are identical with results predicted from geometrical optics.

An interesting ray-optical interpretation may also be given to the diffraction field expressed by the formula for G'_{sb} in Eq. (6) when both dielectrics are lossless and the medium containing the source is *denser* than the exterior region (i.e., $\epsilon_1 > \epsilon_2$, or $\epsilon < 1$ and real).¹¹ The phase of the exponential term, $k_1 \sqrt{1 - \epsilon} |z + z'| + k_1 \sqrt{\epsilon} \rho$, can be reexpressed as $k_1(L_1 + L_3) + k_2 L_2$, where L_1 , L_2 , and L_3 are the distances defined in Fig. 5.5.2(b). This is verified readily upon noting that $k_2 = k_1 \sqrt{\epsilon}$, $\rho = (L_1 + L_3) \sin \hat{\theta} + L_2$, $|z + z'| = (L_1 + L_3) \cdot \cos \hat{\theta}$, where $\hat{\theta} = \sin^{-1} \sqrt{\epsilon}$ is the angle of total reflection, or of critical refrac-

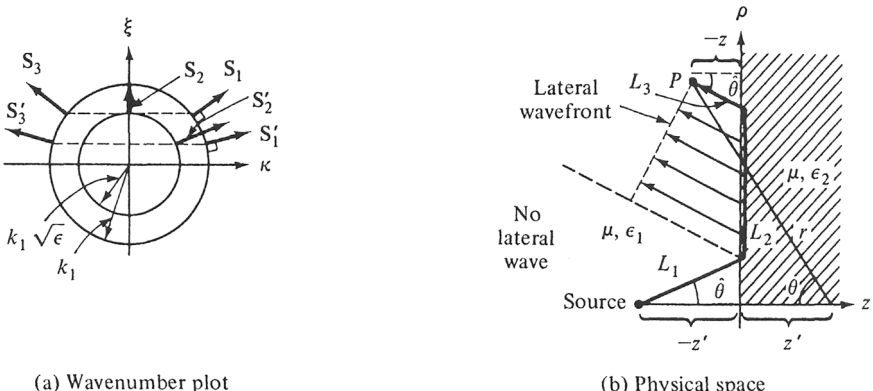


FIG. 5.5.2 The lateral wave.

tion, when $\epsilon < 1$ and real [see Eq. (6a)]. Thus, the phase of the branch-cut wave can be interpreted as arising from a ray that propagates from the source to the interface at the angle $\hat{\theta}$, is refracted parallel to the interface in the *second* medium (since the wavenumber associated with L_2 is k_2), and leaves the interface by refraction at the angle $\hat{\theta}$ to reach the observation point P . The name "lateral" arises from the "sideways" nature of the propagation of this wave along the interface. Furthermore, $L_2 = \rho - |z + z'| \tan \hat{\theta}$, with $\sin \hat{\theta} = \sqrt{\epsilon}$,

$\cos \hat{\theta} = \sqrt{1 - \epsilon}$, so the spatially dependent portion of Eq. (6) may be written as

$$G'_{sb} \propto \frac{e^{i(k_1 L_1 + k_2 L_2 + k_3 L_3)}}{\sqrt{\rho/k_1(k_1 L_2)^{3/2}}} U(\theta - \hat{\theta}). \quad (10)$$

One observes that the domain of existence of G'_{sb} coincides precisely with that predicted from Fig. 5.5.2(b) if the need for a finite lateral segment L_2 along the interface is recognized. The solution evidently fails when $L_2 \rightarrow 0$ (dashed line), corresponding to observation points along the angle of total reflection. In this instance, the saddle point at $w = \theta$ in the integrand of Eq. (3b) moves near the branch point $w = \hat{\theta}$, thereby necessitating a more elaborate calculation in terms of parabolic cylinder functions (see Secs 4.4c and 7.5d, where lateral waves on an anisotropic interface are treated in detail). The equiphase surface $(k_2 L_2 + k_3 L_3) = \text{constant}$ is conical (planar in the ρz plane), in contrast to the spherical equiphase surfaces descriptive of the direct and reflected fields [see Fig. 1.7.9(b)]. Owing to the continuous leakage of energy along the lateral path, the amplitude of the wave decays more rapidly with lateral distance than that of the direct or reflected fields. Equation (10) emphasizes succinctly why G'_{sb} may dominate the geometric-optical field in Eq. (5) when ϵ_1 is lossy and ϵ_2 is lossless. The geometric-optical field trajectory is confined entirely to the dissipative region, whereas the lateral portion of the lateral-wave field trajectory proceeds in the lossless region.

The disposition of the incident-reflected-refracted ($\bar{S}'_{1,2,3}$) and incident-lateral-refracted ($\bar{S}_{1,2,3}$) ray groupings is conveniently inferred from the wave-number plot in Fig. 5.5.2(a). For further discussion of these plots, see Sec. 1.7d with Figs. 1.7.3 and 1.7.7.

Analytical details

The three-dimensional E -mode Green's function $G'(\mathbf{r}, \mathbf{r}')$ defined in Eqs. (2), from which the electromagnetic fields can be derived via Eqs. (5.2.1) and (5.2.4c), has the generic integral representation given in Eq. (5.2.11).^{14,15} The one-dimensional modal Green's function $g_{zi}(z, z')$ satisfies a differential equation of the type (5.2.6b) in each region (the subscript i is suppressed):†

$$\left(\frac{d^2}{dz^2} + \kappa_i^2 \right) g_{zi}(z, z') = -\delta(z - z'), \quad -\infty < z' < 0, \quad (11a)$$

$$\left(\frac{d^2}{dz^2} + \kappa_i^2 \right) g_{zi}(z, z') = 0, \quad 0 < z < \infty, \quad (11b)$$

subject to a radiation condition at $|z| \rightarrow \infty$ and to the following continuity conditions at $z = 0$:

$$g_{z1} = g_{z2}, \quad \frac{1}{\epsilon_1} \frac{dg_{z1}}{dz} = \frac{1}{\epsilon_2} \frac{dg_{z2}}{dz}. \quad (11c)$$

†All modal quantities in this section refer to E modes. To simplify the notation, the distinguishing primes will be omitted.

The propagation constants are defined as $\kappa_{1,2} = \sqrt{k_{1,2}^2 - \xi^2}$, with $\text{Im } \kappa_{1,2} < 0$ for the $\exp(j\omega t)$ dependence and $\text{Im } \kappa_{1,2} > 0$ for the $\exp(-i\omega t)$ dependence. The network analogue of Eqs. (11) is shown in Fig. 5.5.3 (g_z is proportional

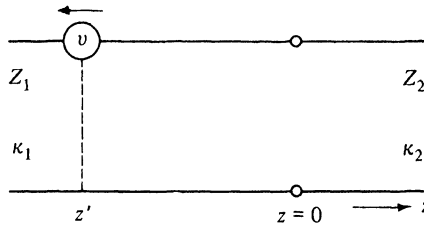


FIG. 5.5.3 Equivalent modal network (E modes).

to the current), and either directly from the differential equation (see Sec. 3.4) or from a network calculation,[†] one may derive the solution for $z < 0$ as in Eq. (5.3.1). Since region 2 is semiinfinite, the input impedance seen to the right from $z = 0$ is equal to the characteristic impedance $Z_2 = \kappa_2/\omega\epsilon_2$, so

$$\vec{\Gamma}_i(0) \equiv \Gamma(\xi) = \frac{Z_2 - Z_1}{Z_2 + Z_1} = \frac{(\kappa_2/\epsilon_2) - (\kappa_1/\epsilon_1)}{(\kappa_2/\epsilon_2) + (\kappa_1/\epsilon_1)}, \quad (12)$$

thus confirming Eq. (3d). Equation (3a) is thereby established (with $j \rightarrow -i$) and Eq. (3b) follows by transforming into the w plane; one recalls that Eq. (5.4.7a) permits the extraction of the infinite space contribution in closed form. Equation (4) follows from the recognition that, from Eqs. (11b) and (11c) and the radiation condition at $z = \infty$,

$$g_{zz}(z, z') = g_{zz}(0, z')e^{-j\kappa_2 z} = g_{zz}(0, z')e^{-j\kappa_2 z}. \quad (13)$$

The integral in Eq. (3b) is in the generic form of the $\exp(-i\omega t)$ equivalent of Eq. (5.3.12a), with $n = 0$. Upon employing the large-argument approximation for the Hankel function in Eq. (5.3.13a), one may reduce the integral for G'_s to the one given in Eq. (5.3.14), with the following identification:

$$f(w) = -\frac{e^{i\pi/4}}{8\pi} \sqrt{\frac{2k_1}{\pi r \sin \theta}} \sqrt{\sin w} \Gamma(k_1 \sin w), \quad \bar{\alpha} = \theta, \quad L = r. \quad (14)$$

An asymptotic evaluation by the steepest-descent procedure then furnishes for real k_1 the contributions listed in Eqs. (5.3.15) and (5.3.16); in particular, the asymptotic formula for the steepest-descent-path integral in Eq. (5.3.16a) yields the result listed in Eq. (5).

To account for the possible contributions from singularities, their location must be clarified. For convenience, the original integration path in the w plane has been redrawn in Fig. 5.5.4(a). In addition to the branch point at $w = 0$ arising from the Hankel function, there are branch point and pole singularities due to the reflection coefficient $\Gamma(k_1 \sin w)$. Let us assume that μ and ϵ_1 are

[†]See Eqs. (2.4.29); Eqs. (11c) specify continuity of voltage and current at $z = 0$.

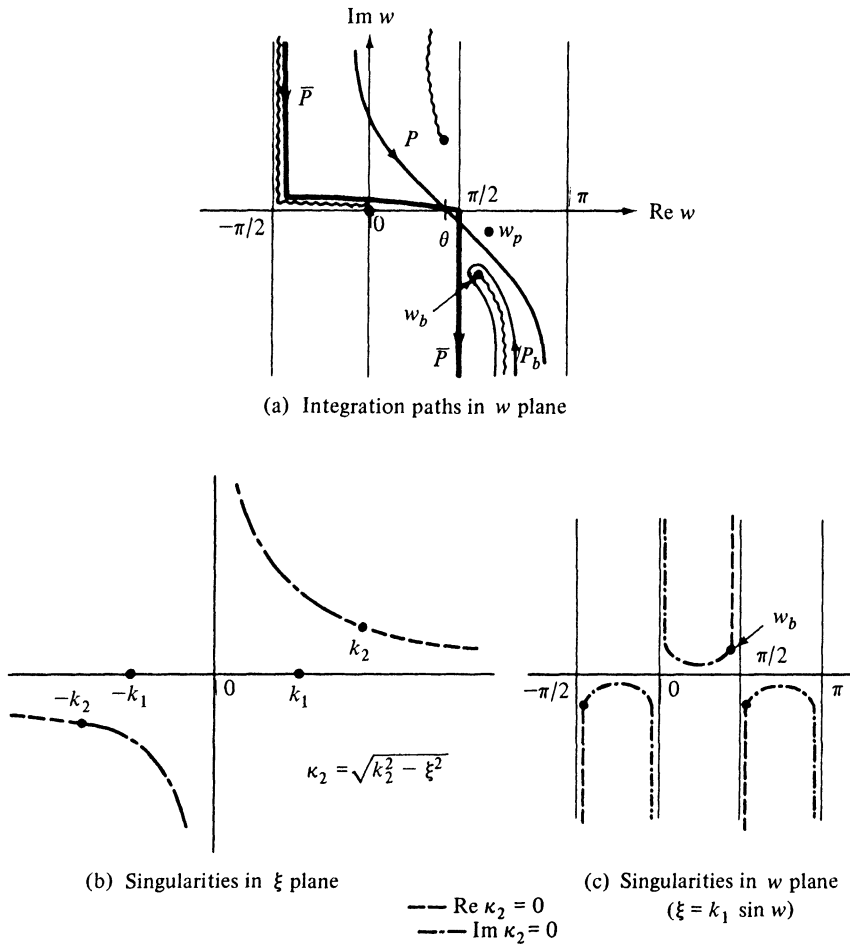


FIG. 5.5.4 Contours of integration and singularities.

real and that ϵ_2 may be dissipative; that is, for an $\exp(-i\omega t)$ time dependence, $\epsilon_2 = \epsilon'_2 + i\epsilon''_2$, where ϵ'_2 and ϵ''_2 are real and $\epsilon'_2 > 0$, $\epsilon''_2 \geq 0$. Thus,

$$\epsilon = \frac{\epsilon_2}{\epsilon_1} = |\epsilon| e^{i2\psi}, \quad 0 \leq \psi < \frac{\pi}{4}, \quad (15a)$$

and

$$\sqrt{\epsilon} = \sqrt{|\epsilon|} e^{i\psi}. \quad (15b)$$

The branch points are located at $w_b = \pm \sin^{-1} \sqrt{\epsilon}$, and with $w_b = w_{br} + iw_{bi}$, w_{br} , w_{bi} real, the relation

$$\sin w_b = \sin w_{br} \cosh w_{bi} + i \cos w_{br} \sinh w_{bi} = \sqrt{|\epsilon|} \cos \psi + i \sqrt{|\epsilon|} \sin \psi, \quad (15c)$$

implies their location as in Fig. 5.5.4(a). If $\psi \rightarrow 0$, with $|\epsilon| > 1$, then $w_b \rightarrow \pi/2 + iw_{bi}$, while if $\psi \rightarrow 0$, with $|\epsilon| < 1$, $w_{bi} \rightarrow 0$. It is recalled that on the top sheet of the four-sheeted Riemann surface shown in Fig. 5.3.6(a) with $k_N = k_2 = k_1\sqrt{\epsilon}$, $\sqrt{k_1^2 - \xi^2} \equiv k_1$ when $\xi = 0$, and $\sqrt{k_1^2\epsilon - \xi^2} \equiv k_1\sqrt{\epsilon}$ when $\xi = 0$. Consequently, on the top sheet of the two-sheeted w plane of Fig. 5.5.4(a), $\sqrt{\epsilon - \sin^2 w} \equiv \sqrt{\epsilon}$ when $w = 0$ (i. e., the square root is positive when the radicand is positive). The behavior of $\operatorname{Re} \kappa_2$ and $\operatorname{Im} \kappa_2$ is clarified in Fig. 5.5.4(b) and (c), which exhibit curves along which $\operatorname{Re} \kappa_2 = 0$ and $\operatorname{Im} \kappa_2 = 0$. Since the algebraic sign of $\operatorname{Re} \kappa_2$ ($\operatorname{Im} \kappa_2$) can change only upon crossing a curve on which $\operatorname{Re} \kappa_2 = 0$ ($\operatorname{Im} \kappa_2 = 0$), a choice of branch cut along the curve(s) $\operatorname{Re} \kappa_2 = 0$ ($\operatorname{Im} \kappa_2 = 0$) assures that the algebraic sign of $\operatorname{Re} \kappa_2$ ($\operatorname{Im} \kappa_2$) is constant on the entire top sheet of the two-sheeted Riemann surface. The sign of $\operatorname{Im} \kappa_2$ ($\operatorname{Re} \kappa_2$), however, changes whenever a curve $\operatorname{Im} \kappa_2 = 0$ ($\operatorname{Re} \kappa_2 = 0$) is crossed.

The pole singularities w_p of $\Gamma(k_1 \sin w)$ in Eq. (3e) are located at

$$\sqrt{\epsilon - \sin^2 w_p} = -\epsilon \cos w_p. \quad (16)$$

Since the real and imaginary parts of $\epsilon(1 + \epsilon)^{-1/2}$ are positive, this relation locates the poles in those regions of the w plane in which the real and imaginary parts of $\kappa_2 = k_1\sqrt{\epsilon - \sin^2 w}$ are also positive. For the choice of branch cuts in Fig. 5.5.4(a), $\operatorname{Re} \kappa_2 > 0$ everywhere on the top sheet. Upon squaring both sides of Eq. (16) and simplifying, and noting from above that the square root is defined to be positive when the radicand is positive, one finds for the pole singularity pertinent to the subsequent asymptotic calculation,

$$\cos w_p = -\frac{1}{\sqrt{1 + \epsilon}}, \quad \sin w_p = \sqrt{\frac{\epsilon}{1 + \epsilon}}. \quad (16a)$$

Since $0 < \arg \sqrt{1 + \epsilon} < \pi/4$, the pole is situated in the strip $\pi/2 < \operatorname{Re} w < \pi$, $\operatorname{Im} w < 0$, in Fig. 5.5.4(a). One may verify that the pole is not intercepted by the steepest-descent path P but that it may move close to the point $w = \pi/2$ when $|\epsilon| \gg 1$. It is therefore effective only when the dielectric in region 2 is very lossy and when the observation point is near the interface $\theta \approx \pi/2$.

A branch point may, however, be intercepted provided that the observation angle $\theta > \hat{\theta}$, where $\hat{\theta}$ is given in Eq. (6a) [see also Eq. (5.3.15a)]. Although its contribution may be written down directly from the general formula (5.3.16b), with Eq. (14), it is instructive to carry out the derivation in detail for the special case at hand. We consider the integral

$$I_b = \int_{P_b} \sqrt{\sin w} e^{ik_1 r \cos(w-\theta)} \Gamma(k_1 \sin w) dw, \quad (17)$$

where P_b is the path in Fig. 5.5.4(a). It is convenient to introduce the transformation,

$$\cos(w - \theta) = \cos(w_b - \theta) + is^2, \quad 0 < s^2 < \infty, \quad (18)$$

which maps the branch point w_b into the origin in the s plane. s is a real variable running from $-\infty$ to $+\infty$. Upon taking the real part of Eq. (18) and employing Eq. (6a), one finds that

$$\cos(w_r - \theta) \cosh w_i = \frac{\cos(w_{br} - \theta)}{\cos(w_{br} - \hat{\theta})}, \quad \theta \geq \hat{\theta}. \quad (18a)$$

Along P_b , which follows the steepest-descent contour through $w = \hat{\theta}$, one has $\cos(w_r - \hat{\theta}) \cosh w_i = 1$. To satisfy Eq. (18a) for $\theta > \hat{\theta}$, the path in Fig. 5.5.4(a) must be distorted toward the right. Since there are no singularities near P_b , such a distortion can be carried out readily and assures the validity of the mapping in Eq. (18). Upon substituting Eq. (18) into Eq. (17), one obtains

$$I_b = e^{ik_1 r \cos(w_b - \theta)} \int_{-\infty}^{\infty} G(s) e^{-k_1 r s^2} ds, \quad (19)$$

where

$$G(s) = \sqrt{\sin w} \Gamma(k_1 \sin w) \frac{dw}{ds}. \quad (19a)$$

An asymptotic evaluation of the integral in Eq. (19) can now be carried out directly via Eq. (4.2.17) provided that $G(s)$ in Eq. (19a) is regular in the vicinity of $s = 0$. To determine the properties of the mapping in Eq. (18), it will be convenient to assume that ϵ is real. If $\epsilon > 1$, the pertinent branch point is located at $w_b = \pi/2 + iw_{bi}$, $w_{bi} < 0$, with $\cosh w_{bi} = \sqrt{\epsilon}$. Then, from Eq. (18),

$$\frac{dw}{ds} = \frac{-i2s}{\pm\sqrt{1 - [\cos(w_b - \theta) + is^2]^2}} \cong \frac{-i2s}{\sin(w_b - \theta)} + O(s^3), \text{ near } s = 0. \quad (20a)$$

The choice of sign in the last term of Eq. (20a) assures that s increases from $-\infty$ to $+\infty$ as w moves along the deformed path (to be called P'_b) in the direction shown in Fig. 5.5.4(a). This is verified upon noting that

$$\sin(w_b - \theta) = \cosh w_{bi} [\cos \theta + i \sin \theta \tanh w_{bi}],$$

whence $0 > \arg \sin(w_b - \theta) > -\theta$. Since $ds > 0$ along P'_b , Eq. (20a) yields, near $w = w_b$,

$$\arg dw = -\arg \sin(w_b - \theta) - \frac{\pi}{2} + \arg s, \quad (20b)$$

which behavior is consistent with Fig. 5.5.4(a) when P_b is distorted as noted above; note that $\arg s = \pi$ when $s < 0$, and $\arg s = 2\pi$ when $s > 0$. Upon expanding $\cos(w - \theta)$ in Eq. (18) in a power series about $w = w_b$, one finds that

$$s \cong \sqrt{i \sin(w_b - \theta)} \sqrt{w - w_b} e^{i\pi}. \quad (20c)$$

The choice of sign in Eq. (20c) is consistent with Eq. (20b), as is verified upon noting that, on the left side of the distorted branch cut in Fig. 5.5.4(a), $s > 0$ and $\arg(w - w_b) = \arg dw$ near w_b . Hence, the first-order branch point at $w = w_b$ maps into the regular point $s = 0$. Since

$$\sqrt{\epsilon - \sin^2 w} = \sqrt{w - w_b} \sqrt{-\sin 2w_b} [1 + O(w - w_b)], \quad (21a)$$

one has

$$\Gamma(k_1 \sin w) = -1 - \frac{2s}{\epsilon \cos w_b} \left[\frac{-\sin 2w_b}{i \sin(w_b - \theta)} \right]^{1/2} + O(s^2). \quad (21b)$$

It is recalled that $\sqrt{\epsilon - \sin^2 w} > 0$ when $\sin w < \sqrt{\epsilon}$ (i.e., for $w = \pi/2 - i|w_i|$, $|w_i| < |w_{bi}|$). This condition is satisfied by the right-hand side of Eq. (21a) since $-\sin 2w_b = -i|\sinh 2w_{bi}|$, while $w - w_b = i[|w_{bi}| - |w_i|]$. Finally,

$$\sqrt{\sin w} = \sqrt{\sin w_b} + O(s^2). \quad (21c)$$

These results apply also to complex ϵ , provided that the square roots are so defined as to reduce to the above when $\arg \epsilon \rightarrow 0$.

Upon substituting Eqs. (21) into Eq. (19a), one notes that $G(0) = 0$. Since only the even-powered terms in the power-series expansion of $G(s)$ about $s = 0$ contribute to the integral in Eq. (19), one finds from Eq. (4.2.17) that the asymptotic approximation of I_b is given for large values of $k_1 r$ by

$$I_b \sim \frac{e^{ik_1 r \cos(w_b - \theta)}}{(k_1 r)^{3/2}} \frac{2\sqrt{2\pi} e^{-i\pi/4} \sin w_b}{\epsilon \sqrt{\cos w_b} [\sin(w_b - \theta)]^{3/2}}, \quad (22)$$

which leads to the form in Eq. (6) since $\sin w_b = \sqrt{\epsilon}$, $\cos w_b = \sqrt{1 - \epsilon}$. The above considerations apply to $|\epsilon| > 1$. If $|\epsilon| < 1$, the branch point w_{b1} in Fig. 5.5.4(a) moves toward the real axis in the interval $\pi/2 < w_r < \pi$, while w_{b2} moves toward the real axis in the interval $0 < w_r < \pi/2$. Hence, w_{b2} is the important branch-point singularity in this range and its contribution can be evaluated using the same procedure as above.

It is to be noted that Eq. (22) is inapplicable when $\theta \rightarrow w_b$ (i.e., when $\theta \rightarrow \hat{\theta}$ for the case $\epsilon < 1$). This is caused by the proximity of the branch-point singularity and the saddle point $w = \theta$, thereby invalidating Eqs. (20) and (21). The behavior of I_b at $\theta = w_b$ is ascertained readily. Upon making the transformation to s via Eq. (18), one finds that dw/ds is finite near $s = 0$, $s \propto w - \theta$, and that I_b becomes proportional to $e^{ik_1 r \int_0^\infty e^{-k_1 r s^2} \sqrt{s} ds}$, whence, upon changing variables to $t = -k_1 r s^2$, I_b is seen to vary like $e^{ik_1 r (k_1 r)^{-3/4}}$. The complete transition from the radial dependence $(k_1 r)^{-3/2}$ when $\theta \neq w_b$ to the dependence $(k_1 r)^{-3/4}$ when $\theta = w_b$ can be expressed in terms of parabolic cylinder functions (for further details, see Secs. 4.4c and 7.5d). It should be emphasized that the steepest-descent evaluation of the reflected-wave integral is likewise influenced when $\theta \rightarrow w_b$, although the geometric-optical result in Eq. (5) remains valid; the effect occurs in the $O(1/k_1^2 r^2)$ term.

While the pole at w_p in Eq. (16a) is not intercepted by the steepest descent path, its proximity to the saddle point when $\theta \approx \pi/2$ and $|\epsilon| \gg 1$ influences the saddle-point calculation; as noted earlier, the branch-point contribution is negligible under these conditions. To appreciate some of the difficulties, we consider an approximation to the reflection coefficient in the saddle-point result (5) valid when $\theta \not\approx \pi/2$:

$$\Gamma(k_1 \sin \theta) \approx \frac{1 - \sqrt{\epsilon} \cos \theta}{1 + \sqrt{\epsilon} \cos \theta} \approx -1 + \frac{2}{\sqrt{\epsilon} \cos \theta}, \quad |\epsilon| \gg 1, \quad (23)$$

where the last relation applies only when $\sqrt{|\epsilon|} \cos \theta \gg 1$. As $\theta \rightarrow \pi/2$, i.e., for source and observation point locations near the interface, the reflection coefficient in Eq. (23) changes very rapidly from $\Gamma \approx -1$ to $\Gamma \approx +1$, so the function $\Gamma(k_1 \sin w)$ in the integrand of Eq. (3b) can no longer be considered as slowly varying in the vicinity of the saddle point $w = \theta \approx \pi/2$. In fact, both the numerator and denominator of $\Gamma(k_1 \sin w)$ may become very small. To circumvent this difficulty in the numerator it is convenient to write

$$\Gamma(k_1 \sin w) = -1 + \hat{\Gamma}(k_1 \sin w), \quad \hat{\Gamma}(k_1 \sin w) = \frac{2\sqrt{\epsilon - \sin^2 w}}{\sqrt{\epsilon - \sin^2 w + \epsilon \cos w}}. \quad (24)$$

The contribution to the integral in Eq. (3b) from the (-1) term on the right-hand side of Eq. (24) is just the free-space Green's function relative to the image point. The $\hat{\Gamma}$ term in Eq. (24) possesses a pole singularity w_p as defined in Eq. (16a), which, for $|\epsilon| \gg 1$, $\arg \epsilon \approx \pi/2$, is located at

$$w_p \approx \frac{\pi}{2} + \frac{e^{-in/4}}{\sqrt{|\epsilon|}} \quad (25)$$

(i.e., near the saddle point). Consequently, the saddle-point evaluation of Eq. (3a) must be modified to account explicitly for the presence of the pole.

The appropriate procedure has been discussed in Sec. 4.4a. One notes first that the function $(w - w_p)\hat{\Gamma}(k_1 \sin w)$ is regular near w_p and hence near the saddle point $w = \theta \approx \pi/2$. Therefore, for a first-order asymptotic evaluation, the contribution to the steepest-descent integral arising from $\hat{\Gamma}$ can be represented as

$$\begin{aligned} I_s &= \int_P \sqrt{\sin w} e^{ik_1 r \cos(w-\theta)} \hat{\Gamma}(k_1 \sin w) dw \\ &\sim (\theta - w_p) \hat{\Gamma}(k_1 \sin \theta) \sqrt{\sin \theta} \int_P \frac{e^{ik_1 r \cos(w-\theta)}}{w - w_p} dw. \end{aligned} \quad (26)$$

The integral in Eq. (26) is identical in form with that in Eq. (4.2.23), the result for which is listed in Eq. (4.4.34). Thus, for large $k_1 r$ and any θ in the range $0 < \theta \leq \pi/2$, one finds ^{10,16}

$$I_s \sim \sqrt{\sin \theta} (\theta - w_p) \hat{\Gamma}(k_1 \sin \theta) e^{ik_1 r} \left[i2\sqrt{\pi} e^{-k_1 r b^2} Q(-ib\sqrt{k_1 r}) + T(0) \sqrt{\frac{\pi}{k_1 r}} \right] \quad (27)$$

where the relevant quantities are defined in Eq. (7b). The result in Eq. (7) follows. For large $\sqrt{k_1 r} |b|$ values (i.e., $w_p - \theta \approx 0$), $Q(-ib\sqrt{k_1 r})$ can be approximated by its asymptotic representation (4.4.20) and then yields for G'_1 the ordinary saddle-point result.

For a derivation of Eqs. (8) via the approximate characterization of the medium by a normalized surface impedance $Z_s = 1/\sqrt{\epsilon}$, see Sec. 5.7.

The asymptotic formula for the transmitted field G'_2 in Eq. (9) results from a saddle-point evaluation of the integral in Eq. (3a), modified according to Eq. (4). Use of the large-argument approximation for the Hankel function renders the form of the integral identical with that in Eq. (5.3.19b), subject to the identifications

$$\eta \rightarrow \xi, \quad y \rightarrow \rho, \quad \bar{f} \rightarrow \frac{e^{i\pi/4}}{4\pi\sqrt{2\pi\rho}} \sqrt{\frac{\xi}{k_1^2 - \xi^2}} [1 - \Gamma(\xi)], \quad \bar{\alpha}_{1,2} \rightarrow \theta_{1,2}.$$

The expression in Eq. (9) follows by substitution into Eq. (5.3.20) [see also Eq. (5.3.23)], with the recognition that the saddle point is given by $\xi_s = k_1 \sin \theta_1 = k_2 \sin \theta_2$. Attention may be called to the use of the wavenumber diagram in Fig. 5.3.10(a) in facilitating the interpretation of the saddle-point condition and of the ray-optical character of the fields.

When the source and observation points are near the interface, complications in the behavior of G'_2 may arise due to the previously mentioned pole and branch-point singularities. These aspects are not pursued further.

5.5b Time-harmonic Transverse Electric Current Element

$$\mathbf{J}(\mathbf{r}, t) = Il\delta(\mathbf{p})\delta(z - z')e^{-i\omega t}\mathbf{x}_0. \quad (28)$$

A transverse current element of strength $J^o = Il$, where I is the current in the element and l is its infinitesimal length, in the presence of a semiinfinite dielectric medium is shown in Fig. 5.5.5. In this instance the source excites

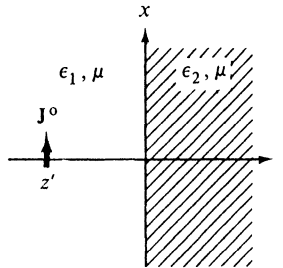


FIG. 5.5.5 Dielectric interface with transverse current element.

both E and H modes along the z direction. The electromagnetic fields are inferred from the functions $\nabla'_i \mathcal{S}'$ and $\nabla'_i \mathcal{S}''$ as in Eqs. (5.2.1) and (5.2.4), where \mathcal{S}' and \mathcal{S}'' satisfy the separate differential equations [see Eqs. (5.2.2)]

$$(\nabla^2 + k_1^2)\nabla_r^2 \begin{cases} \mathcal{S}'_1(\mathbf{r}, \mathbf{r}') \\ \mathcal{S}''_1(\mathbf{r}, \mathbf{r}') \end{cases} = \delta(\mathbf{r} - \mathbf{r}'), \quad z < 0, \quad (29a)$$

$$(\nabla^2 + k_2^2)\nabla_r^2 \begin{cases} \mathcal{S}'_2(\mathbf{r}, \mathbf{r}') \\ \mathcal{S}''_2(\mathbf{r}, \mathbf{r}') \end{cases} = 0, \quad z > 0, \quad (29b)$$

subject to a radiation condition at infinity in both regions, and to the following continuity requirement at $z = 0$ [see Eqs. (2.3.36) et seq.]:

$$\mathcal{S}'_1 = \mathcal{S}'_2, \quad \frac{1}{\epsilon_1} \frac{\partial \mathcal{S}'_1}{\partial z} = \frac{1}{\epsilon_2} \frac{\partial \mathcal{S}'_2}{\partial z} \quad \text{for } E \text{ modes,} \quad (30a)$$

$$\mathcal{S}''_1 = \mathcal{S}''_2, \quad \frac{\partial \mathcal{S}''_1}{\partial z} = \frac{\partial \mathcal{S}''_2}{\partial z} \quad \text{for } H \text{ modes.} \quad (30b)$$

It has been recognized that G and \mathcal{S} have the same continuity conditions across an interface perpendicular to the z axis since they are related by the *transverse* operator $-\nabla_t^2 \mathcal{S} = G$. In a cylindrical-coordinate description of the cross section transverse to z , $\nabla'_t \mathcal{S}$ is given for $z < 0$ and for $\rho' = 0$ by the integral [Eq. (5.2.12)]

$$\begin{aligned} \nabla'_t \mathcal{S}_1(\mathbf{r}, \mathbf{r}') = \rho_0 \frac{i}{8\pi} \int_{-\infty}^{\infty} \frac{H_1^{(1)}(\xi\rho)}{\sqrt{k_1^2 - \xi^2}} & [\exp(i\sqrt{k_1^2 - \xi^2}|z - z'|) \\ & - f(\xi) \exp[-i\sqrt{k_1^2 - \xi^2}(z + z')]] d\xi, \end{aligned} \quad (31)$$

where for the E -mode case $\mathcal{S} = \mathcal{S}'$,

$$f(\xi) = \Gamma'(\xi) = \frac{\sqrt{k_1^2 \epsilon - \xi^2} - \epsilon \sqrt{k_1^2 - \xi^2}}{\sqrt{k_1^2 \epsilon - \xi^2} + \epsilon \sqrt{k_1^2 - \xi^2}}, \quad \epsilon = \frac{\epsilon_2}{\epsilon_1}, \quad (31a)$$

and for the H -mode case $\mathcal{S} = \mathcal{S}''$,

$$f(\xi) = -\Gamma''(\xi) = \frac{\sqrt{k_1^2 \epsilon - \xi^2} - \sqrt{k_1^2 - \xi^2}}{\sqrt{k_1^2 \epsilon - \xi^2} + \sqrt{k_1^2 - \xi^2}}, \quad (31b)$$

with $k_{1,2}^2 = \omega^2 \mu \epsilon_{1,2}$.

The integration path proceeds as in Fig. 5.3.6(a) on the top sheet of the Riemann surface on which all square roots are defined to have positive imaginary parts. The representation for $\nabla'_t \mathcal{S}_2(\mathbf{r}, \mathbf{r}')$ is as in Eq. (31) provided that one replaces the quantity inside the brackets by

$$[] \rightarrow [1 - f(\xi)] \exp(i\sqrt{k_2^2 - \xi^2}z - i\sqrt{k_1^2 - \xi^2}z'). \quad (32)$$

The solution in an unbounded region with wavenumber k_1 , represented by the contribution $\nabla'_t \mathcal{S}_{1f}$ from the first term inside the brackets in Eq. (31), can be expressed in closed form [Eq. (5.4.19b)]; as in Eq. (3), this leaves an integral representation for the interface effect $\nabla'_t \mathcal{S}_s$ observed in region 1. It may also be remarked that the unbounded-space (primary) portion of the field solution is calculated more directly from the formulas

$$\mathbf{H}_{1f} = J^o \nabla \times \mathbf{x}_0 G_{f1}, \quad \mathbf{E}_{1f} = \frac{J^o}{-i\omega\epsilon_1} \nabla \times \nabla \times \mathbf{x}_0 G_{f1}, \quad (33)$$

which follow from Eqs. (5.2.1) and (5.2.4c), with the recognition that the current element in the unbounded region excites only E modes with respect to its axial direction. G_{f1} is defined in Eq. (3).

An asymptotic evaluation of the integral representation for $\nabla'_t \mathcal{S}'_s$ and $\nabla'_t \mathcal{S}''_s$ may be carried out by the techniques described in Sec. 5.5a and yields wave constituents analogous to those encountered in the longitudinal dipole case.

The derivation of Eq. (31) beyond the general form given in Eq. (5.2.12) requires substitution of the modal Green's functions $g'_{zi}(z, z')$ for the E modes and $g''_{zi}(z, z')$ for the H modes. The modal network problem is schematized in Fig. 5.5.6 and the result for the modal Green's function g'_{zi} is the same as in

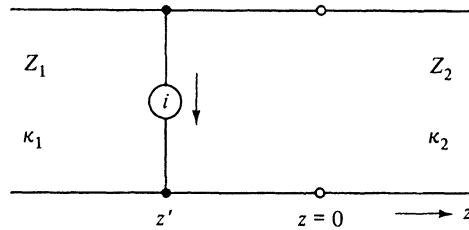


FIG. 5.5.6 Equivalent modal network (E or H modes).

Eqs. (11)–(13). For the H -mode case, g''_{zi} satisfies Eqs. (11) with $g_z \rightarrow g''_z$, provided that the second equation in (11c) is replaced by $dg''_{z1}/dz = dg''_{z2}/dz$ at $z = 0$; this is a consequence of the fact that both regions in Fig. 5.5.5 have the same permeability μ . The H -mode reflection coefficient $\Gamma''(\xi)$ is given by

$$\Gamma''(\xi) = \frac{Z''_2 - Z''_1}{Z''_2 + Z''_1} \quad (34)$$

and yields Eq. (31b) since $Z''_{1,2} = \omega\mu/\kappa''_{1,2}$, $\kappa''_{1,2} = \sqrt{\kappa_{1,2}^2 - \xi^2}$.

An alternative evaluation of the horizontal dipole field has been described by Sommerfeld,^{17,18} wherein he utilizes a Hertzian potential function $\Pi = x_0\Pi_x + z_0\Pi_z$, instead of the z -directed E -and H -mode potentials employed above.

5.5c Time-Harmonic Magnetic Current Element

The electromagnetic fields excited by a magnetic source current density

$$\hat{\mathbf{M}}(\mathbf{r}, t) = Vl\delta(\mathbf{p})\delta(z - z')e^{-i\omega t}\mathbf{u}_0, \quad (35)$$

where V is the source element voltage, l is its infinitesimal length, and $\mathbf{u}_0 = z_0$ or x_0 for the longitudinal and transverse orientations, respectively, can be derived via Eqs. (5.2.1) from the scalar functions $G''_{1,2}$ or $\mathcal{S}'_{1,2}$, $\mathcal{S}''_{1,2}$. The relevant functions $\nabla'\mathcal{S}$ have already been determined in Eqs. (31). The H -mode Green's function G'' is defined as in Eqs. (2) with $G' \rightarrow G''$, except that the second equation in (2c) is replaced by $\partial G'_1/\partial z = \partial G'_2/\partial z$ at $z = 0$. In the resulting representations, as in Eqs. (3) and (4), the E -mode reflection coefficient $\Gamma(\xi) \equiv \Gamma'(\xi)$ in Eq. (3d) is replaced by $[-\Gamma''(\xi)]$ in Eq. (31b). Additional details are left as an exercise for the reader.

5.5d Pulsed Longitudinal Electric Current Element

$$\hat{\mathbf{J}}(\mathbf{r}, t) = \hat{p}\delta(\mathbf{p})\delta(z - z') \frac{d}{dt} \delta(t)\mathbf{z}_0. \quad (36)$$

When the current source in Fig. 5.5.1 has the pulsed behavior prescribed by the impulsive dipole moment of strength \hat{p} in Eq. (36) (see Fig. 5.2.2), and when

the dielectrics ϵ_1 and ϵ_2 are assumed to be frequency independent (non-dispersive), the electromagnetic fields may be derived via Eqs. (5.2.18) from the space and time dependent scalar E -mode Green's function $\hat{G}'(\mathbf{r}, \mathbf{r}'; t, t')$ defined by

$$\left(\nabla^2 - \frac{1}{\bar{c}_1^2} \frac{\partial^2}{\partial t^2} \right) \hat{G}'_1(\mathbf{r}, \mathbf{r}'; t, t') = -\delta(\mathbf{r} - \mathbf{r}')\delta(t - t'), \quad z < 0, \quad (37a)$$

$$\left(\nabla^2 - \frac{1}{\bar{c}_2^2} \frac{\partial^2}{\partial t^2} \right) \hat{G}'_2(\mathbf{r}, \mathbf{r}'; t, t') = 0 \quad z > 0, \quad (37b)$$

subject to quiescence for $t < t'$, and the following continuity requirements at $z = 0$ [see Eqs. (2)]:

$$\hat{G}'_1 = \hat{G}'_2, \quad \frac{1}{\epsilon_1} \frac{\partial \hat{G}'_1}{\partial z} = \frac{1}{\epsilon_2} \frac{\partial \hat{G}'_2}{\partial z} \quad \text{at } z = 0, \quad (37c)$$

with $\bar{c}_{1,2}^2 = (\mu\epsilon_{1,2})^{-1}$. The solution in the region $z < 0$ is given by

$$\hat{G}'_1(\mathbf{r}, \mathbf{r}'; t, t') = \hat{G}_{f1}(\mathbf{r}, \mathbf{r}'; t, t') + \hat{G}'_s(\mathbf{r}, \mathbf{r}'; t, t'), \quad (38)$$

where for $\rho' = 0, t' = 0$, \hat{G}_{f1} is the free-space Green's function in Eq. (5.4.14),

$$\hat{G}_{f1}(\mathbf{r}, \mathbf{r}'; t, t') = \frac{\delta(t - \hat{r}/\bar{c}_1)}{4\pi\hat{r}}. \quad (38a)$$

\hat{G}'_s accounts for the reflection from the interface and is given for $\epsilon_2 > \epsilon_1$ by

$$\hat{G}'_s(\mathbf{r}, \mathbf{r}'; t, t') = \begin{cases} -\frac{1}{4\pi^2} \frac{d}{dt} A(t), & t > \frac{r}{\bar{c}_1}, \\ 0, & t < \frac{r}{\bar{c}_1}, \end{cases} \quad (38b)$$

where

$$A(t) = \frac{2}{r} \int_0^{\pi/2} \operatorname{Re} \Gamma \left[\theta - i \cosh^{-1} \frac{t}{[t^2 + (r/\bar{c}_1)^2 \cos^2 \nu]^{1/2}} \right] d\nu, \quad (39a)$$

with

$$\Gamma(w) = \frac{\epsilon_2 \cos w - \epsilon_1 \sqrt{(\Omega_2/\Omega_1)^2 - \sin^2 w}}{\epsilon_2 \cos w + \epsilon_1 \sqrt{(\Omega_2/\Omega_1)^2 - \sin^2 w}}, \quad (39b)$$

$$\Omega_{1,2} = \sqrt{\frac{1}{\bar{c}_{1,2}^2} + \left[\left(\frac{t}{r} \right)^2 - \frac{1}{\bar{c}_1^2} \right] \sin^2 \nu}. \quad (39c)$$

As in Fig. 5.5.1, \hat{r} and r denote the distance to the observation point (ρ, z) from the source point and the image point, respectively, and θ is the angle between r and the negative z axis. These rather complicated exact results, valid for arbitrary observation times, reduce substantially when $t \approx r/\bar{c}_1$, in which instance one may employ the more direct formulas derivable from the time-harmonic solution [see Eqs. (1.7.80) and (1.7.81)]. The reflected response \hat{G}'_s appears to originate at the image point $r = 0$ and first reaches the observation point after a time interval $t = r/\bar{c}_1$ required for propagation over the dashed-line path in Fig. 5.5.1. When $\epsilon_2 < \epsilon_1$, an additional contribution,

the transient counterpart of the lateral wave in Fig. 5.5.2, must be taken into account (see also Fig. 5.5.8).

Analytical details

Because of the occurrence of the Hankel function in the integral representation (3b), the (cylindrical waveguide) time-harmonic solution is not in the form of Eq. (5.2.20), which admits a direct inversion for recovery of the transient response. Another approach must therefore be taken, and it seems best to proceed from a rectangular waveguide representation as in Eq. (5.2.7).¹⁹ For an $\exp(j\omega t)$ dependence, the rectangular waveguide analogue of Eq. (3b) is

$$G'_s(\mathbf{r}, \mathbf{r}', \omega) = \frac{j}{8\pi^2} \int_{-\infty}^{\infty} d\xi \int_{-\infty}^{\infty} d\eta \frac{e^{-j\xi x - j\eta y - j\kappa_1 Z}}{\kappa_1} \Gamma(\kappa_1, \kappa_2), \quad (40)$$

where $Z = |z + z'|$ and

$$\Gamma(\kappa_1, \kappa_2) = -\frac{\epsilon_2 \kappa_1 - \epsilon_1 \kappa_2}{\epsilon_2 \kappa_1 + \epsilon_1 \kappa_2}, \quad \kappa_{1,2} = \sqrt{\frac{\omega^2}{\tilde{c}_{1,2}^2} - \xi^2 - \eta^2}, \quad \text{Im } \kappa_{1,2} \leq 0. \quad (40a)$$

Next, we let $\omega \rightarrow -js$, $s > 0$, and introduce the change of scale $\xi = \alpha's$, $\eta = \beta's$, which renders Γ independent of s and also allows the factor s to appear explicitly in the exponential:

$$G'_s = -\frac{s}{8\pi^2} \int_{-\infty}^{\infty} \int_{-\infty}^{\infty} \frac{e^{s(-j\alpha'x - j\beta'y - \gamma'_1 Z)}}{\gamma'_1} \Gamma(\gamma'_1, \gamma'_2) d\alpha' d\beta', \quad (41)$$

where

$$\gamma'_{1,2} = \sqrt{\frac{1}{\tilde{c}_{1,2}^2} + \alpha'^2 + \beta'^2}, \quad \text{Re } \gamma'_{1,2} \geq 0. \quad (41a)$$

Cylindrical coordinates (ρ, ϕ) in the xy plane are now introduced via a change of variable that makes the direction of the vector $\mathbf{x}_0 \alpha' + \mathbf{y}_0 \beta'$ identical to that of the radius vector $\mathbf{r} = \rho(\mathbf{x}_0 \cos \phi + \mathbf{y}_0 \sin \phi) \equiv \mathbf{x}_0 x + \mathbf{y}_0 y$.

$$\alpha' = \alpha \cos \phi - \beta \sin \phi, \quad \beta' = \alpha \sin \phi + \beta \cos \phi. \quad (42)$$

Thus,

$$\alpha'x + \beta'y = \alpha\rho, \quad \alpha'^2 + \beta'^2 = \alpha^2 + \beta^2, \quad d\alpha' d\beta' = d\alpha d\beta, \quad (42a)$$

so Eq. (41) can be written as

$$G'_s = -\frac{s}{8\pi^2} \int_{-\infty}^{\infty} d\beta \int_{-\infty}^{\infty} \frac{e^{s(-j\alpha\rho - \gamma_1 Z)}}{\gamma_1} \Gamma(\gamma_1, \gamma_2) d\alpha, \quad (43)$$

where

$$\gamma_{1,2} = \sqrt{\alpha^2 + \Omega_{1,2}^2}, \quad \Omega_{1,2} = \sqrt{\frac{1}{\tilde{c}_{1,2}^2} + \beta^2}, \quad \text{Re } \gamma_{1,2} \geq 0, \quad \Omega_{1,2} > 0. \quad (43a)$$

The integral over α can be cast into the form given in Eq. (5.2.20). First, apply the transformation

$$\alpha = \Omega_1 \sinh \chi, \quad (44)$$

so $\gamma_1 = \Omega_1 \cosh \chi$. Upon also utilizing spherical coordinates (r, θ) via $\rho = r \sin \theta$, $Z = r \cos \theta$, $0 < \theta < \pi/2$, one obtains

$$I = \int_{-\infty}^{\infty} \frac{e^{-s(j\alpha\rho + \gamma_1 Z)}}{\gamma_1} \Gamma(\gamma_1, \gamma_2) d\alpha = \int_{-\infty}^{\infty} e^{-sr\Omega_1 \cosh(\chi + j\theta)} \Gamma(\gamma_1, \gamma_2) d\chi. \quad (45)$$

With $\chi = -jw$,

$$I = -j \int_{-j\infty}^{j\infty} e^{-sr\Omega_1 \cos(w - \theta)} \Gamma(w) dw, \quad (46a)$$

$$\Gamma(w) = \frac{\epsilon_2 \cos w - \epsilon_1 \sqrt{\Omega_2^2/\Omega_1^2 - \sin^2 w}}{\epsilon_2 \cos w + \epsilon_1 \sqrt{\Omega_2^2/\Omega_1^2 - \sin^2 w}},$$

or equivalently,

$$I = -j \int_{-j\infty}^{j\infty} e^{-sr\Omega_1 \cos w} \Gamma(w + \theta) dw. \quad (46b)$$

The transition from Eq. (46a) to Eq. (46b) is permitted if Γ has no singularities in the strip $0 < |\operatorname{Re} w| < \pi/2$. If $\Omega_1 < \Omega_2$ (i.e., $\epsilon_2 > \epsilon_1$), the branch-point singularities w_b lie on the lines $\operatorname{Re} w = \pm\pi/2$. The pole singularities w_p of Γ are located at

$$\cos w_p = -\sqrt{\frac{(\Omega_2/\Omega_1)^2 - 1}{\epsilon - 1}}, \quad \epsilon = \frac{\epsilon_2}{\epsilon_1} = \frac{\bar{c}_1^2}{\bar{c}_2^2}. \quad (47)$$

$\cos w_p$ is real when $\epsilon > 1$, and must be chosen negative since $\sqrt{(\Omega_2/\Omega_1)^2 - \sin^2 w} > 0$ when the radicand is positive. Hence, the poles also lie outside the range $|\operatorname{Re} w| < \pi/2$, and Eq. (46b) is valid for $0 < \theta < \pi/2$ when $\epsilon > 1$. Thus, from Eq. (5.2.22),

$$I = 2 \int_{r\Omega_1}^{\infty} \frac{e^{-st}}{\sqrt{\tau^2 - (r\Omega_1)^2}} \operatorname{Re} \Gamma \left[\theta + j \cosh^{-1} \left(\frac{\tau}{r\Omega_1} \right) \right] d\tau, \quad \epsilon > 1, \quad (48)$$

with Ω_1 defined in Eq.(43a).

The desired formulation in Eq. (5.2.19a) is achieved after substituting Eq. (48) into Eq. (43) and interchanging the orders of integration.¹⁹ The τ integration extends from the curve $\tau = r\sqrt{(1/\bar{c}_1)^2 + \beta^2}$ to $\tau = \infty$, while $-\infty < \beta < \infty$. If the β integration is performed first, one has $[(\tau/r)^2 - 1/\bar{c}_1^2] < |\beta|$, while $r/\bar{c}_1 < \tau < \infty$. Thus,

$$G'_s = -\frac{s}{4\pi^2} \int_0^{\infty} e^{-sr\tau} A(\tau) d\tau, \quad (49)$$

where

$$A(\tau) = \begin{cases} 0 & \tau < \frac{r}{\bar{c}_1}, \\ \int_{-b}^b \frac{\operatorname{Re} \Gamma[\theta + j \cosh^{-1}(\tau/r\Omega_1)]}{\sqrt{\tau^2 - (r\Omega_1)^2}} d\beta, & \tau > \frac{r}{\bar{c}_1}, \end{cases} \quad (50a)$$

and $b = [(\tau/r)^2 - 1/\bar{c}_1^2]^{1/2}$, $\Omega_1^2 = (1/\bar{c}_1^2) + \beta^2$. A final change of variable

$$\beta = \left[\left(\frac{\tau}{r} \right)^2 - \frac{1}{\bar{c}_1^2} \right]^{1/2} \sin \nu, \quad (51)$$

transforms the expression for $A(\tau)$ into the one in Eq. (39), and Eq. (38) follows from Eq. (5.2.19b) and from the equivalence $s \rightarrow d/dt$.

5.5e Time-Harmonic Transverse Electric Line Current

$$\hat{\mathbf{J}}(\mathbf{r}, t) = I\delta(\hat{\mathbf{p}} - \hat{\mathbf{p}}')e^{-i\omega t}\mathbf{x}_0 \quad (52)$$

The fields excited by an electric line current with constant strength I located at $\hat{\mathbf{p}}' = (y', z')$, $z' < 0$, in the presence of a dielectric interface at $z = 0$ can be derived from the scalar two-dimensional (H -mode) Green's function $\bar{G}(\hat{\mathbf{p}}, \hat{\mathbf{p}}')$, which satisfies the differential equations†

$$\left(\frac{\partial^2}{\partial y^2} + \frac{\partial^2}{\partial z^2} + k_1^2 \right) \bar{G}_1(\hat{\mathbf{p}}, \hat{\mathbf{p}}') = -\delta(\hat{\mathbf{p}} - \hat{\mathbf{p}}') \quad z < 0, \quad (53a)$$

$$\left(\frac{\partial^2}{\partial y^2} + \frac{\partial^2}{\partial z^2} + k_2^2 \right) \bar{G}_2(\hat{\mathbf{p}}, \hat{\mathbf{p}}') = 0 \quad z > 0, \quad (53b)$$

subject to a radiation condition at infinity in both regions, and to the continuity requirements

$$\bar{G}_1 = \bar{G}_2, \quad \frac{\partial \bar{G}_1}{\partial z} = \frac{\partial \bar{G}_2}{\partial z} \quad \text{at } z = 0, \quad (53c)$$

with $k_{1,2}^2 = \omega^2 \mu \epsilon_{1,2}$. The solution is given by

$$\bar{G}_1(\hat{\mathbf{p}}, \hat{\mathbf{p}}') = \bar{G}_{f1}(\hat{\mathbf{p}}, \hat{\mathbf{p}}') + \bar{G}_s(\hat{\mathbf{p}}, \hat{\mathbf{p}}'), \quad z < 0, \quad (54)$$

where \bar{G}_{f1} is the free-space Green's function for medium 1 [Eq. (5.4.24) with $k = k_1$] and \bar{G}_s contains the interface effect,

$$\bar{G}_s(\hat{\mathbf{p}}, \hat{\mathbf{p}}') = \begin{cases} \frac{i}{4\pi} \int_{-\infty}^{\infty} \frac{e^{i\eta(y-y')}}{\sqrt{k_1^2 - \eta^2}} \Gamma''(\eta) \exp[-i\sqrt{k_1^2 - \eta^2}(z + z')] d\eta, & (54a) \\ \frac{i}{4\pi} \int_{\tilde{P}} e^{ik_1 R \cos(w-\varphi)} \Gamma''(k_1 \sin w) dw, & (54b) \end{cases}$$

where

$$\Gamma''(\eta) = \frac{\sqrt{k_1^2 - \eta^2} - \sqrt{k_1^2 \epsilon - \eta^2}}{\sqrt{k_1^2 - \eta^2} + \sqrt{k_1^2 \epsilon - \eta^2}}, \quad \epsilon = \frac{\epsilon_2}{\epsilon_1}, \quad (54c)$$

and the transformation $\eta = k_1 \sin w$ has been employed. The integration path \tilde{P} is shown in Fig. 5.3.6(b). For the region $z > 0$,

$$\begin{aligned} \bar{G}_2(\hat{\mathbf{p}}, \hat{\mathbf{p}}') = & \\ \frac{i}{4\pi} \int_{-\infty}^{\infty} & \frac{\exp[i\eta(y - y') + i\sqrt{k_1^2 \epsilon - \eta^2} z]}{\sqrt{k_1^2 - \eta^2}} \exp(-i\sqrt{k_1^2 - \eta^2} z')[1 + \Gamma''(\eta)] d\eta. \end{aligned} \quad (55)$$

The electromagnetic fields are calculated from [see Eq. (5.4.31)]

$$E_{x1,2} = i\omega \mu I \bar{G}_{1,2}, \quad E_y = E_z = 0, \quad (56a)$$

† For simplicity, the distinguishing superscript " for H modes is omitted on \bar{G} .

$$H_{y,1,2} = I \frac{\partial}{\partial z} \bar{G}_{1,2}, \quad H_{z,1,2} = -I \frac{\partial}{\partial y} \bar{G}_{1,2}, \quad H_x = 0. \quad (56b)$$

An asymptotic evaluation for large values of $k_1 R$, where R is the distance from the image point in Fig. 5.5.7, leads to the following approximation for \bar{G}_s :

$$\bar{G}_s = I_s + U(\varphi - \hat{\varphi}) I_b, \quad (57)$$

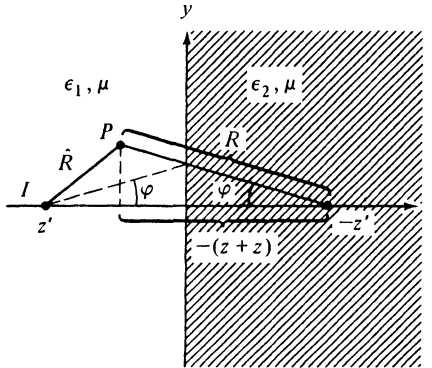


FIG. 5.5.7 Dielectric interface with parallel line current.

I_s being the unit step function, with the steepest-descent path contribution I_s , given by

$$I_s \sim \frac{i}{4\pi} \sqrt{\frac{2\pi}{k_1 R}} e^{i(k_1 R - \pi/4)} \Gamma''(k_1 \sin \varphi) \left[1 + O\left(\frac{1}{k_1 R}\right) \right], \quad (57a)$$

$$\Gamma''(k_1 \sin \varphi) = \frac{\cos \varphi - \sqrt{\epsilon - \sin^2 \varphi}}{\cos \varphi + \sqrt{\epsilon - \sin^2 \varphi}}. \quad (57b)$$

The branch-point contribution I_b is

$$I_b \sim \frac{1}{\sqrt{2\pi}} \frac{\exp[i k_1 (\sqrt{1-\epsilon} |z+z'| + \sqrt{\epsilon} y) + i\pi/4]}{[k_1 (\sqrt{\epsilon} |z+z'| - \sqrt{1-\epsilon} y)]^{3/2}} \left(\frac{\epsilon}{1-\epsilon} \right)^{1/4}. \quad (57c)$$

$\hat{\varphi}$ is the angle given on the right-hand side of Eq. (6a), while φ is the polar angle shown in Fig. 5.5.7 [see also Eq. (10) and Fig. 5.5.2].

When $k_1 \hat{R}$ is also large, one may employ the asymptotic form of the free-space Green's function [see Eq. (5.3.13b)], and the result for \bar{G}_1 may then be written as

$$\begin{aligned} \bar{G}_1 \sim & \frac{e^{i\pi/4}}{2\sqrt{2\pi}} \left[\frac{e^{ik_1 \hat{R}}}{\sqrt{k_1 \hat{R}}} + \Gamma''(k_1 \sin \varphi) \frac{e^{ik_1 R}}{\sqrt{k_1 R}} \right] \left[1 + O\left(\frac{1}{k_1 R}\right) + O\left(\frac{1}{k_1 \hat{R}}\right) \right] \\ & + U(\varphi - \hat{\varphi}) I_b, \quad k_1 \hat{R} \gg 1, \quad k_1 R \gg 1. \end{aligned} \quad (58)$$

The first group of terms on the right-hand side of Eq. (58) represents the two-dimensional (cylindrical wave) geometric-optical field while the contribution from I_b may be interpreted as a lateral wave [see also Fig. 1.7.9 and Eqs. (1.7.64b)

and (1.7.64c)]. The relative importance of these constituents is the same as for the longitudinal dipole problem in Sec. 5.5a and the discussion will therefore not be repeated. The branch-cut integral contribution is $O[(k_1 R)^{-3/2}]$ and therefore smaller than the geometric-optical field except when ϵ is real and $\varphi \rightarrow \pi/2$ (glancing incidence) in which case $\hat{R} \rightarrow R$ and $\Gamma''(k_1) = -1$. In this instance, the entire field is $O[(k_1 R)^{-3/2}]$, and for a calculation of \bar{G} , the asymptotic evaluation of \bar{G}_{f1} and \bar{G}_s must be carried out to the next higher order. The higher-order terms in the asymptotic representation for \bar{G}_{f1} can be obtained from Eq. (5.4.37). For a higher-order evaluation of the steepest-descent integral in Eq. (54b) over the path \tilde{P} , one employs Eqs. (4.2.17), (4.A2c), and (4.A6c), after first introducing the change of variable $\cos(w - \varphi) = 1 + is^2$, $-\infty < s < \infty$.

It may be emphasized that Γ'' in Eq. (57b) is well behaved for $0 \leq \varphi \leq \pi/2$ even when $|\epsilon| \gg 1$, so the field excited by the electric line source does not exhibit a behavior analogous to that described in Eqs. (7) and (8).

Analytical details

The discussion in Eqs. (5.4.31) applies here as well, therefore justifying Eqs. (56). Since the electric field has only an x component, only H modes with respect to z are relevant, so $\bar{G} \equiv \bar{G}''$ is the two-dimensional H -mode Green's function. The differential equations (53a) and (53b) follow from Eqs. (5.2.3b) with $\partial/\partial x \equiv 0$, and the boundary conditions at $z = 0$ may be inferred from the discussion following Eq. (2.3.36).

The integral representations for \bar{G}_s follow from Eqs. (5.2.13a) and (5.3.1) (with $j \rightarrow -i$), the calculation of the H -mode reflection coefficient being described in connection with Eq. (34). It may be noted that the modal network problem is the same as in Fig. 5.5.6 since the present electric source current distribution is also transverse; only the strength of the current generator i differs in the two cases. The integral in Eq. (54b) is exactly in the form given in Eq. (5.3.12b), allowance being made for the different time dependence $\exp(-i\omega t)$, so the results in Eqs. (5.3.15) and (5.3.16) apply directly [see also the analogous treatment of I_b in Eq. (17)]. It may be noted that while $\Gamma''(k_1 \sin w)$ has branch-point singularities at $w_b = \pm \sin^{-1}\sqrt{\epsilon}$, no pole singularities analogous to those for the E -mode case in Eq. (16) are present. Difficulties from an adjacent pole and saddle point therefore do not arise here.

In the construction of \bar{G}_s in Eq. (54a) by the modal network technique, simplification results on direct recognition of the nondependence on x of the total field, and consequent use of x -independent transverse eigenfunctions. Alternatively, and less directly, one may proceed by using the two-dimensional transverse eigenfunctions in Eq. (3.2.40b): $\psi_i(\rho) = (1/2\pi) \exp(-j\xi x - j\eta y)$, $-\infty < (\xi, \eta) < \infty$. On evaluating the source current generator strengths from Eqs. (2.2.14), with $\mathbf{J} = x_0 I \delta(y - y') \delta(z - z')$, one finds that for the E modes, $i'_i \propto \xi \delta(\xi) = 0$, while for the H modes, $i''_i = -jI \delta(\xi) \exp(j\eta y')$. Recalling from Eq. (2.3.9a) that $V''_i(z, z') = -i''_i Z''_i(z, z')$, evaluating $\Pi''(\mathbf{r})$ from Eq.

(2.3.5) (with $\sum_i \rightarrow \int \int_{-\infty}^{\infty} d\xi d\eta$) and noting from Eq. (2.3.6a) that $\mathbf{E} = \mathbf{x}_0 E_x = -\mathbf{x}_0 j \omega \mu \partial \Pi''(\mathbf{r}) / \partial y$, one arrives at Eqs. (54).

5.5f Time-harmonic Transverse Line Distribution of Longitudinally Directed Electric Current Elements

$$\hat{\mathbf{J}}(\mathbf{r}, t) = J^o \delta(\hat{\mathbf{p}} - \hat{\mathbf{p}}') e^{-i\omega t} \mathbf{z}_0. \quad (59)$$

The source configuration at $\hat{\mathbf{p}}' = (0, z')$ in Fig. 5.5.7 has the form sketched in Fig. 5.4.7, and the electromagnetic fields may be derived as in Eqs. (5.4.39) [see also Eqs. (5.2.1) and (5.2.4c)] from a two-dimensional *E*-mode Green's function $\bar{G}'(\hat{\mathbf{p}}, \hat{\mathbf{p}}')$ that satisfies Eqs. (53a) and (53b) subject to a radiation condition at infinity and to boundary conditions as in Eq. (2c) at $z = 0$. The solution for \bar{G}' is the same as in Eqs. (54) except that $-\Gamma''(\eta)$ is replaced by the *E*-mode reflection coefficient $\Gamma(\eta)$ in Eq. (3d) [see Eqs. (77) and (78)]. Asymptotic results valid in the far zone may be derived as in preceding examples.

5.5g Time-harmonic Progressively Phased Transverse Electric Line Currents

Transversely directed current elements

$$\hat{\mathbf{J}}(\mathbf{r}, t) = I \delta(\hat{\mathbf{p}} - \hat{\mathbf{p}}') e^{i\alpha x} e^{-i\omega t} \mathbf{x}_0. \quad (60)$$

If the line source in Fig. 5.5.7 has a linear phase variation $\exp(i\alpha x)$, then the electric field everywhere can no longer be represented by the single component E_x as in Eq. (56a), but both *E* and *H* modes, relative to the *z* direction, are excited [see Eqs. (5.4.68a)]. The electromagnetic fields in this case are inferred from the functions $\nabla'_j \mathcal{S}'$ and $\nabla'_j \mathcal{S}''$ via Eqs. (5.2.1) and (5.2.4), where

$$\mathcal{S}'(\mathbf{r}; \hat{\mathbf{p}}') = \int_{-\infty}^{\infty} \mathcal{S}'(\mathbf{r}, \mathbf{r}') e^{i\alpha x'} dx', \quad (61)$$

and $\mathcal{S}'(\mathbf{r}, \mathbf{r}')$, $\mathcal{S}''(\mathbf{r}, \mathbf{r}')$ are the three-dimensional functions defined in Eqs. (29). The functions \mathcal{S} have the integral representation given in Eq. (5.2.14), with $j \rightarrow -i$, g_{zi} taken from Eqs. (5.3.1) and (13) for $z < 0$ and $z > 0$, respectively, and $\Gamma(\eta)$ taken from Eqs. (31a) and (31b) for the *E*-mode case (\mathcal{S}') and *H*-mode case (\mathcal{S}''), respectively.

Asymptotic approximations for \mathcal{S} may be determined as in Sec. 5.5a.

Longitudinally directed current elements

$$\hat{\mathbf{J}}(\mathbf{r}, t) = J^o \delta(\hat{\mathbf{p}} - \hat{\mathbf{p}}') e^{i\alpha x} e^{-i\omega t} \mathbf{z}_0. \quad (62)$$

In this case, the fields are derivable from the *E*-mode Green's function $\bar{G}'(\mathbf{r}; \hat{\mathbf{p}}')$ defined in terms of $G'(\mathbf{r}, \mathbf{r}')$ [Eqs. (2)] as in Eq. (61). An integral representation analogous to Eq. (61) is obtained by substitution into Eq. (5.2.13).

5.5h Time-harmonic Ring Currents

When ring currents are situated at a dielectric interface perpendicular to the *z* axis (see Fig. 5.4.13), representations for the fields may be obtained as

in Sec. 5.4f, provided that the modal Green's function g_{zi} for the unbounded medium [Eq. (5.4.7)] is replaced by that for the semiinfinite medium described in connection with Eq. (61).

5.5i Pulsed Transverse Electric Line Currents

When the line current in Fig. 5.5.7 has the temporal dependence

$$\hat{\mathbf{J}}(\mathbf{r}, t) = \delta(\hat{\mathbf{p}} - \hat{\mathbf{p}}')\hat{I}(t)\mathbf{x}_0, \quad \hat{I}(t) = I\delta(t) \quad (63)$$

the electromagnetic fields may be inferred from Eqs. (56) (with $i\omega \rightarrow -\partial/\partial t$),

$$\hat{E}_{x1,2} = -\mu I \frac{\partial}{\partial t} \hat{G}_{1,2}, \quad \hat{E}_y = \hat{E}_z = 0, \quad (64a)$$

$$\hat{H}_{y1,2} = I \frac{\partial}{\partial z} \hat{G}_{1,2}, \quad \hat{H}_{z1,2} = -I \frac{\partial}{\partial y} \hat{G}_{1,2}, \quad \hat{H}_x = 0, \quad (64b)$$

where the time-dependent two-dimensional H -mode Green's function $\hat{G}'' \equiv \hat{G}$ satisfies the differential equations

$$\left(\frac{\partial^2}{\partial y^2} + \frac{\partial^2}{\partial z^2} - \frac{1}{\bar{c}_1^2} \frac{\partial^2}{\partial t^2} \right) \hat{G}_1(\hat{\mathbf{p}}, \hat{\mathbf{p}}'; t, t') = -\delta(\hat{\mathbf{p}} - \hat{\mathbf{p}}')\delta(t - t'), \quad z < 0, \quad (65a)$$

$$\left(\frac{\partial^2}{\partial y^2} + \frac{\partial^2}{\partial z^2} - \frac{1}{\bar{c}_2^2} \frac{\partial^2}{\partial t^2} \right) \hat{G}_2(\hat{\mathbf{p}}, \hat{\mathbf{p}}'; t, t') = 0, \quad z > 0, \quad (65b)$$

subject to quiescence for $t < t'$, and to the continuity requirements

$$\hat{G}_1 = \hat{G}_2, \quad \frac{\partial}{\partial z} \hat{G}_1 = \frac{\partial}{\partial z} \hat{G}_2 \quad \text{at } z = 0. \quad (65c)$$

The electromagnetic propagation speeds in the two regions are $\bar{c}_{1,2} = (\mu\epsilon_{1,2})^{-1/2}$; also $\hat{\mathbf{p}} = (y, z)$.

The solution in the region $z < 0$ may be written for $t' = 0$ as

$$\hat{G}_1(\hat{\mathbf{p}}, \hat{\mathbf{p}}'; t, t') = \hat{G}_{f1}(\hat{\mathbf{p}}, \hat{\mathbf{p}}'; t, t') + \hat{G}_s(\hat{\mathbf{p}}, \hat{\mathbf{p}}'; t, t'), \quad (66)$$

where \hat{G}_{f1} , the Green's function for the unbounded medium 1, is given in Eqs. (5.4.42) with $\bar{c} \rightarrow \bar{c}_1$, $\hat{\mathbf{p}} \rightarrow \hat{R}$ (see Fig. 5.5.7), while

$$\hat{G}_s = \begin{cases} \frac{1}{2\pi} \frac{\operatorname{Re} \Gamma[\varphi + j \cosh^{-1}(\bar{c}_1 t/R)]}{\sqrt{t^2 - R^2/\bar{c}_1^2}}, & t > \frac{R}{\bar{c}_1}, \\ 0, & t < \frac{R}{\bar{c}_1}, \end{cases} \quad (67a)$$

$$(67b)$$

with

$$\Gamma(w) = \frac{\cos w - \sqrt{\epsilon - \sin^2 w}}{\cos w + \sqrt{\epsilon - \sin^2 w}}, \quad \epsilon = \frac{\epsilon_2}{\epsilon_1} = \frac{\bar{c}_1^2}{\bar{c}_2^2}. \quad (67c)$$

For $t' \neq 0$, one replaces t by $t - t'$. R and φ are polar coordinates with respect to the image point (Fig. 5.5.7), and the dielectric constants $\epsilon_{1,2}$ are assumed to be frequency independent, with $\epsilon_2 > \epsilon_1$. Thus, when $\epsilon_2 > \epsilon_1$, the field due to an impulsive source located at $(0, z')$, $z' < 0$, observed at the observation

point (y, z) , $z < 0$, comprises the direct wave \hat{G}_{f1} plus a reflected contribution \hat{G}_r , which has an amplitude given by $\operatorname{Re} \Gamma$ and which appears to emanate from the image point $(0, -z')$ located in a medium with wave velocity \bar{c}_1 . When $\epsilon_1 > \epsilon_2$, an additional contribution may arise which represents the transient counterpart of the lateral wave sketched in Fig. 5.5.2 (see also Fig. 5.5.8).

Analytical details

The time-harmonic solution for \bar{G}_s in Eq. (54b) is in the form given in Eq. (5.2.20) (with $j \rightarrow -i$) so that the recovery of the transient result in Eq. (67) follows at once from Eqs. (5.2.19) and (5.2.23). The restriction $\epsilon_2 > \epsilon_1$ (i.e., $\epsilon > 1$) assures that the branch points $w_b = \pm \sin^{-1} \sqrt{\epsilon}$ of $\Gamma(k_1 \sin w)$ are not crossed during the path deformation leading to Eq. (5.2.21); for convenience, $\Gamma(k_1 \sin w)$ has been abbreviated by $\Gamma(w)$ in Eq. (67c).

When $\epsilon < 1$, the branch points lie on the real w axis in the interval $|\operatorname{Re} w| < \pi/2$, and they may contribute a lateral wave (Figs 5.5.2 and 5.5.8) in certain spatial regions. The occurrence of an additional wave solution may be appre-

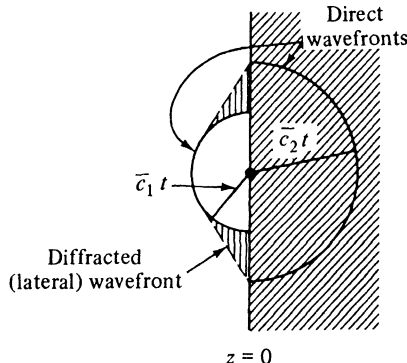


FIG. 5.5.8 Wavefronts when source is on interface. Points in vertically shaded region are reached first by diffracted wave traveling a ray path corresponding to that of lateral wave in Fig. 5.5.2.

ciated on simple physical grounds when the source lies in the interface. The disturbance propagates radially outward in each region with propagation speeds \bar{c}_1 and \bar{c}_2 , where $\bar{c}_2 > \bar{c}_1$. In view of the required continuity across the interface [Eq. (65c)], the field spills over from region 2 into region 1, giving rise to the diffracted wave front. It is not difficult to verify that the diffracted wave front exists precisely in the same spatial domain wherein the lateral wave in Fig. 5.5.2 (with $L_1 = 0$) is present, and that the ray trajectories L_2 and L_3 remain valid.²⁰

5.5j Point Charge in Uniform Straight Motion Parallel to Interface

A point charge q moving with constant speed v parallel to the x axis as in Fig. 5.5.9 may be characterized by the source current density

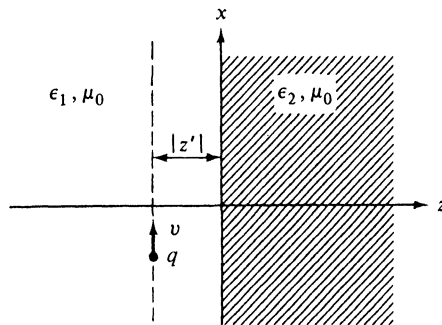


FIG. 5.5.9 Particle moving parallel to a plane interface between two media.

$$\hat{\mathbf{J}}(\mathbf{r}, t) = qv\delta(x - vt)\delta(\hat{\mathbf{p}} - \hat{\mathbf{p}}')\mathbf{x}_0, \quad \hat{\mathbf{p}} = (y, z). \quad (68)$$

As in the latter portion of Sec. 5.4e, we shall emphasize here the radiated energy rather than the actual fields, and consequently deal directly with Eq. (5.2.34), which requires a knowledge of the modal voltage and current solutions $V_i(z, \omega)$ and $I_i(z, \omega)$. The dielectric constants ϵ_1 and ϵ_2 are kept arbitrary although in many practical applications, medium 1 is taken as vacuum ($\epsilon_1 = \epsilon_0$). In the latter instance, radiation may be produced in the denser medium 2 if $(\epsilon_2/\epsilon_0)\beta^2 > 1$, $\beta = v/c$, in which instance the evanescent waves incident from medium 1 (see Sec. 5.4e) are converted into propagating waves in medium 2.

The associated steady-state problem, wherein the line current distribution in Eq. (5.4.62) flows along the particle trajectory in Fig. 5.5.9, has been solved in Sec. 5.4e for an unbounded medium. In the present case, the equivalent modal network problem is shown in Fig. 5.5.6, and its solution is obtained from Eqs. (2.4.23) and (2.4.6) as

$$V_i(z) = -\frac{Z_{ii}i_i}{2} [e^{-j\kappa_{ii}|z-z'|} + \Gamma_i(0)e^{+j\kappa_{ii}(z+z')}], \quad z \leq 0, \quad (69a)$$

$$I_i(z) = -\frac{i_i}{2} [\text{sgn}(z - z')e^{-j\kappa_{ii}|z-z'|} - \Gamma_i(0)e^{+j\kappa_{ii}(z+z')}], \quad z \leq 0, \quad (69b)$$

$$V_i(z) = V_i(0)e^{-j\kappa_{ii}z}, \quad I_i(z) = I_i(0)e^{-j\kappa_{ii}z}, \quad z \geq 0, \quad (69c)$$

when $\text{sgn } x = \pm 1$, $x \geq 0$. Upon defining the relative dielectric constants

$$\bar{\epsilon}_1 = \frac{\epsilon_1}{\epsilon_0}, \quad \bar{\epsilon}_2 = \frac{\epsilon_2}{\epsilon_0}, \quad (70)$$

one may utilize the definitions for Z_i and κ_i given in Eq. (5.4.68b), with $\bar{\epsilon}$ replaced by $\bar{\epsilon}_1$ and $\bar{\epsilon}_2$ in the regions $z < 0$ and $z > 0$, respectively. The modal current generator strengths are the same as in Eq. (5.4.68a), while the reflection coefficients are, from Eq. (2.4.12),

$$\Gamma_i(0) = \frac{Z_{i2} - Z_{ii}}{Z_{i2} + Z_{ii}}. \quad (71)$$

This completes the solution of the modal network problem.

To calculate the energy flow W_ω into region 2, it is convenient to employ Eq. (69c). Since

$$V_i(0) = -\frac{Z_{i1}Z_{i2}i}{Z_{i1}+Z_{i2}} e^{j\kappa_{i1}z'}, \quad I_i(0) = \frac{V_i(0)}{Z_{i2}}, \quad (72)$$

one finds that for imaginary κ_{i2} ,

$$\vec{P}_i = V'_i I_i^* + V''_i I_i^{**} = 0, \quad (73)$$

while for (positive) real κ_{i2} ,

$$\vec{P}_i = \left\{ \begin{array}{l} \frac{q^2 \omega \mu_0 \kappa_{i2}}{2\pi k_{i1}^2} \left[\frac{\kappa_{i1}^2 \bar{\epsilon}_2}{\beta^2 (\bar{\epsilon}_2 \kappa_{i1} + \bar{\epsilon}_1 \kappa_{i2})^2} + \frac{\eta^2}{(\kappa_{i1} + \kappa_{i2})^2} \right], \quad \kappa_{i1} \text{ real}, \\ \frac{q^2 \omega \mu_0 \kappa_{i2} e^{-2|\kappa_{i1} z'|}}{2\pi k_{i1}^2} \left[\frac{|\kappa_{i1}|^2 \bar{\epsilon}_2}{\beta^2 (\bar{\epsilon}_2^2 |\kappa_{i1}|^2 + \bar{\epsilon}_1^2 \kappa_{i2}^2)} + \frac{\eta^2}{|\kappa_{i1}|^2 + \kappa_{i2}^2} \right], \quad \kappa_{i1} \text{ imaginary}. \end{array} \right. \quad (73a)$$

$$(73b)$$

Equation (73b) applies when $\bar{\epsilon}_2 > 1/\beta^2 > \bar{\epsilon}_1$, and only this case is considered further. Upon substituting for $\kappa_{i1,2}$ from Eqs. (5.4.68) and (5.4.67b), one finds after some manipulation that the expression inside the brackets in Eq. (73b) may be written in the form $a k_{i1}^2 (\eta^2 + f)[b(\eta^2 + g)]^{-1}$, where a , b , f , and g are quantities independent of η , so one obtains the following result for the real power carried in a combined E - and H -mode field characterized by the index η :

$$\vec{P}_i \equiv \vec{P}_\eta = \frac{q^2 \omega \mu_0}{2\pi k_0^2 (\bar{\epsilon}_2 - \bar{\epsilon}_1)} \sqrt{k_0^2 \left(\bar{\epsilon}_2 - \frac{1}{\beta^2} \right) - \eta^2} \frac{\eta^2 + f}{\eta^2 + g} \exp \left[-2\sqrt{\eta^2 + k_0^2 \left(\frac{1}{\beta^2} - \bar{\epsilon}_1 \right)} |z'| \right] \quad (74)$$

where $k_0 = \omega/c$ and

$$f = \frac{k_0^2 \bar{\epsilon}_2 (1 - \bar{\epsilon}_1 \beta^2)}{\beta^2 (\bar{\epsilon}_1 + \bar{\epsilon}_2)}, \quad g = \frac{k_0^2 [\bar{\epsilon}_2 (1 - \bar{\epsilon}_1 \beta^2) + \bar{\epsilon}_1]}{\beta^2 (\bar{\epsilon}_1 + \bar{\epsilon}_2)}, \quad \bar{\epsilon}_2 > \frac{1}{\beta^2} > \bar{\epsilon}_1. \quad (74a)$$

Equation (5.2.34) then yields the total energy flowing into the region $z > 0$ in a small frequency interval $d\omega$ centered about ω ; it is recalled that the η integration extends only over those values which render $\kappa_{i1,2}$ real²¹:

$$\begin{aligned} W_\omega &= \frac{1}{\pi} \int_{-\eta_0}^{\eta_0} \vec{P}_\eta d\eta = \frac{q^2 \omega \mu_0 (\bar{\epsilon}_2 - 1/\beta^2)}{2\pi^2 (\bar{\epsilon}_2 - \bar{\epsilon}_1)} \\ &\times \int_{-1}^1 \sqrt{1 - \xi^2} \frac{\xi^2 + \hat{f}}{\xi^2 + \hat{g}} \exp \left[-2k_0 |z'| \sqrt{\left(\bar{\epsilon}_2 - \frac{1}{\beta^2} \right) \xi^2 + \left(\frac{1}{\beta^2} - \bar{\epsilon}_1 \right)} \right] d\xi, \end{aligned} \quad (75)$$

where the change of variable $\eta = \eta_0 \xi$, $\eta_0 = k_0 [\bar{\epsilon}_2 - (1/\beta^2)]^{1/2}$, has been introduced, with

$$\hat{f} = \frac{f}{k_0^2 (\bar{\epsilon}_2 - 1/\beta^2)}, \quad \hat{g} = \frac{g}{k_0^2 (\bar{\epsilon}_2 - 1/\beta^2)}. \quad (75a)$$

The integral in Eq. (75) can be evaluated when the exponential term may be replaced by unity.²¹ This happens when the charge trajectory lies in the interface $z' = 0$, or less stringently, when the parameters in question are such as to make $2k_0|z'|\sqrt{\bar{\epsilon}_2 - \bar{\epsilon}_1} \ll 1$, $k_0 = \omega/c$. The change of variable $\zeta = \xi(\xi^2 - 1)^{-1/2}$ leads to

$$W_o = \frac{q^2\omega\mu_0(\bar{\epsilon}_2 - 1/\beta^2)}{2\pi^2(\bar{\epsilon}_2 - \bar{\epsilon}_1)} \int_{-\infty}^{\infty} \frac{d\xi}{(1 + \zeta^2)^2} \frac{\zeta^2(1 + \hat{f}) + \hat{f}}{\zeta^2(1 + \hat{g}) + \hat{g}}, \quad (76)$$

which may be evaluated in terms of the residues at the poles in the upper or lower halves of the complex ζ plane. The details are left as an exercise for the reader.

5.5k Phenomena in Bounded Regions with Negative Real Dielectric Constant (Time-Harmonic Regime)

The time-harmonic radiation problems considered in the preceding sections have been concerned with conventional dielectric media characterized by a complex dielectric constant with a positive real part. However, the effect of a macroscopically neutral ionized plasma medium on an electromagnetic field can under certain conditions be represented by a complex dielectric constant whose real part may be negative [see Eq. (1.1.64), with $\partial^2/\partial t^2 \rightarrow -\omega^2$, $a \equiv 0$]. To assess the influence of such a medium on the radiation field of an electromagnetic source, and to deal in particular with interface effects associated with a bounded region, we examine the field of a line source of longitudinally directed electric current elements [Eq. (59)]† situated at the point $\hat{\mathbf{p}}' = (0, z')$, $z' < 0$, as in Fig. 5.5.7. The fields may be derived from a two-dimensional E -mode Green's function $\tilde{G}'(\hat{\mathbf{p}}, \hat{\mathbf{p}}') \equiv \tilde{G}(\hat{\mathbf{p}}, \hat{\mathbf{p}}')$, represented as follows [see discussion following Eq. (59)]:

$$\tilde{G}_1 = \tilde{G}_{f1} + \tilde{G}_s, \quad z < 0, \quad (77)$$

where \tilde{G}_{f1} is the free-space Green's function for medium 1 given in Eq. (5.4.25), while \tilde{G}_s represents the reflected contribution

$$\tilde{G}_s = -\frac{i}{4\pi} \int_{-\infty}^{\infty} \frac{e^{i\eta y - i\kappa_1(z+z')}}{\kappa_1} \Gamma(\eta) d\eta, \quad \kappa_1 = \sqrt{k_1^2 - \eta^2}, \quad (77a)$$

and $\Gamma(\eta) = (\epsilon_1\kappa_2 - \epsilon_2\kappa_1)/(\epsilon_1\kappa_2 + \epsilon_2\kappa_1)$ is the reflection coefficient given in Eq. (3d). In region 2 ($z > 0$),

$$\tilde{G}_2 = \frac{i}{4\pi} \int_{-\infty}^{\infty} e^{i\eta y + i\kappa_2 z - i\kappa_1 z'} \left\{ \frac{[1 - \Gamma(\eta)]}{\kappa_1} \right\} d\eta, \quad \kappa_2 = \sqrt{k_2^2 - \eta^2}, \quad \epsilon = \frac{\epsilon_2}{\epsilon_1}. \quad (78)$$

ϵ_1 is taken as real, but ϵ_2 may be arbitrary.

Upon transforming to the w plane via $\eta = k_1 \sin w$, k_1 positive real, one observes that the contour of integration maps into the path \tilde{P} in Fig. 5.3.6(b);

†Surface-wave phenomena encountered subsequently are associated with E modes. A line current as in Eq. (52) excites only H modes.

the branch cut leading to the branch point at $w = 0$ is absent for the line-source problem. The singularities of the integrands in Eqs. (77a) and (78) have been discussed in Eqs. (15) and (16). Since $\operatorname{Re} \epsilon$ may be negative, it is convenient to draw the branch cuts in the w plane along the contours $\operatorname{Im} \kappa_2 = 0$ (see Fig. 5.5.4), whence $\operatorname{Im} \kappa_2$ can be chosen positive on the entire top Riemann sheet. Since $\operatorname{Im} [\epsilon(1 + \epsilon)^{-1/2}] > 0$, $0 \leq \arg \epsilon \leq \pi$, Eq. (16a) still locates the pole singularities on the top sheet, with $\operatorname{Im} \cos w_p > 0$, $\operatorname{Re} \cos w_p \leq 0$, whence the pertinent pole is confined to the strip $0 < \operatorname{Re} w < \pi$, $\operatorname{Im} w < 0$. If ϵ is real, the pole is located on the borders of the strip $\pi/2 < \operatorname{Re} w < \pi$, $\operatorname{Im} w < 0$, in accord with the following:

$$\frac{\pi}{2} < \operatorname{Re} w_p \leq \pi, \quad \operatorname{Im} w_p = 0, \quad \text{for } 0 \leq \epsilon < \infty, \quad (79a)$$

$$\operatorname{Re} w_p = \pi, \quad -\infty < \operatorname{Im} w_p \leq 0, \quad \text{for } -1 < \epsilon \leq 0, \quad (79b)$$

$$\operatorname{Re} w_p = \frac{\pi}{2}, \quad -\infty < \operatorname{Im} w_p \leq 0, \quad \text{for } -\infty < \epsilon < -1. \quad (79c)$$

If $\operatorname{Re} \epsilon < 0$, $\operatorname{Im} \epsilon = 0$, the locations of the pole and branch-point singularities are shown in Fig. 5.5.10. For an asymptotic field evaluation in region 1, it is convenient to introduce cylindrical coordinates as in Fig. 5.5.7, whence the integrand takes on the form shown in Eq. (5.3.14). The steepest-descent path P through the saddle point $w = \varphi$ is also shown in Fig. 5.5.10. For sufficiently

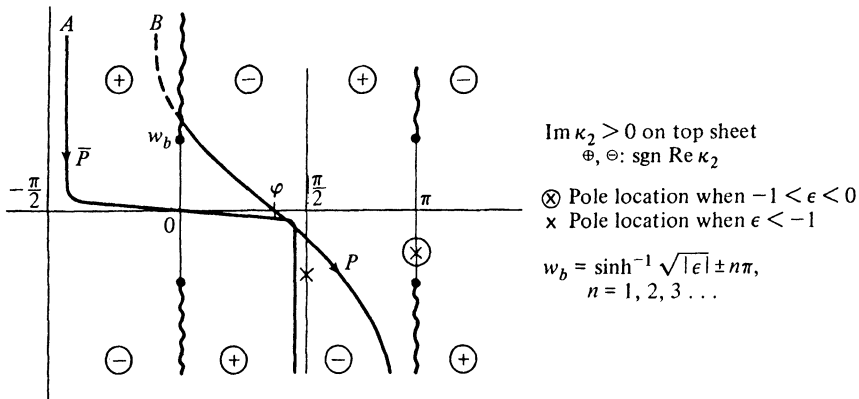


FIG. 5.5.10 Paths of integration and singularities in the w plane when $\epsilon < 0$.

large φ , P passes through the branch cut along the positive imaginary w axis and continues on to the lower Riemann sheet; although $\operatorname{Im} \kappa_2 < 0$ on the lower sheet, the exponential convergence of the integral in Eq. (77a) is not affected, since the exponent contains κ_1 only. The deformation of \bar{P} into P in the lower half of the w plane can be carried out directly provided that one accounts for the possible pole contribution when $\epsilon < -1$. At $\operatorname{Im} w \rightarrow +\infty$, one follows the procedure in Fig. 5.3.6(b). Thus, for large enough φ , whose exact value can be assessed with reference to Eq. (5.3.15a), the original integral can be written as

$$\int_{\bar{P}} = \int_P + \int_{P_s} + (\text{residue at pole}). \quad (80)$$

The steepest-descent integral yields the geometrically reflected wave contribution

$$\bar{G}_{\text{ref}} = -A_2(k_1 R) \Gamma(k_1 \sin \varphi), \quad k_1 R \gg 1, \quad (81)$$

where $A_2(k_1 R)$ is the factor multiplying Γ'' in Eq. (57a). For real $\epsilon < 0$, $|\Gamma(k_1 \sin \varphi)| = 1$, and the half-space region is totally reflecting; this observation follows at once from the imaginary wavenumber $k_2 = k_1 \sqrt{\epsilon}$, which does not permit wave propagation in medium 2. The branch-cut integral contribution has a form similar to that in Eq. (57c) and is negligible because of the presence of $\exp(-|k_2|y)$; this decay factor arises since the lateral wave (see Fig. 5.5.2) travels in the attenuating medium 2. The pole contribution, possible only when $\epsilon < -1$, represents a surface wave that propagates parallel to the interface. This wave is truly guided by the interface since it decays away from the $z = 0$ plane in both media, as will be demonstrated. In region 1, its spatial dependence is given by

$$\bar{G}_{\text{pole}} \sim \exp\left[ik_1\left(\frac{\sqrt{|\epsilon|}}{\sqrt{|\epsilon|-1}}\right)y\right] \exp\left[\frac{k_1(z+z')}{\sqrt{|\epsilon|-1}}\right], \quad z, z' < 0, \quad |\epsilon| > 1 \quad (82)$$

(i.e., the velocity of propagation in the y direction is smaller than that of a uniform plane wave).

Since when $\epsilon < 0$, κ_2 in Eq. (78) is imaginary for all η , the fields in region 2 decay exponentially with increasing z . We therefore restrict our attention to observation points lying near the interface and treat $\exp(ik_2 z)$ as an amplitude factor that does not exhibit rapid fluctuation. While an asymptotic evaluation of the integral in Eq. (78) is readily performed for large values of y and z' [see Eq. (5.3.19)], we assume for convenience that the source point lies near the interface and treat $\exp(-ik_2 z')$ also as a slowly varying factor when compared with $\exp(i\eta y)$. Transforming to the w plane via $\eta = k_1 \sin w$, one then obtains a steepest-descent path as in Fig. 5.5.10, with the saddle point located at $w = \pi/2$. The deformation of \bar{P} into P is carried out as above. The steepest-descent integral yields a space-wave contribution which varies like

$$\bar{G}_{\text{SDP}} \propto (k_1 y)^{-3/2} \exp(ik_1 y - k_1 \sqrt{1+|\epsilon|} |z|), \quad k_1 y \gg 1, \quad z > 0, \quad (83)$$

owing to the fact that $\Gamma(k_1 \sin \varphi) \rightarrow 1$ as $\varphi \rightarrow \pi/2$, so the $O[(k_1 y)^{-1/2}]$ term derived from the saddle-point evaluation vanishes. The branch-cut integral contribution is certainly negligible since it decays exponentially both with y and z . If $\epsilon < -1$, the pole contribution is the most significant and represents a surface wave with a spatial dependence

$$\begin{aligned} G_{\text{pole}} \sim & \exp\left[ik_1\left(\frac{\sqrt{|\epsilon|}}{\sqrt{|\epsilon|-1}}\right)y\right] \exp\left[-k_1\left(\frac{|\epsilon|}{\sqrt{|\epsilon|-1}}\right)z + \frac{k_1 z'}{\sqrt{|\epsilon|-1}}\right], \\ & z > 0, \quad z' < 0, \quad |\epsilon| > 1. \end{aligned} \quad (84)$$

As noted above, the surface wave decays away from the interface in both regions.

The existence of a surface wave on a plane interface between two media, with $\epsilon < -1$, can also be deduced from a transverse resonance argument (see Sec. 2.4e). The resonance relation $Z_1 + Z_2 = 0$ becomes in the present case [see Eq. (12)],

$$\kappa_2 = -\epsilon\kappa_1, \quad \kappa_{1,2} = \sqrt{k_{1,2}^2 - \eta^2}, \quad k_2 = \sqrt{\epsilon} k_1. \quad (85)$$

Since the region extends to $z = \pm\infty$, a proper modal solution satisfying the radiation condition at infinity is possible only if $\kappa_{1,2} = i|\kappa_{1,2}|$. Consequently, Eq. (85) can be satisfied only for negative ϵ and for $\eta^2 > k_1^2$. Solving for the resonant values η_p^2 , one finds

$$\eta_p^2 = \frac{|\epsilon|k_1^2}{|\epsilon| - 1}, \quad (86)$$

which, since $\eta_p^2 > 0$, imposes the restriction $\epsilon < -1$.

5.6 TIME-HARMONIC SOURCES IN THE PRESENCE OF A DIELECTRIC SLAB

5.6a Longitudinal Electric Current Element

$$\hat{\mathbf{j}}(\mathbf{r}, t) = Il\delta(\rho)\delta(z - z')e^{-i\omega t}\mathbf{z}_0. \quad (1)$$

The physical configuration of a longitudinal electric current element of strength $J^o = Il$, where I is the current in the element and l is its infinitesimal length, situated at the point $z' < 0$ on the z axis in the presence of a grounded dielectric slab is shown in Fig. 5.6.1. The slab is characterized by a dielectric

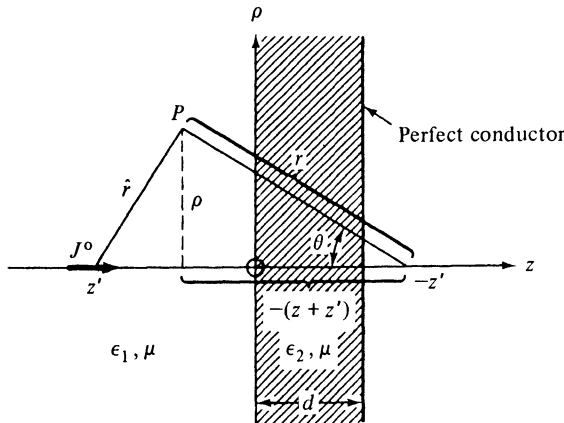


FIG. 5.6.1 Longitudinal current element and grounded dielectric slab.

constant ϵ_2 and permeability μ and occupies the region between the planes $z = 0$ and $z = d$, with a perfect conductor located at $z = d$. The medium properties in the exterior region $z < 0$ are characterized by ϵ_1 and μ . The electromagnetic fields may be derived via Eqs. (5.2.1) and (5.2.4c) from a scalar

E-mode Green's function $G'(\mathbf{r}, \mathbf{r}')$ which satisfies in the two regions the separate differential equations

$$(\nabla^2 + k_1^2)G'_1(\mathbf{r}, \mathbf{r}') = -\delta(\mathbf{r} - \mathbf{r}'), \quad z < 0, \quad (2a)$$

$$(\nabla^2 + k_2^2)G'_2(\mathbf{r}, \mathbf{r}') = 0, \quad 0 < z < d, \quad (2b)$$

subject to a radiation condition at infinity, and to the following boundary conditions at $z = 0$ and $z = d$ [see Eqs. (2.3.36) et seq.]:

$$G'_1 = G'_2; \quad \frac{1}{\epsilon_1} \frac{\partial G'_1}{\partial z} = \frac{1}{\epsilon_2} \frac{\partial G'_2}{\partial z} \quad \text{at } z = 0; \quad (2c)$$

$$\frac{\partial G'_2}{\partial z} = 0 \quad \text{at } z = d. \quad (2d)$$

$k_{1,2} = \omega\sqrt{\mu\epsilon_{1,2}}$ are the wavenumbers in the two regions. In a cylindrical coordinate description of the cross section transverse to z , $G'(\mathbf{r}, \mathbf{r}')$ in the region $z < 0$ may be represented as follows:

$$G'_1(\mathbf{r}, \mathbf{r}') = G_{f,1}(\mathbf{r}, \mathbf{r}') + G'_s(\mathbf{r}, \mathbf{r}'), \quad (3)$$

where $G_{f,1} = (1/4\pi\hat{r}) \exp(ik_1\hat{r})$ is the free-space Green's function for region 1 (see Sec. 5.4a). The scattered component G'_s has the integral representation

$$G'_s = \frac{-ik_1}{8\pi} \int_{\tilde{P}} \sin w H_0^{(1)}(k_1 r \sin \theta \sin w) e^{ik_1 r \cos \theta \cos w} \Gamma(k_1 \sin w) dw \quad (4)$$

with the *E*-mode reflection coefficient given by

$$\Gamma(k_1 \sin w) = \frac{\sqrt{\epsilon - \sin^2 w} \sin \psi - i\epsilon \cos w \cos \psi}{\sqrt{\epsilon - \sin^2 w} \sin \psi + i\epsilon \cos w \cos \psi}, \quad (4a)$$

$$\psi = k_1 d \sqrt{\epsilon - \sin^2 w}, \quad \epsilon = \frac{\epsilon_2}{\epsilon_1}.$$

The contour of integration \tilde{P} is that in Fig. 5.3.6(b) (see also Fig. 5.6.3), and the polar coordinates r, θ relative to the image point $-z'$ are depicted in Fig. 5.6.1 with $\rho = r \sin \theta$, $|z + z'| = r \cos \theta$. In the complex wavenumber plane $\xi = k_1 \sin w$, the integral representation takes the form given in Eq. (5.5.3a), with $\Gamma(\xi)$ taken from Eq. (4a).

For observation points in the slab region $0 < z \leq d$, $G'_2(\mathbf{r}, \mathbf{r}')$ has an integral representation as in Eq. (5.5.3a) provided that one replaces

$$-\exp[-i\sqrt{k_1^2 - \xi^2}(z + z')] \Gamma(\xi)$$

$$\text{by } [1 - \Gamma(\xi)] \exp(-i\sqrt{k_1^2 - \xi^2}z) \frac{\cos[\sqrt{k_1^2 \epsilon - \xi^2}(d - z)]}{\cos(\sqrt{k_1^2 \epsilon - \xi^2}d)}, \quad (5)$$

with $\Gamma(\xi)$ given in Eq. (4a).

For large values of $k_1 r \sin \theta$, the secondary contribution G'_s to the Green's function in the region $z < 0$ may be evaluated asymptotically by the saddle-point method. The resulting $G'_1(\mathbf{r}, \mathbf{r}')$ for arbitrary distances \hat{r} from the source, but for large distances r from the image point, is given by

$$\begin{aligned}
G'_1 \sim & \frac{e^{ik_1 r}}{4\pi r} - \Gamma(k_1 \sin \theta) \frac{e^{ik_1 r}}{4\pi r} \left[1 + O\left(\frac{1}{k_1 r}\right) \right] \\
& + \frac{e^{i\pi/4}}{2\sqrt{2\pi k_1 r} \sin \theta} \left[\sum_v \frac{e^{ik_1 r \cos(w_v - \theta)}}{\epsilon_1 A_v^2 \sqrt{\sin w_v}} U(\theta - \theta_v) \right. \\
& \left. + \sum_\mu \frac{e^{ik_1 r \cos(w_\mu - \theta)}}{\epsilon_1 A_\mu^2 \sqrt{\sin w_\mu}} U(\theta - \theta_\mu) \right] \left[1 + O\left(\frac{1}{k_1 r}\right) \right], \quad (6)
\end{aligned}$$

where $U(\gamma)$ is the Heaviside unit function, which equals unity for $\gamma > 0$ and vanishes for $\gamma < 0$, while

$$\Gamma(k_1 \sin \theta) = \frac{\cos \theta' \tan(k_1 d \sqrt{\epsilon} \cos \theta') - i\sqrt{\epsilon} \cos \theta}{\cos \theta' \tan(k_1 d \sqrt{\epsilon} \cos \theta') + i\sqrt{\epsilon} \cos \theta}, \quad \sin \theta' = \frac{\sin \theta}{\sqrt{\epsilon}}, \quad (6a)$$

and

$$\epsilon_1 A_\alpha^2 = \frac{d}{2} \left\{ \left[1 - \left(\frac{q}{p} \right)^2 \right] \frac{i}{q} + \frac{1}{\epsilon} \left[1 - \epsilon^2 \left(\frac{q}{p} \right)^2 \right] \right\}, \quad \epsilon = \frac{\epsilon_2}{\epsilon_1}, \quad \alpha = v, \mu. \quad (6b)$$

p and q satisfy the transcendental equations

$$\begin{aligned}
\epsilon q &= ip \tan p, \\
p^2 - q^2 &= (k_1 d)^2 (\epsilon - 1) \equiv l^2,
\end{aligned} \quad (7)$$

and are related as follows to $w_\alpha = w_v$ or $w_\alpha = w_\mu$:

$$p = k_1 d \sqrt{\epsilon - \sin^2 w_\alpha}, \quad q = k_1 d \cos w_\alpha. \quad (7a)$$

While the terms in the series have also been approximated for the far zone $k_1 \rho \gg 1$, they may easily be given exactly for arbitrary values of $k_1 \rho$ [see the discussion preceding Eqs. (15)]. The pole singularities w_α of the reflection coefficient in Eq. (4a), defined by Eqs. (7), may be grouped into two categories: (1) surface-wave poles $w_\alpha \equiv w_v$ and (2) leaky-wave poles $w_\alpha \equiv w_\mu$. The sums in Eq. (6) denote corresponding residue contributions to the asymptotic field solution, and they arise at observation angles $\theta > \theta_\alpha$, where

$$\theta_\alpha = \operatorname{Re} w_\alpha - \cos^{-1} \operatorname{sech}(\operatorname{Im} w_\alpha), \quad \alpha = v, \mu. \quad (8)$$

The results are valid exterior to the transition regions $\theta \approx \theta_\alpha$. For modifications in transition regions, see the discussion following Eq. (16).

Discussion

The first two terms on the right-hand side of Eq. (6) (without the quantity in brackets) represent the geometric optical field; they may be interpreted exactly as for the semiinfinite medium in Sec. 5.5a, except that $\Gamma(k_1 \sin \theta)$ now accounts for the reflection from the slab configuration. It may in fact be shown that for lossless media, the slab reflection coefficient in Eq. (6a) may be synthesized by summing up the multiply reflected- and refracted-ray contributions sketched in Fig. 5.6.2.

The residue terms constitute diffraction fields which contribute for observation angles θ sufficiently near the interface. When the region is almost lossless,

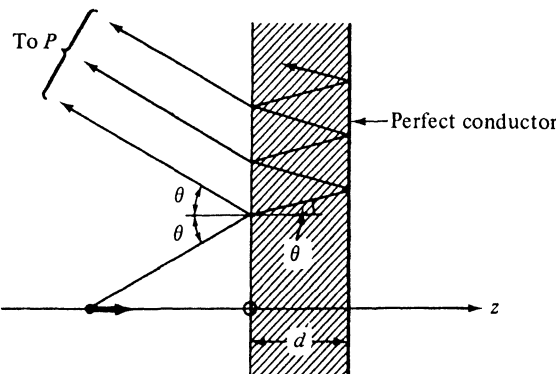
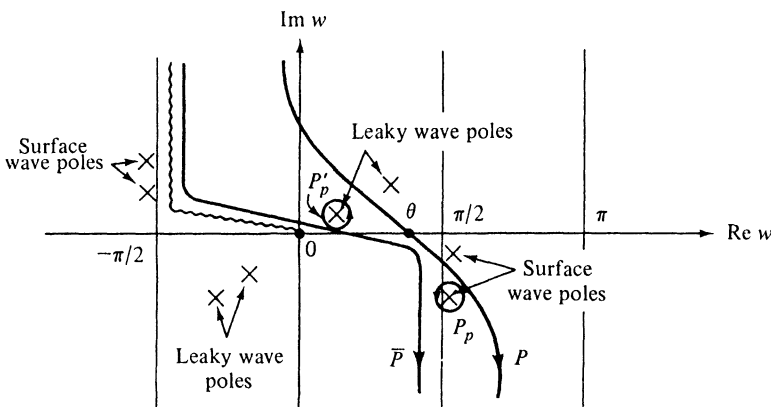


FIG. 5.6.2 Ray-optical interpretation of the reflection coefficient.

FIG. 5.6.3 Contours of integration and singularities in the w plane.

the relevant surface-wave and leaky-wave poles in the complex w plane are situated as in Fig. 5.6.3; in the lossless case, the surface-wave poles are located on the vertical lines $\text{Re } w_\alpha = \pm\pi/2$. One notes that in contrast to the direct-wave and reflected-wave contributions which possess a $1/k_1 r$ or $1/k_1 r$ variation characteristic of spherically diverging waves, the surface-wave and leaky-wave fields behave like cylindrical waves with a $1/\sqrt{k_1 r \sin \theta} = 1/\sqrt{k_1 \rho}$ dependence. Thus, from purely geometrical considerations, the decay of the fields in a surface wave or leaky wave is slower than that in the geometric-optical field contributions. However, the behavior of the amplitude factors and the exponential terms must likewise be considered in assessing the importance of a particular residue term.

For real ϵ greater than 1, Eqs. (7) can be satisfied for imaginary values of $q = i|q|$ and real values of p . These solutions, finite in number, characterize surface waves with the exponential dependence

$$e^{ik_1 r \cos(w_p - \theta)} = e^{-|q||z+z'|/d} \exp[ik_1 \sqrt{1 + (|q|/k_1 d)^2} \rho], \quad (9)$$

undamped in the coordinate ρ parallel to the slab surface, but appreciable only when both the source and observation points are situated near the surface. The name "surface wave" derives from the field being confined near the interface in this wave species. In the assumed absence of dissipation, if $|z + z'| \rightarrow 0$, the surface waves in the dielectric constitute the dominant contribution to the field because of their above-mentioned cylindrical wave character, as opposed to the spherical wave behavior of the geometric optical field. In fact, in the range $\theta \rightarrow \pi/2$ where the surface-wave contribution is most pronounced, one notes that $\Gamma(k_1 \sin \theta) \rightarrow 1$, $r \rightarrow \hat{r} \rightarrow \rho$, so the geometric optical field vanishes to $O(1/k_1 \rho)$. The surface-wave variation $O(1/\sqrt{k_1 \rho})$ is therefore to be compared with a contribution of $O(1/k_1^2 \rho^2)$ arising from a second-order evaluation of the steepest-descent integral in Eq. (5.3.16a). It is noted from Eq. (9) that the undamped propagation constant of the surface wave in the ρ direction, κ_ρ , is given by $\kappa_\rho = k_1 \sqrt{1 + (|q|/k_1 d)^2} > k_1$, so its phase velocity $v = \omega/\kappa_\rho$ is less than the phase velocity $v_f = \omega/k_1$ of a plane wave in free space. Hence, these surface waves are also referred to as "slow" waves (see Sec. 5.4d).

Concerning the leaky-wave contributions in Eq. (6), corresponding to complex roots of Eqs. (7), we note from Fig. 5.6.3 that, in their domains of existence, $(w_{\mu r} - \theta) < 0$, $w_{\mu i} > 0$, where $w_{\mu r}$ and $w_{\mu i}$ are the real and imaginary parts of w_μ , respectively. Since

$$e^{ik_1 r \cos(w_{\mu r} - \theta)} = \exp\{ik_1 r [\cos(w_{\mu r} - \theta) \cosh w_{\mu i} - i \sin(w_{\mu r} - \theta) \sinh w_{\mu i}]\}, \quad (10a)$$

$$= \exp\{ik_1 [\gamma|z + z'| + \beta\rho]\}, \quad (10b)$$

where

$$\gamma = \cos w_{\mu r} \cosh w_{\mu i} - i \sin w_{\mu r} \sinh w_{\mu i}, \quad (10c)$$

$$\beta = \sin w_{\mu r} \cosh w_{\mu i} + i \cos w_{\mu r} \sinh w_{\mu i},$$

a typical leaky-wave contribution decreases exponentially in all directions $\theta > \theta_\mu$. These contributions to the far field are therefore negligible unless $w_{\mu i} \rightarrow 0$ (i.e., for leaky-wave poles situated very near the real w axis). As noted in Sec. 5.3e, although the leaky-wave fields increase exponentially with $|z + z'|$ [see Eqs. (10b) and (10c)], their restricted domain of existence $\theta > \theta_\mu$ limits the maximum allowable value of $|z + z'|$ (for a given ρ) in such a manner that the decay along ρ overcomes the growth along $|z|$ (see Fig. 5.3.8). In view of the decay with ρ , the wave leaks energy continually into the direction perpendicular to the surface.

In reference to the asymptotic reduction of Eqs. (5.3.12) and (5.3.14), which represent the generic form of Eq. (4), the following observation is relevant. In Eq. (5.3.15), the restricted domain of existence of a typical residue contribution appears as the result of the transformation of an exact integral representation along path \bar{P} into another along path P . Since residues represent surface waves or leaky waves, while the steepest-descent integral gives rise (asymptotically) to a space wave or radiation field, it is suggestive to conclude that surface

or leaky waves exist only when $\bar{\alpha} > \bar{\alpha}_p$ in Eq. (5.3.15) or in its asymptotic approximation. The latter supposition does not follow, since the asymptotic approximation, unlike the exact representation, contains an exponentially small error against which exponentially small residue terms must be compared [see remarks following Eqs. (4.2.18)]. Only upon specification of the error term, which depends on the radius of convergence of the power-series expansion of the integrand in Eq. (4) about the saddle point, may Eq. (6) be made consistent. It then follows that the absence of the surface-wave residue terms when $\theta < \theta_v$ need not imply the nonexistence of these waves but merely that their amplitude is so small as to be beyond the accuracy of the approximation.

If $\epsilon_2 < \epsilon_1$ (i.e., $\epsilon < 1$), the region $z < 0$ is occupied by the denser medium, so the configuration in Fig. 5.6.1 can be viewed as a dielectric "gap." In this instance, Eqs. (7) do not admit of surface-wave solutions for which p is real and $q = i|q|$; hence, the leaky-wave contributions may be important for the evaluation of the fields in the region $z < 0$. To illustrate this possibility, let us consider the case $0 < \epsilon \ll 1$. Since the gap region $0 < z < d$ appears to be a waveguide bounded by highly reflecting walls at $z = 0, d$, it is suggestive to look for solutions of the resonance equations (7) which differ from the resonant solutions $p_0 = \kappa_{20}d = m\pi$, $m = 0, 1, 2, \dots$, appropriate to $\epsilon = 0$, by the small quantity δ :

$$p = m\pi + \delta. \quad (11)$$

Upon substituting Eq. (11) into Eqs. (7) and retaining terms to $O(\delta)$ only, one obtains as a first approximation,

$$\delta \approx \frac{-i\epsilon}{m\pi} \sqrt{(m\pi)^2 + (k_1 d)^2(1 - \epsilon)}, \quad m = 1, 2, \dots, \quad (12a)$$

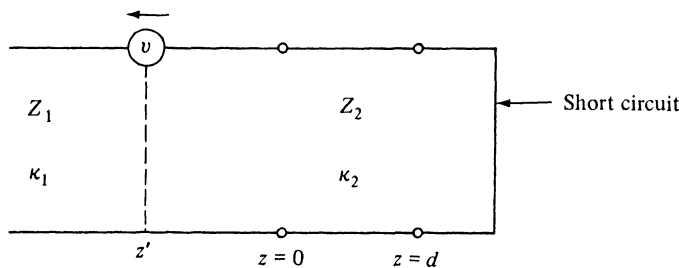
valid when $0 < \epsilon \ll 1$, $\epsilon \sqrt{1 + (1 - \epsilon)(k_1 d/m\pi)^2} \ll 1$. For $m = 0$, one must retain terms to $O(\delta^2)$ and finds

$$\delta = e^{-i\pi/4} \sqrt{\epsilon a}, \quad a = k_1 d \sqrt{1 - \epsilon}, \quad \epsilon a \ll 1, \quad \epsilon \ll a. \quad (12b)$$

For Eq. (12a), $\text{Im } q = -\sin w_{\mu r} \sinh w_{\mu i} = -\epsilon$, while for Eq. (12b), $\text{Im } q = -\epsilon/2$. Since $\epsilon \ll 1$, one finds that the pertinent leaky-wave poles are situated near the real w axis and the attenuation of the leaky waves noted in the preceding paragraph can be small; for δ given in Eq. (12b), one finds $w_{\mu} \approx \sqrt{\epsilon} \cdot \sqrt{1 + (i/k_1 d)}$. Thus, their contribution for observation points with large $k_1 r$ but small $k_1 r \sin(\theta - w_{\mu r}) \sinh w_{\mu i}$ may be appreciable.⁵

Analytical details

The integral representation for G'_s in Eq. (4) is derived by considerations directly analogous to those utilized in connection with Eqs. (5.5.11), except that for the modal Green's function, the boundary condition $dg_{z2}/dz = 0$ at $z = d$ must be added [see Eq. (2d)]. The corresponding modal network problem is sketched in Fig. 5.6.4, and g_z is proportional to the current in the network. The solution for $z < 0$ is given in Eq. (5.3.1), where $Z_1 = \kappa_1/\omega\epsilon_1$ (E modes)

FIG. 5.6.4 Equivalent modal network (E modes).

and $\vec{Z}(0)$, the input impedance of the short-circuited transmission line seen from $z = 0$, is given via Eq. (2.4.24a) as

$$\vec{Z}(0) = jZ_2 \tan \kappa_2 d, \quad Z_2 = \frac{\kappa_2}{\omega \epsilon_2}, \quad \kappa_{1,2} = \sqrt{k_{1,2}^2 - \xi^2}. \quad (13)$$

Equation (5.3.1a) with $\xi = k_1 \sin w$ thus yields the reflection coefficient in Eq. (4a), and Eqs. (3) and (4) follow from the general integral representation in Eq. (5.2.11), with $j \rightarrow -i$ to account for the difference in time dependence [see also Eq. (5.4.7a)]. When the source point z' is located inside the slab region $0 < z \leq d$, the modal Green's function g_z has the more general form given in Eqs. (2.4.28) or (2.4.29) (see also Sec. 3.4a).

The solution for observation points in the slab region $0 < z \leq d$ may be derived by inspection from that for g_{z1} in the exterior region $z < 0$ [Eq. (5.3.1)]. Since $dg_{z2}/dz = 0$ at $z = d$, g_{z2} must be proportional to $\cos \kappa_2(d - z)$. Then from the continuity $g_{z1} = g_{z2}$ at $z = 0$, one has

$$g_{z2}(z, z') = g_{z2}(0, z') \frac{\cos \kappa_2(d - z)}{\cos \kappa_2 d} = g_{z1}(0, z') \frac{\cos \kappa_2(d - z)}{\cos \kappa_2 d}, \quad (14)$$

thereby justifying Eq. (5).

The asymptotic evaluation of the integral in Eq. (4) proceeds as in Sec. 5.5a, except that in the function $f(w)$ in Eq. (5.5.14), the reflection coefficient is taken from Eq. (4a). A first-order saddle-point evaluation yields the second term on the right-hand side of Eq. (6), and higher-order terms, denoted by the symbol $O(1/k_1 r)$, may be derived by the procedure in Sec. 4.2b.

Concerning the singularities of the integrand in Eq. (4) in the complex w plane, we note first the branch points at $\sin w = 0$ arising from the argument of the Hankel function. The pertinent branch point at $w = 0$, and the associated branch cut, are shown in Fig. 5.6.3. No branch points are located at $w_b = \pm \sin^{-1} \sqrt{\epsilon}$, or correspondingly at $\xi_b = \pm k_2$, since $\Gamma(k_1 \sin w)$ is an even function of $\sqrt{\epsilon - \sin^2 w}$. This is in accord with the general observation made in Sec. 5.3a because region 2 is terminated at $z = d$ (i.e., $z = +\infty$ is inaccessible). The branch-point pair at $z_b = \pm k_1$ in the complex wavenumber plane has been removed by the transformation $\xi = k_1 \sin w$. However, $\Gamma(k_1 \sin w)$ has pole singularities at the zeros w_α of the denominator on the right-hand side

of Eq. (4a). Upon introducing the new parameters p and q in Eq. (7a), one obtains the simultaneous equations (7) defining the location of the pole singularities. These equations can also be derived from an application of the transverse resonance argument in Eq. (2.4.36). As seen from the $z = 0$ terminal in Fig. 5.6.4, $\vec{Z}(0)$ is given in Eq. (13), $\vec{Z}(0) = Z_1$, whence the transverse resonance relation $\vec{Z}(0) + \vec{Z}(0) = 0$ yields Eqs. (7) (with $j \rightarrow -i$).

For non-dissipative media, ϵ and k^2 are positive; Eqs. (7) can then be satisfied for imaginary values of $q = i|q|$ and real values of p . Simple poles corresponding to these values of q are finite in number and are located at $w_{\nu} = \pi/2$, $w_{\nu} < 0$.[†] From Eq. (4), residue terms arising from such poles have a z dependence $\exp[i|z + z'| \cos w_{\nu}] = \exp[-|q||z + z'|/d]$ [see Eq. (9)] and a ρ dependence $H_0^{(1)}(k_1\rho \sin w_{\nu})$, the latter behaving like $(k_1\rho)^{-1/2} \exp(ik_1\rho \sin w_{\nu})$ for large $k_1\rho \sin w_{\nu}$. These residues represent the surface waves discussed previously. They constitute proper solutions of the transverse resonance equations (7), carry no real power in the direction perpendicular to the surface, and play an important role in the determination of the spectrum of waves that can be guided along the dielectric surface (see Sec. 3.4a). A “proper” modal solution satisfies the source-free Maxwell field equations, the boundary conditions on the perturbing surface, and it decays at infinity.

One observes from Eqs. (7) that for $q = i|q|$ and p real, $|q| = -k_1 d \sinh w_{\nu}$ must lie between the limits $0 \leq |q| < k_1 d \sqrt{\epsilon - 1}$. Equations (7) can be solved graphically by a construction analogous to that in Fig. 3.4.3, yielding the same general picture except that the non-circular contours in Fig. 3.4.3 are displaced to the left through an interval $\pi/2$. It is then evident that for real ϵ and k_1 , and $\epsilon > 1$, N solutions exist in the range $(N-1)\pi < k_1 d \sqrt{\epsilon - 1} < N\pi$, $N = 1, 2, \dots$. In particular, one solution exists for arbitrarily small $k_1 d \sqrt{\epsilon - 1}$ (i.e., there is no low-frequency cutoff). For ϵ positive real and less than unity, and k_1 real, no solutions are possible for real p and positive imaginary q .

In addition to the surface-wave roots, Eqs. (7) possess an infinity of other complex roots²² in the half-strip $0 < \operatorname{Re} w < \pi/2$, $\operatorname{Im} w > 0$, to mention only those pertinent to the present problem. For these “leaky-wave” roots $w_{\alpha} = w_{\mu}$, $|\exp[i|z + z'|k_1 \cos w_{\mu}]| = \exp[k_1|z + z'| \sin w_{\mu}, \sinh w_{\mu}]$ increases with distance from the surface of the dielectric. The field variation along the slab is given by $H_0^{(1)}(k_1\rho \sin w_{\mu})$, thereby leading for large $k_1\rho \sin w_{\mu}$ to the dependence noted in Eqs. (10). The leaky waves cannot represent a field solution everywhere in space because of their unlimited growth at $z \rightarrow -\infty$. Therefore, they do not belong to the proper spectrum of waves (modes) that can be guided along the dielectric slab. These “non-modal” waves may arise, however, in a field representation for a limited region of space wherein they decay [region $\theta > \theta_{\mu}$ in Eq. (6); see also Fig. 5.3.8].

[†]It is evident from Eqs. (7) that if w_{α} is a solution of these equations, then $-w_{\alpha}$ is also a solution. Moreover, when ϵ is real, one notes upon taking the complex conjugate that Eqs. (7) are also satisfied by $-q^*$, implying for real k_1 that $\pi - w_{\alpha}^*$ is also a solution.

To ascertain the disposition of the surface-wave poles with respect to the path of integration \bar{P} in Fig. 5.6.3, we assume for the moment that ϵ_1 and ϵ_2 are slightly complex but that $\arg \epsilon_2 = \arg \epsilon_1$, so ϵ is real. Since $p = \kappa_2 d$, $q = \kappa_1 d$, and $\text{Im } \kappa_{1,2} > 0$ for the assumed $\exp(-i\omega t)$ time dependence, it follows that $\text{Im } p > 0$, $\text{Im } q > 0$. From Eq. (7), one then has $\text{Re } q < 0$. From Eqs. (5.3.5a) and (5.3.8), it is noted that the requirement $\text{Re } q < 0$, $\text{Im } q > 0$, is satisfied in the strip $\pi/2 < \text{Re } w < \pi$, $\text{Im } w < 0$. This establishes the location of the pertinent surface-wave poles and path of integration as shown in Fig. 5.6.3. Typical leaky-wave poles located in the strip $-\pi/2 < \text{Re } w < \pi/2$ are also shown. In the limit $\arg \epsilon_1 \rightarrow 0$, it is evident that the path \bar{P} is to be indented to the left around the surface-wave poles situated on the half-line $\text{Re } w = \pi/2$, $\text{Im } w < 0$. During the deformation of the path \bar{P} into the steepest-descent path P through the saddle point at $w = \theta$, surface-wave or leaky-wave poles may be intercepted, and these give rise to the residue terms expressed by the sums in Eq. (6). As noted above, the residue contributions can be obtained *exactly* by retaining the Hankel function in Eq. (4). The form in Eq. (6) has been simplified by employing the condition $k_1 \rho \gg 1$ for the Hankel function [see Eq. (5.3.13)], a condition imposed on the evaluation of the saddle-point integral. The residue at a typical pole w_α is proportional to [see Eqs. (4) and (5.3.15)]

$$R_\alpha = \sqrt{\sin w_\alpha} e^{ik_1 r \cos(w_\alpha - \theta)} B_\alpha, \quad (15)$$

where

$$B_\alpha = [(w - w_\alpha) \Gamma(k_1 \sin w)]_{w=w_\alpha} = \frac{2p \sin p}{\left[\frac{d}{dw} (p \sin p + i\epsilon q \cos p) \right]_{w=w_\alpha}}. \quad (15a)$$

After carrying out the differentiation and recalling Eqs. (7), one obtains, for B_α ,

$$B_\alpha = \frac{i}{\epsilon_1 A_\alpha^2 k_1 \sin w_\alpha}, \quad (16)$$

with A_α^2 given in Eq. (6b). For the surface waves, $q = i|q|$, p real; $A_\alpha^2 \equiv A_v^2$ in Eq. (6b) is then identical with the normalization term for the surface-wave spectrum in Eq. (3.4.26c), save for the replacement $\epsilon_1 \leftrightarrow \epsilon_2$ arising because of the different medium designations in Figs. 5.6.1 and 3.4.5.

It should be emphasized that the result in Eq. (6) is valid when $\theta \neq \theta_{v,p}$ (i.e., when the steepest-descent path does not pass near a pole singularity). To effect a continuous transition in Eq. (6) as the steepest-descent path crosses a pole, or when a pole is near the saddle point, one employs the modified saddle-point procedures in Sec. 4.4a.

Alternative representation (radial transmission formulation)

As noted in the preceding section, near the surface of the dielectric slab configuration of Fig. 5.6.1, with $\epsilon_2 > \epsilon_1$, the dominant contribution to the far electromagnetic fields due to a longitudinal electric current situated near the

slab arises from surface waves which propagate in the ρ direction like cylindrical waves and decay exponentially away from the interface. The amplitudes of excitation of these waves given in Eq. (6) were not obtained directly from the z -transmission formulation leading to Eq. (4), but emerged only after an asymptotic evaluation of the far fields observed near the interface. Because the surface waves represent fields that propagate *along* the interface, it is suggestive that a radial transmission formulation (i.e., a representation in terms of the mode spectrum in the z domain) of the scalar E -mode Green's function G' yields their excitation amplitudes in a more direct manner.

A ρ -transmission representation for G' can be written down at once from Eq. (3.3.39b), wherein $u \equiv \rho$, $v \equiv \phi$. The orthonormal eigenfunctions for the ϕ and z domains were obtained in Sec. 3.4 and are repeated below for convenience. In the z domain, the scalar eigenfunctions $\Phi_r(z)$ must satisfy boundary conditions appropriate to E modes along z in the configuration of Fig. 5.6.1. This configuration is identical with that in Fig. 3.4.5, provided that $x, x', \epsilon_1, \epsilon_2$ in the latter are replaced by $-z, -z', \epsilon_2, \epsilon_1$, respectively. As noted from Eqs. (3.4.25)–(3.4.27), the mode spectrum has a discrete (surface wave) and a continuous part; we list only the functions required for a field representation in the region $z < 0$, with $z' < 0$.

z domain

Discrete part:

$$\Phi_r(z) \equiv \Phi_\nu(z) = \frac{e^{iq_\nu|z|/d}}{\sqrt{\epsilon_1} A_\nu}, \quad (17a)$$

where $q_\nu = i|q_\nu|$ is a solution of the transverse resonance equations (7), and A_ν is given by Eq. (6b).

Continuous part:

$$\Phi_r(z) \equiv \Phi(\zeta, z) = \frac{1}{\sqrt{2\pi}} [e^{i\zeta z} - \vec{\Gamma}(\zeta) e^{-i\zeta z}], \quad 0 < \zeta < \infty, \quad (17b)$$

where

$$\vec{\Gamma}(\zeta) \equiv \Gamma(\zeta) = \frac{-i\xi_1 \tan \xi_1 d - \zeta \epsilon}{-i\xi_1 \tan \xi_1 d + \zeta \epsilon}, \quad \xi_1 = \sqrt{k_1^2(\epsilon - 1) + \zeta^2}. \quad (17c)$$

The replacement $j \rightarrow -i$, appropriate to an assumed $\exp(-i\omega t)$ time dependence, has been made above. Also, the variable ξ in Eqs. (3.4.25)–(3.4.27) has been replaced by ζ to avoid confusion with the notation in the present chapter.

ϕ domain

The appropriate eigenfunctions are listed in Eq. (3.2.51b):

$$\Phi_m(\phi) = \frac{1}{\sqrt{2\pi}} e^{im\phi}, \quad m = 0, \pm 1, \pm 2, \dots \quad (18)$$

The radial characteristic Green's function $g'_r(\rho, \rho'; \lambda_\rho, \lambda_{\phi m})$ is identical with that listed in Eq. (3.4.93):

$$g'_p(\rho, \rho'; \lambda_p, \lambda_{\phi_m}) = \frac{\pi i}{2} J_m(\eta \rho_<) H_m^{(1)}(\eta \rho_>), \quad \eta = \sqrt{\lambda_p} = \sqrt{k_1^2 - \lambda_z}. \quad (19)$$

The relation $\lambda_p = k_1^2 - \lambda_z$ follows from Eq. (3.3.38b); λ_z is defined as

$$[-1/\Phi(z)][d^2\Phi(z)/dz^2].$$

Upon substituting Eqs. (17) and (18) into Eq. (3.3.39b), one obtains for the radial transmission representation of $G'(\mathbf{r}, \mathbf{r}')$ [$\rho' = 0$ in Fig. 5.6.1, hence only the $m = 0$ term in Eq. (18) contributes since $J_m(0) = 0$ for $m \neq 0$]:

$$\begin{aligned} G'(\mathbf{r}, \mathbf{r}') &= \frac{1}{2\pi} \frac{\pi i}{2} \sum_v \frac{e^{iq_v(z+z')/d}}{\epsilon_1 A_v^2} H_0^{(1)}(\sqrt{k_1^2 + |q_v|^2/d^2} \rho) \\ &\quad + \frac{1}{2\pi} \frac{\pi i}{2} \int_0^\infty \Phi(\zeta, z) \Phi^*(\zeta, z') H_0^{(1)}(\sqrt{k_1^2 - \zeta^2} \rho) d\zeta, \end{aligned} \quad (20)$$

where $\sqrt{k_1^2 - \zeta^2}$ is positive when real, and equal to $i\sqrt{\zeta^2 - k_1^2}$ when $|\zeta| > k_1$. The sum in Eq. (20) extends over all solutions $q_v = i|q_v|$, p_v real, of the transverse resonance equations (7), and represents the spectrum of surface waves excited by the source in the presence of the dielectric slab. Upon approximating the Hankel function by its asymptotic form in Eq. (5.3.13) and recalling Eq. (7a), one verifies that the surface-wave amplitudes in Eq. (20) are identical with those in Eq. (6). Hence, as anticipated, the excitation amplitudes of the surface-wave spectrum are determined directly from the radial transmission representation. However, to assess the influence of the continuous spectrum, one must still estimate the contribution from the integral in Eq. (20).

It is instructive to trace in detail the transition from the z -transmission formulation to the ρ -transmission representation in Eq. (20). It is convenient to begin in the ζ plane, wherein G' is represented via Eqs. (5.2.11) and (5.3.1) for $z, z' < 0$ and for a time dependence $\exp(-i\omega t)$ as

$$G'(\mathbf{r}, \mathbf{r}') = \frac{i}{8\pi} \int_{-\infty e^{i\pi}}^\infty \xi H_0^{(1)}(\xi \rho) [e^{i\xi|z-z'|} - \Gamma(\zeta) e^{-i\xi(z+z')}] \frac{d\xi}{\zeta}, \quad \zeta = \sqrt{k_1^2 - \xi^2}, \quad (21)$$

where $\Gamma(\zeta)$ is the reflection coefficient given in Eq. (4a). The transformation $\zeta = k_1 \sin \vartheta$ in Eq. (21) then yields the formulations in Eqs. (3) and (4). Equation (21) involves a *modal* representation in the radial domain and therefore constitutes a *transmission* formulation along z . The path of integration proceeds as in Fig. 5.3.6(a) relative to the branch-point singularities in the complex ζ plane; no branch points exist at $\zeta = \pm k_2$. The ρ -transmission formulation is to be obtained from Eq. (21) by a deformation of the integration path into the upper half of the ζ plane around the singularities of $g_z(z, z')$.† Since this deformation is possible for arbitrary \mathbf{r} and \mathbf{r}' only in those regions wherein $\text{Im } \zeta >$

†There exists an intimate relation between the procedure carried out here in the ζ plane, and the characteristic Green's-function technique described in Sec. 3.3c. In the notation of Eqs. (3.3.37) and (3.3.38), $\zeta \equiv \sqrt{\lambda_u}$ and $\lambda_z = k_1^2 - \lambda_u = \zeta^2$.

0, it is convenient to choose branch cuts emanating from the branch points $\xi = \pm k_1$ as in the second of Figs. 5.3.3(a), so $\text{Im } \zeta > 0$ on the entire top sheet of the two-sheeted ξ plane. In the discussion carried out in connection with Fig. 5.6.3, it is noted that the singularities of $\Gamma(\zeta)$ are either surface-wave poles ξ_ν for which $\text{Im } \zeta_\nu > 0$, $\text{Re } \zeta_\nu < 0$, or leaky-wave poles ξ_μ for which $\text{Im } \zeta_\mu < 0$. Thus, only the surface-wave poles appear on the top sheet of the two-sheeted ξ -plane, as shown in Fig. 5.6.5. To highlight the progress of the contour of

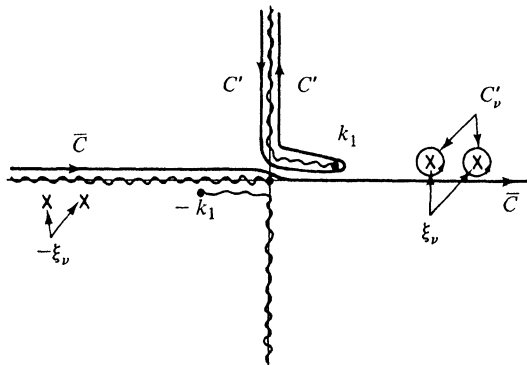


FIG. 5.6.5 Contours of integration and singularities in the ξ plane.

integration $\tilde{\mathcal{C}}$, the various singularities at $\xi = \pm k_1$ and $\xi = \xi_\nu$ have been given small complex parts.

A deformation of the contour $\tilde{\mathcal{C}}$ about the singularities of the integrand in Eq. (21) in the upper half of the ξ plane can now be carried out directly. By virtue of Eq. (5.3.13), the Hankel function vanishes exponentially at $|\xi| \rightarrow \infty$, $\text{Im } \xi > 0$. Since $\text{Im } \zeta > 0$ on the entire top sheet, the terms inside the brackets of Eq. (21) vanish exponentially at $|\xi| \rightarrow \infty$. Thus, there is no contribution to the integral from a contour at $|\xi| \rightarrow \infty$, $0 < \arg \xi < \pi$; the integral taken over the contour $\tilde{\mathcal{C}}$ is by Cauchy's theorem equal to the integral taken over the contour C' surrounding the branch cut plus the integrals taken over the contours C'_ν surrounding the surface-wave poles of $\Gamma(\zeta)$. The latter formulation constitutes the desired radial transmission representation since, as in Eq. (20), it involves the mode spectrum in the z domain. The discrete spectrum arises from the residue contributions at the surface-wave poles and yields identically the series portion of Eq. (20). To show that the contribution from the continuous spectrum in Eq. (20) is the same as that arising from the branch-cut integral taken over the contour C' , one introduces ζ as a new variable in Eq. (21) [see Eq. (5.4.10) et seq.] and simplifies, noting that $\Gamma(-\zeta) = \Gamma^*(\zeta)$ when ζ is real.

In the w plane, the contour $\tilde{\mathcal{C}}$ in Fig. 5.6.5 transforms into the contour \tilde{P} in Fig. 5.6.3, whereas the contour C' maps into a path P' which runs along the imaginary axis from $w = i\infty$ to $w = 0$, along the real axis from $w = 0$ to $w =$

π , and then along the vertical line from $w = \pi$ to $w = \pi - i\infty$. In a far-field asymptotic calculation of the contribution to Eq. (20) from the continuous spectrum as represented on the infinite contour P' , one deforms P' into the steepest-descent path P in Fig. 5.6.3 and evaluates the steepest-descent integral as in Eq. (6). Unless $\theta = \pi/2$, there exists the possibility of crossing during the path deformation one or more of those surface-wave poles which lie closest to the real w axis of Fig. 5.6.3. The resulting residue contributions cancel corresponding terms in the sum on the right-hand side of Eq. (20), so not all of the possible surface waves are included in the asymptotic representation of the fields observed above the dielectric interface. Moreover, one or more of the leaky-wave poles may have to be taken into account. The final result then agrees with that in Eq. (6), which is derived from an initial z -transmission formulation.

Modifications for an ungrounded slab

When the source is located exterior to an ungrounded slab as in Fig. 5.6.6(a), the preceding analysis must be modified only through the insertion of the appropriate modal Green's function g , whose evaluation is schematized in network form in Fig. 5.6.6(b). Instead of treating the problem in Fig. 5.6.6 directly, it

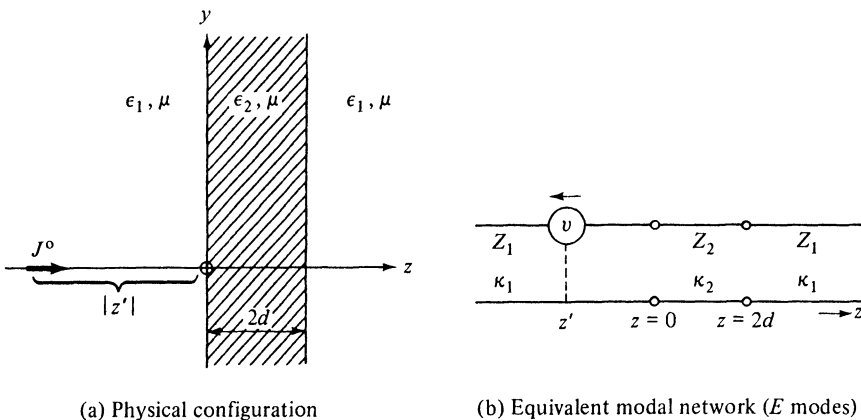


FIG. 5.6.6 Longitudinal current element and ungrounded dielectric slab.

is convenient, because of the network symmetry about the plane $z = d$, to consider two auxiliary problems arising from symmetric and antisymmetric voltage excitations, as shown in Figs 5.6.7(b) and 5.6.7(a), respectively. The corresponding electromagnetic field problems are also shown.

From the network picture one notes that the antisymmetric voltage excitation gives rise to a voltage null (short circuit) at the symmetry plane $z = d$, while the symmetric voltage excitation gives rise to a current null (open circuit) at $z = d$. Correspondingly, the tangential electric and magnetic fields vanish

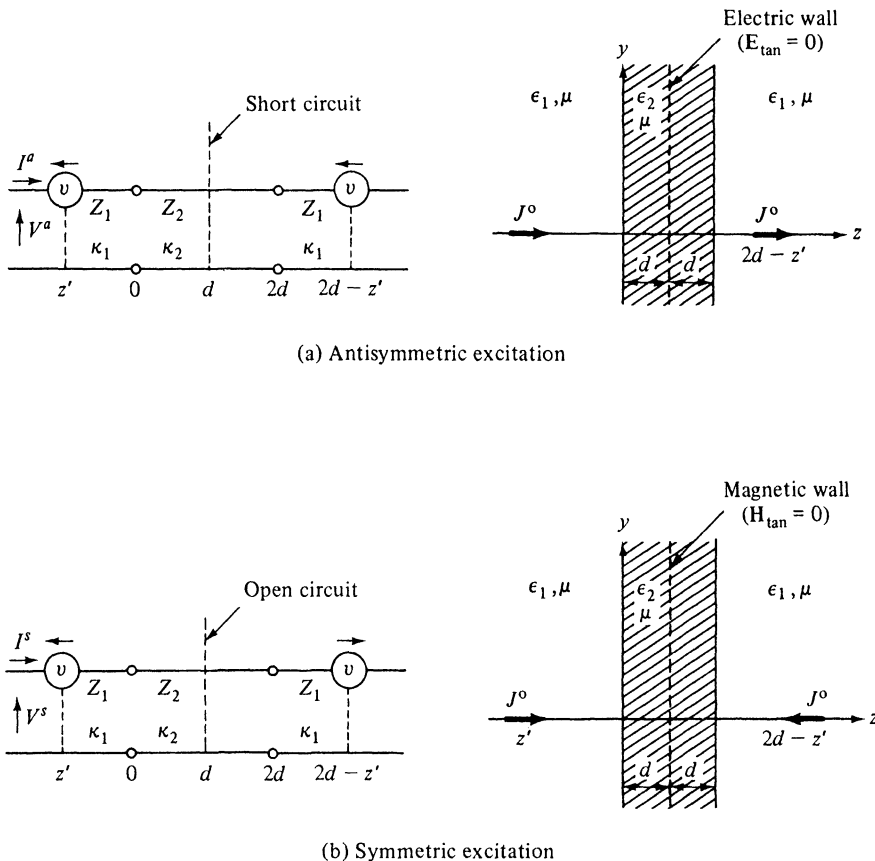


FIG. 5.6.7 Auxiliary field and network problems.

at the symmetry plane $z = d$ for the antisymmetric and symmetric longitudinal electric current excitations, respectively. It is evident that a superposition of field and network responses for the configurations in Fig. 5.6.7(a) and (b) yields twice the response for the structure in Fig. 5.6.6. Let \mathbf{E}^a , \mathbf{H}^a , and \mathbf{E}^s , \mathbf{H}^s denote at any point the electromagnetic fields arising from the excitation by the antisymmetric and symmetric current elements, respectively. Then the electromagnetic fields in Fig. 5.6.6(a) are given by

$$\mathbf{E} = \frac{1}{2}(\mathbf{E}^s + \mathbf{E}^a), \quad \mathbf{H} = \frac{1}{2}(\mathbf{H}^s + \mathbf{H}^a). \quad (22)$$

The electric and magnetic walls in Fig. 5.6.7(a) and (b), respectively, isolate the region $z < d$ from the region $z > d$, so it suffices to treat only the bisected problems in the region $z < d$.

The antisymmetric excitation, leading to the configuration in Fig. 5.6.1, has already been treated. For the symmetric excitation, the requirement $g_z^s = 0$ at $z = d$ leads via Eq. (2.4.24b) to the replacement of $\vec{Z}(0)$ in Eq. (13) by [exp($j\omega t$) dependence]

$$\vec{Z}^s(0) = -jZ_2 \cot \kappa_2 d, \quad Z_2 = \frac{\kappa_2}{\omega \epsilon_2}; \quad (23)$$

the corresponding reflection coefficient Γ^s is

$$\Gamma^s(\xi) = \frac{j\kappa_2 \cot \kappa_2 d + \epsilon \kappa_1}{j\kappa_2 \cot \kappa_2 d - \epsilon \kappa_1}, \quad \kappa_{1,2} = \sqrt{\kappa_{1,2}^2 - \xi^2}, \quad (23a)$$

and the three-dimensional Green's function $G'(\mathbf{r}, \mathbf{r}')$ is readily constructed therefrom. For a field evaluation in the slab region, g_{z2} in Eq. (14) is replaced by [see Eq. (5)]

$$g_{z2}^s(z, z') = g_{z2}(0, z') \frac{\sin \kappa_2(d - z)}{\sin \kappa_2 d} = g_{z1}(0, z') \frac{\sin \kappa_2(d - z)}{\sin \kappa_2 d}. \quad (24)$$

It may be noted that while the asymptotic field solution for the open-circuit bisection (symmetric excitation) takes the same form as in Eq. (6), the transcendental equations defining the pole singularities of $\Gamma(k_1 \sin w)$ are now, instead of Eqs. (7),

$$\epsilon q = -ip \cot p, \quad p^2 - q^2 = (k_1 d)^2(\epsilon - 1), \quad (25)$$

with p and q defined as in Eq. (7a). Surface-wave solutions of these equations for real $\epsilon > 1$, with $q = i|q|$, p real, may be found by a graphical construction as in Fig. 3.4.3; one observes that N solutions exist in the range $(N + \frac{1}{2})\pi < k_1 d \sqrt{\epsilon - 1} < (N + \frac{3}{2})\pi$, $N = 0, 1, 2, \dots$. No solution is found when $k_1 d \sqrt{\epsilon - 1} < \pi/2$, so the surface waves are now subject to a low-frequency cutoff, in contrast to the short-circuit bisection case; $\epsilon < 1$ likewise does not yield surface-wave solutions.

It may be mentioned that in view of Fig. 5.6.7, a knowledge of the field solutions for the bisected structures in the region $z < 0$ implies a knowledge of the solution for the configuration in Fig. 5.6.6 both for $z < 0$ and $z > 2d$. With reference to Figs. 5.6.6 and 5.6.7 and Eq. (22), the field on the side $z < 0$ containing the source is obtained by adding the contributions due to *identically oriented* sources, whereas the transmitted field on the side $z > 2d$ is obtained by adding the contributions due to *oppositely oriented* sources, in the bisected arrangement.

5.6b Other Source Configurations

Transverse electric current element

$$\hat{\mathbf{J}}(\mathbf{r}, t) = Il\delta(\mathbf{p})\delta(z - z')e^{-i\omega t}\mathbf{x}_0. \quad (26)$$

If the current element in Fig. 5.6.1 or 5.6.6(a) is directed along the x axis, the equivalent excitation in the modal network of Fig. 5.6.4 or 5.6.6(b) is a shunt current generator located at z' as in Fig. 5.5.6, and both E and H modes must be considered. The analysis for observation points $z < 0$ proceeds exactly as in Sec. 5.5b, wherein the transverse current element is situated in front of a semiinfinite dielectric medium. The only difference is that $\Gamma'(\xi)$ and $\Gamma''(\xi)$ in Eqs. (5.5.31) must be replaced by the E - and H -mode reflection coefficients,

respectively, seen looking to the right at the $z = 0$ plane in Fig. 5.6.1 or 5.6.7(b). As in Sec. 5.6a, the fields radiated in the presence of the dielectric slab can be inferred by superposition from those in the two auxiliary configurations wherein an electric and magnetic wall, respectively, is placed along the $z = 0$ plane as in Fig. 5.6.7. The electric wall bisection arises from an excitation by the x -directed current element at z' and an oppositely directed element of the same strength at $2d - z'$, while the magnetic wall bisection occurs when the direction of both current elements is the same. The E -mode reflection coefficients for the bisected configurations seen looking to the right at $z = 0$ are given in Eqs. (4a) and (23a). For the H modes, Eqs. (13) and (23) for $\vec{Z}(0)$ remain valid except that the formulas for the characteristic impedances are now $Z''_{1,2} = \omega\mu/\kappa'_{1,2}$. It may also be recalled that in view of the unbounded cross section transverse to z , $\kappa'_{1,2} = \kappa''_{1,2} = \sqrt{k_{1,2}^2 - \xi^2}$. Thus, the modal reflection coefficient for the short-circuit bisection is

$$\Gamma''(\xi) = \frac{j\kappa_1 \tan \kappa_2 d - \kappa_2}{j\kappa_1 \tan \kappa_2 d + \kappa_2}, \quad (27a)$$

whereas for the open-circuit bisection,

$$\Gamma''^s(\xi) = \frac{j\kappa_1 \cot \kappa_2 d + \kappa_2}{j\kappa_1 \cot \kappa_2 d - \kappa_2}. \quad (27b)$$

When these formulas (with $j \rightarrow -i$) are inserted into Eqs. (5.5.31), they yield integral representations for the functions $\nabla'_i \mathcal{G}'_i$ and $\nabla'_i \mathcal{G}''_i$ for both the open- and short-circuit bisections, from which the electromagnetic fields in the region $z < 0$ may be derived via Eqs. (5.2.1). For the region $0 < z \leq d$, modifications analogous to those in Eqs. (5) and (24) are required.

An asymptotic evaluation in the region $z < 0$ in Figs. 5.6.1 and 5.6.7 or $z > 2d$ in Fig. 5.6.6 may be carried out as before and leads to expressions analogous to those in Eq. (6). It may be noted that the H -mode resonance conditions are quite similar to those for the E modes in Eqs. (7) and (25). In particular, the short-circuit bisection in Eq. (27a) yields pole singularities of $\Gamma''(\xi)$; these are specified by Eq. (25) provided that the term ϵq is replaced by q , and the same replacement makes Eq. (7) applicable to the open-circuit bisection case in Eq. (27b).

Transverse electric line current

$$\hat{\mathbf{J}}(\mathbf{r}, t) = I\delta(\hat{\mathbf{p}} - \hat{\mathbf{p}}')e^{-i\omega t}\mathbf{x}_0. \quad (28)$$

This problem is directly analogous to the line-source excitation of a semi-infinite medium (Sec. 5.5d), provided that the half-space region $z > 0$ is replaced by the slab configurations in Fig. 5.6.1 or 5.6.7. In the analysis, it is implied that the input impedances $\vec{Z}(0)$ and reflection coefficients Γ are replaced by their counterparts for the slab region, as specified in the preceding sections. The asymptotic evaluation of the resulting integrals, which have the same form as in Eq. (5.5.54b), is almost identical with that for the point-source problem

since the Hankel function in Eq. (3b) is replaced by its asymptotic approximation in Eq. (5.3.13). The derivation of explicit results is left as an exercise for the reader.

5.7 TIME-HARMONIC SOURCES IN THE PRESENCE OF A CONSTANT-IMPEDANCE SURFACE

For a half-space or layered region $z > 0$, it is possible to define in certain parameter ranges a surface impedance Z_s that characterizes in an *approximate* fashion the relation between the tangential electric and magnetic fields at the $z = 0$ plane:

$$\mathbf{E}_t(\mathbf{p}, 0) = Z_s \mathbf{H}_t(\mathbf{p}, 0) \times \mathbf{z}_0. \quad (1)$$

When the surface impedance concept can be employed, it simplifies substantially the solution of an electromagnetic boundary-value problem in the region $z < 0$ since it eliminates the need for a detailed exploration of the fields in the region $z > 0$. In effect, the surface impedance on the $z = 0$ plane terminates the region $z < 0$ [see Figs. 5.6.1 and 5.3.1 and Eq. (1.5.40)].

5.7a Longitudinal Electric Current Element

$$\hat{\mathbf{J}}(\mathbf{r}, t) = Il\delta(\mathbf{p})\delta(z - z')e^{-i\omega t}\mathbf{z}_0. \quad (2)$$

We consider the physical configuration in Fig. 5.7.1, wherein a longitudinal electric current element of strength $J^o = Il$, I being the current in the element

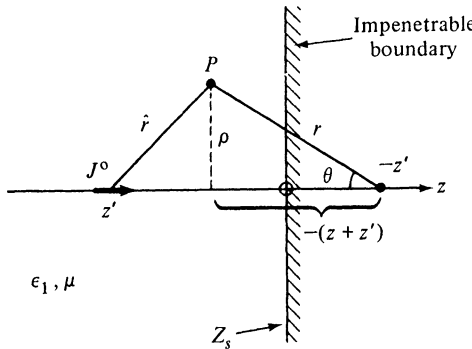


FIG. 5.7.1 Longitudinal current element and constant-impedance surface.

and l its infinitesimal length, is situated at the point $z' < 0$ on the z axis in the presence of a plane surface at $z = 0$ having a constant surface impedance Z_s (Fig. 5.7.1). The electromagnetic fields may be derived via Eqs. (5.2.1) and (5.2.4c) from a scalar E -mode Green's function $G'(\mathbf{r}, \mathbf{r}')$ which satisfies the differential equation

$$(\nabla^2 + k_1^2)G'(\mathbf{r}, \mathbf{r}') = -\delta(\mathbf{r} - \mathbf{r}'), \quad z, z' < 0, \quad (3)$$

subject to a radiation condition at infinity, and to the following boundary condition [obtained by utilizing Eqs. (1) and (5.2.1)]:

$$\frac{\partial G'}{\partial z} = i\omega\epsilon_1 Z_s G' = ik_1 \bar{Z}_s G' \quad \text{at } z = 0. \quad (3a)$$

$\bar{Z}_s = Z_s / \sqrt{\mu/\epsilon_1}$ is the surface impedance normalized to the wave impedance in the unbounded medium described by the constitutive parameters ϵ_1 , μ , and $k_1 = \omega\sqrt{\mu\epsilon_1}$ is the wavenumber. In a cylindrical coordinate description of the cross section transverse to z , G' may be represented as follows:

$$G'(\mathbf{r}, \mathbf{r}') = G_{f1}(\mathbf{r}, \mathbf{r}') + G'_s(\mathbf{r}, \mathbf{r}'), \quad (4)$$

where $G_{f1} = (1/4\pi\hat{r}) \exp(ik_1\hat{r})$ is the free-space Green's function for the unbounded region [Eq. (5.4.2b)], and G'_s , which arises from the presence of the boundary at $z = 0$, has the integral representation:

$$G'_s = \frac{-ik_1}{8\pi} \int_{\bar{P}} \sin w H_0^{(1)}(k_1 r \sin \theta \sin w) e^{ik_1 r \cos \theta \cos w} \Gamma(k_1 \sin w) dw, \quad (5)$$

where

$$\Gamma(k_1 \sin w) = \frac{\bar{Z}_s - \cos w}{\bar{Z}_s + \cos w}. \quad (5a)$$

The path of integration is given in Fig. (5.3.6b) and the coordinates \hat{r} , r , and θ are defined in Fig. 5.7.1.

For large values of $k_1 r \sin \theta$, the integral in Eq. (5) may be evaluated asymptotically and yields a saddle-point contribution as well as a possible residue contribution arising from the pole w_p of the reflection coefficient in Eq. (5a):

$$G' \sim \frac{e^{ik_1 \hat{r}}}{4\pi\hat{r}} - \Gamma(k_1 \sin \theta) \frac{e^{ik_1 r}}{4\pi r} \left[1 + O\left(\frac{1}{k_1 r}\right) \right] + \frac{e^{-i\pi/4}}{\sqrt{\sin w_p}} \sqrt{\frac{k_1}{2\pi r \sin \theta}} \cos w_p e^{ik_1 r \cos(w_p - \theta)} U(\theta - \theta_p) \left[1 + O\left(\frac{1}{k_1 r}\right) \right], \quad (6)$$

where

$$\cos w_p = -\bar{Z}_s, \quad (6a)$$

and θ_p , the observation angle for which the steepest-descent path P in Fig. 5.3.6(b) crosses the pole w_p , is defined as in Eq. (5.6.8). $U(\theta - \theta_p)$ is the Heaviside unit function defined in Eq. (5.6.6), and its contributing range is limited to inductive surface impedances for which $\text{Im } \bar{Z}_s < 0$ [$\exp(-i\omega t)$ dependence].

Discussion

The physical interpretation of the above solution in terms of geometric-optical and surface-wave contributions is identical with that for Eq. (5.6.6). The solution is valid for those observation points $\theta > 0$ for which the steepest-descent path P does not pass near the pole w_p ($\theta \neq \theta_p$). If the pole is located near the steepest-descent path, in particular near the saddle point, the asymptotic evaluation must be carried out by the modified saddle-point procedure described in Sec. 4.4a. For the case where the surface impedance Z_s is equal

to $\sqrt{\mu/\epsilon_2}$ representative of a highly lossy medium with complex dielectric constant ϵ_2 occupying the half-space region $z > 0$, one has $\bar{Z}_s \approx 1/\sqrt{\epsilon}, \epsilon = \epsilon_2/\epsilon_1$. For corresponding ranges of source and observation point coordinates, the asymptotic field solution then becomes identical with that in Eq. (5.5.7) which is derived from an exact analysis.

In view of Eq. (6a), the propagation characteristics of the residue contribution in Eq. (6) can be expressed simply in terms of the surface impedance \bar{Z}_s :

$$\frac{e^{ik_1 r \cos(w_p - \theta)}}{\sqrt{r \sin \theta}} = \frac{1}{\sqrt{\rho}} \exp(-ik_1 \bar{Z}_s |z + z'|) \exp(ik_1 \sqrt{1 - \bar{Z}_s^2} \rho). \quad (7)$$

Thus, one notes that the residue field contribution decays exponentially away from the surface $z = 0$ if $\text{Im } \bar{Z}_s < 0$ and constitutes a proper solution of the Maxwell field equations in this case where $\text{Im } \sqrt{1 - \bar{Z}_s^2} > 0$. By an extension of the notion of a surface wave on a lossless structure ($\bar{Z}_s = -i|\bar{Z}_s|$), the wave on a dissipative surface with $\text{Im } \bar{Z}_s < 0$ might be termed a “lossy” surface wave. For the highly lossy case, $\bar{Z}_s \approx \epsilon^{-1/2}$, $\sin w_p \approx 1 + i/2|\epsilon|$, a comparison at $z = z' = 0$ of the amplitude of excitation of the surface wave in Eq. (6) with that given by the second term in Eq. (5.5.8b) yields a value for the latter half as large as for the former. This discrepancy occurs since, for $\theta = \pi/2$, the pole is located on the steepest-descent path near the saddle point, and the path of integration is indented around the pole in the form of a semicircle. Hence only a half-residue contributes, instead of the full residue given in Eq. (6) (see Sec. 4.4a).

Analytical details

The integral representation in Eq. (5) is derived in a manner directly analogous to that employed in Sec. 5.6. The schematic representation of the modal Green's function problem of determining $g_{zi}(z, z')$ in Eq. (5.3.1) is given in Fig. 5.7.2, with the surface impedance Z_s representing the termination on the modal

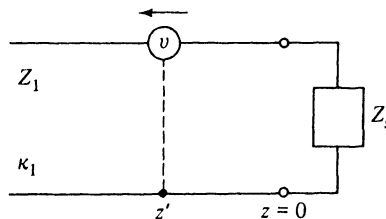


FIG. 5.7.2 Equivalent modal network (E modes).

transmission line. To deduce the above result one employs the field in Eq. (5.2.11) (with $j \rightarrow -i$) and Eq. (3a) to derive the modal boundary condition $dg'_{zi}/dz = i\omega\epsilon_1 Z_s g'_{zi}$, and thence, via Eqs. (5.2.6a) and (2.2.15), the network in Fig. 5.7.2. It is recalled that $Y'_i(z, z')$ and therefore g'_{zi} represents a normalized current; from the E -mode transmission-line equations (2.2.15), $(1/i\omega\epsilon_1)(dg'_{zi}/dz)$

is the corresponding voltage, and the ratio of the voltage to the current at $z = 0$ yields the surface impedance Z_s . The formula for the reflection coefficient in Eq. (5a) follows from Eq. (5.3.1a), with $\vec{Z}_i(0) = Z_s$ and $k_{ni} = \xi = k_1 \sin w$.

The asymptotic evaluation of the integral in Eq. (5) proceeds as in Sec. 5.6. Instead of the infinite set of leaky-wave poles and the finite set of surface-wave poles encountered in the slab problem, there exists now only a single relevant pole at

$$\cos w_p = -\bar{Z}_s, \quad \text{i.e., } w_p = \cos^{-1}(-\bar{Z}_s) \pm 2m\pi, \quad m = 0, 1, 2, \dots \quad (8a)$$

For passive surface impedances, which absorb a finite (or zero) amount of power, the requirement of real power flow into the surface [i.e., $\operatorname{Re} \int_S \mathbf{E}_t \times \mathbf{H}_t^* \cdot \mathbf{z}_0 dS \geq 0$] implies via Eq. (1) that $\operatorname{Re} \bar{Z}_s \geq 0$. It then follows from Eq. (8a) that, at the pertinent pole singularity,

$$\frac{3\pi}{2} > \operatorname{Re} w_p \geq \frac{\pi}{2}; \quad \operatorname{Im} w_p \geq 0 \quad \text{if } \operatorname{Im} \bar{Z}_s \geq 0. \quad (8b)$$

For lossless surfaces ($\operatorname{Re} \bar{Z}_s = 0$), $\operatorname{Re} w_p = \pi/2$. From Eqs. (8) it is evident that the pole approaches the line $\operatorname{Re} w_p = \pi/2$ from the right as $\operatorname{Re} \bar{Z}_s \rightarrow 0$. If $\operatorname{Im} \bar{Z}_s < 0$, $\operatorname{Re} \bar{Z}_s = 0$, it then follows that the path of integration is indented to the left around the pole situated on the half-line $\operatorname{Re} w_p = \pi/2$, $\operatorname{Im} w_p < 0$. As noted from the discussion in Secs. 5.6 and 5.3e, this latter pole is identified as a “surface-wave pole” since its residue contribution to the integral in Eq. (5) gives rise to a surface wave [see Eq. (7)]. The requirement for the existence of a surface wave on a lossless (reactive) surface is, therefore, $\bar{Z}_s = -i|\bar{Z}_s|$ [i.e., the surface is inductive; one recalls that the assumed time dependence is $\exp(-i\omega t)$]. This behavior follows at once from a transverse resonance argument which requires via Eq. (2.4.36) that $\vec{Z}_i(0) + \vec{Z}'_i(0) = 0$ at a pole. In the present case, wherein only E modes are involved, $Z_s + Z'_s = 0$ from Fig. 5.7.2. In a surface wave, the fields decay exponentially away from the surface implying that the associated mode is non-propagating. Since, for a non-propagating E mode, $Z'_s = i|Z'_s|$ is capacitative, the resonance equation can be satisfied only if $\bar{Z}_s = -i|\bar{Z}_s|$. The pole is not intercepted when $\operatorname{Im} \bar{Z}_s > 0$.

An alternative representation in terms of the waves *guided along the surface* may be carried out as in Sec. 5.6 (see also Sec. 5.7b).

An image formulation

It is of interest to note a formulation²³ in which the perturbing properties of the constant impedance surface on fields radiated by a given source distribution can be taken into account rigorously by a suitably defined distribution of image sources. For excitation by a longitudinal electric current element, the effect of the impedance surface on the field is contained in the scattered contribution G_s to the scalar Green's function G . For the present discussion it is convenient to employ the integral representation in the ξ plane as in Eq. (5.5.3a), with $\Gamma(\xi)$ defined in Eq. (5a) (note: $\xi = k_1 \sin w$). Upon substituting

$$\Gamma(\xi) = \frac{k_1 \bar{Z}_s - \kappa(\xi)}{k_1 \bar{Z}_s + \kappa(\xi)} = -1 + \frac{2k_1 \bar{Z}_s}{k_1 \bar{Z}_s + \kappa(\xi)}, \quad \kappa(\xi) = \sqrt{k_1^2 - \xi^2}, \quad (9)$$

into Eq. (5.5.3a), one obtains

$$G'_s = G'_{s1} + G'_{s2}, \quad (10)$$

$$G'_{s1} = \frac{i}{8\pi} \int_{-\infty e^{i\pi}}^{\infty} \xi H_0^{(1)}(\xi\rho) \frac{e^{-ik(z+z')}}{\kappa} d\xi = \frac{\exp[ik\sqrt{\rho^2 + (z+z')^2}]}{4\pi\sqrt{\rho^2 + (z+z')^2}}, \quad (10a)$$

$$G'_{s2} = -\frac{ik_1 \bar{Z}_s}{4\pi} \int_{-\infty e^{i\pi}}^{\infty} \xi H_0^{(1)}(\xi\rho) \frac{e^{-ik(z+z')}}{\kappa} \frac{1}{k_1 \bar{Z}_s + \kappa} d\xi. \quad (10b)$$

The closed-form evaluation of G'_{s1} , carried out via Eq. (5.4.12c), is interpretable as a contribution from an image source of strength (+1) located at $z = -z'$ as in Fig. 5.7.1. To reformulate G'_{s2} , one employs the identity

$$\frac{1}{k_1 \bar{Z}_s + \kappa} = \int_0^{\infty} e^{-(k_1 \bar{Z}_s + \kappa)\gamma} d\gamma, \quad (11)$$

which is valid when $\operatorname{Re} \bar{Z}_s > 0$; k_1 is assumed to be real, and $\operatorname{Re} \kappa \geq 0$ for all ξ on the path of integration in Eq. (10b). Upon inserting Eq. (11) into Eq. (10b) and performing a permissible interchange of the orders of integration, one obtains

$$G_{s2} = -2k_1 \bar{Z}_s \int_0^{\infty} d\gamma e^{-k_1 \bar{Z}_s \gamma} \frac{i}{8\pi} \int_{-\infty e^{i\pi}}^{\infty} \xi H_0^{(1)}(\xi\rho) \frac{e^{i\kappa(-z+z'+i\gamma)}}{\kappa} d\xi, \quad (12a)$$

$$= \int_0^{\infty} [-2k_1 \bar{Z}_s e^{-k_1 \bar{Z}_s \gamma}] \frac{e^{i k_1 \psi}}{4\pi \psi} d\gamma, \quad \psi = \sqrt{\rho^2 + [-(z+z') + i\gamma]^2}. \quad (12b)$$

The transition from Eq. (12a) to (12b) is accomplished via Eq. (10a), wherein $\sqrt{\rho^2 + \chi^2}$ has been continued analytically from positive real values into a permitted domain of complex values of $\chi = -(z+z') + i\gamma$, $(z+z') < 0$, $\gamma \geq 0$, for which $\operatorname{Im} \sqrt{\rho^2 + \chi^2} > 0$. One notes from Fig. 5.3.3(a) (upon substituting $\xi = i\chi$) that the latter condition is satisfied in the first and third quadrants of the complex χ plane, thus resulting in the analytic continuation of the right-hand side of Eq. (10a) from real values of χ to $\chi = -(z+z') + i\gamma$. Since $\operatorname{Re} \kappa \geq 0$ along the path of integration, this continuation is also valid for the integral on the left-hand side of Eq. (10a). Equation (12b) can be interpreted as arising from a continuous distribution of image point sources situated in an infinite medium at the complex location $z = -z' + i\gamma$ and having an exponentially decaying strength denoted by the factor inside the brackets in the integrand.

For the special case $\operatorname{Im} \bar{Z}_s > 0$, the image formulation above can be made physical by locating the image sources at *real* values of the coordinates. We note that $\operatorname{Im} \psi > 0$ throughout the fourth quadrant of the complex γ plane [branch points are located at $\gamma = \pm\rho - i(z+z')$, $(z+z') < 0$], so the $\exp(i k_1 \psi)$ term in the integrand of Eq. (12b) vanishes at $|\gamma| \rightarrow \infty$ in the fourth

quadrant of the γ plane. The same is true for $\exp(-k_1 \bar{Z}_s \gamma)$ provided that $\text{Im } \bar{Z}_s > 0$. Thus, there is no contribution to the integral from a quarter-circle of infinite radius in the fourth quadrant, and the contour of integration can be deformed into the negative imaginary axis of the γ plane. Upon introducing the change of variable $\gamma = i\mu$, one obtains

$$G_{s2} = \int_0^{-\infty} [-2ik_1 \bar{Z}_s e^{-ik_1 \bar{Z}_s \mu}] \frac{\exp\{ik_1 \sqrt{\rho^2 + [z + (z' + \mu)]^2}\}}{4\pi \sqrt{\rho^2 + [z + (z' + \mu)]^2}} d\mu, \quad \text{Im } \bar{Z}_s > 0, \quad (13)$$

which now comprises the contributions from a continuous set of image point sources situated along the segment $z' \leq z < \infty$ of the positive z axis (Fig. 5.7.3). It is noted that the condition $\text{Im } \bar{Z}_s > 0$, which admits of an exact

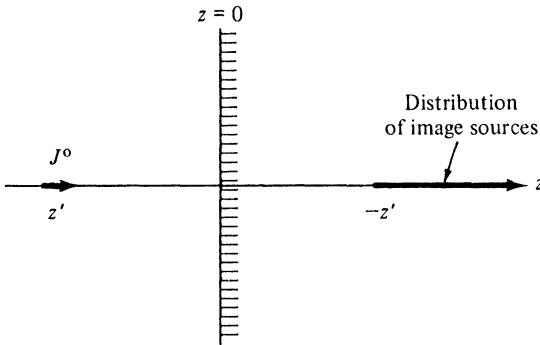


FIG. 5.7.3 Image formulation when $\text{Im } Z_s > 0$.

representation of the perturbing effect of the constant impedance surface in terms of physical image sources, excludes the case wherein a surface wave can be propagated along the structure. This implies that an image source distribution of the type noted above cannot produce in the region $z < 0$ a field that behaves in accordance with Eq. (7).

5.7b Transverse Magnetic Line Current

$$\hat{\mathbf{M}}(\mathbf{r}, t) = V \delta(\hat{\mathbf{p}} - \hat{\mathbf{p}}') e^{-i\omega t} \mathbf{x}_0. \quad (14)$$

When the dipole in Fig. 5.7.1 is replaced by a magnetic line current of strength V parallel to the x axis, the electromagnetic field has the non-vanishing components H_x, E_y, E_z [see the dual of Eqs. (5.5.56) or (5.4.31)],

$$H_x = i\omega \epsilon_1 V \bar{G}', \quad E_y = -V \frac{\partial \bar{G}'}{\partial z}, \quad E_z = V \frac{\partial \bar{G}'}{\partial y}, \quad (15)$$

which are derivable from a two-dimensional scalar E -mode Green's function \bar{G}' satisfying the differential equation

$$\left(\frac{\partial^2}{\partial y^2} + \frac{\partial^2}{\partial z^2} + k_1^2 \right) \bar{G}'(\hat{\mathbf{p}}, \hat{\mathbf{p}}') = -\delta(\hat{\mathbf{p}} - \hat{\mathbf{p}}'), \quad \hat{\mathbf{p}} = (y, z) \quad (16)$$

subject to a radiation condition at infinity, and to the boundary condition

$$\frac{\partial \bar{G}'}{\partial z} = i\omega\epsilon_1 Z_s \bar{G}' = ik_1 \bar{Z}_s \bar{G}' \quad \text{at } z = 0, \quad (16a)$$

with k_1 the wavenumber in the medium and $\bar{Z}_s = Z_s / \sqrt{\mu/\epsilon_1}$. The solution may be written as

$$\bar{G}'(\hat{\mathbf{p}}, \hat{\mathbf{p}}') = \bar{G}_f(\hat{\mathbf{p}}, \hat{\mathbf{p}}') + \bar{G}'_s(\hat{\mathbf{p}}, \hat{\mathbf{p}}'), \quad (17)$$

where \bar{G}_f is the free-space Green's function [Eq. (5.4.25)],

$$\bar{G}_f = \frac{i}{4} H_0^{(1)}(k_1 |\hat{\mathbf{p}} - \hat{\mathbf{p}}'|), \quad (17a)$$

while \bar{G}'_s accounts for the presence of the impedance sheet at $z = 0$ and may be written in a z -transmission modal representation as

$$\bar{G}'_s(\hat{\mathbf{p}}, \hat{\mathbf{p}}') = \begin{cases} -\frac{i}{4\pi} \int_{-\infty}^{\infty} \frac{e^{i\eta(y-y')}}{\sqrt{k_1^2 - \eta^2}} \exp[-i\sqrt{k_1^2 - \eta^2}(z + z')] \Gamma(\eta) d\eta, & (17b) \\ -\frac{i}{4\pi} \int_{\bar{P}} e^{ik_1 R \cos(w - \varphi)} \Gamma(k_1 \sin w) dw. & (17c) \end{cases}$$

$\Gamma(k_1 \sin w)$ is given in Eq. (5a) and the path \bar{P} is defined in Fig. 5.3.6b. R and φ are polar coordinates measured from the image point, whence $|z + z'| = R \cos \varphi$, $y - y' = R \sin \varphi$.

For large values of $k_1 R$, the integral in Eq. (17c) may be evaluated asymptotically to yield a reflected-wave and a surface-wave contribution as in Eq. (6):

$$\begin{aligned} \bar{G}'_s \sim & -\frac{1}{4\pi} \sqrt{\frac{2\pi}{k_1 R}} e^{i(k_1 R + \pi/4)} \Gamma(k_1 \sin \varphi) \left[1 + O\left(\frac{1}{k_1 R}\right) \right] \\ & + e^{ik_1 R \cos(w_p - \varphi)} \cot w_p U(\varphi - \varphi_p), \end{aligned} \quad (18)$$

where $\cos w_p = -\bar{Z}_s$, $U(\varphi - \varphi_p)$ is the Heaviside unit function, φ_p is defined as in Eq. (5.6.8), and Eq. (7) applies with $\theta \rightarrow \varphi$, $y \rightarrow p$. When $k_1 \hat{R}$ is also large, where $\hat{R} = |\hat{\mathbf{p}} - \hat{\mathbf{p}}'|$ is the distance from the source to the observation point, the Hankel function in Eq. (17a) may be approximated as in Eq. (5.3.13) and one finds that

$$\bar{G}' \sim \frac{e^{i\pi/4}}{2\sqrt{2\pi}} \left[\frac{e^{ik_1 \hat{R}}}{\sqrt{k_1 \hat{R}}} - \Gamma(k_1 \sin \varphi) \frac{e^{ik_1 R}}{\sqrt{k_1 R}} \right] + e^{ik_1 R \cos(w_p - \varphi)} \cot w_p U(\varphi - \varphi_p). \quad (19)$$

The interpretation of this result is directly analogous to that for the point-source excitation in Sec. 5.7a except that the geometric-optical fields, the first two terms in Eq. (19), are now in the form of cylindrical waves emanating from $\hat{R} = 0$ and $R = 0$, respectively, while the surface-wave contribution is in the form of a *plane wave*. Evidently, when a surface wave is excited ($\text{Im } \bar{Z}_s < 0$)

and when the surface impedance is purely reactive, the surface-wave contribution dominates near the boundary plane $z = 0$.

Equation (17) follows from Eqs. (5.2.13a) (with $\alpha = 0$), (5.4.33), and from the considerations in Sec. 5.7a (see also Fig. 5.7.2), so no additional details need be given.

Alternative representation

As in Sec. 5.6, Eq. (5.6.20), it is possible to reformulate Eqs. (17) in such a manner that they emphasize the guiding properties of the surface along the y direction. This is accomplished by deforming the integration contour in the complex η plane about the singularities of g_{zi} in the integral representation for \tilde{G}' [see Eq. (5.2.13a), with $j \rightarrow -i$]. To this end, one requires in addition to Eq. (17b) the integral representation in Eq. (5.4.36b) for the free-space field \tilde{G}_f . We note first that the composite integral representation is insensitive to the algebraic sign of $y - y'$ (as verified by letting $\eta \rightarrow -\eta$), so $y - y'$ can be replaced by $|y - y'|$. The singularities of $\Gamma(\eta)$ in Eq. (17b) are simple poles at

$$\sqrt{k_1^2 - \eta_p^2} = -k_1 \bar{Z}_s, \quad \text{i.e., } \eta_p = \pm k_1 \sqrt{1 - \bar{Z}_s^2}, \quad (20)$$

and branch points at $\eta = \pm k_1$. The branch cuts are chosen as in Fig. 5.6.5 to assure $\text{Im} \sqrt{k^2 - \eta^2} > 0$ on the entire top sheet of the two-sheeted Riemann surface in the complex η plane. One notes from Eq. (20) that the poles η_p lie on the top sheet only when $\text{Im} \bar{Z}_s < 0$, in which case they are located in the first and third quadrants. A deformation of the contour of integration about the singularities of the integrand in the upper half of the η plane can now be carried out by considerations analogous to those following Eq. (5.6.21) and yields the desired reformulation

$$\begin{aligned} \tilde{G}'(\hat{\mathbf{p}}, \hat{\mathbf{p}}') = & \frac{-\bar{Z}_s}{\sqrt{1 - \bar{Z}_s^2}} e^{ik_1 \sqrt{1 - \bar{Z}_s^2} |y - y'|} e^{ik_1 Z_s(z + z')} U(-\text{Im} \bar{Z}_s) \\ & + \frac{i}{4\pi} \int_{-\infty}^{\infty} \frac{e^{i\sqrt{k_1^2 - \zeta^2} |y - y'|}}{\sqrt{k_1^2 - \zeta^2}} \left[e^{i\zeta(z - z')} - \frac{k_1 \bar{Z}_s - \zeta}{k_1 \bar{Z}_s + \zeta} e^{-i\zeta(z + z')} \right] d\zeta, \end{aligned} \quad (21)$$

where $\text{Im} \sqrt{k_1^2 - \zeta^2} \geq 0$. The replacement of $|z - z'|$ by $(z - z')$ in the integrand of Eq. (21) is justified by noting that the portion of the integral containing the $\exp[i\zeta(z - z')]$ term is insensitive to the algebraic sign of $(z - z')$ (let $\zeta \rightarrow -\zeta$ in the integrand). From Eq. (5.4.36b), the contribution to the integral from the $\exp[i\zeta(z - z')]$ term is equal to the free-space Green's function

$$(i/4) H_0^{(1)}[k_1 \sqrt{(y - y')^2 + (z - z')^2}].$$

The first term on the right-hand side of Eq. (21) represents a surface wave (discrete spectrum) propagating in the y direction [see Eq. (19)], while the remaining integral represents the continuous spectrum of reflected waves. For imaginary values of \bar{Z}_s , the continuous spectrum contribution can be written in a form analogous to that in Eq. (5.6.20).

5.7c Other Elementary Source Configurations

If the constant impedance surface in Fig. 5.7.1 is excited by other fundamental source distributions, such as a transverse current element, line currents, or ring currents, the solution for the radiated fields is obtained by a modal analysis and synthesis procedure as in the corresponding treatments in Secs. 5.5 and 5.6, provided only that the modal reflection coefficients defined therein are replaced by those appropriate to the present problem. The E -mode reflection coefficient has already been stated in Eq. (5a). For the H modes, the modal characteristic impedance is $Z_i'' = \omega\mu/\kappa_i''$ [see Eq. (5.3.1c)], so that, from Eq. (5.3.1a),

$$\vec{\Gamma}_i''(0) = \frac{\kappa_i'' - k_1 \bar{Y}_s}{\kappa_i'' + k_1 \bar{Y}_s}, \quad \bar{Y}_s = \frac{1}{Z_s}, \quad (22a)$$

which becomes for $\kappa_i'' = \sqrt{k_1^2 - \xi^2} = k_1 \cos w$,

$$\Gamma''(k_1 \sin w) = \frac{\cos w - \bar{Y}_s}{\cos w + \bar{Y}_s}. \quad (22b)$$

Asymptotic field calculations are carried out as in Secs. 5.7a and 5.7b.

5.7d Continuous Distribution of Transverse Magnetic Line Currents

Excitation of surface waves by an aperture

Consider the configuration in Fig. 5.7.4(a), wherein a space bounded by the plane $z = 0$ with surface impedance Z_s is excited by electromagnetic fields

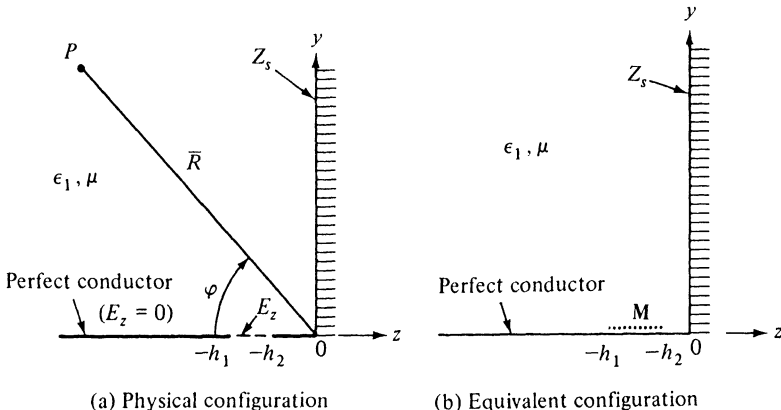


FIG. 5.7.4 Excitation of surface waves by an aperture.

in an aperture perforating a perfectly conducting plane located at $y = 0$.²⁴ The surrounding medium is characterized by the material constants ϵ_1 and μ . The aperture is in the form of a slit of width $h = h_1 - h_2$ and extends to infinity in the x direction; the aperture field is assumed to be independent of x , with a single magnetic-field component $\mathbf{H} = \mathbf{x}_0 H$ and a tangential electric-field com-

ponent E_z . This type of aperture field arises, for example, if the aperture is excited from the region $y < 0$ by a parallel-plate waveguide operating in the TEM mode, with the waveguide walls extending along the planes $z = -h_1$ and $z = -h_2$. By the equivalence relation in Eq. (1.5.33a), the effect of the aperture field can be represented in terms of an equivalent magnetic current distribution $\mathbf{M} = \mathbf{E} \times \mathbf{y}_0 = -\mathbf{x}_0 E_z$ flowing on a perfectly conducting surface as shown in Fig. 5.7.4(b). From the considerations in Sec. 1.5b, the electromagnetic fields everywhere in the region $z < 0, y > 0$, are determined uniquely from a knowledge of $M_x = -E_z$. In view of the invariance of the configuration with respect to the x coordinate, it follows that everywhere in the region $z < 0, y > 0$, the magnetic field has only an x component, $H_x(\hat{\mathbf{p}})$, in terms of which the electric-field components E_y and E_z are calculable as in Eq. (15). From Eq. (15), one obtains the fields due to a line source of magnetic currents having a strength V , so that by superposition, the magnetic field due to the aperture source distribution is given by

$$H_x(\hat{\mathbf{p}}) = 2i\omega\epsilon_1 \int_{-h_1}^{-h_2} V(z') \bar{G}'(\hat{\mathbf{p}}; 0, z') dz', \quad \hat{\mathbf{p}} = (y, z), \quad (23)$$

where \bar{G}' is the Green's function in Eq. (17), and the factor 2 arises from the imaging effect of the perfect conductor along the $y = 0$ plane in Fig. 5.7.4(b).

For an exact calculation, it is convenient to employ the y -guided-wave representation in Eq. (21) since the dependence on z' is continuous, thereby facilitating the integration required in Eq. (23). This is not the case for the z -transmission formulation [see Eq. (5.4.36b)]. At large distances from the aperture, one may insert the asymptotic approximation for \bar{G}' which takes the form shown in Eq. (19). If $R \gg h_1$, where h_1 is the coordinate defining the upper edge of the aperture (Fig. 5.7.4), one may approximate \hat{R} and R as follows:

$$\hat{R} = \bar{R} + z' \cos \varphi, \quad R = \bar{R} - z' \cos \varphi, \quad (24)$$

where $\bar{R} = (y^2 + z^2)^{1/2}$ is the distance from the origin to the observation point (y, z) . Thus,

$$\begin{aligned} H_x(\hat{\mathbf{p}}) &\sim \frac{-\omega\epsilon}{\sqrt{2\pi k_1 \bar{R}}} e^{i(k_1 \bar{R} - \pi/4)} [A(\cos \varphi) - \Gamma(k_1 \sin \varphi) A(-\cos \varphi)] \\ &\quad - 2i\omega\epsilon_1 \frac{A(\bar{Z}_s) \bar{Z}_s}{\sqrt{1 - \bar{Z}_s^2}} [\exp(ik_1 \sqrt{1 - \bar{Z}_s^2} y + ik_1 \bar{Z}_s z)] U(\varphi - \varphi_p), \end{aligned} \quad (25)$$

where

$$A(y) = \int_{-h_1}^{-h_2} V(z') e^{ik_1 z' \gamma} dz'. \quad (25a)$$

In the limit $\varphi \rightarrow \pi/2$, $\Gamma(k_1 \sin \varphi) \rightarrow 1$ and the contributions from the direct and reflected waves cancel to $O(1/\sqrt{k_1 \bar{R}})$. Hence, for surface impedance values such that $\varphi_p < \pi/2$, the field near the surface is given by the last term in Eq. (25), which represents the surface wave propagating along the sheet.

In a true diffraction problem wherein the aperture is excited by an appropriate source distribution located in the region exterior to the quarter space shown in Fig. 5.7.4(a), the equivalent aperture current $M_x = V$ is unknown and must be determined from a self-consistent solution of the *total* electromagnetic boundary-value problem. Such a solution is usually difficult to attain. In many instances, however, the feeding mechanism is such that one may use a suitable approximation for M_x . A frequent technique, described variously as the “Kirchhoff” or “physical optics” procedure, is suitable for aperture widths large compared with the free-space wavelength; it involves the approximation of the aperture field by the value of the incident field in the aperture domain. For example, if the aperture is excited by a parallel-plate waveguide, the incident field (TEM mode) in the waveguide is constant in the $y = 0$ plane. Hence, as a first approximation, M_x would be a constant, and the integrals in Eq. (25) can be evaluated at once. While the physical optics approximation is usually poor for near-field evaluations (it is definitely wrong near the aperture edges where the fields change rather violently), it generally yields a good approximation of dominant effects in the far field provided that the aperture width is large.

Alternatively, when the slot is very narrow, one may write

$$-A(\gamma) \cong e^{-ikh\gamma}V, \quad h_{1,2} = h \pm \delta, \quad 0 < \delta \ll \lambda, \quad (26a)$$

where h is the coordinate at the slot center and V is the voltage across the slot,

$$V = \int_{-h-\delta}^{-h+\delta} V(z') dz' = \int_{-h-\delta}^{-h+\delta} E_z(z') dz'. \quad (26b)$$

A comparison of Eqs. (25) and (26) with Eqs. (15) and (19) establishes the equivalence between the radiation from a voltage V excited narrow slot centered at $z = -h$ in a perfectly conducting plane and that from a magnetic current source of strength V located at $z = -h$ on a similar plane.

Radiation from a terminated reactive surface—comparison of various approximations

In surface-wave antenna applications, one is frequently interested in the radiation from a terminated surface along which a surface wave can be propagated.²⁵ The physical configuration is shown in Fig. 5.7.5(a), wherein a reactive surface with constant normalized surface impedance $\bar{Z}_s = -i\bar{X}_s$, $\bar{X}_s > 0$ (i.e., an inductance for the implied time dependence $\exp(-i\omega t)$) occupies the half-plane $z = 0$, $y < 0$, while the half-plane $z = 0$, $y > 0$, is a perfect conductor ($\bar{Z}_s = 0$). We assume that a plane surface wave, whose magnetic field vector is directed parallel to the x axis, propagates along the reactive surface in the $+y$ direction:

$$H_{\text{inc}}(\hat{\mathbf{p}}) = H_0 e^{iky} e^{k_1 \bar{X}_s z}, \quad \kappa = k_1 \sqrt{1 + \bar{X}_s^2}, \quad \bar{X}_s > 0, \quad z < 0, \quad (27)$$

where the subscript _{inc} denotes the incident field, and H_0 is a constant amplitude factor. One verifies at once that H_{inc} in Eq. (27) satisfies the homogeneous wave equation $(\nabla^2 + k^2)H_{\text{inc}} = 0$, the impedance boundary condition

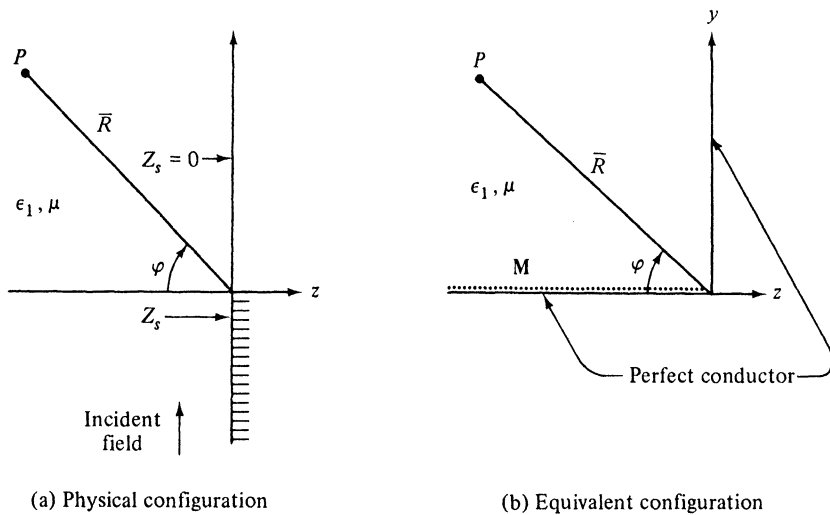


FIG. 5.7.5 Terminated reactive surface.

$(E_{\text{inc}})_y = (i/\omega\epsilon_1)\partial H_{\text{inc}}/\partial z = -Z_s H_{\text{inc}}$ on the reactive surface, and possesses at $y = -\infty$ the ingoing behavior characteristic of an idealized plane-wave excitation. The required functional dependence in a surface wave is inferred directly from the first term on the right-hand side of Eq. (21).

As in the problem sketched in Fig. 5.7.4, the field in the quarter-space region $y > 0, z < 0$, of Fig. 5.7.5(a) can be viewed as arising from an equivalent magnetic current distribution $M_x = -E_z$ flowing on a perfectly conducting plane at $y = 0$ [Fig. 5.7.5(b)]. Since the “aperture” in the present problem occupies the entire half-plane $z < 0, y = 0$, the equivalent magnetic current distribution extends from $z = 0$ to $z = -\infty$. The magnetic field H_x in the region $z < 0, y > 0$ [Fig. 5.7.5(b)] can then be calculated as in Eq. (23), provided that $h_1 = \infty$, $h_2 = 0$, and \bar{G}' represents the Green’s function for the half-space region bounded by a perfect conductor at $z = 0$. The result for the latter is obtained at once from either of Eqs. (17) or (21) by letting $\bar{Z}_s = 0$, as appropriate to a perfect conductor. The far field at $\bar{R} \rightarrow \infty, \varphi > 0$, in Fig. 5.7.5(b) is then given via Eq. (25) by

$$H_x(\hat{\mathbf{p}}) \sim \frac{-2\omega\epsilon_1}{\sqrt{2\pi k_1 \bar{R}}} e^{i(k_1 \bar{R} - \pi/4)} \int_{-\infty}^0 V(z') \cos(k_1 z' \cos \varphi) dz', \quad (28)$$

a result that demands a knowledge of $M_x(z') = V(z')$, or equivalently of E_z , in the aperture plane $y = 0$.

If the surface reactance \bar{X}_s is small, more precisely, if $k_1 \bar{X}_s$ is small, the surface wave is “loosely bound” [i.e., the field in Eq. (27) extends appreciably away from the reactive surface]. The discontinuity in reactance at the junction of the two surfaces in Fig. 5.7.5(a) is likewise small, and it is reasonable to assume as a first approximation that the actual aperture field is approximated by the incident field

$$(E_{\text{inc}})_z = \frac{i}{\omega\epsilon_1} \frac{\partial H_{\text{inc}}}{\partial y} = \frac{-\kappa}{\omega\epsilon_1} H_{\text{inc}}, \quad (29a)$$

whence

$$V(z') \cong \frac{\kappa}{\omega\epsilon_1} H_0 e^{k_1 \bar{X}_s z'}. \quad (29b)$$

One then obtains the following result for the radiated far field, on performing the elementary integration required in Eq. (28):

$$H_x(\hat{p}) \sim \frac{e^{i(k_1 R - \pi/4)}}{\sqrt{2\pi k_1 \bar{R}}} H_0 \frac{2\bar{X}_s \sqrt{1 + \bar{X}_s^2}}{\bar{X}_s^2 + \cos^2 \varphi}. \quad (30)$$

It is of interest to compare the approximate result in Eq. (30), whose validity is expected to be greatest for very small values of \bar{X}_s , with an exact formula^{25,26} obtained via an integral equation procedure. The exact expression for the square of the radiated far-field magnitude is

$$|H_x|^2 \sim \frac{|H_0|^2}{\pi k_1 \bar{R}} \frac{\bar{X}_s^2 v \cos^2 \varphi}{(1+v)(1-\sin \varphi)(\bar{X}_s^2 + \cos^2 \varphi)(v-\sin \varphi)}, \quad v = \sqrt{1 + \bar{X}_s^2}, \quad (31a)$$

while the approximate expression in Eq. (30) yields

$$|H_x|^2 \sim \frac{|H_0|^2}{\pi k_1 \bar{R}} \frac{2\bar{X}_s^2 v^2}{(\bar{X}_s^2 + \cos^2 \varphi)^2}. \quad (31b)$$

A variety of additional approximations can be built about the procedure wherein an induced field in an infinite aperture is approximated by the value of the incident field. Consider the region S in Fig. 5.7.5(a), wherein $y > 0, z < 0$, and apply Green's theorem to the two functions \bar{G}' and H_x which, together with their first and second derivatives, are defined within S and on its boundary s :

$$\begin{aligned} & \int_s [\bar{G}'(\hat{p}, \hat{p}') \nabla'^2 H_x(\hat{p}') - H_x(\hat{p}') \nabla'^2 \bar{G}'(\hat{p}, \hat{p}')] dS' \\ &= \oint_s \left[\bar{G}'(\hat{p}, \hat{p}') \frac{\partial}{\partial n'} H_x(\hat{p}') - H_x(\hat{p}') \frac{\partial}{\partial n'} \bar{G}'(\hat{p}, \hat{p}') \right] ds', \end{aligned} \quad (32)$$

where n is normal to s and increases in the direction out of S . H_x is the magnetic field which satisfies in S the homogeneous wave equation

$$(\nabla^2 + k^2) H_x(\hat{p}) = 0, \quad \hat{p} = (y, z). \quad (33a)$$

On the perfectly conducting boundary $y > 0, z = 0$, denoted by s_1 , it is required that $E_y = 0$, whence

$$\frac{\partial H_x}{\partial z} = 0 \text{ on } s_1. \quad (33b)$$

On the quarter circle at $\bar{R} \rightarrow \infty$, denoted by s_2 , H_x is to satisfy a radiation condition [see Eq. (1.5.34c)] since all sources of the field are contained in the region $y < 0$. Correspondingly, it is convenient to choose \bar{G}' as a Green's function satisfying the inhomogeneous wave equation

$$(\nabla^2 + k_1^2)\bar{G}'(\hat{\mathbf{p}}, \hat{\mathbf{p}}') = -\delta(\hat{\mathbf{p}} - \hat{\mathbf{p}}'), \quad \hat{\mathbf{p}} \text{ and } \hat{\mathbf{p}}' \text{ in } S, \quad (34a)$$

the boundary condition

$$\frac{\partial \bar{G}'}{\partial z} = 0 \text{ on } s_1, \quad (34b)$$

and a radiation condition on s_2 . Its behavior in the aperture plane $y = 0$, required for uniqueness, is left open for the moment. Upon substituting Eqs. (33) and (34) into Eq. (32), one obtains an expression for H_x in S in terms of its value and that of its derivative in the aperture plane:

$$H_x(\hat{\mathbf{p}}) = - \int_{-\infty}^0 \left[\bar{G}'(\hat{\mathbf{p}}, \hat{\mathbf{p}}') \frac{\partial}{\partial y'} H_x(\hat{\mathbf{p}}') - H_x(\hat{\mathbf{p}}') \frac{\partial}{\partial y'} \bar{G}'(\hat{\mathbf{p}}, \hat{\mathbf{p}}') \right]_{y'=0} dz'. \quad (35)$$

The contributions to the boundary integral arising from the contours s_1 and s_2 vanish in view of Eqs. (33b), (34b), and the radiation condition, respectively.

Alternative formulations for H_x can now be obtained from Eq. (35) by specifying the behavior of \bar{G}' in the aperture plane, thus completing the definition of \bar{G}' and permitting its evaluation. Three convenient choices are the following:

$$\bar{G}' = 0 \text{ at } y' = 0, \quad (36a)$$

$$\frac{\partial \bar{G}'}{\partial y'} = 0 \text{ at } y' = 0, \quad (36b)$$

$$\bar{G}' = \bar{G}'_h. \quad (36c)$$

Use of the first two functions eliminates the first and second terms, respectively, in the integrand of Eq. (35). The third choice, the half-space Green's function \bar{G}'_h , is that appropriate to an unlimited y domain and satisfies a radiation condition at $\bar{R} \rightarrow \infty$ in the entire half-space region $z < 0$, as well as condition (34b) on the entire $z = 0$ plane; its use retains both terms in the integrand of Eq. (35). If values of H_x and $\partial H_x / \partial y$ in the aperture plane are known *exactly* from a rigorous solution of the given diffraction problem, then H_x is uniquely determined in S and its calculation via Eq. (35) with any of the above-mentioned Green's functions leads to the same result. On the other hand, if *approximate* values are employed for H_x and $\partial H_x / \partial y$ in the aperture plane, the fields in S calculated via different Green's functions are generally different.

To illustrate these remarks we consider once again the problem sketched in Fig. 5.7.5(a), with the assumption that H_x and (or) $\partial H_x / \partial y$ in the aperture plane are approximated by the value of H_{inc} and (or) $\partial H_{\text{inc}} / \partial y$ in Eq. (27), respectively. The Green's function satisfying Eqs. (34) and (36b) is evidently the one described in Fig. 5.7.5(b), so the resulting expression for H_x in Eq. (35) is identical with that in Eq. (28), with the recognition that $-V(z') = E_z = (1/i\omega\epsilon_1)\partial H_x / \partial y$. Thus, the choice of \bar{G}' as in Eq. (36b) leads to the far-magnetic-field formula in Eq. (30).

For a choice of \bar{G}' in accord with Eq. (36a), we note by inspection that the required boundary condition at $y' = 0$ can be met by imaging two half-space Green's functions \bar{G}'_h in the $y = 0$ plane. Thus,

$$H_x(\hat{p}) = \int_{-\infty}^0 H_x(\hat{p}') \left[\frac{\partial}{\partial y'} [\bar{G}'_h(\hat{p}; y', z') - \bar{G}'_h(\hat{p}; -y', z')] \right]_{y'=0} dz'. \quad (37)$$

It might be pointed out that Eq. (37) can be interpreted as representing an equivalent configuration wherein the aperture plane has been replaced by a magnetic wall carrying an equivalent electric current distribution $J_z \propto H_x$. Upon performing the derivative operation on the asymptotic formula for \bar{G}'_h , substituting into Eq. (37), and employing the value H_{inc} from Eq. (27) for H_x , one obtains

$$H_x(\hat{p}) \sim \frac{e^{i(k_1 \bar{R} - \pi/4)}}{\sqrt{2\pi k_1 \bar{R}}} H_0 \frac{2\bar{X}_s \sin \varphi}{\bar{X}_s^2 + \cos^2 \varphi}. \quad (38)$$

Finally, we employ the half-space Green's function \bar{G}'_h directly. From simple image considerations, $\bar{G}'_h(\hat{p}; 0, z')$ is equal to one half the Green's function satisfying condition (36b), while $(\partial \bar{G}'_h / \partial y')_{y'=0}$ is equal to one half the y' derivative of the Green's function satisfying condition (36a), all functions being

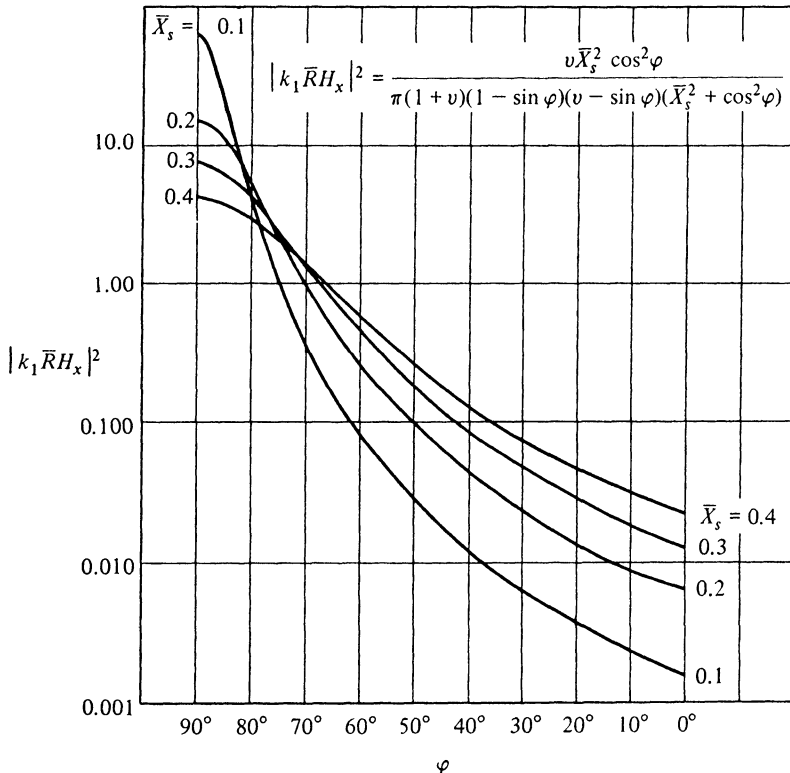


FIG. 5.7.6(a) Radiation pattern of a terminated surface-wave antenna.

evaluated at $y' = 0$. Thus, an approximate evaluation, utilizing for H_x and $\partial H_x / \partial y$ in the $y = 0$ plane the values H_{inc} and $\partial H_{\text{inc}} / \partial y$, respectively, yields a result for H_x in S which is the average of that obtained through use of the two other Green's functions in Eqs. (36a) and (36b). The far field is in this case

$$H_x(\hat{\mathbf{p}}) \sim \frac{e^{i(k_1 \bar{R} - \pi/4)}}{\sqrt{2\pi k_1 \bar{R}}} H_0 \frac{\bar{X}_s (\sin \varphi + \sqrt{1 + \bar{X}_s^2})}{\bar{X}_s^2 + \cos^2 \varphi}. \quad (39)$$

The far-field power patterns $|k_1 \bar{R} H_x|^2$ calculated from Eqs. (31a), (31b), (38), and (39) are plotted in Figs. 5.7.6(a)–(d) for values of $\bar{X}_s = 0.1, 0.2, 0.3, 0.4$. All patterns are peaked in the endfire direction $\varphi = 90^\circ$, as expected from a surface-wave illumination of the aperture plane. The fields obtained from the approximate solution in Eq. (39) and the exact solution in Eq. (31a) agree almost perfectly in the entire quarter-space region $0 \leq \varphi \leq 90^\circ$. The results from Eqs. (31b) and (38) are larger and smaller, respectively, than the correct values, with the greater deviations occurring at larger angles of elevation from

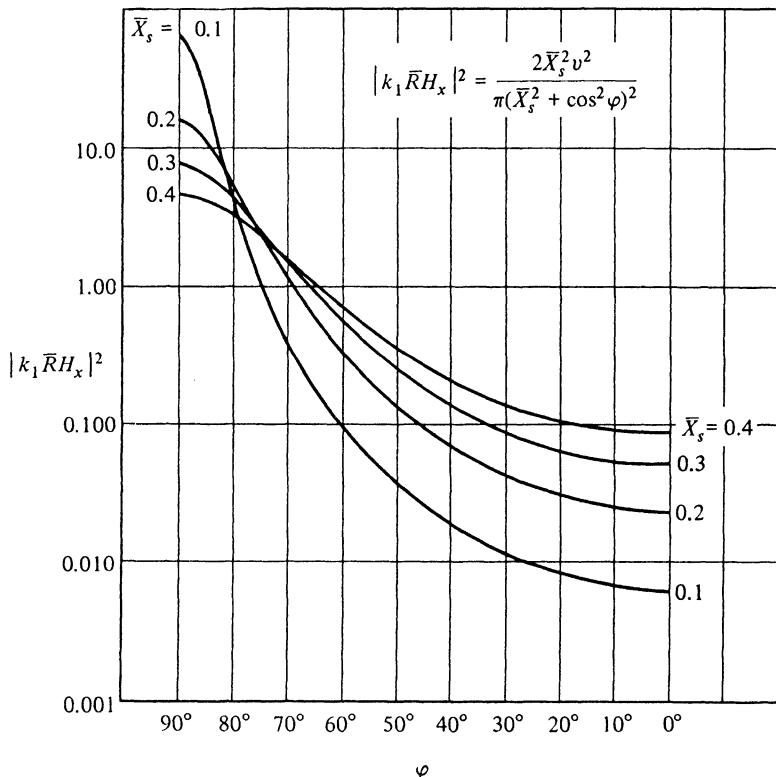


FIG. 5.7.6(b) Radiation pattern of a terminated surface-wave antenna.

the surface. For $\bar{X}_s = 0.1$, the field amplitudes decay sharply as φ decreases from 90° , and any of the above formulations yield acceptable results down to $\varphi \approx 55^\circ$, at which point $|H_x|^2$ decreases to approximately $\frac{1}{1000}$ of its maximum value. The deviations for smaller values of φ are exaggerated on the logarithmic scale but are associated with negligibly small field amplitudes. This agreement will improve further for $\bar{X}_s < 0.1$, thereby justifying any of the above approximation procedures for very small values of surface reactance. For larger values of \bar{X}_s , Eq. (39) is to be preferred.

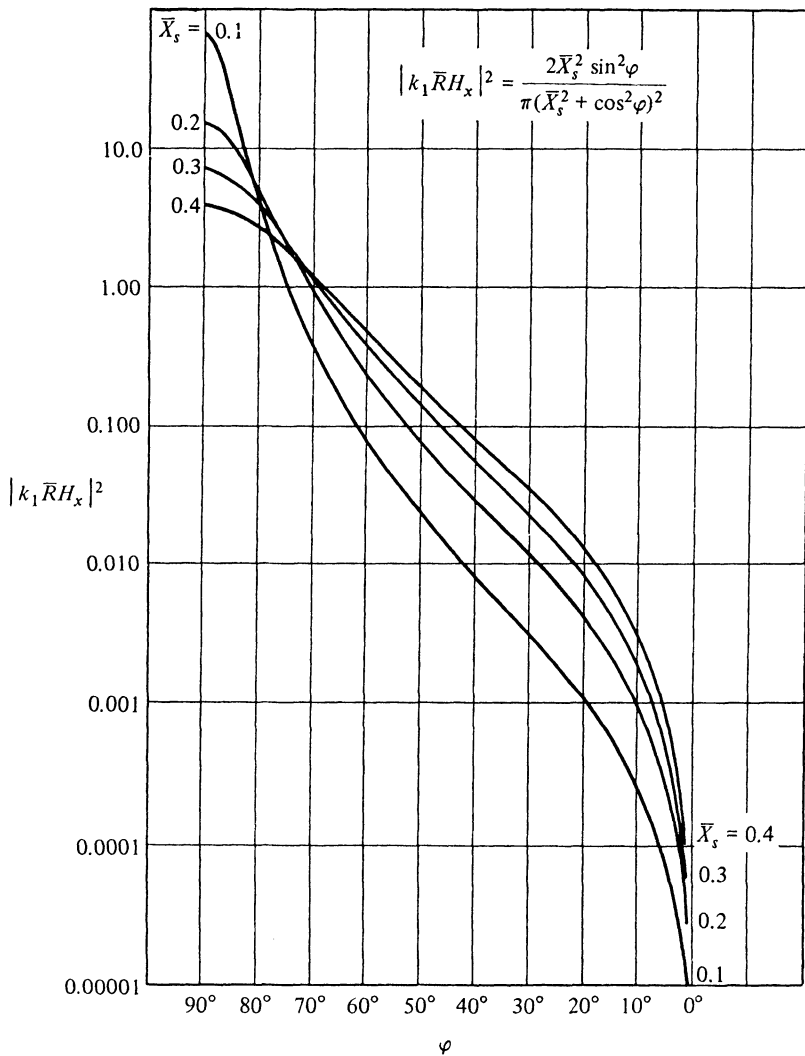


FIG. 5.7.6(c) Radiation pattern of a terminated surface-wave antenna.

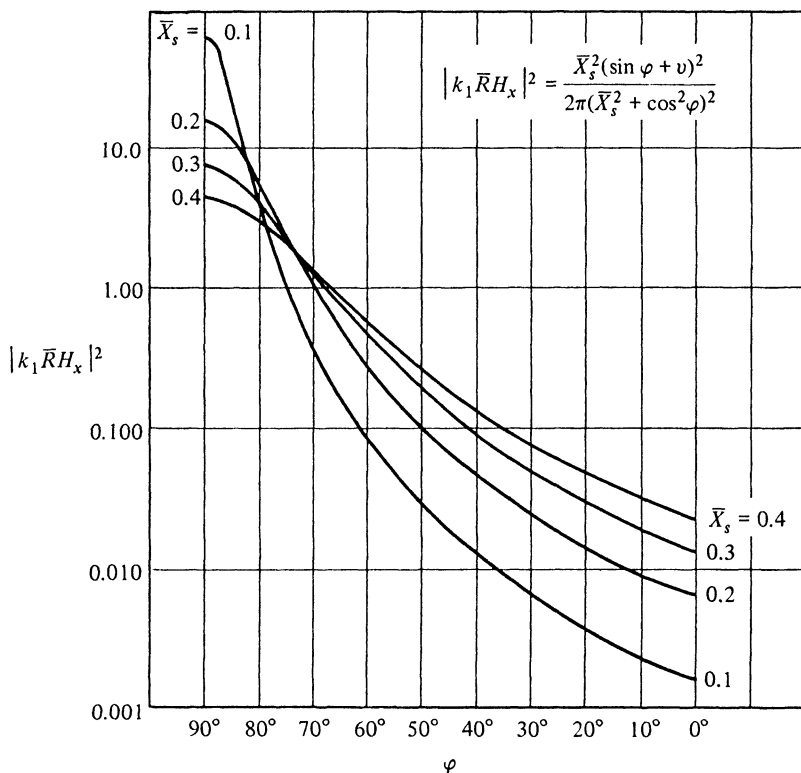


FIG. 5.7.6(d) Radiation pattern of a terminated surface-wave antenna.

5.8 SOURCES IN THE PRESENCE OF MEDIA WITH CONTINUOUS PLANAR STRATIFICATION—ARBITRARY PROFILES

5.8a General Field Properties

The radiation problems in the preceding sections have dealt with regions whose material properties along a rectilinear z coordinate may change discontinuously, as for example, at an interface between two different constant or homogeneous dielectric media. In this section and in Sec. 5.9 we consider the effects of a continuously varying medium on fields radiated by prescribed source distributions. The terms "constant" and "continuously varying" apply only to the macroscopic properties of the medium and represent averages of microscopic effects arising from the more detailed physical structure. The characterization of macroscopically homogeneous isotropic media by a constant permittivity and permeability requires sufficiently long wavelengths. However, many important electromagnetic propagation problems in nature take place under conditions where the macroscopic properties vary in a continuous manner, even for microwave, or lower, frequencies. This is true of such gaseous

media as the earth's atmosphere, or for the "electron plasma gas" constituting the ionosphere, where variations in particle density give rise to macroscopic inhomogeneities. Artificial inhomogeneous media also find application, for example, in microwave lenses.

Exact solutions for fields radiated by prescribed sources in an inhomogeneous medium can be obtained only for those special variations in medium constants that lead to differential equations whose solutions are known (see Sec. 5.9 for illustrative examples). However, if the properties of the medium vary slowly over an interval of length equal to the local wavelength, it is possible to derive approximate expressions for the fields that apply for any slow functional variation of permittivity $\epsilon(\mathbf{r})$ and (or) permeability $\mu(\mathbf{r})$ or, to use the terminology of geometrical optics, of the refractive index $n(\mathbf{r}) = [\mu(\mathbf{r})\epsilon(\mathbf{r})/\mu_0\epsilon_0]^{1/2}$, ϵ_0 and μ_0 being the permittivity and permeability of free space. These approximate expressions are shown to be equal to those obtained from geometric-optical considerations. The corresponding propagation phenomena can be interpreted in terms of real geometric-optical rays that proceed along curved paths determined by the detailed structure of the refractive index; a geometric-optical ray through a point is tangent to the direction of energy flow at that point. Because of the curvature of the rays, there may exist regions of space that are not penetrated by any real rays (see Fig. 5.8.4); in these "shadow" regions, the usual geometric-optical description must be augmented by an alternative analysis. Also, geometrical optics fails in the vicinity of caustics and focal points, and results in these transition regions must be derived from a more rigorous approach. These general observations have been made in Secs. 1.6 and 1.7.

To fit within the framework of plane-stratified regions, the discussion is confined to media whose refractive index varies along the z direction only [i.e., $n(\mathbf{r}) = n(z)$]. Consequently, the electromagnetic fields may be derived from two scalar potential functions as in Sec. 5.2; however, the differential equations satisfied by these potentials are modified by the continuous stratification. The required formulation was given in Sec. 2.3e and is summarized below. For slow variations of medium properties, the differential equations for the potential functions are solved directly by asymptotic techniques that yield geometrical optics as the first approximation exterior to the above-mentioned transition regions (see also Sec. 1.7). Thereafter, a solution is obtained by applying the WKB approximation to rigorous integral representations for the potentials, and it is shown that the result justifies the direct use of geometrical optics in certain regions of space; but, as before, a modification is required in transition regions where rapid field variations take place. These general conclusions are verified in Sec. 5.9, where exact solutions for certain special profiles $n(z)$ are examined.

5.8b Derivation of the Time-Harmonic Field from Scalar Potentials

It is shown in Sec. 2.3e that the electromagnetic fields excited by time-harmonic electric point currents $\hat{\mathbf{J}}(\mathbf{r}, t) = \mathbf{J}^0\delta(\mathbf{r} - \mathbf{r}')\exp(j\omega t)$ and magnetic

point currents $\hat{\mathbf{M}}(\mathbf{r}, t) = \mathbf{M}^o \delta(\mathbf{r} - \mathbf{r}') \exp(j\omega t)$ in a region with continuously varying permittivity $\epsilon(z)$ and permeability $\mu(z)$ can be represented as [see Eqs. (2.3.26) and (2.3.40)]

$$\mathbf{E}(\mathbf{r}, \mathbf{r}') = \frac{\epsilon(z')}{\epsilon(z)} \nabla \times \nabla \times \mathbf{z}_0 \Pi'(\mathbf{r}, \mathbf{r}') - j\omega \mu(z') \nabla \times \mathbf{z}_0 \Pi''(\mathbf{r}, \mathbf{r}'), \quad (1a)$$

$$\mathbf{H}(\mathbf{r}, \mathbf{r}') = j\omega \epsilon(z') \nabla \times \mathbf{z}_0 \Pi'(\mathbf{r}, \mathbf{r}') + \frac{\mu(z')}{\mu(z)} \nabla \times \nabla \times \mathbf{z}_0 \Pi''(\mathbf{r}, \mathbf{r}'), \quad (1b)$$

where the E - and H -mode Hertz potentials Π' and Π'' , respectively, are related via Eqs. (2.3.39) to the scalar functions \mathcal{S}'_d and \mathcal{S}''_d :

$$j\omega \epsilon(z') \Pi'(\mathbf{r}, \mathbf{r}') = \frac{1}{j\omega \epsilon(z')} \mathbf{J}^o \cdot \nabla' \times \nabla' \times \mathbf{z}_0 \mathcal{S}'_d(\mathbf{r}, \mathbf{r}') - \mathbf{M}^o \cdot \nabla' \times \mathbf{z}_0 \mathcal{S}'_d(\mathbf{r}, \mathbf{r}'), \quad (1c)$$

$$j\omega \mu(z') \Pi''(\mathbf{r}, \mathbf{r}') = \mathbf{J}^o \cdot \nabla' \times \mathbf{z}_0 \mathcal{S}''_d(\mathbf{r}, \mathbf{r}') + \frac{1}{j\omega \mu(z')} \mathbf{M}^o \cdot \nabla' \times \nabla' \times \mathbf{z}_0 \mathcal{S}''_d(\mathbf{r}, \mathbf{r}'), \quad (1d)$$

with the vector operators reducible as in Eqs. (5.2.1e) and (5.2.1f). The functions \mathcal{S}'_d and \mathcal{S}''_d are related as follows to the scalar Green's functions G' and G'' [see footnote to Eq. (5.2.3a)],

$$-\nabla_t^2 \mathcal{S}'_d(\mathbf{r}, \mathbf{r}') = j\omega \epsilon(z') G'(\mathbf{r}, \mathbf{r}'), \quad -\nabla_t^2 \mathcal{S}''_d(\mathbf{r}, \mathbf{r}') = j\omega \mu(z') G''(\mathbf{r}, \mathbf{r}'), \quad (2)$$

which, subject to appropriate boundary conditions, satisfy the equations

$$[\mathcal{D}_\epsilon^2(z) + \nabla_t^2 + k^2(z)] G'(\mathbf{r}, \mathbf{r}') = -\delta(\mathbf{r} - \mathbf{r}'), \quad k^2(z) = \omega^2 \mu(z) \epsilon(z), \quad (3a)$$

$$[\mathcal{D}_\mu^2(z) + \nabla_t^2 + k^2(z)] G''(\mathbf{r}, \mathbf{r}') = -\delta(\mathbf{r} - \mathbf{r}'), \quad (3b)$$

with

$$\mathcal{D}_\alpha^2(z) \equiv \alpha(z) \frac{\partial}{\partial z} \frac{1}{\alpha(z)} \frac{\partial}{\partial z}. \quad (3c)$$

By inserting Eqs. (2) into Eqs. (3), one obtains the differential equations satisfied by \mathcal{S}'_d and \mathcal{S}''_d (see Eqs. 5.2.2 for a homogeneous medium). It may be verified that Eqs. (3a) and (3b) can also be written in the alternative form

$$[\nabla^2 + \tilde{k}_\epsilon^2(z)] \frac{G'(\mathbf{r}, \mathbf{r}')}{\sqrt{\epsilon(z)}} = -\frac{\delta(\mathbf{r} - \mathbf{r}')}{\sqrt{\epsilon(z')}}, \quad (4a)$$

$$[\nabla^2 + \tilde{k}_\mu^2(z)] \frac{G''(\mathbf{r}, \mathbf{r}')}{\sqrt{\mu(z)}} = -\frac{\delta(\mathbf{r} - \mathbf{r}')}{\sqrt{\mu(z')}}, \quad (4b)$$

where $\tilde{k}_\alpha(z)$ is the modified wavenumber

$$\tilde{k}_\alpha(z) = \left[k^2(z) - \sqrt{\alpha(z)} \frac{d^2}{dz^2} \frac{1}{\sqrt{\alpha(z)}} \right]^{1/2}. \quad (4c)$$

In a z -transmission modal formulation, the solutions for the scalar functions may be expressed in the following manner:

$$\mathcal{S}'_d(\mathbf{r}, \mathbf{r}') = \sum_i \frac{\Phi_i(\mathbf{p}) \Phi_i^*(\mathbf{p}')}{k_{ii}^2} Y'_i(z, z'), \quad k_{ii}' \neq 0, \quad (5a)$$

$$\mathcal{S}''_d(\mathbf{r}, \mathbf{r}') = \sum_i \frac{\psi_i(\mathbf{p}) \psi_i^*(\mathbf{p}')}{k_{ii}'^2} Z_i''(z, z'), \quad k_{ii}' \neq 0, \quad (5b)$$

and

$$G'(\mathbf{r}, \mathbf{r}') = \frac{1}{j\omega\epsilon(z')} \sum_i \Phi_i(\mathbf{p}) \Phi_i^*(\mathbf{p}') Y_i'(z, z'), \quad (6a)$$

$$G''(\mathbf{r}, \mathbf{r}') = \frac{1}{j\omega\mu(z')} \sum_i \psi_i(\mathbf{p}) \psi_i^*(\mathbf{p}') Z_i''(z, z'). \quad (6b)$$

$\Phi_i(\mathbf{p})$ and $\psi_i(\mathbf{p})$ are the scalar eigenfunctions in the cross sections transverse to z and were discussed in Chapter 3. $Y_i'(z, z')$ and $Z_i''(z, z')$ are, respectively, the E -mode current excited by a unit voltage generator and the H -mode voltage excited by a unit current generator on a nonuniform transmission line with propagation constant $\kappa_i(z)$ and characteristic impedance $Z_i(z)$ (see Figs. 2.4.6 and 2.4.7). The comments pertaining to Eqs. (5.2.4) apply also in the present case, and the entire formulation is in fact analogous to that in Sec. 5.2a, to which it reduces when ϵ and μ are piecewise constant. In view of the z -dependent functions $\epsilon(z)$ and $\mu(z)$, it is convenient to deal with the functions \mathcal{S}'_d and \mathcal{S}''_d rather than with their counterparts \mathcal{S}' and \mathcal{S}'' in Eqs. (5.2.5).

The functions $Y_i'(z, z')$ and $Z_i''(z, z')$ may be related as in Eq. (5.2.6a) to the one-dimensional modal Green's functions

$$g'_{zi}(z, z') = \frac{1}{j\omega\epsilon(z')} Y_i'(z, z'), \quad g''_{zi}(z, z') = \frac{1}{j\omega\mu(z')} Z_i''(z, z'), \quad (7)$$

which satisfy the differential equations

$$[D_\epsilon^2(z) + \kappa_i'^2(z)] g'_{zi}(z, z') = -\delta(z - z'), \quad (7a)$$

$$[D_\mu^2(z) + \kappa_i''^2(z)] g''_{zi}(z, z') = -\delta(z - z'), \quad (7b)$$

where $D_\alpha^2(z)$ is defined as in Eq. (3c), with $\partial/\partial z \rightarrow d/dz$, and

$$\kappa_i^2(z) = k^2(z) - k_{ii}^2. \quad (7c)$$

General methods for solving these equations subject to appropriate boundary conditions are discussed in Chapter 3. If ϵ and (or) μ are discontinuous at a plane $z = z_1$, the required continuity of the voltage and current across the junction point in the equivalent modal network implies via Eqs. (2.3.10) the continuity of the following quantities:

$$g'_{zi}, \quad \frac{1}{\epsilon(z)} \frac{d}{dz} g'_{zi}; \quad g''_{zi}, \quad \frac{1}{\mu(z)} \frac{d}{dz} g''_{zi}. \quad (8)$$

In view of Eqs. (5) and (6), continuity conditions of the same type apply to the three-dimensional Green's functions G' and G'' , and to the functions \mathcal{S}'_d and \mathcal{S}''_d .

Since the transverse eigenfunctions for media with piecewise constant or with continuously variable characteristics along z are identical, the treatment in Sec. 5.2b pertaining to eigenfunction representations in transversely unbounded regions remains valid provided that the modal Green's functions g_{zi} are deter-

mined from Eqs. (7). A basic feature employed in Eqs. (5.2.8) and subsequently, namely the evenness of g_{zi} with respect to the transverse wavenumber $k_{ii} = \xi$, still obtains as one may realize by considering the continuously varying medium with permittivity $\epsilon(z)$ and permeability $\mu(z)$ to be approximated by a series of thin layers. A typical layer extends from $(z_j - \delta)$ to $(z_j + \delta)$ and has a constant permittivity $\epsilon(z_j)$ and permeability $\mu(z_j)$. $g_{zi}(z, z')$ evaluated as in Sec. 5.3a is now a function of the various $\kappa_j = [\omega^2 \mu(z_j) \epsilon(z_j) - \xi^2]^{1/2}$ (i.e., an even function of ξ). This property continues to hold in the limiting case where the number of layers increases indefinitely and each layer width 2δ approaches 0, in which instance one obtains the original continuous medium. From this consideration, it may also be anticipated that when the wavenumber $k(z)$ varies continuously and approaches a *finite* value k_N at $z = \infty$, the function $g_{zi}(z, z')$ has branch points at $k_{ii} = \pm k_N$ (see Fig. 5.3.1), while a finite value k_1 of $k(z)$ at $z = -\infty$ implies existence of branch points at $k_{ii} = \pm k_1$.

5.8c Direct Ray-Optical Solution in a Slowly Varying Medium

Although it is not possible to solve Eqs. (3) or the corresponding equations for $\mathcal{S}'_d, \mathcal{S}''_d$ for arbitrarily prescribed variations in $k(z)$, approximate methods are applicable when the relative variation is small over a length interval equal to the local wavelength $2\pi/k(z)$. It is convenient to characterize this condition in terms of the refractive index $n(z)$ as

$$\left| \frac{dn/dz}{k_0 n^2} \right| \ll 1, \quad (9)$$

where k_0 is the wavenumber in vacuum and $k(z) = k_0 n(z)$, so that this slow variability criterion for a specified $n(z)$ may be met by choosing k_0 large enough (short wavelength limit). Since k_0 is a large parameter, it is suggestive to seek an approximate representation for the field or the scalar potentials in a series involving inverse powers of k_0 . This development, which may be carried out directly from the differential equations, has been described in Sec. 1.7b; to a lowest order of approximation, it yields a solution that can be interpreted in geometric-optical terms. The general discussion in Sec. 1.7b is now specialized to the case of planar stratification. We seek field or potential solutions of the form

$$u(\mathbf{r}) \sim u_0(\mathbf{r}) e^{ik_0 \psi(\mathbf{r})}, \quad (10)$$

where u_0 and ψ are k_0 -independent amplitude and phase functions, respectively [however, see remarks following Eq. (1.7.22a)]. Basic to the evaluation of these functions is the determination of the ray trajectories.

Ray trajectories

Ray trajectories are specified by the ray equation [see Eq. (1.7.23)]

$$\frac{d}{ds} n \frac{d\mathbf{R}}{ds} = \nabla n, \quad \text{with } \left(\frac{d\mathbf{R}}{ds} \right)^2 = 1, \quad (11)$$

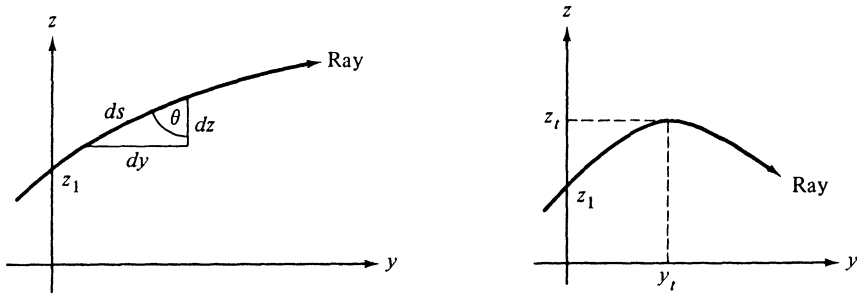
where s is the distance coordinate along the ray and $\mathbf{R} = x_0x + y_0y + z_0z$ is the radius vector from an arbitrarily chosen coordinate center to a point on the ray (coordinates along a ray are denoted by \mathbf{R} instead of \mathbf{r} as in Sec. 1.7b). When n varies only with z , this equation can be written in component form as follows:

$$\frac{d}{ds} n \frac{dx}{ds} = 0 = \frac{d}{ds} n \frac{dy}{ds}, \quad (12a)$$

$$\frac{d}{ds} n \frac{dz}{ds} = \frac{dn}{dz}. \quad (12b)$$

From Eq. (12a), $n(dx/ds)$ and $n(dy/ds)$ are constant along a ray, so their ratio, and therefore dy/dx , are constant also. The constancy of dy/dx implies that the projection of a ray curve upon the xy plane is a straight line, whence each ray is a curve confined entirely to a plane perpendicular to the xy plane. Without loss of generality, the coordinate system may be chosen so that the ray under consideration is confined to the plane $x = 0$. With reference to Fig. 5.8.1(a), one notes that

$$\frac{dy}{ds} = \sin \theta, \quad \frac{dz}{ds} = \cos \theta, \quad (13)$$



(a) Without turning point

(b) With turning point

FIG. 5.8.1 Ray trajectories.

where θ is the angle between the ray vector \mathbf{s} and the positive z axis. Hence, from Eq. (12a),

$$n \sin \theta = a = \text{constant along a ray}, \quad (14)$$

which statement is known as Snell's law. From Eq. (12b),

$$\frac{dn}{dz} = \frac{d}{ds} (n \cos \theta) = \cos \theta \frac{dn}{dz} \frac{dz}{ds} - n \sin \theta \frac{d\theta}{ds}, \quad (15)$$

whence

$$\frac{d\theta}{ds} = -\frac{\sin \theta}{n} \frac{dn}{dz}. \quad (16)$$

Thus, $d\theta/ds < 0$ if $dn/dz > 0$, whence the ray inclination angle decreases with increasing s ; the ray bends toward the z axis when the propagation vector has a component in the direction of increasing n .

From Eqs. (13) and (14),

$$\frac{dy}{dz} = \tan \theta = \frac{a}{\sqrt{n^2 - a^2}}, \quad (17)$$

and the ray curve $y = y(z)$ is therefore given by

$$y(z) = a \int_{z_1}^z \frac{dz}{\sqrt{n^2(z) - a^2}}, \quad (18)$$

with the arbitrary reference $y(z_1) = 0$. If a ranges over a certain set of real numbers for which the square root is real, Eq. (18) defines a corresponding family of rays, all passing through the common point $(0, z_1)$. The square root $\sqrt{n^2 - a^2}$ is conveniently defined to be positive when real and if $a > 0$, one observes from Eq. (17) that $dy/dz > 0$ and the ray in the first quadrant of Fig. 5.8.1(a) is upgoing with respect to the reference point z_1 . The solution for a downgoing ray corresponding to the same value of a is obtained upon interchanging the integration limits in Eq. (18), thereby yielding $dy/dz < 0$. With this definition of the square root, θ is restricted to $0 \leq \theta \leq \pi/2$ and measures the inclination with respect to the negative z direction if the ray is downgoing. It is noted that $\tan \theta = \infty$ at a level z_t defined by

$$n(z_t) = a, \quad (19)$$

so the ray becomes horizontal at z_t [see Fig. 5.8.1(b)]. This may occur when the refractive index decreases along the direction of propagation of the incident ray. Since Eq. (18) has real solutions only when $n^2(z) \geq a^2$, the ray does not penetrate the region where $n^2(z) < a^2$ but bends back toward the direction of incidence after reaching the level $z = z_t$, the "turning point" in the z -coordinate space. If a turning point is present, y is a double-valued function of z , and separate equations apply to the upgoing and downcoming parts of the ray. Along the upgoing part, y is given by Eq. (17); for the downgoing part, z and z_1 in Eq. (18) are replaced by z_t and z , respectively, and the value $y(z_t) \equiv y_t$ from Eq. (18) is added to the right-hand side [see Eq. (28)].

Phase change along a ray

With the ray trajectories determined, one may evaluate the phase change in the field as it advances a specified distance along a ray. From Eq. (1.7.28), the phase difference between two points R_1 and R on a ray is given by

$$\psi(R) - \psi(R_1) = \int_{R_1}^R n ds \equiv \psi - \psi_1, \quad (20)$$

which becomes, for the present problem,

$$\psi - \psi_1 = \int_{R_1}^R n[(\mathbf{y}_0 \cdot \mathbf{s}) dy + (\mathbf{z}_0 \cdot \mathbf{s}) dz] = \int_{R_1}^R n(\sin \theta dy + \cos \theta dz), \quad (20a)$$

where \mathbf{s} is a unit vector along the ray, and the integration path proceeds along the ray. In view of Eq. (13), one has, for an upgoing ray,

$$\psi - \psi_1 = a(y - y_1) + \int_{z_1}^z \sqrt{n^2(z) - a^2} dz, \quad (20b)$$

with ψ_1 denoting the phase at the point (y_1, z_1) on the ray. One observes that the phase function ψ is real only at those points for which $n^2(z) \geq a^2$; if $n^2(z) < a^2$, ψ is imaginary and yields via Eq. (10) an exponentially decaying ("non-propagating") solution. The concept of "complex rays" has been introduced to deal with complex solutions of the ray equations, but the physical attributes of complex ray fields (energy transport, etc.) remain to be clarified.²⁷ If there is a turning point, the calculation of the phase is carried out separately for the upward and downward portions along the ray as above. For an upgoing ray and $\sqrt{n^2 - a^2}$ positive, one obtains from Eq. (20b) the required phase increase with z . For a downgoing ray, z has to appear in the lower integration limit in Eq. (20b) in order to yield the required phase increase with decreasing z [see Eq. (29)].

In order to determine the amplitude function u_0 in Eq. (10), details of the source configuration must be given. Two examples, excitation by a line source and a point source, are treated for illustration.

Excitation by a transverse electric line current

As an illustration of how to determine the amplitude of the fields excited by a confined source distribution, consider a line source of electric currents directed parallel to the x axis and located at the point $(0, z')$ in a medium with variable permittivity $\epsilon(z)$ and constant permeability μ_0 , as shown in Fig. 5.8.2.^{27,28}

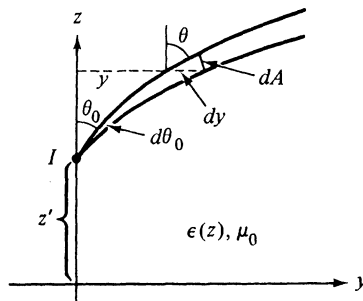


FIG. 5.8.2 Radiation from a line source : $\hat{\mathbf{J}}(\mathbf{r}, t) = I\delta(\hat{\rho} - \hat{\rho}')e^{-i\omega t}\mathbf{x}_0$.

This source generates an electric field which has only an x component, as may be verified from Eqs. (1), with $\partial/\partial x \equiv 0$ [see also Eqs. (5.2.4) and (5.4.31)]. All rays will be plane curves parallel to the yz plane, and each ray may be characterized conveniently by the angle, θ_0 , at which it emerges from the source. To find the ray amplitude from energy conservation in a ray tube [see Eq. (1.7.34)], it is necessary to evaluate the cross-sectional area dA of the tube

bounded by rays leaving the source at angles θ_0 and $\theta_0 + d\theta_0$; a length dimension dx parallel to the x axis is suppressed. From Fig. 5.8.2,

$$dA = dy \cos \theta = \frac{\partial y}{\partial \theta_0} d\theta_0 \cos \theta, \quad (21)$$

where dy , at a fixed value of z , has been related to θ_0 via the parametric form $y = y(\theta_0)$, $z = z(\theta_0)$, of the ray equation. If $P(\theta_0)$ is the angular power density (power per radian) emitted by the source in the direction θ_0 , the power into the ray tube, $P(\theta_0) d\theta_0$, remains constant inside the tube and the intensity (power density) at any point along the ray tube is given by

$$\bar{S} = \frac{P(\theta_0) d\theta_0}{dA} = \frac{P(\theta_0)}{(\partial y / \partial \theta_0) \cos \theta}. \quad (22)$$

The partial derivative $\partial y / \partial \theta$, for a fixed value of z , can be determined from Eq. (18) and the relation $a = n(z) \sin \theta$, whence

$$\frac{\partial y}{\partial \theta_0} = \frac{\partial y}{\partial a} \frac{\partial a}{\partial \theta_0} = n(z') \cos \theta_0 \int_{z'}^z \frac{n^2 dz}{(n^2 - a^2)^{3/2}}, \quad (23)$$

whence, from Eq. (1.7.39),

$$E_0(y, z) = \sqrt{\frac{\zeta \bar{S}(y, z)}{n(z)}} = \left[\frac{\zeta P(\theta_0)}{n(z) \cos \theta_0 n(z') \cos \theta_0 \int_{z'}^z [(n^2 dz) / (n^2 - a^2)^{3/2}]} \right]^{1/2},$$

$$\zeta = \sqrt{\frac{\mu_0}{\epsilon_0}}. \quad (24)$$

This expression, valid for $z > z'$, applies also to $z < z'$ provided that one exchanges z and z' in the integration limits and restricts $0 \leq \theta \leq \pi/2$ as noted previously. The resulting symmetry in the source-point and observation-point coordinates is in accord with the reciprocity principle.

To calculate $P(\theta_0)$ it is necessary to consider the line-source field in the vicinity of the source point $(0, z')$. Since $k_0 \gg 1$ and the relative medium parameters change only slightly over a distance interval equal to the local wavelength, it is possible to choose an observation point $\mathbf{r} = (y, z)$ near enough to the source point \mathbf{r}' to have $n(z) \approx n(z')$ and yet far enough to yield

$$k_0 n(z') |\mathbf{r} - \mathbf{r}'| \gg 1.$$

Thus, the pertinent local power pattern is that produced by the source when embedded in a medium with constant refractive index $n(z')$. If the source strength is chosen as $I = (ik_0 \zeta)^{-1}$, the x component of the electric field, $\mathbf{E}_f = \mathbf{x}_0 E_f$, is given by the free-space Green's function [see Eq. (5.4.25)]:

$$E_f = \frac{i}{4} H_0^{(1)}[k_0 n(z') |\mathbf{r} - \mathbf{r}'|] \sim \frac{1}{4} \sqrt{\frac{2}{\pi k_0 n(z') |\mathbf{r} - \mathbf{r}'|}} e^{ik_0 n(z') |\mathbf{r} - \mathbf{r}'| + i\pi/4}. \quad (25)$$

Thus, the radiation pattern is independent of angle, and $P(\theta_0) = P = \text{constant}$ is given by

$$P = \frac{\text{total power}}{2\pi} = \frac{n(z')|E_f|^2}{2\pi\zeta} 2\pi|\mathbf{r} - \mathbf{r}'| = \frac{1}{8\pi k_0 \zeta}. \quad (26)$$

Substitution of Eq. (26) into Eq. (24) yields an expression for the magnitude E_0 of the electric field, and the actual field $\mathbf{E} = \mathbf{x}_0 E$ is then obtained from $\mathbf{E} \sim E_0 \exp(ik_0\psi)$, with the phase function ψ defined in Eq. (20b). The value of the initial phase ψ_1 depends on the phase of the source function and has to be calculated from the requirement that $E \rightarrow E_f$ as $\mathbf{r} \rightarrow \mathbf{r}'$. Since $(y_1, z_1) \equiv (y', z')$, this comparison yields $k_0\psi_1 = \pi/4$, whence the final result for the line-source Green's function along a ray in a plane-stratified medium is, for $z > z'$,²⁷

$E(\mathbf{R}, \mathbf{R}')$

$$\sim \frac{1}{2\sqrt{2\pi k_0}} \frac{\exp \left[ik_0 ay + ik_0 \int_{z'}^z \sqrt{n^2(z) - a^2} dz + i\pi/4 \right]}{[n^2(z) - a^2]^{1/4} [n^2(z') - a^2]^{1/4} \left[\int_{z'}^z [n^2(z) dz] / [n^2(z) - a^2]^{3/2} \right]^{1/2}} \quad (27)$$

where the identity $n(z) \cos \theta = [n^2(z) - a^2]^{1/2}$ has been utilized, with $a = n(z') \sin \theta_0$ along the ray that emerges from the source at the angle θ_0 . For $z < z'$, one interchanges z and z' in the integration limits. If $n(z) \rightarrow 1$ as $z \rightarrow \infty$, the constant a can likewise be regarded as $\sin \theta_\infty$, where θ_∞ is the angle of emergence of the ray at $z \rightarrow \infty$. The result in Eq. (27) is then identical with that in Eq. (46), which is obtained from an asymptotic analysis of a rigorous solution. It is recalled that $\sqrt{n^2 - a^2}$ is defined to be positive when real; its analytic continuation to the range $n^2 < a^2$ is achieved by the definition $\text{Im } \sqrt{n^2 - a^2} > 0$. In Eq. (27), the field is expressed in terms of the ray parameter a , which is constant on the ray curve of Eq. (18). Alternatively, for prescribed (y, z) , Eq. (18) defines $a = a(y, z)$ and hence permits the elimination of a from Eq. (27) provided that one may solve for $a(y, z)$ explicitly [this is possible only for special profiles $n(z)$].

If $n^2(z)$ decreases as z increases and $n^2(z) = a^2$ at $z = z_t$, a ray that leaves the source at an angle θ_0 propagates up to z_t and is turned back into the region $z < z_t$. The field along the ray up to and including the turning point (y_t, z_t) in Fig. 5.8.1(b) can be calculated from Eq. (27). For the refracted part of the ray in the region $y \geq y_t$, $z \leq z_t$, the ray equation (18) is replaced by

$$y(z) = a \int_z^{z_t} \frac{dz}{\sqrt{n^2(z) - a^2}} + y_t, \quad y_t = y(z_t) = a \int_{z'}^{z_t} \frac{dz}{\sqrt{n^2(z) - a^2}} \quad (28)$$

where y_t is the value of y at the turning point, and the remaining integral traces the ray curve beyond the turning point. Similarly, the phase function ψ is given by

$$\psi = ay + \int_{z'}^{z_t} \sqrt{n^2 - a^2} dz + \int_z^{z_t} \sqrt{n^2 - a^2} dz. \quad (29)$$

The field evaluation along the ray past the turning point can now be carried out as above except that Eq. (28) must be used in the calculation of the cross-section element in Eq. (21), and the phase function taken as that in Eq. (29).

The fields so determined are matched to those obtained from Eq. (27) at the turning point (y_i, z_i) . Details of this evaluation are described in connection with the rigorous analysis in Sec. 5.8d.

Excitation by a longitudinal electric current element

A procedure similar to the above may be employed for the point-source problem. If we are dealing with a z -directed electric or magnetic current element in the region of Fig. 5.8.2, the electromagnetic fields can be determined from a scalar Green's function that satisfies the equation $(\nabla^2 + k_0^2 n^2)G = -\delta(\mathbf{r} - \mathbf{r}')$ [see Eqs. (5.2.4c), (1) and (3)].[†] G is angularly symmetric about the z axis, and rays leaving the source at the angle θ_0 all lie on a surface of revolution defined by Eq. (18) provided that y is replaced by the radial cylindrical variable ρ . The power contained between two such ray surfaces remains constant, and if $P(\theta_0)$ denotes the power per unit solid angle radiated by the source in the direction θ_0 , then the power flow into the two neighboring surfaces bounded by rays with $\theta = \theta_0$ and $\theta_0 + d\theta_0$ is given by $2\pi P(\theta_0) \sin \theta_0 d\theta_0$. Thus, the intensity at any point along a ray leaving the source at angle θ_0 is

$$\tilde{S} = \frac{2\pi P(\theta_0) \sin \theta_0 d\theta_0}{dA} = \frac{P(\theta_0) \sin \theta_0}{\rho \cos \theta [\partial \rho / \partial \theta_0]}, \quad (30)$$

where

$$dA = 2\pi \rho d\rho \cos \theta.$$

All other considerations are now directly analogous to those employed for the line-source problem, with y replaced by ρ . The behavior of G near \mathbf{R}' is given by $(1/4\pi|\mathbf{R} - \mathbf{R}'|) \exp[ik_0 n(z')|\mathbf{R} - \mathbf{R}'|]$ [see Eq. (5.4.2b)], whence for arbitrary \mathbf{R} along the ray characterized by $a = n(z') \sin \theta_0$:

$$G \sim \frac{\sqrt{a} \exp\left(ik_0 a \rho + ik_0 \int_{z'}^z \sqrt{n^2 - a^2} dz\right)}{4\pi \sqrt{\rho} [n^2(z) - a^2]^{1/4} [n^2(z') - a^2]^{1/4} \left\{ \int_{z'}^z n^2 dz / [n^2 - a^2]^{3/2} \right\}^{1/2}}. \quad (31)$$

The modifications when a refracted ray has passed through a turning point are again analogous to those for the line-source problem.

Excitation by an incident plane wave

The limiting case of an incident plane wave, polarized with its electric vector perpendicular to z , may be obtained from Eq. (27) upon letting $y' \rightarrow -\infty$, $z' \rightarrow -\infty$, with $y' = z' \tan \theta_\infty$. To generalize the equation so as to permit arbitrary values of the source-point coordinate y' , we replace y by $y - y'$. If it is assumed that the refractive index approaches the constant value n_1 as $z \rightarrow -\infty$, the integral in the denominator of Eq. (27) can be evaluated as

[†]The differential operator in Eqs. (3a) and (3b) also contains a term of the form $(1/n)(dn/dz)\partial G/\partial z \sim k_0 G(dn/dz)$, which is neglected in comparison with $k_0^2 n^2 G$, in view of Eq. (9).

$n_1^2[n_1^2 - a^2]^{-3/2}(-z')$ in the limit $z' \rightarrow -\infty$. The phase integral cannot be similarly approximated because negligible phase terms must be small compared to unity, rather than small compared to $|z'|$. Since $a = n(z) \sin \theta(z) = n_1 \sin \theta_\infty$, where θ_∞ is the incident ray angle at $z \rightarrow -\infty$, $y \rightarrow -\infty$, one may write Eq. (27) as

$$E \sim A \frac{\sqrt{n_1 \cos \theta_\infty}}{[n^2(z) - n_1^2 \sin^2 \theta_\infty]^{1/4}} \exp \left\{ ik_0 n_1 [y \sin \theta_\infty + z' \cos \theta_\infty] + ik_0 \int_{z'}^z \sqrt{n^2(\eta) - n_1^2 \sin^2 \theta_\infty} d\eta \right\}, \quad (32)$$

where

$$A = \frac{1}{2\sqrt{2\pi k_0 n_1 \hat{\rho}'}} e^{ik_0 n_1 \hat{\rho}' + i\pi/4}, \quad \hat{\rho}' = \sqrt{y'^2 + z'^2}. \quad (32a)$$

The factor A is set equal to unity if the incident plane wave is to have unit amplitude [see Eq. (5.4.30b)]. Upon rearranging the exponent so that the term $n_1 z' \cos \theta_\infty$ is absorbed into the integrand, one may pass to the limit $z' \rightarrow -\infty$ to obtain the expression for the field due to a plane wave of unit amplitude, incident from $z = -\infty$ at an angle θ_∞ with the positive z axis,

$$E \sim \frac{\sqrt{n_1 \cos \theta_\infty}}{[n^2(z) - n_1^2 \sin^2 \theta_\infty]^{1/4}} \exp \left\{ ik_0 n_1 [y \sin \theta_\infty + z \cos \theta_\infty] + ik_0 \int_{-\infty}^z [\sqrt{n^2(\eta) - n_1^2 \sin^2 \theta_\infty} - n_1 \cos \theta_\infty] d\eta \right\} \quad (33)$$

This expression applies when $n(z) > n_1 \sin \theta_\infty$ for all z .

If there is a turning point z_t , Eq. (33) applies up to z_t ; the corresponding expression for the refracted-ray field requires consideration of a “canonical” problem and can be deduced from the limit of Eq. (55) as $z' \rightarrow -\infty$. The result for $z \rightarrow \infty$ is given in Eq. (57), and the formula for $z' \rightarrow \infty$ is obtained therefrom by interchanging z and z' since \tilde{G}_2'' is symmetrical in z and z' . In Eq. (57), it is assumed that $z, z' > z_t$ and that $n(\infty) = 1$. Adapting the result to the present case where $z' \rightarrow -\infty$, $y' \rightarrow -\infty$, $z_t > z, z', n(-\infty) = n_1$, and using Eq. (32a), one finds, for the field along the refracted ray,

$$E_r \sim e^{-i\pi/2} \frac{\sqrt{n_1 \cos \theta_\infty}}{[n^2(z) - n_1^2 \sin^2 \theta_\infty]^{1/4}} e^{ik_0 [n_1 y \sin \theta_\infty - n_1 z \cos \theta_\infty] + ik_0 \psi_r}, \quad (34)$$

where

$$\begin{aligned} \psi_r = & 2 \int_{-\infty}^{z_t} \left[\sqrt{n^2(\eta) - n_1^2 \sin^2 \theta_\infty} - n_1 \cos \theta_\infty \right] d\eta \\ & - \int_{-\infty}^z \left[\sqrt{n^2(\eta) - n_1^2 \sin^2 \theta_\infty} - n_1 \cos \theta_\infty \right] d\eta + 2z_t n_1 \cos \theta_\infty. \end{aligned} \quad (34a)$$

The ray envelope, the caustic, is in this case the straight line $z = z_t$ in Fig. 5.8.3, and the factor $\exp(-i\pi/2)$ represents the phase shift introduced when a ray passes through the caustic. If a physical reflecting plane is located at $z = z_0$, with $n(z_0) > n_1 \sin \theta_\infty$, the reflected field is also given by Eq. (34),

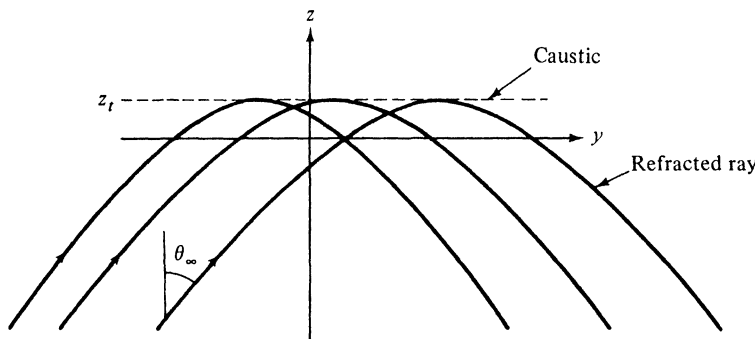


FIG. 5.8.3 Incident plane wave and turning point.

except that z_t is replaced by z_0 and the reflection coefficient $\exp(-i\pi/2)$ is replaced by the one for the plane surface. Since the ray is reflected at the incident angle, the ray trajectories are symmetrical about the reflection point.

5.8d Asymptotic Evaluation of a Typical Radiation Integral for a Medium with Monotonic Variation

The electromagnetic fields excited by arbitrary source distributions can be evaluated in terms of the scalar functions \mathcal{S}'_d and \mathcal{S}''_d , or for special source configurations, in terms of the scalar Green's functions G' or G'' [see Eqs. (1) and (2)]. General modal expansions for these functions, derived from a z -transmission analysis, are given in Eqs. (5) and (6); when the excitation is in the form of point or line currents in a transversely unbounded region, they reduce to the integral representations in Eqs. (5.2.11)–(5.2.14), with g_{zi} specified by Eqs. (7). The nonuniform transmission line equations for g_{zi} can be solved in terms of known functions only for special functional variations $k(z)$. However, for a slowly varying medium satisfying condition (9) (it is convenient to characterize this relation in terms of the large wavenumber k_0), one may approximate $g_{zi}(z, z')$ without specifying its detailed functional form. The nature of the approximation depends on the analytic properties of $[\kappa_i(z)/k_0]^2 = [n^2(z) - (k_{ii}/k_0)^2]$. In Sec. 3.5, this aspect has been pursued in regard to the functional dependence on z and z' , with k_{ii} taken as a fixed parameter, whereas for the present application, the functional dependence on k_{ii} remains to be explored for any specific choice of the space coordinates z and z' . Since the wavenumber variable k_{ii} ranges over an infinite interval, $(\kappa_i/k_0)^2$ may take on positive and negative values (when n^2 is real), and the differential Eqs. (7a) and (7b) possess turning points where κ_i vanishes. The asymptotic forms of the solutions of Eqs. (7a) and (7b) may then be given in terms of Airy functions and remain valid over the entire range of variation of κ_i . Comparison of Eqs. (7) and Eq. (3.5.34) shows that $x \rightarrow z$, $\Omega \rightarrow k_0$, $\alpha(x, \Omega) = \alpha_0(x) \rightarrow [\kappa_i(z)/k_0]^2$, and with these identifications, the relevant asymptotic approximations may be

synthesized from Eqs. (3.5.45)–(3.5.48). Over most of the range of interest where $\kappa_i \neq 0$, one may employ the WKB approximations for the Airy functions as given in Eq. (3.5.47).

Since $-\infty < k_{ii} < \infty$, different k_{ii} -intervals correspond to positive or negative values of $(\kappa_i/k_0)^2$, and these intervals change with the location of the source and observation points z' and z , respectively. The detailed construction of the asymptotic form for $g_{zi}(z, z')$ depends on the algebraic sign of $(\kappa_i/k_0)^2$ as well as on the boundary conditions at the endpoints of the z -domain, and must in general be carried out separately in each of the above-mentioned ranges of k_{ii} . For a subsequent asymptotic evaluation of the integrals representing the scalar potential functions G' , G'' or S'_d , S''_d in the limit of large k_0 , only the wave functions corresponding to real κ_i will be considered since they alone represent propagating wave processes; regions wherein κ_i^2 is negative ($\text{Im } \kappa_i > 0$) yield exponentially decaying contributions.

To illustrate these remarks, we take a refractive index profile that increases monotonically from a positive value n_1 at $z = -\infty$ to a positive value n_2 at $z = +\infty$. When $k_{ii}^2 < k_0^2 n_1^2$, κ_i is real for all values of z and waves may propagate toward infinity in both directions. The corresponding one-dimensional Green's function g_{zi} must satisfy the radiation condition at $|z| \rightarrow \infty$ and is given in Eq. (3.5.39b):

$$g_{zi}(z, z') \sim \frac{\exp \left\{ ik_0 \int_{z_i}^{z'} [\kappa_i(\zeta)/k_0] d\zeta \right\}}{-2ik_0 \left[\frac{\kappa_i(z)}{k_0} \frac{\kappa_i(z')}{k_0} \right]^{1/2}}, \quad k_{ii}^2 < k_0^2 n_1^2. \quad (35a)$$

When $k_0^2 n_1^2 < k_{ii}^2 < k_0^2 n_2^2$, the interval contains turning points z_i at which $\kappa_i(z_i) = 0$: $k_{ii} = \pm k_0 n(z_i)$. Since $n_1 < n(z_i)$, κ_i^2 is negative when $z < z_i$ so that no propagation toward $z = -\infty$ is possible. To assure that the solution remains bounded at $z = -\infty$, a decaying exponential must be chosen, with the consequent appearance of an additional reflected wave in the region $z > z_i$ when $z' > z_i$ [see Eq. (3.5.39e)]:

$$g_{zi}(z, z') \sim \frac{\exp \left\{ ik_0 \int_{z_i}^{z'} [\kappa_i(\zeta)/k_0] d\zeta \right\}}{-2ik_0 \left[\frac{\kappa_i(z)}{k_0} \frac{\kappa_i(z')}{k_0} \right]^{1/2}} - i \frac{\exp \left\{ ik_0 \left(\int_{z_i}^z + \int_{z_i}^{z'} \right) [\kappa_i(\zeta)/k_0] d\zeta \right\}}{-2ik_0 \left[\frac{\kappa_i(z)}{k_0} \frac{\kappa_i(z')}{k_0} \right]^{1/2}}. \quad (35b)$$

No propagating solutions exist in the remaining interval $k_{ii}^2 > k_0^2 n_2^2$ wherein g_{zi} decays exponentially. The factor $-i$ multiplying the second term in Eq. (35b) represents the “reflection coefficient” at the caustic $z = z_i$ of the continuously refracted ray system [see Fig. 5.8.3, with $z \rightarrow -z$, and remarks following Eq. (58)]; if a physical reflecting boundary is located at the fixed coordinate $z = z_0$, $z_0 > z_i$, Eq. (35b) applies as well provided that $z_i \rightarrow z_0$ and the appropriate reflection coefficient Γ at the boundary is inserted instead of $-i$. While the expressions in Eqs. (35) have been deduced for k_{ii} -intervals on the real axis,

they remain valid for neighboring complex values of k_{ii} and therefore define g_{zi} in the corresponding portions of the complex k_{ii} -plane.

An example: Excitation by an electric line current

When the solutions in Eqs. (35) are inserted into Eqs. (5.2.11)–(5.2.14), one obtains explicit integral representations for the scalar functions from which the electromagnetic fields can be calculated. Further reduction of these integrals may be achieved by saddle point techniques since the integrands contain the large parameter k_0 . Although expressions for g_{zi} have been given only in the range κ_i real, they suffice for the location of real stationary points which contribute propagating fields. No such contribution arises from the remaining ranges of k_{ii} , and no further attention is given to the specific structure of the integrand therein. The asymptotic procedure will be illustrated for the specific example of a line source of electric current directed parallel to x and located at $z = z'$ (see Fig. 5.8.2) in a region wherein the refractive index decreases monotonically from $n_2^2 = 1$ at $z = \infty$ to $n_1^2 = -\infty$ at $z = 0$, with $n^2(z_0) = 0$, $z_0 > 0$. The results may then be compared with the exact solution in Sec. 5.9a for a special profile of this type. The fields can in this instance be derived from the scalar H -mode Green's function $\bar{G}''(\hat{\mathbf{p}}, \hat{\mathbf{p}}')$, $\hat{\mathbf{p}} = (y, z)$ [see Eq. (5.2.13a), with $j \rightarrow -i$ to account for the $\exp(-i\omega t)$ dependence, and Eq. (5.4.31)]:

$$\bar{G}''(\hat{\mathbf{p}}, \hat{\mathbf{p}}') = \frac{1}{2\pi} \int_{-\infty}^{\infty} e^{i\eta(y-y')} g_{zi}(z, z') d\eta, \quad k_{ii} = \eta, \quad (36)$$

where g_{zi} is given in Eq. (35b) for the significant range of the integration interval.

As in Sec. 5.3c, it is convenient to introduce the complex angle variable w via the transformation $\eta = k_0 \sin w$, with the contributions arising from the first and second terms in Eq. (35b) denoted by \bar{G}_1'' and \bar{G}_2'' , respectively;

$$\bar{G}''(\hat{\mathbf{p}}, \hat{\mathbf{p}}') \sim \bar{G}_1''(\hat{\mathbf{p}}, \hat{\mathbf{p}}') + \bar{G}_2''(\hat{\mathbf{p}}, \hat{\mathbf{p}}'), \quad (37)$$

where, with $y' = 0$,

$$\bar{G}_{1,2}''(\hat{\mathbf{p}}, \hat{\mathbf{p}}') = \frac{i}{4\pi} \int_{\tilde{P}} f_{1,2}(w) e^{i k_0 q_{1,2}(w)} dw, \quad (38)$$

$$f_1(w) = \frac{\cos w}{\{[n^2(z) - \sin^2 w][n^2(z') - \sin^2 w]\}^{1/4}}, \quad f_2(w) = -if_1(w), \quad (38a)$$

$$q_1(w) = y \sin w + \int_{z_w}^{z'} \sqrt{n^2(\zeta) - \sin^2 w} d\zeta, \quad (39a)$$

$$q_2(w) = y \sin w + \int_{z_w}^z \sqrt{n^2(\zeta) - \sin^2 w} d\zeta + \int_{z_w}^{z'} \sqrt{n^2(\zeta) - \sin^2 w} d\zeta, \quad (39b)$$

and $n^2(z_w) = \sin^2 w$ defines z_w . The asymptotic approximation introduces spurious branch points w_b at $\sin^2 w_b = n^2(z)$ or $n^2(z')$; the exact solution only has branch points at $\sin^2 w_b = 1$, corresponding to $\eta_b = k_0 n_2 = k_0$ at $z = \infty$ [see the remarks following Eq. (8)]. The path \tilde{P} is shown in Fig. 5.3.6(b). Asymp-

totic approximations for \tilde{G}_1'' and \tilde{G}_2'' are derived below and lead to the results in Eqs. (46) and (55), respectively, which represent the geometric-optical field in the illuminated region. Near the caustic separating the illuminated and shadow regions (Fig. 5.8.4) or in the shadow region, Eqs. (60) and (61) are relevant.

Asymptotic evaluation

The saddle points w_s of $q_1(w)$ are determined by

$$0 = \frac{dq_1(w_s)}{dw_s} = \cos w_s \left[y - \sin w_s \int_{z<}^{z>} \frac{d\zeta}{\sqrt{n^2(\zeta) - \sin^2 w_s}} \right]. \quad (40)$$

The solution $\cos w_s = 0$ is excluded because the resulting $\sin^2 w_s = 1$ is greater than $n^2(z)$ in the medium, thereby falling outside the range of propagating solutions. Hence, the relevant saddle points of $q_1(w)$ are specified implicitly by the equation

$$y = \sin w_s \int_{z<}^{z>} \frac{d\zeta}{\sqrt{n^2(\zeta) - \sin^2 w_s}}. \quad (41)$$

Since $n^2(z)$ varies monotonically between z and z' , this equation admits of real solutions for w_s provided that $\sin w_s$ does not exceed the smaller of the values $n(z)$ or $n(z')$. Conversely, for each $\sin w_s < n(z)$ or $n(z')$, Eq. (41) defines a real curve in the yz domain which is precisely the geometric-optical ray trajectory [see Eq. (18)]. Thus, the real saddle points $0 \leq w_s \leq \sin^{-1} n(z)$ or $\sin^{-1} n(z')$ can be associated with real ray solutions, which define the trajectories of energy flow from the source point z' to the observation point z . Since $n(z) \rightarrow 1$ as $z \rightarrow \infty$, one has, from Eq. (41),

$$y \rightarrow z> \tan w_s, \quad \text{as } z> \rightarrow \infty. \quad (42)$$

If the source is located at some finite point z' , then $z> = z$, and w_s can be identified as the angle between the emerging ray at $z = \infty$ and the z axis (see Fig. 5.8.4). Conversely, if the source is located at $z' = \infty$, w_s represents the inclination of an incident ray. Each ray can thus be characterized by a particular value of w_s . For a source location $z' < \infty$, the maximum value of w_s is given by

$$w_{sm} = \sin^{-1} n(z'), \quad (43)$$

whence the region illuminated by real rays is confined at $z = \infty$ to the wedge $|\varphi| < w_{sm}$, with the observation angle φ measured from the positive z axis. For the refractive index in Eq. (5.9.19a), the rays form a family of hyperbolas as shown in Fig. 5.9.5. If $z < z'$, Eq. (41) is valid up to the point z_t which satisfies the equation

$$n(z_t) = \sin w_s. \quad (44)$$

When $z = z_t$, $dy/dz = \infty$ from Eq. (41), whence the “turning point” $z = z_t$ (starting point of refracted ray portion in Fig. 5.8.4) defines the level at which

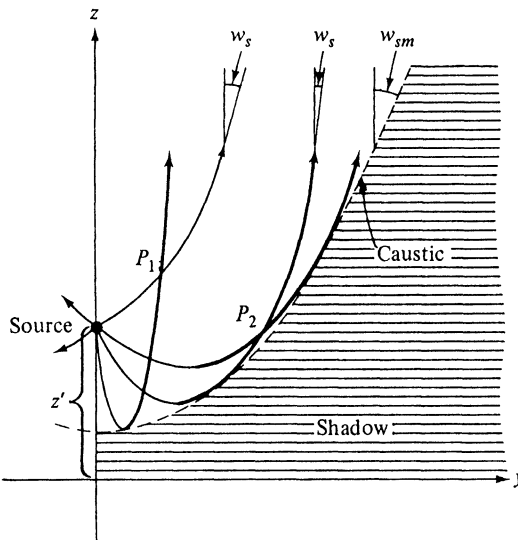


FIG. 5.8.4 Graphical interpretation of saddle-point condition. Direct rays [Eq. (41)] shown light; refracted rays [Eq. (52)] shown heavy.

the ray is parallel to the y axis and is bent back toward the positive z direction.

The first-order asymptotic approximation to \bar{G}_1'' can now be inferred from Eqs. (4.2.1). Utilizing the result,

$$\frac{d^2q_1}{dw_s^2} \Big|_{w_s} \equiv q''(w_s) = -\cos^2 w_s \int_{z<}^{z>} \frac{n^2(\zeta) d\zeta}{[n^2(\zeta) - \sin^2 w_s]^{3/2}}, \quad (45)$$

one obtains²⁷

$$\begin{aligned} \bar{G}_1'' &\sim \frac{1}{2\sqrt{2\pi k_0}} \\ &\times \frac{\exp \left\{ ik_0 \left[y \sin w_s + \int_{z<}^{z>} \sqrt{n^2(\zeta) - \sin^2 w_s} d\zeta \right] + i/\pi 4 \right\}}{\{[n^2(z) - \sin^2 w_s][n^2(z') - \sin^2 w_s]\}^{1/4} \left[\int_{z<}^{z>} \left[[n^2(\zeta) d\zeta]/[n^2(\zeta) - \sin^2 w_s]^{3/2} \right] \right]^{1/2}}, \end{aligned} \quad (46)$$

with w_s determined from the solution of the ray equation (41) and all roots taken positive. This expression can be interpreted as describing the geometric-optical field along a “direct” ray that proceeds from the source to the observation point without having been turned by refraction; it agrees with the result in Eq. (27) derived from purely geometric-optical considerations. When $z \rightarrow \infty$, with z' finite, the integral in the denominator of Eq. (46) can be approximated by $z/\cos^3 w_s$. Since $n(z) \rightarrow 1$ as $z \rightarrow \infty$, and $z/\cos w_s = \hat{p}$, with w_s representing

the ray inclination at $z = \infty$ and \hat{p} denoting the radius vector [see Fig. 5.9.3(a)], Eq. (46) reduces to

$$\bar{G}_1'' \sim \frac{\sqrt{\cos w_s}}{2\sqrt{2\pi k_0 \hat{p}}} \frac{\exp\left\{ik_0 \left[y \sin w_s + \int_{z_t}^z \sqrt{n^2(\zeta) - \sin^2 w_s} d\zeta \right] + i\pi/4\right\}}{[n^2(z') - \sin^2 w_s]^{1/4}},$$

$$z \rightarrow \infty, \quad (47)$$

which result agrees with that derived for the special case in Eq. (5.9.15a). For another check, assume a homogeneous medium with $n(z) = 1$, in which instance one obtains, from Eq. (46),

$$\bar{G}_1'' \sim \frac{e^{ik_0[y \sin w_s + |z-z'| \cos w_s] + i\pi/4}}{2\sqrt{2\pi k_0 \hat{p}}}, \quad n(z) = 1, \quad (48)$$

the correct expression for the free-space Green's function.

It is of interest to note that Eq. (46) tends to a finite limiting value at the turning points $n(z_t) = \sin w_s$ or $n(z'_t) = \sin w_s$, although the asymptotic formulas (35) are not valid there. A power-series expansion of $n^2(z)$ and $n^2(\zeta)$ about the point z_t yields the limiting expression

$$\lim_{z \rightarrow z_t} [n^2(z) - \sin^2 w_s]^{1/4} \left\{ \int_z^{z'} \frac{n^2(\zeta) d\zeta}{[n^2(\zeta) - \sin^2 w_s]^{3/2}} \right\}^{1/2} \rightarrow \left[\frac{n(z_t)}{(d/dz_t)n(z_t)} \right]^{1/2}, \quad (49)$$

whence

$$\bar{G}_1'' \sim \frac{1}{2\sqrt{2\pi k_0}} \frac{\exp\left\{ik_0 \left[y \sin w_s + \int_{z_t}^{z'} \sqrt{n^2(\zeta) - \sin^2 w_s} d\zeta \right] + (i\pi/4)\right\}}{[n^2(z') - \sin^2 w_s]^{1/4} (n(z_t)/\{dn(z_t)/dz_t\})^{1/2}}, \quad z = z_t. \quad (50)$$

The asymptotic evaluation of \bar{G}_2'' in Eq. (38) can be carried out in a similar manner and yields the field along a "refracted" ray. Since

$$\begin{aligned} & \frac{d}{dw} \int_{z_w}^z \sqrt{n^2(\zeta) - \sin^2 w} d\zeta \\ &= \int_{z_w}^z \frac{d}{dw} \sqrt{n^2 - \sin^2 w} d\zeta - [n^2(z_w) - \sin^2 w]^{1/2} \frac{dz_w}{dw}, \end{aligned} \quad (51)$$

and $n^2(z_w) = \sin^2 w$, one obtains the following equation for the saddle points w_s of $q_2(w)$:

$$F(y, z, w_s) = 0, \quad (52a)$$

where $z_w \equiv z_t$, with $n(z_t) = \sin w_s$, and

$$F(y, z, w) = y - \sin w \left[\int_{z_w}^z \frac{d\zeta}{\sqrt{n^2(\zeta) - \sin^2 w}} + \int_{z_w}^{z'} \frac{d\zeta}{\sqrt{n^2(\zeta) - \sin^2 w}} \right]. \quad (52b)$$

Equation (52a) is precisely the equation for a refracted geometric-optical ray that has passed through the turning point z_t and emerges at $z \rightarrow \infty$ with an

inclination given by the angle w_s [see Eq. (28) and darkly drawn rays in Fig. 5.8.4]. In the calculation of

$$q''_2(w_s) = \cos w_s \frac{d}{dw_s} F(y, z, w_s), \quad (53)$$

required for the asymptotic evaluation from Eq. (4.2.1b), the operation d/dw_s cannot be carried out directly on Eq. (52b) since the contribution from differentiation of the integrand and the lower integration limit diverges. However, after integration by parts,

$$\int_{z_t}^z \frac{d\zeta}{\sqrt{n^2 - \sin^2 w_s}} = \frac{\sqrt{n^2(z) - \sin^2 w_s}}{n(z)n'(z)} - \int_{z_t}^z \sqrt{n^2 - \sin^2 w_s} \frac{d}{d\zeta} \left(\frac{1}{nn'} \right) d\zeta, \quad (54)$$

with a similar result for the z' -dependent integral, the ensuing expression can be differentiated, and yields

$$\begin{aligned} \sec w_s \frac{d}{dw_s} F(y, z, w_s) \\ = \sin^2 w_s \left[\frac{1}{n(z)n'(z)\sqrt{n^2(z) - \sin^2 w_s}} + \frac{1}{n(z')n'(z')\sqrt{n^2(z') - \sin^2 w_s}} \right] \\ - \left[\int_{z_t}^z + \int_{z_t}^{z'} \right] \frac{1 + \sin^2 w_s (d/d\xi)[n'(\xi)n(\xi)]^{-1}}{\sqrt{n^2(\xi) - \sin^2 w_s}} d\xi, \end{aligned} \quad (54a)$$

where $n'(\alpha) \equiv dn/d\alpha$. The asymptotic approximation of \bar{G}_2'' is then found from Eqs. (4.2.1b) or (4.2.1c):²⁷

$$\begin{aligned} \bar{G}_2'' \sim \frac{1}{2\sqrt{2\pi k_0}} \times \\ \frac{\exp \left\{ ik_0 \left[y \sin w_s + \int_{z_t}^z \sqrt{n^2(\zeta) - \sin^2 w_s} d\zeta + \int_{z_t}^{z'} \sqrt{n^2(\zeta) - \sin^2 w_s} d\zeta \right] \mp i\pi/4 \right\}}{[(n^2(z) - \sin^2 w_s)(n^2(z') - \sin^2 w_s)]^{1/4} \sqrt{\sec w_s |dF(y, z, w_s)/dw_s|}}, \end{aligned} \quad (55)$$

which formula could again have been derived from geometrical optics (Sec. 5.8c). w_s is defined in Eq. (52a), and the upper and lower signs in Eq. (55) apply when $dF/dw_s < 0$ and $dF/dw_s > 0$, respectively. All roots are taken as positive.

As $z \rightarrow z_t$, one finds, from Eqs. (44) and (54a),

$$\sec w_s \frac{dF}{dw_s} \rightarrow \frac{n(z_t)}{n'(z_t)} \frac{1}{\sqrt{n^2(z) - \sin^2 w_s}}, \quad (56)$$

so Eqs. (55) and (50) agree at the turning point z_t . As $z \rightarrow \infty$, $dF/dw_s \rightarrow -z/\cos^2 w_s = -\hat{p}/\cos w_s$,[†] and

[†]This result follows at once from Eq. (52b), which reduces to $F = y - z \tan w + \text{constant}$ as $z \rightarrow \infty$. After some manipulation it can also be derived from the limiting form of Eq. (54a) if one assumes that $1 - n^2(z) \sim bz^{-m}[1 + O(z^{-1})]$, where m and b are positive constants.

$$\begin{aligned} \bar{G}_2'' &\sim \frac{\sqrt{\cos w_s}}{2\sqrt{2\pi k_0\hat{\rho}}} e^{-i\pi/2} \times \\ &\exp \left[ik_0 \left(y \sin w_s + \int_{z_1}^z \sqrt{n^2 - \sin^2 w_s} d\zeta + \int_{z_1'}^{z'} \sqrt{n^2 - \sin^2 w_s} d\zeta \right) + i\pi/4 \right], \\ &[n^2(z') - \sin^2 w_s]^{1/4} \end{aligned} \quad (57)$$

which result agrees with that derived for the special case in Eq. (5.9.15). Since for a monotonically increasing refractive index profile with $n'(z) > 0$, one has dF/dw_s positive when $z \approx z_1$ and negative when $z \rightarrow \infty$, dF/dw_s has a zero at an intermediate coordinate location. The elimination of w_s from the simultaneous equations

$$F(y, z, w_s) = 0, \quad \frac{d}{dw_s} F(y, z, w_s) = 0, \quad (58)$$

yields a curve, the caustic, which forms the envelope of the refracted-ray family (Fig. 5.8.4). A ray characterized by a given w_s touches the caustic at the coordinates (\bar{y}, \bar{z}) for which dF/dw_s vanishes. It is noted from Eq. (55) that a phase change of $\pi/2$ is introduced into the ray field after emerging from the caustic.

It has been mentioned that the solution of Eqs. (41) and (52) for real saddle points w_s is easily visualized from the ray diagram in Fig. 5.8.4 that represents a plot of these equations, with each ray curve characterized by a certain w_s . One finds that every observation point (y, z) in the illuminated region is reached by two rays; the values of w_s belonging to these rays represent the saddle points. In the vicinity of the source (point P_1 in Fig. 5.8.4), one of the rays is a direct ray arising from Eq. (41) while the other is refracted and corresponds to a saddle point of Eq. (52). However, if the observation point (y, z) lies near the caustic (point P_2 in Fig. 5.8.4), both rays are refracted and arise from saddle points of Eq. (52); Eq. (41) has no pertinent solution. \bar{G}'' is then given by the sum of two expressions of the form in Eq. (55), with w_s replaced by the two solutions w_1 and w_2 of Eq. (52). It is also noted from Fig. 5.8.4 that of the two rays passing through a point near the caustic, one ray has already touched the caustic while the other has not; if the saddle points corresponding to the former and the latter are denoted by w_1 and w_2 respectively, then $w_1 < w_2$ since it is recalled that $w_{1,2}$ represent the angles of emergence of the two rays at $z \rightarrow \infty$. Moreover, from the preceding discussion, $(dF/dw)_{w_2} > 0$ and $(dF/dw)_{w_1} < 0$. As the observation point approaches the caustic, $w_1 \rightarrow w_2$ and $(dF/dw)_{w_1} \rightarrow 0$, whence a point on the caustic gives rise to a second-order saddle point of $q_2(w)$.

Evaluation near the caustic

The asymptotic formula (55) fails for observation points on the caustic since $dF/dw_s = 0$. The required modification of the asymptotic expression is obtained from Eq. (4.5.7) and is valid for observation points on or near the caustic [for a uniform approximation at arbitrary observation points, see Eq. (4.5.2)]:

$$\bar{G}_2''|_{w_{1,2}} \sim \pm \frac{1}{4} f_2(w_0) \left[\frac{2}{k_0 q_2^{(3)}(w_0)} \right]^{1/3} e^{ik_0[q_2(w_1) + q_2(w_2)]/2} \{ \text{Bi}(x) \pm i \text{Ai}(x) \}, \quad (59)$$

where the upper and lower signs are appropriate to contributions from path segments leading over the saddle points w_1 and w_2 , respectively, with $q''(w_1) < 0$ and $q''(w_2) > 0$. $\text{Ai}(x)$ and $\text{Bi}(x)$ are the Airy functions defined in Sec. 4.2e, and

$$x = k_0^{2/3} X, \quad (59a)$$

where

$$\frac{4}{3} X^{3/2} = i[q_2(w_1) - q_2(w_2)], \quad X^{1/2} \cong \left[\frac{1}{2} q_2^{(3)}(w_0) \right]^{1/3} \left(\frac{w_1 - w_2}{2} \right) e^{i\pi/2}, \quad (59b)$$

with $q^{(3)}(w_0) > 0$ since $w_1 < w_2$ and $q''(w_{1,2}) \leq 0$. In these equations, $w_1 \approx w_2$, $w_0 \approx (w_1 + w_2)/2$, $q_2''(w_0) = 0$, whence $q_2(w_1) > q_2(w_2)$, and

$$q_2'(w_0) \approx -\frac{q^{(3)}(w_0)}{8} (w_1 - w_2)^2, \quad q^{(3)} \equiv \frac{d^3 q}{dw^3}. \quad (59c)$$

For large values of $|x|$ [since $k_0 \gg 1$, this condition can be satisfied for very small $(w_1 - w_2)$], use of the asymptotic approximation for the Airy functions in Eqs (4.2.51) reduces Eq. (59) to the expression given in Eq. (55), subject to $f_2(w_{1,2}) \approx f_2(w_0)$. On the other hand, when $x \rightarrow 0$, formula (59) must be retained and yields for the sum of the contributions from w_1 and w_2 :

$$\bar{G}'' \sim \bar{G}_2'' \sim \frac{i}{2} f(w_0) \left[\frac{2}{k_0 q_2^{(3)}(w_0)} \right]^{1/3} e^{ik_0[q_2(w_1) + q_2(w_2)]/2} \text{Ai}(x). \quad (60a)$$

In particular, when $x = 0$,

$$\bar{G}'' \sim \frac{i}{2} f(w_0) \left[\frac{2}{k_0 q_2^{(3)}(w_0)} \right]^{1/3} e^{ik_0 q_2(w_0)} \text{Ai}(0), \quad (60b)$$

whence the dependence on $k_0^{-1/3}$ here, as compared with the smaller $k_0^{-1/2}$ in Eq. (55) at an ordinary point along a ray, is indicative of the field enhancement on the caustic.

To determine the field behavior on the dark side of the caustic, we consider the real function $F(y, z, w_0) = q_2'(w_0) \sec w_0$ in Eq. (52b), which vanishes for observation points y and z on the caustic. If the observation point moves along the line $z = \text{constant}$, $y > 0$, the algebraic sign of F changes as the caustic is traversed, and since $q^{(3)}(w_0)$ is positive, one notes from Eq. (59c) that $q_2'(w_0)$ is negative on the illuminated side where w_1 and w_2 are real. Consequently, $q_2'(w_0) > 0$ on the dark side [this is also evident from Eq. (52b) since F is surely positive for sufficiently large y], whence $(w_1 - w_2)^2 < 0$. The parameter X in Eq. (59b) is therefore positive, and the field decays in view of the behavior of $\text{Ai}(x)$ for large positive x [see Eq. (4.2.42a)]:

$$\text{Ai}(x) \sim \frac{1}{2\sqrt{\pi} x^{1/4}} e^{-(2/3)x^{3/2}}, \quad x \gg 1. \quad (61)$$

Because X is positive, one notes from Eq. (59b) that $\arg(w_1 - w_2) = -\pi/2$, so w_2 and w_1 move into the upper and lower halves of the complex w plane,

respectively. The asymptotic formula resulting from Eqs. (60a) and (61) has the same characteristics as the analytic continuation of $\tilde{G}_2''|_{w_2}$ in Eq. (55) from real to complex values of w_2 .

It is of interest to observe the similarity between the description of the field near the caustic in the present example, which involves curved ray trajectories and a curved ray envelope, and the problem in Sec. 7.5e, wherein the rays are straight lines (see also References 28–30).

5.8e Propagation in Ducts (Guided Modes)

If the refractive index profile is not a monotonic function of z but has a maximum n_m at some finite value z_m as shown in Fig. 5.8.5(a), then a ray characterized by the parameter a [see Eq. (18)] lying in the range $n_\beta < a < n_m$ has two turning points z_1 and z_2 since $n(z_{1,2}) = a$. For propagation, $n(z) \geq a$, whence the ray in question is guided or “trapped” in the region $z_1 \leq z \leq z_2$,

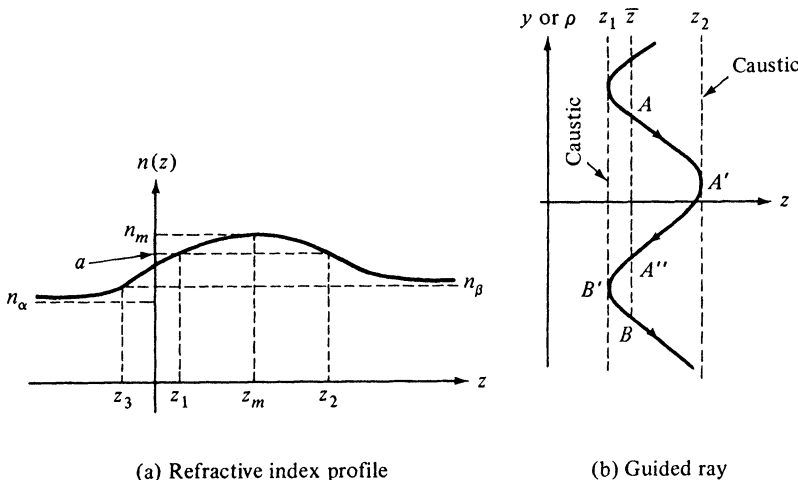


FIG. 5.8.5 Duct propagation.

which forms an effective waveguide or duct, as shown in Fig. 5.8.5(b). Outside the duct, $n(z) < a$ and the associated fields are exponentially damped. The duct width changes with a ; for the profile in Fig. 5.8.5(a), ray trapping occurs only when $n_\beta < a < n_m$. Rays with $n_\alpha < a < n_\beta$ are turned once at some point z_t , where $-\infty < z_t < z_3$, while those with $a < n_\alpha$ are not turned at all and progress from $-\infty$ to $+\infty$. All rays characterized by the parameter $a = n(z_{1,2})$ touch the lines $z = z_1$ and $z = z_2$, which therefore form the caustics or envelopes of the ray system.

If the field associated with the ray in Fig. 5.8.5(b) is to be a guided or trapped mode that maintains itself indefinitely along the transverse y or ρ direction, certain demands of self-consistency must be met. These can be phrased as the requirement that the magnitude and phase of the field at B is equal to that at A , where the points A and B are separated by a single spatial period.

Let the mode in question be characterized by the transverse (to z) wavenumber $k_0 a$; the longitudinal variation is then defined via Eqs. (7), with solutions given in Sec. 3.3b. If the field amplitude at A is arbitrarily set equal to unity, the reflected wave field at A'' in Fig. 5.8.5(b) has an amplitude $\vec{\Gamma}(\bar{z})$, where $\vec{\Gamma}(\bar{z})$ is the modal reflection coefficient seen from the point $z = \bar{z}$ when looking in the direction of increasing z . In passing from A'' to B , the reflected wavefield with amplitude $\vec{\Gamma}(\bar{z})$ is incident upon the boundary $z = z_1$ and emerges at B with an amplitude $\vec{\Gamma}(\bar{z}) \vec{\Gamma}(\bar{z})$, where $\vec{\Gamma}(\bar{z})$ is the reflection coefficient observed at \bar{z} when looking in the direction of decreasing z . Imposition of the above-mentioned self-consistency requirement then leads to the condition

$$\vec{\Gamma}(\bar{z}) \vec{\Gamma}(\bar{z}) = 1, \quad (62)$$

which must be satisfied if the field in question is to represent a guided mode. Equation (62) is simply an alternative statement of the transverse resonance relation

$$\overleftarrow{Z}(\bar{z}) + \vec{Z}(\bar{z}) = 0, \quad (63)$$

phrased in terms of the impedances seen by the mode at $z = \bar{z}$ [see Eq. (3.3.30)]. Equations (62) or (63) can generally be satisfied only for a certain set of discrete values of a , the eigenvalues for the modes in question.

If the medium is slowly varying, the reflection coefficients can be determined from the WKB approximation or from geometrical optics [see Eqs. (35b) or (20b)]. The z -dependent part of the phase change along a ray traveling from A to A' in Fig. 5.8.5(b) is then given by the phase integral $k_0 \int_{z_1}^{z_2} \sqrt{n^2(\eta) - a^2} d\eta$. At the boundary z_2 , the wave amplitude is changed by the reflection coefficient $\vec{\Gamma}(z_2)$;† in passing from A' to B' and from B' to B , the appropriate phase increments are added, as well as the reflection coefficient $\vec{\Gamma}(z_1)$ arising from the boundary at z_1 . Thus, Eq. (62) can be written as

$$\vec{\Gamma}(z_2) \vec{\Gamma}(z_1) \exp\left(i 2 k_0 \int_{z_1}^{z_2} \sqrt{n^2(\eta) - a^2} d\eta\right) = 1. \quad (64)$$

In the assumed absence of dissipation, the reflection coefficient magnitudes are equal to unity and may be expressed as $\Gamma(z_{1,2}) = \exp(ic_{1,2})$, where c_1 and c_2 are real constants. If losses are present, these considerations still apply, with complex values for $c_{1,2}$.^{31,32} Thus, the transverse resonance condition becomes

$$k_0 \int_{z_1}^{z_2} \sqrt{n^2(\eta) - a_m^2} d\eta = m\pi - \frac{c_1 + c_2}{2}, \quad (65)$$

where the values of a corresponding to different m have been denoted by a_m , the eigenvalues for the m th mode. Since the left-hand side of the equation is positive, m takes on those integer values (or zero) that render the right-hand

†This discussion applies to the general case where plane reflecting boundaries are present at z_1 and z_2 ; if the boundary is formed by a caustic, the phase of the ray is changed by $-\pi/2$, thereby giving rise to an effective reflection coefficient $\exp(-i\pi/2)$ [see Eq. (35b) and remarks following Eq. (58)].

side positive. For the case where physical boundaries are located at z_1 and z_2 and $a_m^2 < n^2(z_{1,2})$, the points $z_{1,2}$ remain fixed; if the ray turns before reaching the physical boundary (if any), z_1 and (or) z_2 are defined by $n^2(z_{1,2}) = a_m^2$, and c_1 and (or) c_2 are equal to $-\pi/2$, accounting for the phase change at the caustic. The distance L between points A and B along the ray path can be evaluated from the ray equation (28),

$$L_m = 2 \int_{z_1}^{z_2} \frac{a_m dz}{\sqrt{n^2(z) - a_m^2}}, \quad (66)$$

where $a_m = n(z) \sin \theta(z)$ is a constant along the ray.

From the preceding remarks, showing the connection between the guided modes in a variable medium and the transverse resonance relations (62) or (63), it is apparent that the guiding effect of the inhomogeneity is observed most directly if a radiation problem is analyzed in terms of transmission along the transverse (y or ρ) coordinate. The transformation of the z -transmission representations in Eqs. (5), (6), or (36) into an alternative form highlighting propagation transverse to z has been discussed in general terms in Sec. 3.3c and has been illustrated in detail for the dielectric slab problem in Sec. 5.6. Analytically, the transformation involves the deformation of the integration contour away from the real axis to enclose the singularities of the longitudinal characteristic Green's function $g_z(z, z'; \lambda_z)$. If the z domain is unbounded, the singularities comprise branch points, but poles may also arise if the transverse resonance equations have discrete solutions that satisfy the radiation condition at infinity. The associated spectrum of modes capable of propagating in the transverse direction then has both a continuous and a discrete part. In the presence of impenetrable physical boundaries at $z_{1,2}$, one has a conventional, although inhomogeneously filled, waveguide, and the spectrum is usually purely discrete. If trapped modes can exist and the source and observation points are located in or near the duct region, the contribution from the continuous spectrum is usually negligible and the fields are well represented in terms of the guided modes alone [see remarks following Eq. (5.6.9)]. In the problem of radiation from a longitudinally directed electric current element, the resulting formulation is directly analogous to that for the homogeneous dielectric slab problem [Eq. (5.6.20)]. If an exact solution of the eigenvalue problem cannot be found, the specific form of the eigenfunctions $\Phi_r(z)$ can be ascertained from the WKB approximation provided that the duct is wide and the medium is slowly varying. The utility of the various representations for the evaluation of the fields in the duct region is discussed in connection with a specific example in Sec. 5.9b.

5.9 SOURCES IN THE PRESENCE OF MEDIA WITH CONTINUOUS PLANAR STRATIFICATION—SPECIAL PROFILES

While the formal presentation in Sec. 5.8a is appropriate to radiation problems in continuously varying media with arbitrary refractive index profiles, explicit solutions (albeit in the form of representations) can be constructed only

for special variations of $n^2(z)$ for which Eqs. (5.8.7a) and (5.8.7b) can be solved in terms of known functions. From the by-no-means-exhaustive sampling of profiles in Sec. 3.6, the inverse-square dependence has been selected for detailed study since it incorporates many features associated with a general category of monotonic variation. Another example, the Epstein profile descriptive of a continuous transition, is discussed in a more condensed fashion.

5.9a Inverse-square Profile

Properties of the medium

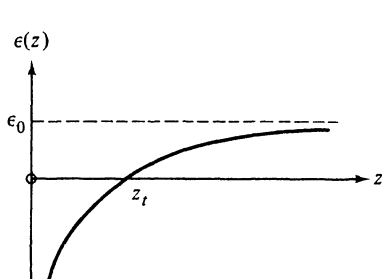
We begin our discussion of the radiation characteristics of sources in the presence of special inhomogeneous media by considering a region whose permittivity varies from a finite, constant value ϵ_0 at $z \rightarrow \infty$ in a monotonic manner characterized by the equation

$$\epsilon(z) = \epsilon_0 \left(1 - \frac{p^2}{k_0^2 z^2}\right), \quad k_0^2 = \omega^2 \mu_0 \epsilon_0. \quad (1)$$

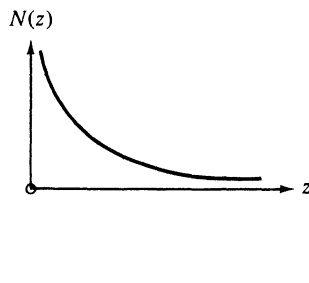
p is an arbitrary constant and the permeability μ_0 is assumed to be constant throughout the region. As will be seen below, the nonuniform transmission-line equations (5.8.7a) and (5.8.7b) have a particularly simple solution in this case. For p^2 positive real and independent of ω , the permittivity $\epsilon(z)$ in Eq. (1) may represent approximately the effect of a lossless, cold, isotropic, electron plasma medium whose electron density $N(z)$ [or equivalently the plasma frequency $\omega_p(z)$ as in Eq. (1.1.60)] is given by

$$N(z) = \frac{p^2 m}{\mu_0 e^2} \frac{1}{z^2} = \frac{\omega_p^2(z) m \epsilon_0}{e^2}, \quad (1a)$$

where m and e signify the electronic mass and charge, respectively. A sketch of both $\epsilon(z)$ and $N(z)$ for real values of p is shown in Fig. 5.9.1.



(a) Permittivity



(b) Electron density

FIG. 5.9.1 Inverse-square profile (lossless plasma).

For real p , the permittivity passes through zero at the turning point $z_t = p/k_0$. For $z > z_t$, $k(z) = \omega \sqrt{\mu_0 \epsilon(z)}$ is real, while for $z < z_t$, $k(z)$ is imaginary [$\text{Im } k \geq 0$ for $\exp(-i\omega t)$ time dependence]. If the continuously variable me-

dium is approximated by a series of thin layers, with a typical layer between the planes $z_i - \delta$ and $z_i + \delta$ characterized by the constant permittivity $\epsilon(z_i)$, then for the $\exp(j\omega t)$ dependence, a plane wave propagating in the \pm direction in the i th layer has a variation $\exp(\mp jk_i z)$, where $k_i = \omega\sqrt{\mu_0\epsilon(z_i)}$. Hence, the wave propagates when $z_i > z_r$, and attenuates when $z_i < z_r$. Although the electron density in the above model increases indefinitely as $z \rightarrow 0$, thus invalidating the physical conditions required for a collision-free (i. e., lossless) plasma, this mathematical singularity has little effect on the radiation characteristics of a source located at finite z values in this medium provided that z_r is reasonably large. Since the region $|z| < z_r$ is essentially impenetrable to electromagnetic waves, the detailed nature of the medium for $|z| \ll z_r$ is immaterial. A physically more realistic density profile, as in Fig. 5.9.2, wherein $N(z)$ in-

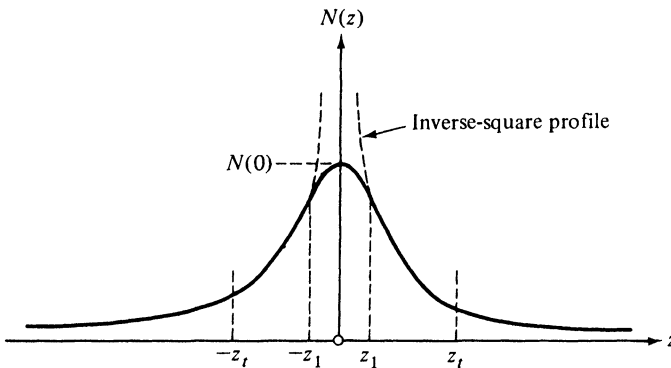


FIG. 5.9.2 Physical profile with monotonically increasing electron density.

creases monotonically to a finite maximum value $N(0)$, can be well approximated by the inverse-square profile provided that the deviation of $N(z)$ from the inverse-square variation occurs only in the region $|z| < z_1$, where $z_1 \ll z_r$, and that the source is located at $z' > z_1$. To demonstrate the validity of these remarks concerning the lack of sensitivity of the radiated field on the detailed medium properties in the region $z \ll z_r$, we shall consider the problem wherein a perfectly conducting plane is located at $z = d$, and will show that the influence of this perturbing structure is negligible when $d \ll z_r$. In the preceding discussion it has been assumed that $\epsilon(z)$ is real. The effect of losses in the medium can be taken into account at any fixed frequency ω by an appropriate complex choice of p in Eq. (1).

Although the inverse-square medium is a special case, it is to be expected that the radiation characteristics of sources therein are representative of those encountered in other media with monotonic variations of $\epsilon(z)$ that pass from a constant value at $|z| \rightarrow \infty$ to negative values at $z \rightarrow 0$. The present model has the virtue of simplicity.

Solution for excitation by a longitudinal magnetic dipole or by a transverse electric line current

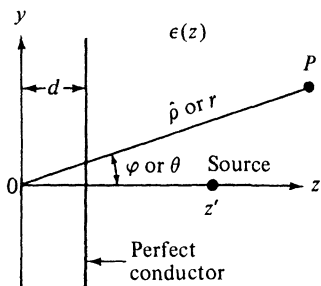
Consider the problem of radiation from either a time-harmonic longitudinal magnetic current element

$$\mathbf{M}(\mathbf{r}) = M^{\circ} \delta(\mathbf{r} - \mathbf{r}') \mathbf{z}_0, \quad (2a)$$

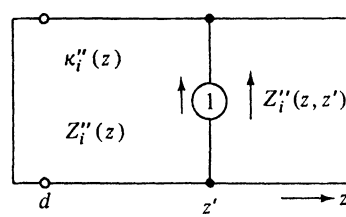
or from a transverse electric line current,

$$\mathbf{J}(\mathbf{r}) = I \delta(\hat{\mathbf{p}} - \hat{\mathbf{p}}') \mathbf{x}_0, \quad \hat{\mathbf{p}} = (y, z), \quad (2b)$$

located in the variable medium shown in Fig. 5.9.3(a), with a perfectly conducting plane at $z = d$. From Eqs. (5.8.1), (5.2.4), (5.4.31a), and (5.4.31b) the solutions for the electromagnetic fields can be inferred from the scalar H -mode



(a) Physical configuration



(b) Equivalent modal network (H modes)

FIG. 5.9.3 Physical configuration and network equivalent in the presence of a perfectly conducting plane.

Green's functions $G''(\mathbf{r}, \mathbf{r}')$ and $\bar{G}''(\hat{\mathbf{p}}, \hat{\mathbf{p}}')$, respectively, which satisfy the differential equation (5.8.3b) (with $\partial/\partial x \equiv 0$ for the line source) subject to a radiation condition at infinity, and to $G'' = \bar{G}'' = 0$ at $z = d$. The solution may be obtained in a z -transmission representation as in Eq. (5.8.6b) and therefore requires a knowledge of the modal Green's function $g_{zi}''(z, z') = (j\omega\mu_0)^{-1}Z_i''(z, z')$. g_{zi}'' satisfies the differential equation (5.8.7b) subject to vanishing at $z = d$ and to a radiation condition at $z \rightarrow \infty$; its determination is equivalent to finding the voltage $Z_i''(z, z')$ excited in the modal network of Fig. 5.9.3(b). As noted in conjunction with Eqs. (5.8.7), the characteristic impedance $Z_i''(z)$ and propagation constant $\kappa_i''(z)$ are given by $Z_i''(z) = \omega\mu_0/\kappa_i''(z)$, $\kappa_i''(z) = [\omega^2\mu_0\epsilon(z) - k_i'^2]^{1/2}$.

Substitution of the expression for $\epsilon(z)$ in Eq. (1) into Eq. (5.8.7b) yields the differential equation for the modal Green's function

$$\left[\frac{d^2}{dz^2} + k_0^2 \left(1 - \frac{p^2}{k_0^2 z^2} \right) - k_i^2 \right] g_{zi}''(z, z') = -\delta(z - z'). \quad (3)$$

This equation is identical with Eq. (3.3.3); its solution is given in Eq. (3.3.14a), with Eq. (3.3.4), in terms of homogeneous solutions $\tilde{V}_i(z)$ and $\tilde{V}_i(z)$ below,

which satisfy the boundary conditions at the upper and lower z termini, respectively. The homogeneous equation (3) is solved by the spherical Bessel functions

$$c_\nu(\kappa z) \equiv \sqrt{\frac{\pi \kappa z}{2}} C_{\nu+1/2}(\kappa z), \quad \kappa = \sqrt{k_0^2 - k_t^2}, \quad p^2 = \nu(\nu + 1), \quad (3a)$$

where $C_\mu(z)$ represents any linear combination of the cylinder functions $J_\mu(z)$, $N_\mu(z)$, $H_\mu^{(1)}(z)$, $H_\mu^{(2)}(z)$. In contrast to the z -dependent $\kappa(z)$, κ denotes the value of $\kappa(z)$ at $z \rightarrow \infty$. From the network picture in Fig. 5.9.3(b) it is recognized that the solution must be outgoing at $z = \infty$, whence one selects via Eqs. (5.3.13) [for an $\exp(j\omega t)$ dependence],

$$\vec{V}_i(z) = h_\nu^{(2)}(\kappa z). \quad (4a)$$

At the lower endpoint $z = d$, the voltage vanishes, so

$$\overleftarrow{V}_i(z) = j_\nu(\kappa z) - \frac{j_\nu(\kappa d)}{h_\nu^{(2)}(\kappa d)} h_\nu^{(2)}(\kappa z). \quad (4b)$$

The particular combination of functions chosen in Eq. (4b) simplifies the determination of the Wronskian required in Eq. (3.3.14a). Since

$$J_\mu(z) \frac{d}{dz} N_\mu(z) - N_\mu(z) \frac{d}{dz} J_\mu(z) = \frac{2}{\pi z}, \quad (5a)$$

it follows from Eq. (3) that

$$j_\nu(z) \frac{d}{dz} n_\nu(z) - n_\nu(z) \frac{d}{dz} j_\nu(z) = 1, \quad (5b)$$

and the Wronskian of \overleftarrow{V} and \vec{V} is evaluated as

$$W(\overleftarrow{V}, \vec{V}) = \overleftarrow{V} \frac{d\vec{V}}{dz} - \vec{V} \frac{d\overleftarrow{V}}{dz} = -jk. \quad (5c)$$

Thus, the solution is given by [see also Eq. (2.7.12a) for a related problem in spherical regions],

$$g''_{zi}(z, z') = -\frac{j}{\kappa} \left[j_\nu(\kappa z_<) - \frac{j_\nu(\kappa d)}{h_\nu^{(2)}(\kappa d)} h_\nu^{(2)}(\kappa z_<) \right] h_\nu^{(2)}(\kappa z_>). \quad (6)$$

Regarding the definition of $\kappa = \sqrt{k_0^2 - k_t^2}$, the requirements $\kappa = k_0$ when $k_t = 0$, and $\text{Im } \kappa < 0$ when $k_t > k_0$, are imposed.

A check of Eq. (6) is possible for the limiting case $p = 0$ (i. e., $\nu = 0$), for which the medium in Eq. (1) reduces to the vacuum $\epsilon(z) = \epsilon_0$. Since

$$j_0(x) = \sin x, \quad h_0^{(1,2)}(x) = \mp j e^{\pm jx}, \quad (7)$$

one finds, from Eq. (6),

$$g''_{zi}(z, z') = \frac{1}{\kappa} \left[\sin \kappa z_< - \sin \kappa d e^{-j\kappa(z_<-d)} \right] e^{-j\kappa z_>}, \quad (8)$$

which agrees with the result in Eqs. (3.4.4) and (3.4.5), with Eqs. (3.4.21), upon letting $\epsilon_1 = \epsilon_2 = \epsilon_0$, and replacing d by $-d$ as appropriate to the geometry in Fig. 5.9.3(a).

Substitution of Eq. (6) into Eq. (5.2.11) or (5.2.13a) yields the formal solution for the scalar Green's functions appropriate to problems of radiation from a longitudinal magnetic dipole and a transverse electric line current, respectively. For the former case, $\kappa = (k_0^2 - \xi^2)^{1/2}$, while for the latter case, $\kappa = (k_0^2 - \eta^2)^{1/2}$. Pertinent singularities of $g''_{zi}(z, z')$ near the real axis (on the real axis for k_0 real) in the complex ξ or η plane are the branch points located at $\kappa = 0$ (i.e., $\xi = \pm k_0$ and $\eta = \pm k_0$, respectively), in agreement with the general observations at the end of Sec. 5.8b. The path of integration avoids these singularities as in Fig. 5.3.5(a). Additional singularities exist at the zeros κ_p , determined by the equation $h_v^{(2)}(\kappa_p d) = 0$. The location of these complex zeros will be discussed below.

As in previous examples, subsequent considerations will be carried out for an $\exp(-i\omega t)$ dependence. In this instance,

$$g''_{zi}(z, z') = \frac{i}{\kappa} \left[j_v(\kappa z_<) - \frac{j_v(\kappa d)}{h_v^{(1)}(\kappa d)} h_v^{(1)}(\kappa z_<) \right] h_v^{(1)}(\kappa z_>), \quad (9a)$$

$$= \frac{i}{2\kappa} \left[h_v^{(2)}(\kappa z_<) - \frac{h_v^{(2)}(\kappa d)}{h_v^{(1)}(\kappa d)} h_v^{(1)}(\kappa z_<) \right] h_v^{(1)}(\kappa z_>). \quad (9b)$$

The requirement on κ is now $\text{Im } \kappa \geq 0$. The frequently more useful form in Eq. (9b) follows from Eq. (9a) upon writing $j_v = \frac{1}{2}(h_v^{(1)} + h_v^{(2)})$. The preceding remarks concerning integration paths and singularities now refer to Fig. 5.3.6a. In particular, one obtains for the two-dimensional Green's function $\bar{G}''(\hat{\mathbf{p}}, \hat{\mathbf{p}}')$ in Eq. (5.2.13a), upon letting $j \rightarrow -i$ to account for the $\exp(-i\omega t)$ dependence and introducing the change of variable $\eta = k_0 \sin w$,

$$\bar{G}''(\hat{\mathbf{p}}, \hat{\mathbf{p}}') = \frac{i}{4\pi} \int_{\hat{\mathbf{p}}} e^{ik_0 y \sin w} h_v^{(1)}(k_0 z_> \cos w) A(z_<, w) dw, \quad (10)$$

$$A(z_<, w) = h_v^{(2)}(k_0 z_< \cos w) - \frac{h_v^{(2)}(k_0 d \cos w)}{h_v^{(1)}(k_0 d \cos w)} h_v^{(1)}(k_0 z_< \cos w), \quad (10a)$$

$$= 2 \left[j_v(k_0 z_< \cos w) - \frac{j_v(k_0 d \cos w)}{h_v^{(1)}(k_0 d \cos w)} h_v^{(1)}(k_0 z_< \cos w) \right]. \quad (10b)$$

The path of integration in the complex w plane is shown in Fig. 5.3.6(b). Instead of the branch point at $w = 0$, there exists in the present case a branch point, and associated branch cut, at $w = \pi/2$. The analogous representation for the three-dimensional Green's function $G''(\mathbf{r}, \mathbf{r}')$ may be derived from Eq. (5.2.11).

Asymptotic evaluation as $z_> \rightarrow \infty$

Since the integral in Eq. (10) cannot be evaluated in closed form, we consider an approximate calculation of the far field. It is convenient to introduce polar coordinates via $z = \hat{\mathbf{p}} \cos \varphi$, $y = \hat{\mathbf{p}} \sin \varphi$ as shown in Fig. 5.9.3(a), and

assume that $k_0 z > \equiv k_0 z \rightarrow \infty$. As long as the integration path avoids the vicinity of $w = \pi/2$, one has $|k_0 z \cos w| \gg |\nu|$, so the asymptotic formula in Eq. (5.3.13) may be employed for the representation of $h_\nu^{(1)}(k_0 z \cos w)$, whence

$$\bar{G}''(\hat{\rho}, \hat{\rho}') \sim \frac{1}{4\pi} e^{-iv\pi/2} \int_{\bar{P}} e^{ik_0 \hat{\rho} \cos(w-\varphi)} A(z', w) dw. \quad (11)$$

In the asymptotic evaluation of this integral, $A(z', w)$ is considered a slowly varying amplitude function as compared to $\exp[ik_0 \hat{\rho} \cos(w-\varphi)]$. Hence, the saddle point, determined by the exponential function, is located at $w = \varphi$, and the steepest descent path P through the saddle point proceeds as shown in Fig. 5.3.6(b). In the deformation of \bar{P} into P , the only pertinent singularities of $A(z', w)$ are poles located at the zeros w_p of $h_\nu^{(1)}(k_0 d \cos w)$. These poles are complex³³; those relevant for the present problem are finite in number and lie in the half-strip $0 < \operatorname{Re} w < \pi/2$, $\operatorname{Im} w > 0$. The pole singularities belong to the “leaky-wave” category (see Sec. 5.3e) and their contribution to the far field is exponentially small since $\operatorname{Im} w_p > 0$. Even for $k_0 d \gg 1$, when $w_p \rightarrow \pi/2$,† their effect is unimportant, since the range $w \approx \pi/2$ (i.e., $\varphi \approx \pi/2$) is excluded from consideration in view of the restriction previously imposed on the integration path. Hence, the contribution from the leaky-wave poles can be neglected, and the asymptotic evaluation of the integral in Eq. (11) yields the first-order result [Eq. (5.3.16a)]

$$\bar{G}'' \sim \bar{G}_f B(z', \varphi), \quad z \rightarrow \infty, \quad \varphi \not\approx \pi/2, \quad (12)$$

where \bar{G}_f is the free-space field due to a line source at $\hat{\rho} = 0$ [Eqs. (5.4.25) et seq.],

$$\bar{G}_f = \frac{i}{4} \sqrt{\frac{2}{\pi k_0 \hat{\rho}}} e^{i(k_0 \hat{\rho} - \pi/4)}, \quad (12a)$$

while $B(z', \varphi)$ expresses the distortion of the free-space pattern

$$B(z', \varphi) = -ie^{-iv\pi/2} A(z', \varphi). \quad (13)$$

The expression for $A(z', \varphi)$ is given in Eqs. (10a) or (10b).

For the point-source Green's function $G''(\mathbf{r}, \mathbf{r}')$ [see Eq. (5.2.11)], substitution of Eq. (9b) yields an integral representation as in Eq. (10) provided that $\exp(i k_0 y \sin w)$ is replaced by $\frac{1}{2} k_0 \sin w H_0^{(1)}(k_0 \rho \sin w)$. If $|k_0 \rho \sin w| \gg 1$, $|k_0 z \cos w| \gg |\nu|$ (i.e., $k_0 \rho \gg 1$, $k_0 z \gg |\nu|$, $w \not\approx 0, \pi/2$), the Hankel functions $H_0^{(1)}(k_0 \rho \sin w)$ and $h_\nu^{(1)}(k_0 z \cos w)$ can be replaced by their asymptotic approximations. The resulting integrand has the same form as that in Eq. (11), save for a factor $\sqrt{\sin w}$, and the integral is evaluated asymptotically as before, yielding the result

$$G''(\mathbf{r}, \mathbf{r}') \sim G_f B(z', \theta), \quad r \rightarrow \infty, \quad \theta \not\approx 0, \quad \frac{\pi}{2}, \quad (14)$$

[†]Since the zeros α_p of $h_\nu^{(1)}(\alpha)$ are located at finite values of $|\alpha|$ (see Reference 33), $\cos w_p = \alpha_p/k_0 d \rightarrow 0$ when $k_0 d \gg 1$.

where $r = \sqrt{\rho^2 + z^2}$, $z = r \cos \theta$ [see Fig. 5.9.3(a)], and G_f is the free-space Green's function

$$G_f = \frac{e^{ik_0 r}}{4\pi r}. \quad (14a)$$

In Eqs. (11)–(14) it has been assumed that the source is located at finite z' while the observation point moves to $z \rightarrow \infty$. Manifestly, via the replacement $\mathbf{r} \leftrightarrow \mathbf{r}'$, the above results remain valid for the reciprocal situation wherein the source point moves to infinity and the observation point is situated arbitrarily.

Ray-optical interpretation

While the pattern function $B(z', \varphi)$, and hence the electromagnetic fields derived from the asymptotic forms of the Green's functions \bar{G}'' and G'' , can be calculated from available numerical tables of the cylinder functions, it is desirable for an interpretation utilizing the concepts of geometrical optics to approximate the cylinder functions comprised in $B(z', \varphi)$ by their representations in Eqs. (5.4.77a). If v is assumed to be large, one may use the approximation $p^2 \approx (v + \frac{1}{2})^2$ in Eq. (3a) and represent the Hankel function as in Eq. (19). Equation (12) can then be written as

$$\bar{G}''(\hat{\mathbf{p}}, \hat{\mathbf{p}}') \sim \bar{G}_1''(\hat{\mathbf{p}}, \hat{\mathbf{p}}') + \bar{G}_2''(\hat{\mathbf{p}}, \hat{\mathbf{p}}'), \quad (15)$$

where

$$\bar{G}_1''(\hat{\mathbf{p}}, \hat{\mathbf{p}}') = \frac{\sqrt{\cos \varphi} \exp \left[ik_0 y \sin \varphi + ik_0 \int_{z_i}^z \sqrt{n^2(\zeta) - \sin^2 \varphi} d\zeta + i\pi/4 \right]}{2\sqrt[4]{2\pi k_0 \hat{\rho}} \sqrt[4]{n^2(z') - \sin^2 \varphi}}, \quad (15a)$$

$$\begin{aligned} \bar{G}_2''(\hat{\mathbf{p}}, \hat{\mathbf{p}}') = & - \frac{\sqrt{\cos \varphi} \exp \left[ik_0 y \sin \varphi + ik_0 \left[\int_d^{z'} + \int_d^z \right] \sqrt{n^2(\zeta) - \sin^2 \varphi} d\zeta + (i\pi/4) \right]}{2\sqrt[4]{2\pi k_0 \hat{\rho}} \sqrt[4]{n^2(z') - \sin^2 \varphi}}. \end{aligned} \quad (15b)$$

Equation (15a) applies in the range $\sin \varphi \leq \sin \varphi_c \equiv n(z')$, while Eq. (15b) is limited to observation angles $\sin \varphi \leq \sin \varphi_0 \equiv n(d)$. If $\varphi_0 < \varphi < \varphi_c$, the argument of the Hankel functions $H_p^{(1,2)}(k_0 d \cos \varphi)$ is smaller than the order p and $H_p^{(1)} \sim -H_p^{(2)}$ [see Eq. (5.4.77b)]. In this case, \bar{G}_2'' is still found to be given by Eq. (15b) provided that the lower integration limits are changed from d to z_i , where z_i is defined by the equation

$$n(z_i) = \sin \varphi, \quad (16)$$

and that the multiplicative constant -1 is replaced by $\exp(-i\pi/2)$. When $\varphi > \varphi_c$, the arguments of all the Hankel functions appearing in $A(z', \varphi)$ are smaller than their order p , whence $A(z', \varphi)$ becomes a decaying function with increasing φ . The corresponding implication in Eqs. (15) is $[n^2(\zeta) - \sin^2 \varphi]^{1/2} = i[\sin^2 \varphi - n^2(\zeta)]^{1/2}$ when $\sin \varphi > n(\zeta)$. Near the transition regions $\varphi \approx \varphi_0$

or $\varphi \approx \varphi_c$, one must employ the Airy-function approximations in Eq. (5.4.77c) [see also Eq. (5.8.60)].

Equations (15a) and (15b) distinguish three different ranges of observation angles φ when the observation point P is located at infinity. In all cases, the radiation field is described locally by plane waves propagating at the angle φ , since $n(\zeta) \rightarrow 1$ as $\zeta \rightarrow \infty$, so the essential behavior of the exponentials is represented by $\exp[ik_0y \sin \varphi + ik_0z \cos \varphi] = \exp(ik_0\hat{\rho})$ [see also Eq. (12)]. However, Eqs. (15) have been expressed in a manner that permits a study of the

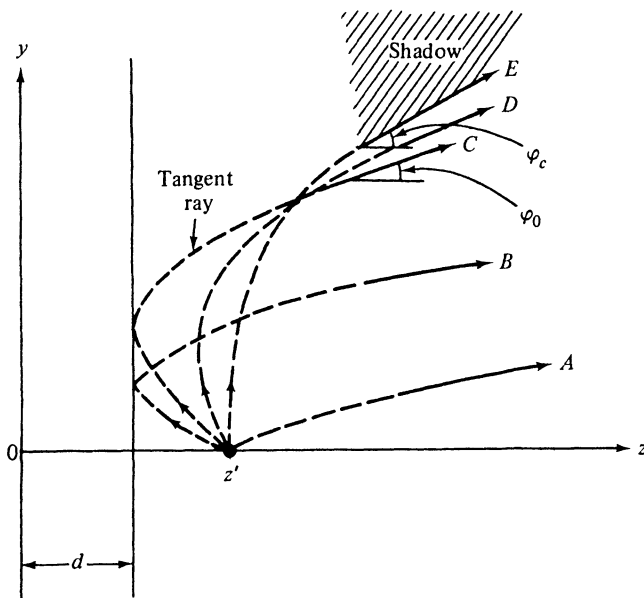


FIG. 5.9.4 Ray picture.

progress of each wave contribution from the source point to $z \rightarrow \infty$. As shown in Sec. 5.8d [see Eq. (5.8.47) and (5.8.57)], \bar{G}_1'' and \bar{G}_2'' represent precisely the fields along geometric-optical rays following curved trajectories in the variable medium, thereby lending significance to what might otherwise appear as an arbitrary rearrangement of Eq. (12). The complete ray trajectories are shown dashed in Fig. 5.9.4 (see Fig. 5.8.4), but their asymptotic direction, to which Eqs. (15) apply, is indicated by the solid arrows. Ray A reaches the observation point P directly from the source while ray B first travels to the plane at $z = d$, is reflected, and then proceeds to P . Comparison of the phase behavior of \bar{G}_1'' (ray A) and \bar{G}_2'' (ray B) lends direct support to this interpretation; one also observes in the reflected ray term the additional factor -1 , which represents the reflection coefficient of the perfectly conducting plane; for a plane having another value of surface impedance, -1 would be replaced by the appropriate plane-wave reflection coefficient. The domain of existence of ray B

is bounded by the tangent ray C , which just grazes the surface and emerges with the angle φ_0 .[†]

When $\varphi_0 < \varphi < \varphi_c$, Eq. (15a) yields the direct ray A as before, but the modified Eq. (15b) now describes the field along ray D which is refracted back toward the positive z axis before reaching the boundary. Its maximum penetration into the medium is given by the coordinate z_r defined in Eq. (16). The factor $\exp(-i\pi/2)$ replacing the reflection coefficient (-1) arises from the phase change experienced by this ray when touching the caustic, which forms the envelope of the refracted ray system [see Fig. 5.8.4 and Eq. (5.8.55)]. Ray E , whose initial direction at the source point z' is parallel to the y axis, emerges at $z \rightarrow \infty$ at the angle $\varphi_c = \sin^{-1} n(z')$, which also defines the asymptote of the caustic curve. This exhausts the class of propagating geometric-optical rays; observation points specified by angles $\varphi > \varphi_c$ lie in the geometric-optical shadow region and can be reached only by diffraction. The fields in the shadow region can be calculated from Eq. (12) or, equivalently, from the analytic continuation of the appropriately modified ray formulas (15). The general conclusions arrived at in Sec. 5.8d are therefore verified.

Implied in the preceding remarks is the assumption that $n^2(z') > 0$, $n^2(d) > 0$, so both the source point and the bounding plane are located in parts of the medium which can support propagating waves. If $n^2(d) < 0$, $n^2(z') > 0$, the boundary cannot be reached by propagating waves (real rays) and the ray picture comprises only types A and D ; the ray traveling along the negative z axis shows the deepest penetration to the point z_0 where $n(z) = 0$ (Fig. 5.8.4). The deeper the plane is embedded in the nonpropagating portion of the medium, the smaller is its effect on the refracted wave field. An estimate can be obtained from $A(z', \varphi)$ in Eq. (10b), which contains a factor of the form

$$Q = H_p^{(2)}(k_0 z' \cos \varphi) + (1 - \Delta)H_p^{(1)}(k_0 z' \cos \varphi), \quad \Delta = \frac{2J_p(k_0 d \cos \varphi)}{H_p^{(1)}(k_0 d \cos \varphi)}. \quad (17)$$

When $n^2(d) < 0$, one has $k_0 d \cos \varphi < p$ and Δ is a small quantity for any φ ; when $n^2(d) > 0$, these remarks apply to the rays of type D in Fig. 5.9.4. If $n^2(z') < 0$, the source point lies in the nonpropagating portion; no real geometric-optical rays exist in this case, $H_p^{(1)} \sim -H_p^{(2)}$, and the factor Q is small for all values of φ . If $n^2(z') > 0$, these remarks apply to observation points in the shadow region $(k_0 z' \cos \varphi) < p$. Since the $H_p^{(1)}$ term in Eq. (17) is associated with a refracted ray when $\varphi_c > \varphi > \varphi_0$, one may interpret Δ as the correction to the refracted-wave amplitude introduced by the plane boundary. The magnitude of $1/\Delta$ increases with the ratio z_r/d , where $z_r = p/(k_0 \cos \varphi)$ is the z coordinate at the turning point (i. e., at the point of maximum penetration)

[†]It has been postulated²⁷ that the tangent ray C excites at its point of contact with the surface a diffracted ray which travels along the surface into the shadow region and sheds energy continually as it progresses. Since the emerging diffracted ray is congruent to ray C and its amplitude decays exponentially during the part of its travel along the boundary, its contribution is negligible at $\hat{\rho} \rightarrow \infty$.

along the ray; the farther the turning point is located from the plane, the smaller is the correction of the refracted-wave field. The correction can be interpreted as arising from a decaying wave that has entered the refraction shadow, has been reflected by the plane, and has emerged again into the propagating wave domain.

The far-field calculation above has been carried out under the assumption $z_> \rightarrow \infty$, thereby justifying the use of the simple asymptotic formula (5.3.13) for $h_v^{(1)}(k_0 z \cos w)$ in the integrand of Eq. (10). A better approximation is obtained via the Debye formula (5.4.77a). If k_0 is assumed to be the large parameter, a short-wavelength representation of the radiated field can be derived by employing this expression for all the cylinder functions appearing in the integrand of Eq. (10). This formulation is then valid for arbitrary observation points provided that they are located many wavelengths away from the source. In order to phrase the result in a manner which highlights its validity for general refractive index variations, rather than only the special one in Eq. (1), it is pertinent to write Eq. (5.4.77a) in the WKB form [see Eq. (3.5.37)]:

$$H_s^{(1,2)}(k_0 z \cos w)$$

$$\sim \left(\frac{2}{\pi k_0 z \cos w \cos \beta} \right)^{1/2} e^{\pm ik_0 z \cos w [\cos \beta + (\beta - \pi/2) \sin \beta] \mp i\pi/4}, \quad (18)$$

$$\sim \left(\frac{2}{\pi k_0 z \sqrt{n^2(z) - \sin^2 w}} \right)^{1/2} \exp \left[\pm ik_0 \int_{z_w}^z \sqrt{n^2(\zeta) - \sin^2 w} d\zeta \mp i\pi/4 \right], \quad (19)$$

where

$$n^2(z) = 1 - \frac{s^2 - 1/4}{k_0^2 z^2}, \quad s^2 = p^2 + \frac{1}{4}; \quad z_w = \frac{s}{k_0 \cos w}, \quad n(z_w) = \sin w, \quad (19a)$$

and

$$\sin \beta \equiv \frac{s}{k_0 z \cos w} \approx \sqrt{1 - n^2(z \cos w)}, \quad \cos \beta \approx n(z \cos w). \quad (19b)$$

The asymptotic representation in Eq. (18) can be employed along the entire integration path provided that the path avoids the vicinity of $w = \pi/2$ (see Sec. 6.A1). The approximation in Eq. (19b) is valid when s is reasonably large, so $s^2 - 1/4 \approx s^2$. This assumption, together with the formula

$$\int_{z_w}^z \sqrt{1 - \frac{s^2}{k_0^2 \zeta^2} - \sin^2 w} d\zeta = z \cos w \left[\cos \beta + \left(\beta - \frac{\pi}{2} \right) \sin \beta \right], \quad (20)$$

has been employed in going from Eq. (18) to (19). Via Eq. (19), the solution (10a) of the differential equation (3) can be expressed in a form valid (asymptotically, for large k_0) for *any* variation of refractive index that increases monotonically to the value of unity at $z = \infty$ and contains no turning points or singularities in the interval in question. This follows from a comparison with the more generally derived Eq. (5.8.35b), which corresponds to the special case $d = 0$. The subsequent asymptotic evaluation may then be performed as

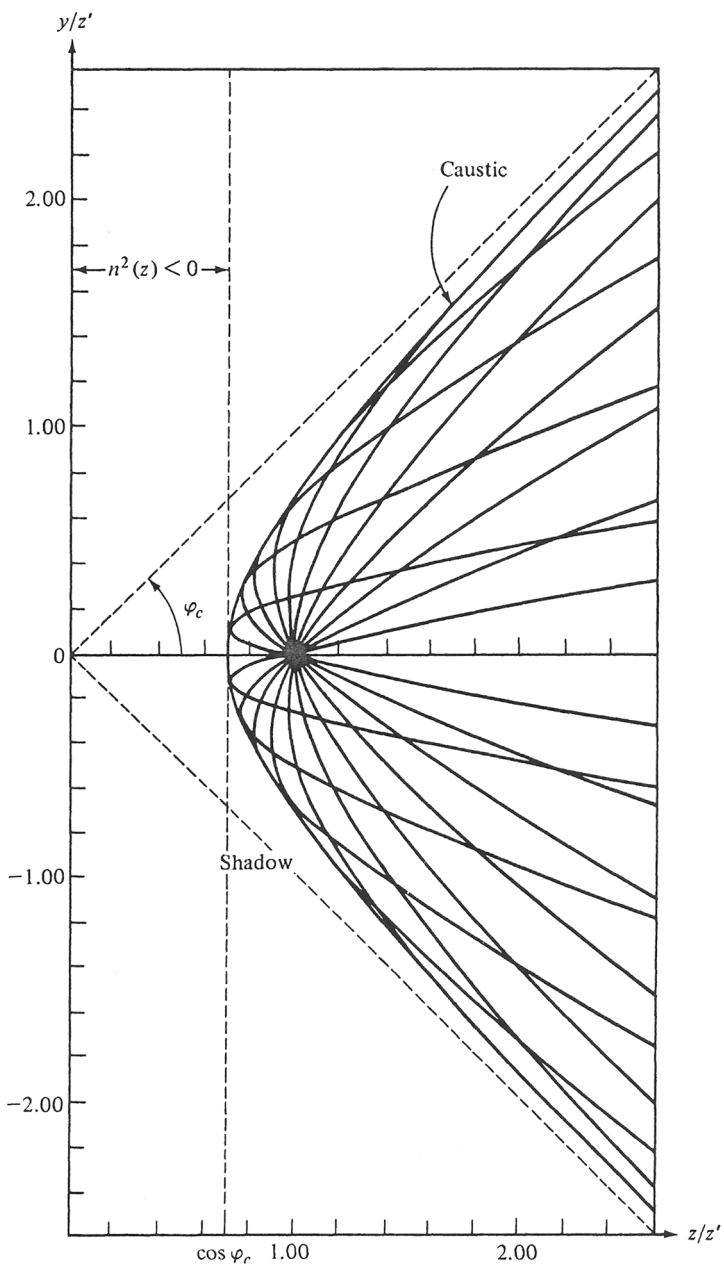


FIG. 5.9.5 Ray configuration and caustic : [$\varphi_c = \cos^{-1}(p/k_0 z') = \pi/4$].

in Sec. 5.8d and yields a ray-optical interpretation valid everywhere along the trajectories in Fig. 5.9.4.

The geometric-optical ray configuration

We consider now the geometric-optical ray family, defined by the ray equations (5.8.18) and (5.8.28), in the inverse-square profile whose refractive index $n(z) = \sqrt{\epsilon(z)/\epsilon_0}$ is given in Eq. (1). The integration may be performed explicitly and one finds that the rays form a family of hyperbolas described by the equation

$$(z'^2 - z^2) \sin^2 \varphi_c + y^2(\cos^2 \varphi_c + \cot^2 \alpha) + 2z'y \sin^2 \varphi_c \cot \alpha = 0, \quad (21)$$

where $\varphi_c = \sin^{-1} [n(z')]$ defines the extent of the illuminated region at infinity (see Fig. 5.9.4) and α or $\pi + \alpha$ is the angle with the positive z axis at which the ray leaves the line source at $(0, z')$. The relation between α and the angle of emergence $\varphi = w_s$ of the ray at infinity is obtained from Eq. (5.8.18) [see also Eq. (5.8.41)]:

$$\frac{dy}{dz} \Big|_{(0,z')} = \frac{\sin \varphi}{\sqrt{\cos^2 \varphi - (p^2/k_0^2 z'^2)}} = \tan \alpha. \quad (22)$$

The caustic is also found to be a hyperbola whose equation is determined by eliminating the parameter $\cot \alpha$ between Eq. (21) and its derivative with respect to $\cot \alpha$:³⁴

$$\frac{z^2}{z'^2 \cos^2 \varphi_c} - \frac{y^2}{z'^2 \sin^2 \varphi_c} = 1. \quad (23)$$

The caustic is tangent to the line $z = z' \cos \varphi_c = p/k_0$ on which the refractive index $n(z) = 0$. A plot of the ray configuration for $\varphi_c = \pi/4$ is given in Fig. 5.9.5. If a plane surface is inserted as in Fig. 5.9.4, rays in Fig. 5.9.5 that are intercepted by the surface give rise to reflected rays. The illuminated region is then bounded by the tangent ray C in Fig. 5.9.4 up to its point of tangency with the caustic, and by the caustic thereafter.

5.9b Radiation in a Duct

The guided-mode spectrum

To illustrate the general procedure concerning duct propagation as discussed in Sec. 5.8e, we consider a region bounded at $z = d$ by a perfectly conducting infinite plane surface; in the space $z \leq d$, the dielectric constant is assumed to vary as in Eq. (1), with p^2 large. The refractive index profile is shown in Fig. 5.9.6(a) and passes through zero at z_0 . Thus, no wave propagation is possible when $z < z_0$, and the effective maximum waveguide height is $d - z_0$. The rays are again the hyperbolas described at the end of Sec. 5.9a; however, because of the presence of the wall, reflections take place as shown in Fig. 5.9.6(b). Since a reflected ray emerges at the angle of incidence, it traces out identical trajectories between reflections. In terms of the picture in Fig. 5.9.6(b) and

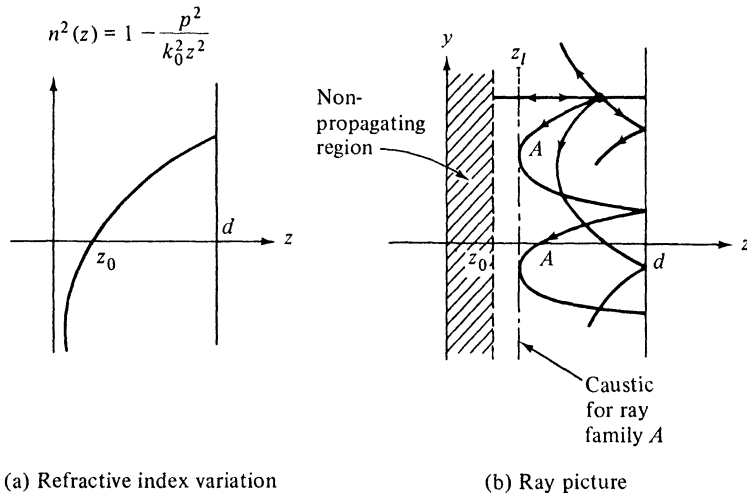


FIG. 5.9.6 Inhomogeneously filled waveguide.

with reference to Eq. (5.8.62), $\vec{\Gamma}(z_2) \equiv \Gamma(d) = -1$, while $\vec{\Gamma}(z_1) = \exp(-i\pi/2)$ since z_1 represents the caustic for the mode in question. Thus, the transverse resonance equation is

$$k_0 \int_{z_1}^d \sqrt{n^2(\eta) - a_m^2} d\eta = (m + \frac{3}{4})\pi, \quad m = 0, 1, 2, \dots \quad (24)$$

with $n^2(z_1) = a_m^2$. The integral has been evaluated in Eq. (20) and yields the implicit relation

$$k_0 d \cos \theta_m \left[\cos \beta_m + \left(\beta_m - \frac{\pi}{2} \right) \sin \beta_m \right] = \left(m + \frac{3}{4} \right) \pi, \quad (24a)$$

where

$$a_m = \sin \theta_m, \quad \beta_m = \sin^{-1} \left(\frac{p}{k_0 d \cos \theta_m} \right).$$

The implications of this equation are studied by comparison with the exact result. For two-dimensional *H*-mode propagation with respect to *z* (i. e., $\mathbf{E} = E_x \mathbf{x}_0$ and $\partial/\partial x \equiv 0$), we seek solutions $Q(y, z)$ of the homogeneous equation (5.8.3b), $[\nabla^2 + k^2(z)]Q(y, z) = 0$, that remain bounded at $z = 0$ and vanish at $z = d$. Via Eq. (3a), such solutions are

$$Q(y, z) = \exp(i\eta_l y) \sqrt{z} J_s(\sqrt{k_0^2 - \eta_l^2} z), \quad s = \sqrt{p^2 + \frac{1}{4}} \approx p, \quad (25)$$

provided that the η_l satisfy the condition

$$J_s(\sqrt{k_0^2 - \eta_l^2} d) = 0. \quad (25a)$$

If χ_l denotes the *l*th non-vanishing solution of $J_s(\chi) = 0$, then

$$\eta_l = \sqrt{k_0^2 - \frac{\chi_l^2}{d^2}}. \quad (26)$$

The pertinent roots χ_i are positive real and form an increasing sequence whence the wavenumber η_i along y is real only as long as $\chi_i < k_0 d$; for $\chi_i > k_0 d$, η_i is imaginary and this implies that the wave does not propagate along the y direction. The modes in question are seen to be quite similar to those in a perfectly conducting circular waveguide filled with a homogeneous dielectric ϵ_0 ; the refractive index singularity at $x = 0$ produces a virtual boundary, thereby making the region effectively a closed waveguide. The Bessel function in Eq. (25) can be rewritten as $J_s(\chi_i z/d)$. Since $J_s(\chi)$ is a decaying function when $s \gtrsim \chi$, the l th-mode pattern in the z direction oscillates when $z > sd/\chi_i$ and decays when $z < sd/\chi_i$. The effective height of the duct for the l th mode is given by $d - z_l$, where

$$z_l = \frac{s}{\chi_i} d = z_0 \frac{k_0 d}{\chi_i}, \quad (27)$$

and the last equality results from the definition $n^2(z_0) = 0$. Thus, the duct height increases with increasing l . The wavefunction Q is unchanged when $\eta_i y$ changes by multiples of 2π ; the modal wavelength λ_l is given by

$$\lambda_l = \frac{2\pi}{\eta_l}, \quad (28)$$

and increases with increasing l .

The zeros χ_i may be evaluated approximately if $J_s(\chi)$ is represented by its asymptotic representation in Eq. (5.4.77a), valid when s is large and $[1 - (s/\chi)] \gg \chi^{-2/3}$. The resulting condition is

$$\cos \left\{ \chi \left[\cos \beta + \left(\beta - \frac{\pi}{2} \right) \sin \beta \right] - \frac{\pi}{4} \right\} = 0, \quad \sin \beta = \frac{s}{\chi} \approx \frac{p}{\chi}. \quad (29)$$

If one puts $\eta = k_0 \sin \theta$, $\chi = k_0 d \cos \theta$, Eq. (29) yields the same result as Eq. (24), whence the geometric-optical formula is certainly adequate to approximate the higher-order zeros of $J_s(\chi)$.

Radiation from a line source

If an electric line current is located in the region $0 < z < d$ in Fig. 5.9.3(a) [see also Fig. 5.9.6(b)], the modal network problem in Fig. 5.9.3(b) must be

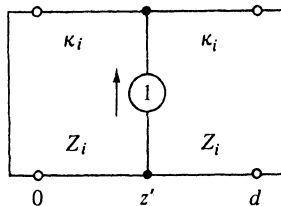


FIG. 5.9.7 Modal network problem.

modified and replaced by the one in Fig. 5.9.7. \vec{V}_i and \vec{V}'_i in Eqs. (4) are now

taken as

$$\overleftarrow{V}_i(z) = j_\nu(\kappa z), \quad \overrightarrow{V}_i(z) = h_\nu^{(1)}(\kappa z) - \frac{h_\nu^{(1)}(\kappa d)}{h_\nu^{(2)}(\kappa d)} h_\nu^{(2)}(\kappa z), \quad (30)$$

in order to satisfy the boundary conditions $\overleftarrow{V}_i(0) = 0 = \overrightarrow{V}_i(d)$. From Eq. (3.3.14a), the modal Green's function is then found to be [exp $(-i\omega t)$ dependence]

$$g''_{zi}(z, z') = \frac{i\pi}{4} \sqrt{zz'} [H_s^{(1)}(\kappa z_>) H_s^{(2)}(\kappa d) - H_s^{(2)}(\kappa z_>) H_s^{(1)}(\kappa d)] \frac{J_s(\kappa z_<)}{J_s(\kappa d)}, \quad (31)$$

where $s = (\nu + \frac{1}{2})$ and $\kappa = \sqrt{k_0^2 - \eta^2}$. Substitution into Eq. (5.2.13a) (with $j \rightarrow -i$) or into Eq. (5.8.36) completes the formal solution of the problem in a z -transmission representation, and convergence of the integral is assured by the choice $\text{Im } \kappa \geq 0$.

The disposition of the integration path with respect to possible singularities of g''_{zi} on the real η axis remains to be clarified. Upon use of the circuit relations for the cylinder functions,

$$J_s(\chi e^{i\pi}) = e^{is\pi} J_s(\chi), \quad H_s^{(1)}(\chi e^{i\pi}) = -e^{-is\pi} H_s^{(2)}(\chi), \quad (32a)$$

$$H_s^{(2)}(\chi e^{i\pi}) = e^{is\pi} H_s^{(1)}(\chi) + \frac{\sin 2s\pi}{\sin s\pi} H_s^{(2)}(\chi), \quad \chi = \kappa d, \quad (32b)$$

one verifies that g''_{zi} is an even function of κ , whence $\kappa = 0$ is a regular point in the complex η plane (see Sec. 5.3a). Thus, the only singularities are the simple poles η_l arising from the simple zeros of $J_s(\kappa d)$,

$$\eta_l = \pm \sqrt{k_0^2 - \kappa_l^2}, \quad l = 1, 2, \dots, \quad (33a)$$

where $\kappa_l d$ is the l th non-vanishing zero defined by

$$J_s(\kappa_l d) = 0. \quad (33b)$$

The absence of branch-point singularities in g''_{zi} implies that the mode spectrum in the z domain is wholly discrete. If s is assumed positive real, the κ_l constitute an infinite discrete set of real numbers [one notes from Eq. (32a) that $-\kappa_l$ also satisfies Eq. (33b)]. The corresponding η_l are real if $\kappa_l^2 < k_0^2$ and imaginary if $\kappa_l^2 > k_0^2$, as noted in connection with Eq. (26). If slight dissipation is assumed

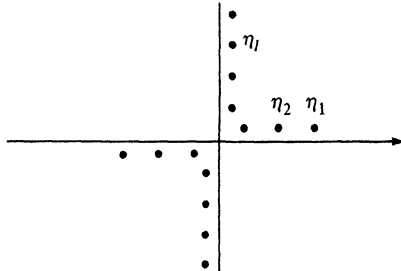


FIG. 5.9.8 Singularities in the complex η plane.

by giving k_0^2 a small positive imaginary part, then the poles are displaced into the complex plane as shown in Fig. 5.9.8, and their location relative to the integration path is unambiguous as $\text{Im } k_0 \rightarrow 0$.

The guided-mode expansion

A guided-wave representation utilizing y in Fig. 5.9.6(b) as the propagation direction is achieved upon deforming the contour of integration about the pole singularities in the upper or lower halves of the complex η plane.²⁸ Since g''_{zi} is an even function of η , the integrand in Eq. (5.8.36) remains unchanged if $y - y'$ is replaced by $|y - y'|$ [see Eqs. (5.4.11) and (5.4.12d)]. After verifying from the asymptotic formula for the Hankel function that g''_{zi} decays exponentially as $|\eta| \rightarrow \infty$, one may deform the integration path around the poles η_i in the upper half of the η plane to obtain, after a residue evaluation,

$$\tilde{G}'' = \left\{ -\frac{\pi\sqrt{zz'}}{2d} \sum_{l=1}^{\infty} \frac{\kappa_l}{\eta_l} \frac{H_s^{(1)}(\kappa_l d)}{J_s'(\kappa_l d)} J_s(\kappa_l z) J_s(\kappa_l z') e^{i\eta_l |y-y'|}, \quad (34a) \right.$$

$$\left. \frac{i\sqrt{zz'}}{d^2} \sum_{l=1}^{\infty} \frac{1}{\eta_l [J_s'(\kappa_l d)]^2} J_s(\kappa_l z) J_s(\kappa_l z') e^{i\eta_l |y-y'|}, \quad (34b) \right.$$

with $\text{Im } \eta_l \geq 0$. These alternative formulations follow from the expressions

$$H_s^{(1)}(\kappa_l d) = -H_s^{(2)}(\kappa_l d) = iN_s(\kappa_l d) = \frac{-2i}{J_s(\kappa_l d)\pi\kappa_l d}, \quad (34c)$$

which are a direct consequence of Eq. (33b) when applied to Eq. (5a) and to the definition $H_s^{(1,2)} = J_s \pm iN_s$. Since only a finite number of the η_l are real, the field far from the source plane $y = y'$ is given by a finite number of the guided modes. The series is particularly well suited for direct calculation of the field if only a small number of propagating guided modes exists.

The geometric-optical series

In order to derive a representation that is easily identifiable in terms of the geometric-optical rays sketched in Fig. 5.9.6(b), it is desirable to express g''_{zi} as a superposition of terms containing only products of traveling wave (i.e., Hankel) functions. Such a formulation leads to integrals similar to those in Eqs. (5.8.38), whose stationary-phase approximation is directly interpretable as the geometric-optical solution. The Bessel function in the numerator of Eq. (31) is easily decomposed to yield two additive terms involving the constituent Hankel functions. To achieve a similar additive decomposition of $J_s(\kappa d)$ in the denominator, we use the power-series expansion

$$\frac{1}{2J_s(\kappa d)} = \frac{1}{H_s^{(2)}(\kappa d)} [1 + t(\kappa d)]^{-1} = \frac{1}{H_s^{(2)}(\kappa d)} \sum_{m=0}^{\infty} (-t)^m, \quad t = \frac{H_s^{(1)}(\kappa d)}{H_s^{(2)}(\kappa d)}, \quad (35)$$

which converges if $|t| < 1$. The integration path can be slightly distorted so that this condition is satisfied, and substitution into Eqs. (31) and (5.8.36) yields the series

$$\tilde{G}'' = \sum_{m=0}^{\infty} G_m, \quad (36)$$

where G_m comprises the four integrals

$$G_m = \sum_{i=1}^4 g_i, \quad (37)$$

$$g_{1,2} = (-1)^m \frac{i\sqrt{zz'}}{8} \int_{-\infty}^{\infty} H_s^{(2,1)}(\kappa z_<) H_s^{(1)}(\kappa z_>) t^m e^{i\eta|y-y'|} d\eta, \quad (37a)$$

$$g_{3,4} = (-1)^{m+1} \frac{i\sqrt{zz'}}{8} \int_{-\infty}^{\infty} H_s^{(2,1)}(\kappa z_<) H_s^{(2)}(\kappa z_>) t^{m+1} e^{i\eta|y-y'|} d\eta. \quad (37b)$$

Since $z, z' < d$ and $\text{Im } \kappa \geq 0$, one verifies upon use of the asymptotic formula (5.3.13) that the integrals are convergent. However, each term in the series representation for g''_i is no longer an even function of κ , so branch points exist at $\kappa = 0$ and we define $\text{Im } \kappa \geq 0$ on the path of integration.

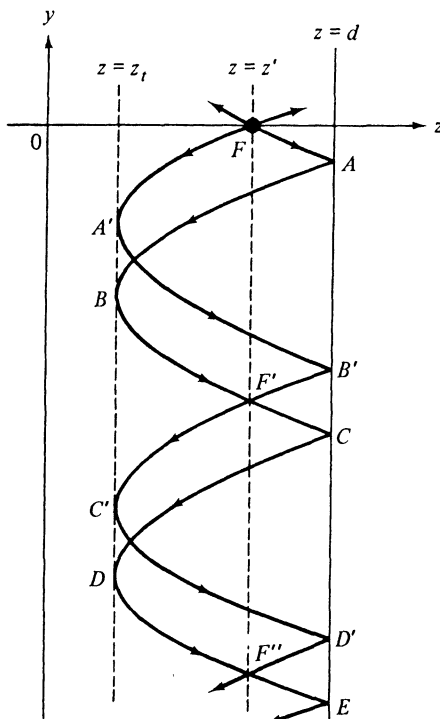
Substitution of the WKB formula (19) for the various Hankel functions casts these expressions into a general form that remains valid even for slow refractive index variations other than the special one in Fig. 5.9.6(a). The asymptotic evaluation of each integral, after introducing the transformation $\eta = k_0 \sin w$, proceeds as in Sec. 5.8d and will not be repeated here. It is of interest, however, to examine the various saddle-point conditions and their relation to the ray diagram sketched in Fig. 5.9.6(b). The saddle-point conditions are (for convenience, $y' = 0$)

$$y =$$

$$\begin{cases} \sin w_s \left[\int_{z<}^{z>} \frac{d\zeta}{\sqrt{n^2(\zeta) - \sin^2 w_s}} + 2m \int_{z_t}^d \frac{d\zeta}{\sqrt{n^2(\zeta) - \sin^2 w_s}} \right], & \text{for } g_1, \\ \sin w_s \left[\int_{z_t}^z + \int_{z_t}^{z'} + 2m \int_{z_t}^d \right], & \text{for } g_2, \\ \sin w_s \left[\int_z^{z_t} + \int_{z'}^{z_t} + (2m+2) \int_{z_t}^d \right] = \sin w_s \left[\int_{z'}^d + \int_z^d + 2m \int_{z_t}^d \right], & \text{for } g_3, \\ \sin w_s \left[\int_{z>}^{z<} + (2m+2) \int_{z_t}^d \right] = \sin w_s \left[\int_{z>}^d + \int_{z_t}^{z<} + \int_{z_t}^d + 2m \int_{z_t}^d \right], & \text{for } g_4, \end{cases} \quad (38d)$$

where all the integrands have the same form as in Eq. (38a), and $n(z_t) = \sin w_s$.

For an interpretation of these geometric-optical ray equations, let us consider the curves described when w_s is a fixed positive number lying in the range $0 < \sin w_s < n(d)$, where $n(d)$ is the refractive index value at the conducting plane $z = d$. If the source point F at $(0, z')$ is located so that $n(z') > 0$, and if $\sin w_s < n(z')$, then Eqs. (38) define the rays shown in Fig. 5.9.9. As noted in Sec. 5.8d, the ray trajectories are tangent to the line $z = z_t$ and would emerge at $z \rightarrow \infty$ with an angle of inclination w_s . Two separate ray systems exist: the first is associated with a ray that travels directly from the source F

FIG. 5.9.9 Ray trajectories for specified w_s .

to the boundary point A , while the second arises from a ray departing in the opposite direction and being turned back at A' . It is recalled that a ray travels to the right or left when the observation-point coordinate z appears in the upper or lower integration limit, respectively. Equation (38a), with $m = 0$, describes the direct ray segments FA' and FA when $z < z'$ and $z > z'$, respectively; when $m = 1$, the corresponding segments are $F'C'$ and $F'C$ on the first repetition of the cycle; when $m = 2$, one has $F''E'$ and $F''E$, etc. Equation (38b) accounts for the refracted ray $A'B'$ when $m = 0$, ray $C'D'$ when $m = 1$, etc. Equation (38c) describes the reflected ray AB when $m = 0$, CD when $m = 1$, etc. Finally, Eq. (38d), with $m = 0$, yields the ray segments $B'F'$ and BF' when $z > z'$ and $z < z'$, respectively, and correspondingly for $m \geq 1$. Thus, the integrals g_i in Eq. (37) account separately for the fields associated with the various portions of the ray trajectories listed above. The factors $(-1)^m$ arise from the m th reflection of a ray at the plane $z = d$ (reflection coefficient = -1), while the factors $[\exp(-i\pi/2)]^m$ entering into the asymptotic approximation of t in Eq. (35) characterize the m contacts of the pertinent ray with the caustic surfaces. The geometric-optical series is convenient for field calculations in a wide duct if the observation point P is located not too far from the source point F , since the effect of the multiply reflected rays, whose amplitude decreases with the path length between F and P [see Eq. (5.8.55)], is small in this case.

While either the guided mode or the geometric-optical expansion can be derived from the contour integral representation (5.8.36) as above, it is of interest to note that one series can also be transformed into the other via the Poisson transformation.³⁵

5.9c An Equivalence Relation for Fields in a Homogeneous and an Inverse-Square Medium

An interesting equivalence may be established between a class of two-dimensional (x -independent) field problems in the inhomogeneous medium described by Eq. (1), and a class of field problems with certain rotational symmetry in vacuum.³⁶ In consequence of the orthogonality of the exponential functions in the interval $0 \leq \phi \leq 2\pi$, the scalar Green's function \hat{G}_f for a ring source with a progressive phase variation $\exp(i\hat{p}\phi)$, $\hat{p} = 0, \pm 1, \pm 2..$ [see Eq. (5.4.72a)] excites in vacuum a field having this ϕ dependence everywhere. Thus, one may write [Eqs. (5.4.78)]

$$\hat{G}(\mathbf{r}; \rho', z') = e^{i\hat{p}\phi} \hat{G}(\hat{\mathbf{p}}, \hat{\mathbf{p}}'), \quad \hat{\mathbf{p}} = (y, \rho), \quad (39)$$

where \hat{G} is the two-dimensional Green's function defined by

$$\left(\hat{\nabla}^2 + k_0^2 - \frac{\hat{p}^2}{\rho^2} \right) \hat{G}(\hat{\mathbf{p}}, \hat{\mathbf{p}}') = -\delta(\rho - \rho')\delta(y - y'), \quad \hat{\nabla}^2 = \nabla^2 - \frac{1}{\rho^2} \frac{\partial^2}{\partial \phi^2}. \quad (39a)$$

To facilitate subsequent interpretation, the axis of the ring source has been chosen as y , with $(x, z) \rightarrow (\rho, \phi)$ in the transverse plane. If $(k_0^2 - \hat{p}^2/\rho^2)^{1/2}$ is viewed as an effective wavenumber in a variable medium, the structure of Eq. (39a) is the same as for Green's-function problems involving the inverse-square profile with ρ regarded as a *rectilinear* coordinate, except that the operator $\hat{\nabla}^2 = (1/\rho)(\partial/\partial\rho)(\rho\partial/\partial\rho) + (\partial^2/\partial y^2)$ is not in the rectilinear form $(\partial^2/\partial\rho^2) + (\partial^2/\partial y^2)$. The latter deficiency may be removed by the transformation

$$\hat{G}(\hat{\mathbf{p}}, \hat{\mathbf{p}}') = \sqrt{\frac{\rho'}{\rho}} \bar{G}(\hat{\mathbf{p}}, \hat{\mathbf{p}}'), \quad (40)$$

which yields the following defining equation for \bar{G} :

$$\left[\frac{\partial^2}{\partial \rho^2} + \frac{\partial^2}{\partial y^2} + k^2(\rho) \right] \bar{G}(\hat{\mathbf{p}}, \hat{\mathbf{p}}') = -\delta(\rho - \rho')\delta(y - y'), \quad (41)$$

with

$$k^2(\rho) = k_0^2 \left(1 - \frac{\hat{p}^2 - \frac{1}{4}}{k_0^2 \rho^2} \right). \quad (41a)$$

If ρ is now interpreted as the rectilinear coordinate z and $p^2 = \hat{p}^2 - \frac{1}{4}$, then $\bar{G}(y, z; y', z')$ is exactly the two-dimensional *H*-mode Green's function for the variable medium in Eq. (1).

The equivalence applies also in the presence of rotationally symmetric obstacles with a contour S described by the equation $f(y, \rho) = 0$, on which \bar{G} satisfies the boundary condition

$$\hat{G} = \gamma \frac{\partial \hat{G}}{\partial n} \quad \text{on } S, \quad (42a)$$

where n is in the direction of the normal to S and γ is a constant. After transforming according to Eq. (40), one observes the relation

$$\bar{G} = \gamma \left(\frac{\partial}{\partial n} - \frac{1}{2\rho} \frac{\partial \rho}{\partial n} \right) \bar{G} \quad \text{on } S, \quad (42b)$$

which implies that when $\gamma = 0$, the boundary condition $\hat{G} = 0$ on S also yields $\bar{G} = 0$ on S . Since $\bar{G}(y, z; y', z')$ is proportional to the electric field E_x in the problems considered [see Eqs. (5.8.1) and (5.4.31)], the latter condition is relevant for perfectly conducting obstacles that are embedded in the inhomogeneous medium and are described by the equation $f(y, z) = 0$. This class of cylindrical diffraction problems in the line-source-excited inhomogeneous medium is therefore equivalent to a corresponding class of problems in vacuum wherein the obstacle is rotationally symmetric and the excitation is due to a phased ring source (see Fig. 5.9.10). Since the refractive index $n^2(0) = -\infty$,

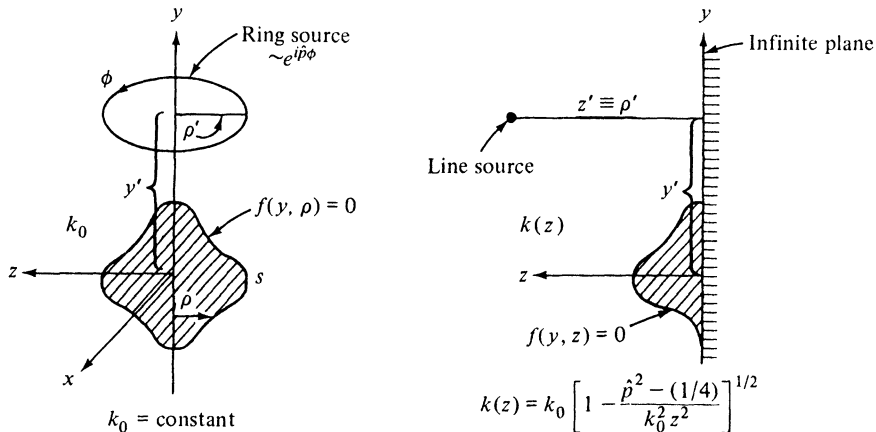


FIG. 5.9.10 Related diffraction problems.

the field vanishes on the plane $z = 0$ and is therefore not disturbed by the insertion of a conducting plane. Various specific configurations are shown in Fig. 5.9.11. It is worth noting that the refractive index varies in a relatively arbitrary (though monotonic) manner over the surfaces shown in Fig. 5.9.11(c), (d), and (e), for which exact solutions of the three-dimensional analogue are known. This refractive index behavior in the presence of an obstacle is not usually found in problems studied in the literature, and the solutions may therefore serve as a valuable check on approximate methods that have been proposed for the analysis of diffraction problems under more general conditions.

The far-field formulas for the ring source [Eq. (5.4.74)] and for the line source in the variable medium [Eq. (12), with $A(z', \phi) = 2j_{p+1/2}(k_0 z' \cos \phi)$] may

be compared as a simple illustration. After allowing for the different coordinate designation in Eq. (5.4.74) (see also Fig. 5.4.14), one finds readily that the two results are related via Eqs. (39) and (40).

The above-described equivalence may also be employed for the derivation of geometric-optical ray characteristics in one problem in terms of those in another. The ray structure in the plane of the ring source has already been described in Fig. 5.4.14 and is found to be confined to a region of space exterior

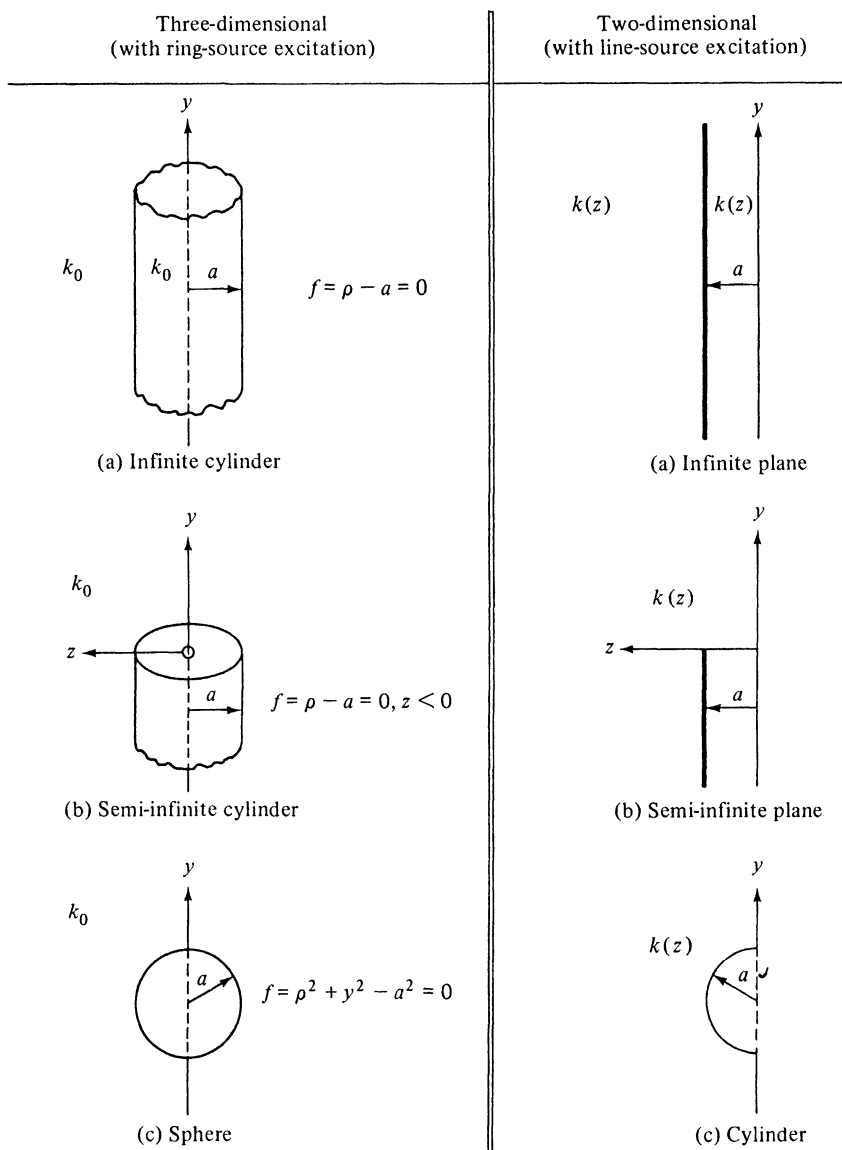


FIG. 5.9.11 Some equivalent configurations.

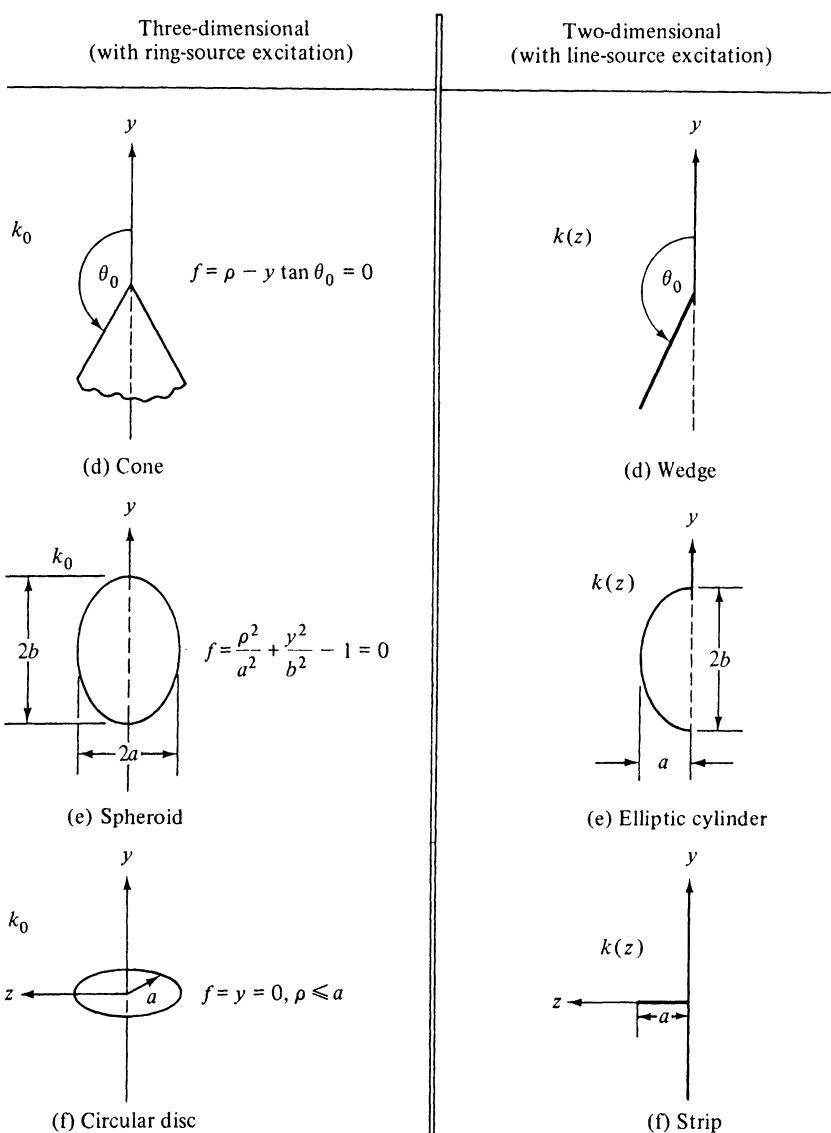


FIG. 5.9.11 Some equivalent configurations (cont.)

to a centered circular shadow zone. To determine the ray picture everywhere, it is convenient to go back to Eq. (5.4.72b) and to perform a first-order asymptotic evaluation of this integral when k_0 is large and \hat{p}/k_0 is finite. The stationary points ϕ_s , located where $(\partial/\partial\phi')[|\mathbf{r} - \mathbf{r}'| + (m/k_0)\phi'] = 0$, are found to be specified implicitly by

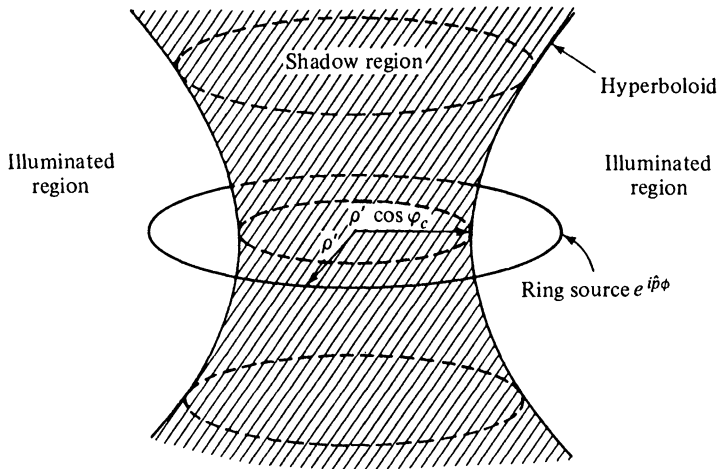
$$\frac{\rho \sin(\phi - \phi_s)}{\sqrt{\rho^2 + \rho'^2 + y^2 - 2\rho\rho' \cos(\phi - \phi_s)}} = \cos \varphi_c, \quad (43)$$

or, upon solving for $\cos(\phi - \phi_s)$, with $0 < \phi - \phi_s < \pi$,

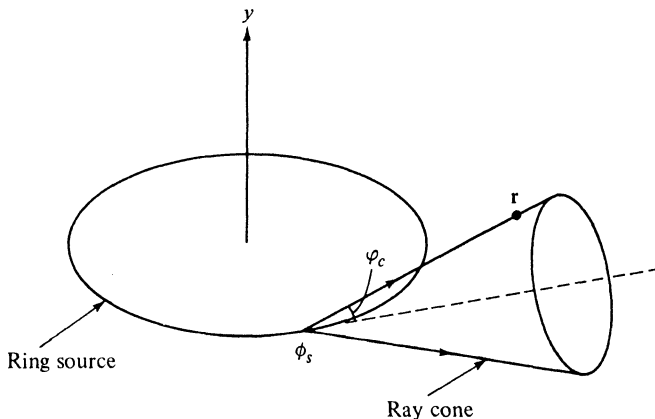
$$\cos(\phi - \phi_s) = \frac{\cos \varphi_c}{\rho} \left[\rho' \cos \varphi_c \pm \sin \varphi_c \sqrt{\frac{\rho^2}{\cos^2 \varphi_c} - \frac{y^2}{\sin^2 \varphi_c} - \rho'^2} \right], \quad (44)$$

where it is recalled that the y and z coordinates in Eq. (5.4.72b) are to be interchanged (with $z' = 0$), and

$$\cos \varphi_c = \frac{p}{k_0 \rho'} < 1, \quad p \approx \hat{p}. \quad (45)$$



(a) Ray-optical domains



(b) Ray cone

FIG. 5.9.12 Ray structure for phased ring source.

One observes that there are two real stationary points when $(\rho/\cos \varphi_c)^2 - (y/\sin \varphi_c)^2 > \rho'^2$, and no real stationary points when the inequality is reversed. Since real ϕ_s gives rise to undamped propagating fields, the region illuminated by the ring source is bounded by the surface

$$\frac{\rho^2}{\rho'^2 \cos^2 \varphi_c} - \frac{y^2}{\rho'^2 \sin^2 \varphi_c} = 1, \quad (46)$$

a hyperboloid as shown in Fig. 5.9.12(a). All field points (ρ, y) corresponding to the same value of ϕ_s in Eq. (43) lie on a right circular cone of total angle $2\varphi_c$, with its apex situated at $\phi' = \phi_s$ and with its axis tangent to the ring, as shown in Fig. 5.9.12(b). This cone is formed by the geometric-optical rays emanating from the ring-source element at $\phi' = \phi_s$, as seen by combining Figs. 5.4.10 and 5.4.14 (with $\psi \rightarrow \varphi_c$). The caustic in Eq. (46) is generated by revolving the ray cone in Fig. 5.9.12(b) about the ring axis y .

The ray trajectories associated with the line source in the inhomogeneous medium may be obtained from those above after recalling that the phase function in the former is derived from the latter by suppressing the ϕ variable [see Eqs. (39) and (40)], substituting z for ρ , and leaving y invariant. Interpreted in geometrical terms, a ray element at (ρ, ϕ, y) in the ring-source problem maps into an element at $(\rho = z, y)$, with the z and y components in the transformed configuration equal to the original ρ and y components, respectively. A two-dimensional ray is therefore constructed as in Fig. 5.9.13 by rotating the points

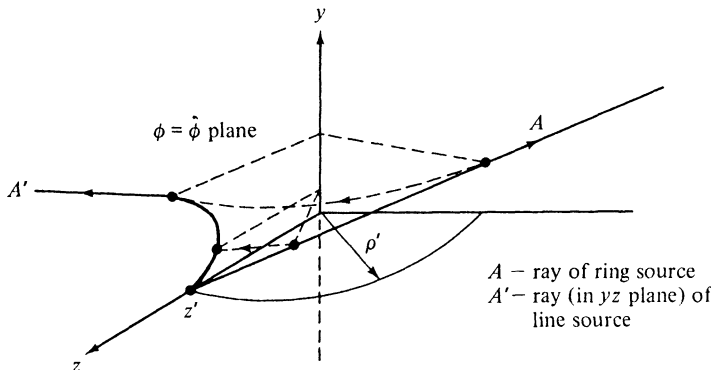


FIG. 5.9.13 Mapping of rays.

on a three-dimensional ray about the y axis into the radial plane $\phi = \hat{\phi}$, which intersects the ring at the point of emergence of the ray. This construction makes evident that the turning point on a ray in the variable medium corresponds in the ring-source problem to the point of nearest approach to the y axis; that a direct and a refracted ray pass through each point (z_1, y_1) in the illuminated region (the plane $y = y_1$ cuts the ray cone in a hyperbolic trace which is intersected at two points by the cylinder $\rho = z_1$; that the pertinent rays are the mapping of those which pass through the points of intersection);

and that the illuminated region is bounded by the hyperbolic caustic in Eq. (23).

To determine the equation of a ray that leaves the source in the inhomogeneous medium at an angle α with the positive z axis, one must select the appropriate ray on the three-dimensional cone. This may be accomplished by considering a plane surface through the cone axis which must intersect the ray cone at the appropriate angle. Since the cone axis is given by $\rho \cos(\phi - \hat{\phi}) = \rho'$, the equation of a plane inclined at the angle β with the $y = 0$ plane is

$$\rho \cos(\phi - \hat{\phi}) - \rho' = y \cot \beta. \quad (47)$$

According to the mapping prescription, a ray contained in this plane has an initial slope equal to $\tan \beta$, whence the desired angle is $\beta = \alpha$. The corresponding ray, found upon eliminating $\cos(\phi - \hat{\phi})$ between Eqs. (47) and (43) (with $\hat{\phi} = \phi_s$), is then transformed into the $\phi = \hat{\phi}$ plane by letting $\rho = z$, $\rho' = z'$. The resulting equation is that of a hyperbola and may be reduced to Eq. (21).

5.9d Continuous Transition (Epstein Profile)

When the permittivity in the medium varies continuously and monotonically from a constant value $\epsilon(-\infty) = (1 + \nu)\epsilon_0$ at $z = -\infty$ to $\epsilon(+\infty) = \epsilon_0$ at $z = +\infty$, the following functional dependence of $\epsilon(z)$ may be employed to represent such a variation:

$$\epsilon(z) = \left(1 + \frac{\nu}{1 + e^{\tau z}}\right)\epsilon_0, \quad (48)$$

where ν and τ are positive constants (Fig. 5.9.14). The resulting differential equation for the H -mode Green's function G'' [Eq. (5.8.3b)] can be solved in this instance; only this function is required when the excitation is in the form

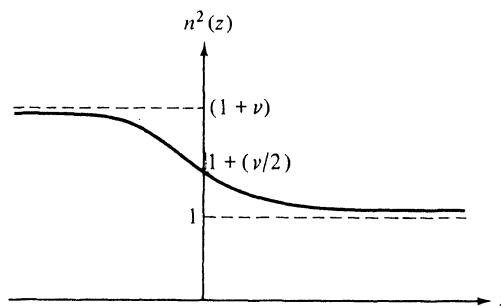


FIG. 5.9.14 Continuous transition.

of a longitudinal magnetic dipole or a transverse electric line current as in Eqs. (2). The resulting z -transmission modal representation [see Eqs. (5.2.11) and (5.2.13)] requires a knowledge of the modal Green's function g''_{zi} which satisfies the differential equation (5.8.7b) with $\mu = \mu_0$, $k^2(z) = k_0^2 \epsilon(z)$, and $k_0^2 = \omega^2 \mu_0 \epsilon_0$. The solution can be expressed in terms of hypergeometric functions as shown

in Sec. 3.6b.³⁷⁻³⁹ In particular, from Eqs. (3.5.16) and the discussion preceding Eq. (3.6.43),

$$g''_{zi}(z, z') = \frac{\hat{V}_s(z_<) \hat{V}_3(z_>)}{W[\hat{V}_3, \hat{V}_s]}, \quad (49)$$

where the expressions for \hat{V}_3 , \hat{V}_s , and W are obtained from Eqs. (3.6.18)–(3.6.23), (3.6.37), and (3.6.44). The explicit functional form of \hat{V}_3 and \hat{V}_s depends on the relative location of the source- and observation-point coordinates z and z' , and we shall consider here only the case $z < 0$, $z' < 0$, where both the source and observation points are situated in the optically denser medium. Modifications for other cases, including those where the medium in Eq. (48) is joined at some point z_0 to one with constant $\epsilon(z_0)$, have been considered in Reference 40. From the above-mentioned reference to Sec. 3.6b, one infers the following representations for \hat{V}_3 and \hat{V}_s , suitable when $z < 0$, $z' < 0$ [†]:

$$\hat{V}_s(z) = \zeta^{(1-\gamma)/2} (1 - \zeta) F(\alpha - \gamma + 1, \beta - \gamma + 1; 2 - \gamma; \zeta), \quad (50a)$$

$$\begin{aligned} \hat{V}_3(z) = & \zeta^{\gamma-1/2} (1 - \zeta) \left[\frac{\Gamma(1 - \gamma)\Gamma(\alpha + 1 - \beta)}{\Gamma(1 - \beta)\Gamma(\alpha + 1 - \gamma)} F(\alpha, \beta; \gamma; \zeta) \right. \\ & + \frac{\Gamma(\gamma - 1)\Gamma(\alpha + 1 - \beta)}{\Gamma(\gamma - \beta)\Gamma(\alpha)} e^{i\pi(\gamma-1)} \zeta^{(1-\gamma)} \\ & \cdot F(\alpha - \gamma + 1, \beta - \gamma + 1; 2 - \gamma; \zeta) \Big], \end{aligned} \quad (50b)$$

where $\zeta = -e^{\tau z}$, and α , β , and γ are defined in Eqs. (3.6.37). Substitution into Eq. (49) yields

$$g''_{zi}(z, z') = g_1(z, z') + g_2(z, z'), \quad (51)$$

where

$$\begin{aligned} g_1(z, z') = & \frac{e^{i\kappa_1|z-z'|}}{-2i\kappa_1} [(1 + e^{\tau z})(1 + e^{\tau z'}) F(\alpha, \beta; \gamma; -e^{\tau z}) \\ & \times F(\alpha - \gamma + 1, \beta - \gamma + 1; 2 - \gamma; -e^{\tau z})], \end{aligned} \quad (51a)$$

$$\begin{aligned} g_2(z, z') = & A \frac{e^{-i\kappa_1(z+z')}}{-2i\kappa_1} [(1 + e^{\tau z})(1 + e^{\tau z'}) \\ & \times F(\alpha - \gamma + 1; \beta - \gamma + 1; 2 - \gamma; -e^{\tau z}) \\ & \times F(\alpha - \gamma + 1; \beta - \gamma + 1; 2 - \gamma; -e^{\tau z})], \end{aligned} \quad (51b)$$

$$A = \frac{\Gamma(1 - \beta)\Gamma(\alpha + 1 - \gamma)\Gamma(\gamma - 1)}{\Gamma(\gamma - \beta)\Gamma(\alpha)\Gamma(1 - \gamma)}, \quad \kappa_1 = \sqrt{k_0^2(1 + \nu) - \zeta^2}. \quad (51c)$$

κ_1 is the propagation constant in the medium to the left of the transition region whose effective width is defined by τ . If $|z|$ and $|z'|$ are large enough so that $\exp(\tau z)$ and $\exp(\tau z')$ are very small, the factors inside the brackets in Eqs. (51a) and (51b) are slowly varying and almost equal to unity [see Eq. (3.6.21c)]

[†]In this section, $\Gamma(w)$ denotes the gamma function and should not be confused with the same symbol used elsewhere for the reflection coefficient.

and may therefore be regarded as distortions of the incident- and reflected-wave fields, respectively.

As a check on Eqs. (51) we examine the limiting cases $\nu = 0$ (homogeneous medium from $z = -\infty$ to $z = +\infty$) and $\tau = \infty$ (abrupt change of dielectric constant at $z = 0$). When $\nu = 0$, one has $\alpha = 1$, $\beta = 1 + (2ik_2/\tau) = \gamma$, $k_2 = \sqrt{k_0^2 - \xi^2}$; since $\Gamma(0) = \infty$, one finds that $A = 0$ in Eq. (51c). Moreover,

$$F(\alpha, \beta; \beta; \zeta) = (1 - \zeta)^{-\alpha}, \quad F(\alpha, \beta; \alpha; \zeta) = (1 - \zeta)^{-\beta}, \quad (52)$$

so the expression inside the brackets in Eq. (51a) equals unity, thereby yielding the correct value for the free-space Green's function. When $\tau = \infty$, the expressions inside the brackets in Eqs. (51a) and (51b) again have the value unity. In this case, $\alpha = \beta = \gamma \rightarrow 1$, or, more precisely,

$$1 - \beta = -\frac{i}{\tau}(k_1 + k_2), \quad 1 - \gamma = -\frac{2i}{\tau}k_1, \quad \gamma - \beta = \frac{i}{\tau}(k_1 - k_2), \quad (53a)$$

which, with the formula

$$\Gamma(w) = \frac{1}{w} + O(1), \quad \text{as } w \rightarrow 0, \quad (53b)$$

yields the following result for the reflection coefficient A [see also Eq. (3.6.30b)]:

$$A = \frac{k_1 - k_2}{k_1 + k_2}, \quad k_1 = \sqrt{k_0^2(1 + \nu) - \xi^2}, \quad k_2 = \sqrt{k_0^2 - \xi^2}, \quad (54)$$

the correct expression for an abrupt transition as given in Eq. (5.5.54c). The modal Green's function then reduces correctly to that in Sec. 5.5d.

Substitution of Eq. (49) into Eqs. (5.2.11) or (5.2.13) yields the Green's functions required for the solution of the problem of radiation from a longitudinal magnetic current element or from a transverse electric line current, respectively, in the medium characterized by the spatially varying permittivity in Eq. (48). To render the integrand unique along the integration contour that extends from $\xi = -\infty$ to $\xi = \infty$ along the real ξ axis (or similarly along the real η axis), it is necessary to investigate the singularities of $g''_{zi}(z, z')$. We recall first [see Eqs. (3.6.37)] that the square roots k_1 and k_2 are defined to have positive imaginary parts when the radicands are non-positive. One may then easily verify that the integrals converge exponentially as $|\xi| \rightarrow \infty$. $g''_{zi}(z, z')$ has first-order branch-point singularities at $k_{1,2} = 0$, i.e., at

$$\xi = \pm k_0, \quad \xi = \pm k_0\sqrt{1 + \nu}. \quad (55)$$

As regards pole singularities, we note that $\Gamma(w)$ has simple poles at $w = -n = 0, -1, -2, \dots$, that $F(\alpha, \beta; \gamma; \zeta)$ has simple poles at the poles of $\Gamma(\gamma)$, and that, in particular,⁴

$$\begin{aligned} \lim_{\gamma \rightarrow -n} \frac{F(\alpha, \beta; \gamma; \zeta)}{\Gamma(\gamma)} &= \frac{\alpha(\alpha + 1) \cdots (\alpha + n)\beta(\beta + 1) \cdots (\beta + n)}{(n + 1)!} \\ &\times \zeta^{n+1} F(\alpha + n + 1, \beta + n + 1; n + 2; \zeta). \end{aligned} \quad (56)$$

Moreover, $\Gamma(w)$ has no zeros. From these remarks it appears that both g_1 and g_2 have simple pole singularities at $\gamma = -n$; however, detailed study utilizing Eq. (56) shows that the sum $(g_1 + g_2)$ is regular at $\gamma = -n$. g_1 and (or) g_2 also have poles at points in the complex ξ plane at which

$$2 - \gamma = -n, \quad 1 - \beta = -n, \quad \alpha + 1 - \gamma = -n, \quad n = 0, 1, 2, \dots \quad (57)$$

Equation (57) can be satisfied only if γ , β , and $\alpha - \gamma$ are real (i.e., if κ_1 and κ_2 are imaginary). If there are solutions of this equation with $\kappa_{1,2} = +i|\kappa_{1,2}|$, they represent surface waves which individually satisfy the radiation condition at $z \rightarrow \pm \infty$; they comprise discrete components in the spectrum of waves that can be guided along the inhomogeneity in the direction transverse to z . Examination of Eqs. (57) and (3.6.37) reveals, however, that such solutions do not exist. If branch cuts are chosen so that $\text{Im } \kappa_{1,2} > 0$ on the top sheet of the four-sheeted Riemann surface representing the complex ξ plane, then no pole singularities are present on the top sheet, and the integration path proceeds as in Fig. 5.3.6(a).

An asymptotic evaluation of the integrals in Eqs. (5.2.11) or (5.2.13) for arbitrary z and z' is quite difficult. However, if $|z|$ and $|z'|$ are large enough so that the factors inside the braces in Eqs. (51a) and (51b) may be considered as slowly varying, the integrals can be evaluated asymptotically as in Sec. 5.3d. The saddle points corresponding to the g_1 and g_2 portions of the integrands are located at $\xi_s = k_0(1 + v) \sin \theta$, where θ is, respectively, the angle between the z axis and the radius vector from the source point (ρ', z') and the image point $(\rho', -z')$ to the observation point (ρ, z) . The resulting first-order asymptotic approximation (in which branch-cut integral contributions yielding lateral-wave effects are neglected) then looks like that in Eqs. (5.5.5) or (5.5.58) except that the distortion factors inside the brackets in Eqs. (51a) and (51b) are included in the incident- and reflected-field contributions, respectively, and that the reflection coefficient is given by A in Eq. (51c), with ξ replaced by ξ_s . The behavior of the reflection coefficient was discussed in connection with Eq. (3.6.39).

P R O B L E M S

1. An azimuthally directed electric current element

$$\hat{\mathbf{J}}(\mathbf{r}, t) = Il\delta(\rho - \rho')\delta(z - z')e^{-i\omega t}\phi'_0, \quad \phi'_0 = y_0 \cos \phi' - x_0 \sin \phi', \quad (1)$$

where I is the current in the element and l is its length, is located at (ρ', ϕ', z') inside a perfectly conducting circular waveguide with radius b .

(a) Referring to Sec. 5.2a, show that the longitudinal electric and magnetic fields excited by the current element are given by:

$$E_z(\mathbf{r}, \mathbf{r}') = \frac{Il}{-i\omega\epsilon} \frac{\partial}{\rho'\partial\phi'} \frac{\partial}{\partial z'} \sum_i \Phi_i(\rho)\Phi_i^*(\rho') \frac{e^{i\kappa_i' |z-z'|}}{-2ik_i'}, \quad (2a)$$

$$H_z(\mathbf{r}, \mathbf{r}') = -Il \frac{\partial}{\partial \rho'} \sum_i \psi_i(\rho)\psi_i^*(\rho') \frac{e^{i\kappa_i'' |z-z'|}}{-2ik_i''}, \quad (2b)$$

where Φ_i and ψ_i are the scalar mode functions in Eqs. (3.2.75) and (3.2.76).

(b) An electric ring current with radius ρ' and azimuthal variation $\exp(iv\phi')$, $v = \text{integer}$, can be synthesized by multiplying Eq. (1) by $\exp(iv\phi')$ and integrating over ϕ' between the limits 0 and 2π . Show that the longitudinal electric fields $\dot{\vec{E}}_z$ and $\dot{\vec{H}}_z$ excited by the ring current are given by:

$$\dot{\vec{E}}_z(\mathbf{r}; \rho', z') = \frac{Il \operatorname{sgn}(z - z') v e^{iv\phi}}{\omega \epsilon \rho' b^2} \sum_n \frac{J_v(\beta_n \rho) J_v(\beta_n \rho') e^{i\sqrt{k^2 - \beta_n^2}|z - z'|}}{J_v''(\beta_n b)} \quad (3a)$$

and

$$\dot{\vec{H}}_z(\mathbf{r}; \rho', z') = \frac{i l v e^{iv\phi}}{b^2} \sum_n \frac{\beta'_n}{J_v(\beta'_n b) J_v''(\beta'_n b)} \frac{J_v(\beta'_n \rho) J_v(\beta'_n \rho')}{\sqrt{k^2 - \beta'^2_n}} e^{i\sqrt{k^2 - \beta'^2_n}|z - z'|}, \quad (3b)$$

where $\beta_n = x_{nm}/b$, $\beta'_n = x'_{nm}/b$, with $J_m(x_{nm}) = J'_m(x'_{nm}) = 0$.

(c) Repeat the calculations in parts (a) and (b) for excitation by a magnetic current element and magnetic current ring source, respectively.

2. Referring to Fig. 5.3.4, discuss the behavior of $\kappa(\xi) = \sqrt{k^2 - \xi^2}$ on a two-sheeted Riemann surface cut along the straight line segment connecting $-k$ and $+k$. Also discuss the corresponding mapping to the w plane via the transformation $\xi = k \sin w$ and compare with the discussion in Sec. 5.3c, which pertains to an alternative choice of branch cuts.
3. Show that when f in the integrand of Eq. (5.2.21) has pole singularities located at $w = \pm jw_1$, w_1 positive real, the time function $A(\tau)$ contains in addition to the result in Eq. (5.2.23) the contribution:

$$A_1(\tau) = \mp \pi j [(w + jw_1)[f(\bar{\alpha} + w) - f(\bar{\alpha} - w)]]_{w=-jw_1} \delta\left(\tau - \frac{L}{c} \cosh w_1\right), \quad (4)$$

where the upper and lower signs apply when the integration path around the poles is indented into the half-planes $\operatorname{Re} w < 0$ and $\operatorname{Re} w > 0$, respectively. Note that $A_1(\tau) = 0$ when f is an even function of w .

4. Derive the two-dimensional free-space Green's function representation in Eq. (5.4.36b) by integrating over x' the cylindrical waveguide representation (5.4.10) of the three-dimensional Green's function. Hint: Show first that for $\alpha > 0$, $s > 0$ [cf. Eq. (5.4.12d)]

$$\frac{e^{-j\alpha s}}{s} = \frac{-j}{2} \int_{-j\infty}^{j\infty} H_0^{(2)}(\sqrt{\alpha^2 - \zeta^2}s) d\zeta = \frac{1}{2} \int_{-\infty}^{\infty} H_0^{(2)}(\sqrt{\alpha^2 + \mu^2}s) d\mu. \quad (5)$$

5. The cylindrical waveguide representation for the free-space Green's function G_f in Eq. (5.4.10) may be written alternatively as

$$G_f = \frac{i}{4\pi} \int_0^\infty \zeta J_0(\zeta \rho) \frac{e^{i\sqrt{k^2 - \zeta^2}|z|}}{\sqrt{k^2 - \zeta^2}} d\zeta. \quad (6)$$

By employing the steepest-descent procedure to evaluate the integral, show that on the axis $\rho = 0$, G_f is given by

$$G_f \sim \frac{e^{ik|z|}}{4\pi|z|}, \quad (7)$$

thereby verifying that the asymptotic result in Eq. (5.4.9) applies also at $\theta = 0$.

6. Electric line currents flowing parallel to z are distributed over a cylindrical surface $\rho = \rho'$; the current distribution has an azimuthal phase variation $\exp(im\phi)$,

$m = \text{integer}$. The electric field E_z generated by this source configuration is proportional to a scalar potential $u(\rho, \phi; \rho')$ defined by

$$\left(\frac{1}{\rho} \frac{\partial}{\partial \rho} \rho \frac{\partial}{\partial \rho} + \frac{1}{\rho^2} \frac{1}{\partial \phi^2} + k^2 \right) u(\rho, \phi; \rho') = -\frac{\delta(\rho - \rho')}{\rho'} e^{im\phi}, \quad (8)$$

subject to a radiation condition at infinity. A time-dependence $\exp(-i\omega t)$ is implied.

Show that u is given by

$$u(\rho, \phi; \rho') = \frac{\pi i}{2} J_m(k\rho') H_m^{(1)}(k\rho) e^{im\phi}. \quad (9)$$

Assuming $k\rho' \gg 1$ and $(m/k\rho') < 1$, use the Debye asymptotic formulas in Eqs. (5.4.77) to derive an asymptotic approximation for u . Show that this approximation agrees with the ray-optical result in Problem 29 of Chapter 1.

7. Use the asymptotic expansion of the time-harmonic, two-dimensional free space Green's function,

$$\tilde{G}_f(\hat{\rho}) = \frac{i}{4} H_0^{(1)}(k\hat{\rho}) = \frac{e^{i[k\hat{\rho} + (\pi/4)]}}{2\sqrt{2\pi k\hat{\rho}}} \sum_{m=0}^{\infty} \frac{(0, m)}{(2ik\hat{\rho})^m}, \quad k = \frac{\omega}{c} \quad (10)$$

where

$$(0, m) \equiv \frac{(1)(3^2)(5^2)\dots(2m-1)^2}{2^{2m}m!}, \quad (0, 0) \equiv 1, \quad (10a)$$

to construct via Eqs. (1.7.80) and (1.7.81) the behavior of the time-dependent Green's function \hat{G}_f near the wavefront. Verify the validity of this result by expanding the exact solution in Eq. (5.4.42), $\hat{G}_f = \{4\pi^2[t^2 - (\hat{\rho}/\bar{c})^2]\}^{-1/2}U(\bar{c}t - \hat{\rho})$, in a series about $\bar{c}t = \hat{\rho}$.

8. An x -directed electric line current with impulsive behavior $\hat{\mathbf{J}}(\mathbf{r}, t) = I\delta(t) \cdot \delta(\hat{\rho} - \hat{\rho}')\mathbf{x}_0$ is situated at $\hat{\rho}' = (0, z')$, $z' < 0$, in the presence of a non-dispersive lossless dielectric half-space (see Fig. 5.5.7). The electromagnetic fields can be derived from the two-dimensional, time-dependent Green's functions $\hat{G}_{1,2}$ defined in Eqs. (5.5.65). When $\epsilon_2 > \epsilon_1$, where ϵ_1 and ϵ_2 are the dielectric constants for the regions $z < 0$ and $z > 0$, respectively, the result for \hat{G}_1 in $z < 0$ is given in Eqs. (5.5.66)-(5.5.67).

When $\epsilon_1 > \epsilon_2$, show the result in Eqs. (5.5.66)-(5.5.67) remains valid for $\varphi < \sin^{-1}\sqrt{\epsilon}$, $\epsilon = \epsilon_2/\epsilon_1$, where φ is the observation angle measured from the image point as in Fig. 5.5.7. Show that for $\varphi > \sin^{-1}\sqrt{\epsilon}$ in the half-space $z < 0$, one must add to this result a contribution \hat{G}_b whose time-harmonic form [for an $\exp(-i\omega t)$ dependence] is as follows:

$$\hat{G}_b = \frac{i}{4\pi} \int_{P_1} e^{-s(R/\bar{c}_1) \cos(w-\varphi)} \Gamma(k_1 \sin w) dw, \quad (11)$$

where R is the distance from the image point, \bar{c}_1 is the propagation speed in the region $z < 0$, and

$$\Gamma(k_1 \sin w) = \frac{\cos w - \sqrt{\epsilon - \sin^2 w}}{\cos w + \sqrt{\epsilon - \sin^2 w}}, \quad (11a)$$

and the path P_1 runs from $w = \varphi + i0$ to $w = \varphi - i0$ around the branch point at $w_b = \sin^{-1}\sqrt{\epsilon}$, with the branch cut chosen along the contour $\text{Re } \sqrt{\epsilon - \sin^2 w} = 0$. Use the procedure in Eqs. (5.2.19)–(5.2.23) to show that the time-dependent result is as follows:

$$\hat{\sigma}_b = -\text{Im} \left(\frac{\cos \beta + i\sqrt{\sin^2 \beta - \epsilon}}{\cos \beta - i\sqrt{\sin^2 \beta - \epsilon}} \right) \times \frac{U(\varphi - \sin^{-1}\sqrt{\epsilon}) U[t - \{(R/\bar{c}_1) \cos(w_b - \varphi)\}] U[(R/\bar{c}_1) - t]}{2\pi\sqrt{(R/\bar{c}_1)^2 - t^2}}, \quad (12)$$

where $\beta = \varphi + \cos^{-1}(\bar{c}_1 t / R)$ and $U(\alpha) = 1$ or 0 for $\alpha > 0$ or $\alpha < 0$, respectively. Show that Eq. (12) defines a lateral wave whose relation to the direct and reflected waves is as shown in Fig. 5.5.8 when $z' = 0$. Sketch the incident, reflected, and lateral wavefronts when $z' \neq 0$ and indicate on this sketch the domain of existence of the lateral wave contribution.

9. Assume the semiinfinite dielectric medium in Fig. 5.5.7 to be excited by a source distribution that gives rise only to H modes with respect to the z direction and is confined to the interface (i.e., $z' = 0$).

(a) Show that for observation point locations on the interface ($z = 0$), the voltage in a typical mode is given by:

$$V = -\frac{2}{k_1^2 - k_2^2} \left[\frac{d^2}{dz^2} V_{f1} - \frac{d^2}{dz^2} V_{f2} \right]_{z=z'=0}, \quad (13)$$

where $k_\alpha^2 = \omega^2 \mu_0 \epsilon_\alpha$, $\alpha = 1, 2$ and $V_{f\alpha}$ is the voltage on an *infinite* transmission line characteristic of medium α .

(b) Since only H modes are excited, the electromagnetic fields can be inferred from an appropriate scalar Green's function, to be called $G(\mathbf{r}, \mathbf{r}')$. Show via modal synthesis that for $z = z' = 0$, G can be expressed in terms of the elementary Green's functions $G_{f\alpha}$ for an *infinite* medium having a dielectric constant ϵ_α :

$$G(\mathbf{r}, \mathbf{r}')|_{z=z'=0} = -\frac{2}{k_1^2 - k_2^2} \left[\frac{\partial^2}{\partial z^2} G_{f1}(\mathbf{r}, \mathbf{r}') - \frac{\partial^2}{\partial z^2} G_{f2}(\mathbf{r}, \mathbf{r}') \right]_{z=z'=0} \quad (14)$$

(c) For the case of an electric line source as in Fig. 5.5.7, show that Eq. (14) can be written for an $\exp(-i\omega t)$ time dependence as:

$$G|_{z=z'=0} = \frac{i}{2(k_1^2 - k_2^2)} \left[\left(\frac{d^2}{dy^2} + k_1^2 \right) H_0^{(1)}(k_1 y) - \left(\frac{d^2}{dy^2} + k_2^2 \right) H_0^{(1)}(k_2 y) \right] \\ = \frac{i}{2(h_1^2 - h_2^2)} [h_1 H_1^{(1)}(h_1) - h_2 H_1^{(1)}(h_2)], \quad h_\alpha = k_\alpha y, \quad y > 0. \quad (15)$$

For $y < 0$, replace y by $|y|$. It is noted that the far field ($k_\alpha y \gg 1$) varies like $y^{-3/2}$; compare this with the results in Eq. (5.5.58).

(d) For the case of a longitudinal magnetic current element located at $\mathbf{r}' = 0$, show that Eq. (14) can be written for an $\exp(-i\omega t)$ time dependence as:

$$G|_{z=z'=0} = -\frac{1}{2\pi(g_1^2 - g_2^2)} \left[(ig_1 - 1) \frac{e^{ig_1}}{\rho} - (ig_2 - 1) \frac{e^{ig_2}}{\rho} \right], \quad g_\alpha = k_\alpha \rho, \quad (16)$$

where ρ is the radial distance from the source to the observation point. Verify that $G \rightarrow 1/4\pi\rho$ as $\rho \rightarrow 0$.

10. A source distribution with assumed time-dependence $\exp(j\omega t)$ is located in the presence of a highly lossy dielectric half-space as shown in Fig. P5.1a. Referring

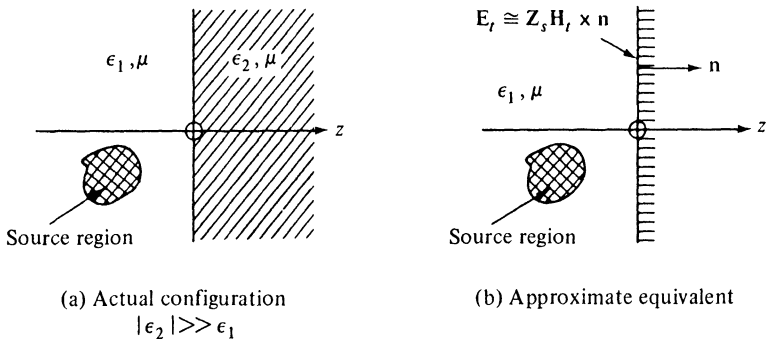


FIG. P5.1 Approximate equivalent configurations.

to the equivalent modal network problems in Fig. 5.5.3 or 5.5.6 and assuming that $\epsilon_2 = \epsilon_{2r} - j\sigma/\omega \approx -j\sigma/\omega$, where ϵ_{2r} is the real part of the dielectric constant in the lossy medium and $\sigma \gg \omega\epsilon_{2r}$ is its conductivity, show that for modes with $k_{ti}^2 \ll |k_i^2 \epsilon|$, the modal impedance Z_{2i} for the i th E or H mode is given approximately by:

$$Z_{2i} \approx \sqrt{\frac{\mu}{\epsilon_2}} = \frac{\omega \mu e^{j\pi/4}}{\sqrt{2}} \delta, \quad \delta = \sqrt{\frac{2}{\omega \mu \sigma}}, \quad (17)$$

where k_{ti} is the transverse wavenumber for the i th mode, $k_{1,2}^2 = \omega^2 \mu \epsilon_{1,2}$, $\epsilon = \epsilon_2/\epsilon_1$, and δ is the skin depth. When the source region is not too near the interface (give a criterion!), show that the approximation in Eq. (17) can be used for all modes whose contribution to the reflected field is not negligible, and that the equivalent network problem reduces to that in Fig. 5.7.2 or its H -mode analogue, with $Z_s = \sqrt{\mu/\epsilon_2}$ denoting the surface impedance [see also Eq. (5.7.1) and Fig P5.1b]. By applying the concept of a locally plane boundary, show that the surface impedance approximation remains valid also for a curved interface provided that the skin depth δ and the wavelength inside the lossy medium are much smaller than (1) the wavelength $2\pi/k_1$ in the exterior medium, (2) the smallest radius of curvature of the boundary surface, and (3) the distance from the source region to the observation point.[†] Show that when $\epsilon_2 \gg \epsilon_1$, with ϵ_2 real (lossless medium), the surface impedance approximation remains valid for the plane interface but not, in general, for a curved interface if the latter gives rise to multiple internal reflections.

11. A source distribution is located exterior to the grounded dielectric slab shown in Fig. 5.6.1. If the slab width d is so small that $|k_2 d| \ll 1$, with k_2 either real or complex, and if the source configuration excites only H modes with respect to the z direction (perpendicular to the slab), show that under restrictions analogous to those in Problem 10, the grounded slab may be replaced by the surface impedance

[†]M. A. Leontovich, *Investigations of Propagation of Radio Waves*, Part II, Moscow (1948). Also T. B. A. Senior, "Impedance boundary conditions for imperfectly conducting surfaces," *Appl. Sci. Res.* **8**, Sec. B.

$$Z_s = j \sqrt{\frac{\mu}{\epsilon_1}} k_1 d \quad (\text{for } H \text{ modes}). \quad (18)$$

Show also that no such replacement is possible for the *E*-mode case.

12. For the grounded dielectric slab in Fig. 5.6.1 calculate the far fields when the source and/or the observation point is located inside the slab region. Obtain and interpret a radial transmission representation analogous to that discussed in Sec. 5.6a.
13. The ray-optical approximation of the field radiated by a time-harmonic line source of electric currents in a plane stratified medium with refractive index $n = n(z)$ is given in Eq. (5.8.27). This result is applicable for observation points on rays emanating from the source point, before such rays reach a turning point z_t (if any) where $n(z_t) = a$, a being the ray parameter. Use the refracted ray equation (5.8.28) to derive a corresponding expression for the field valid on ray segments after turning. Show that the result agrees with the asymptotic evaluation of the exact solution in Eq. (5.8.55).

R E F E R E N C E S

1. STRATTON, J. A., *Electromagnetic Theory*, Secs. 6.9-6.11. New York: McGraw-Hill, 1941.
2. MORSE, P. M. and H. FESHBACH, *Methods of Theoretical Physics*, Sec. 4.8. New York: McGraw-Hill, 1953.
3. KNOPP, K., *Theory of Functions*, Part II, Sec. II. New York: Dover Publications, 1947.
4. MAGNUS, W. and F. OBERHETTINGER, *Formulas and Theorems for the Special Functions of Mathematical Physics*, p. 22. New York: Chelsea Publishing Co., 1954.
5. TAMIR, T. and A. A. OLINER, "Guided complex waves. I. Fields at an interface. II. Relation to radiation patterns," *Proc. IEE (London)* 110 (1963), pp. 310-334.
6. CLEMMOW, P. C., "The resolution of a dipole field into transverse electric and transverse magnetic waves," *Proc. IEE (London)* 110 (1963), p. 107.
7. SOMMERFELD, A. N., *Partial Differential Equations in Physics*, Sec. 19. New York: Academic Press, 1949.
8. FRANK, I. M. and I. G. TAMM, *Dokl. Akad. Nauk. (USSR)* 14 (1937), p. 109.
9. PANOFSKY, W. K. H. and M. PHILLIPS, *Classical Electricity and Magnetism*, Chapter 19. Reading, Mass.: Addison-Wesley Publishing Co., 1962.
10. SOMMERFELD, A. N., *Partial Differential Equations in Physics*, Chapter 6; in particular, pp. 256-257. New York: Academic Press, 1949.
11. BREKHOVSKIKH, L. M. *Waves in Layered Media*, Secs. 21-23. New York: Academic Press, 1960.

12. BAÑOS, A., *Dipole Radiation in the Presence of a Conducting Half Space*, Sec. 4.10. New York: Pergamon Press, 1966.
13. STRATTON, J. A., *Electromagnetic Theory*, Secs. 9.5-9.6. New York: McGraw-Hill, 1941.
14. WAIT, J. R., *Electromagnetic Waves in Stratified Media*, Chapter 2. New York: Macmillan, 1962.
15. CLEMMOW, P. C., *The Plane Wave Spectrum Representation of Electromagnetic Fields*, Chapter 5. New York: Pergamon Press, 1966.
16. FOCK, V. A., *Electromagnetic Diffraction and Propagation Problems*, Sec. 11.1. New York: Pergamon Press, 1965.
17. SOMMERFELD, A. N., *Partial Differential Equations in Physics*, Sec. 33. New York: Academic Press, 1949.
18. BANOS, A., *Dipole Radiation in the Presence of a Conducting Half Space*, Chapter 1. New York: Pergamon Press, 1966.
19. deHOOP, A. T. and H. J. FRANKENA, "Radiation of pulses generated by a vertical electric dipole above a plane, non-conducting earth," *Appl. Sci. Res.*, Sec. B 8 (1960), p. 369.
20. JONES, D. S., *The Theory of Electromagnetism*, Sec. 10.1. New York: Macmillan, 1964.
21. SITENKO, A. G. and V. S. TALICH, "Cerenkov effect in the motion of a charge above a boundary between two media," *J. Tech. Phys. (Russian)* 29 (1959), pp. 1074-1085.
22. COLLIN, R. E., *Field Theory of Guided Waves*, Chapter 11. New York: McGraw-Hill, 1960.
23. SOMMERFELD, A. N., *Partial Differential Equations in Physics*, p. 250. New York: Academic Press, 1949.
24. CULLEN, A. L., "The excitation of plane surface waves," *Proc. IEE (London)* 101, Part IV, 1954; "A note on the excitation of surface waves," *ibid.*, 104, Part C, 1957.
25. BARLOW, H. E. M. and J. BROWN, *Radio Surface Waves*, Chapter 12. London: Oxford University Press, 1962.
26. KAY, A. F., "Scattering of a surface wave by a discontinuity in reactance," *IRE Trans. on Antennas and Propagation AP-7* (Jan. 1959).
27. SECKLER, B. D. and J. B. KELLER, "Geometrical theory of diffraction in inhomogeneous media," *J. Acoust. Soc.* 31(1959), pp. 192-205. Also B. D. SECKLER and J. B. KELLER, "Asymptotic theory of diffraction in inhomogeneous media," *J. Acoust. Soc.* 31 (1959), pp. 206-216.
28. BREKHOVSKIKH, L. M., *Waves in Layered Media*, Sec. 38. New York: Academic Press, 1960.
29. LUDWIG, D., "Uniform asymptotic expansions at a caustic," *Comm. Pure and Appl. Math.* 19 (1966), pp. 215-260.

30. KRAVTSOV, Yu. A., "A modification of the geometrical optics method," *Radiofizika* 7 (Russian) (1964), pp. 664-673.
31. BREKHOVSKIKH, L. M., *Waves in Layered Media.*, Sec. 27. New York: Academic Press, 1960.
32. BUDDEN, K. G., *The Waveguide Mode Theory of Wave Propagation*, Chapter 8. Englewood Cliffs: Prentice-Hall, 1961.
33. WATSON, G. N., *A Treatise on the Theory of Bessel Functions*, Chapter 15. Cambridge, England: Cambridge University Press, 1944.
34. COURANT, R., *Differential and Integral Calculus*, Vol. II, Sec. 3.5. New York: Interscience, 1947.
35. BREMMER, H., *Terrestrial Radio Waves*, Chapters 8 and 9. New York: Elsevier Publishing Co., 1949. See also *Handbuch der Physik* 16, p. 350.
36. FELSEN, L. B. and L. LEVEY, "A relation between a class of boundary value problems in a homogeneous and an inhomogeneous region," *IEEE Trans. on Antennas and Propagation AP-14* (1966), pp. 308-317.
37. EPSTEIN, P. S., "Reflection of waves in an inhomogeneous absorbing medium," *Proc. Natl. Acad. Sci. (USA)* 16 (1930), p. 627.
38. ECKART, C., *Phys. Rev.* 35 (1930), p. 1303.
39. RAWER, K., *Ann. d. Physik* 35 (1939), p. 385.
40. ECKART, G., "Wellenoptische Behandlung der Strahlung eines magnetischen Dipols in einem eben geschichteten Medium mittels der Methode von Epstein," *Bayerische Akad. d. Wissenschaften, Mathematisch-Naturwissenschaftliche Klasse*, Munich, Germany, December 1960.